REPORT DOCUMENTATION PAGE

Form Approved
OMB No. 0704-0188

1. REPORT DATE *(DD-MM-YYYY)*	2. REPORT TYPE	3. DATES COVERED *(From - To)*
MARCH 2021	TECHNICAL PAPER	DEC 2019 - DEC 2020

4. TITLE AND SUBTITLE

TDoA Geolocation Accuracy as a Function of the Number of Randomly Placed Sensors

5a. CONTRACT NUMBER
IN-HOUSE - R1LP

5b. GRANT NUMBER
N/A

5c. PROGRAM ELEMENT NUMBER
62788F

6. AUTHOR(S)

Warren H. Debany Jr.

5d. PROJECT NUMBER
RIGI

5e. TASK NUMBER
HR

5f. WORK UNIT NUMBER
DR

7. PERFORMING ORGANIZATION NAME(S) AND ADDRESS(ES)

Air Force Research Laboratory/Information Directorate
Rome Research Site/RIG
525 Brooks Road
Rome NY 13441-4505

8. PERFORMING ORGANIZATION REPORT NUMBER
N/A

9. SPONSORING/MONITORING AGENCY NAME(S) AND ADDRESS(ES)

Air Force Research Laboratory/Information Directorate Rome Research Site/RIG
525 Brooks Road
Rome NY 13441-4505

10. SPONSOR/MONITOR'S ACRONYM(S)
AFRL/RI

11. SPONSORING/MONITORING AGENCY REPORT NUMBER
AFRL-RI-RS-TP-2021-003

12. DISTRIBUTION AVAILABILITY STATEMENT

Approved for public release; distribution unlimited. PA# AFRL-2021-0842
Cleared Date: 15 MAR 2021

13. SUPPLEMENTARY NOTES

Work was performed by member of AFRL's Volunteer Emeritus Corps (VEC).This is a work of the United States Government and is not subject to copyright protection in the United States.

14. ABSTRACT

This paper addresses the problem of locating a radio frequency (RF) emitter on the ground using a set of ground-based or airborne sensors. Time-difference-of-arrival (TDoA) measurements at pairs of sensors are combined to obtain an estimate of the emitter location. The central question is to determine the trend of the relative reductions in statistical metrics for Location Distance Error (LDE), in the presence of sensor position and timing errors, as the number of sensors increases. Analysis is based on Monte Carlo simulations of randomly generated geometries of an emitter and the sensors. It is shown that, even in the error-free case, a minimum of five sensors should be used to avoid significant percentages of bad geometries with intrinsically large LDE. Combining the measurements of all pairs of sensors, rather than subsets of pairs, consistently provides the smallest LDE although at increased computational cost. This paper determines the sensitivity of LDE to sensor altitude as well as position errors and timing errors. Regression models relate LDE statistical metrics to the number of sensors and the specific configurations; the double logarithm of each of the LDE statistical metrics is closely estimated by a linear function of the double log of the number of sensors. The improvement in LDE statistical metrics as the number of sensors increases can be approximated by simpler power law regression models. Rough estimates of LDE improvement are provided as multiples of the reciprocal of the number of sensors. This paper also determines the improvement in LDE achieved by the simple rule of enforcing minimum separation between the sensors.

15. SUBJECT TERMS

Time-Difference of Arrival, TDoA, Geolocation, Location Distance Error, Sensors

16. SECURITY CLASSIFICATION OF:			17. LIMITATION OF ABSTRACT	18. NUMBER OF PAGES	19a. NAME OF RESPONSIBLE PERSON
a. REPORT	b. ABSTRACT	c. THIS PAGE			**WARREN H. DEBANY JR.**
U	U	U	UU	223	19b. TELEPHONE NUMBER (*Include area code*) N/A

TDoA Geolocation Accuracy as a Function of the Number of Randomly Placed Sensors

Warren H. Debany Jr., Ph.D., P.E.
AFRL/RIG
525 Brooks Rd.
Rome NY 13441-4505

Abstract

This paper addresses the problem of locating a radio frequency (RF) emitter on the ground using a set of sensors. Time-difference-of-arrival (TDoA) measurements at pairs of sensors are combined to obtain an estimate of the emitter location. The sensors may be stationary or in motion and may be on the ground or airborne. The sensors are networked and processing is centralized.

The central question addressed in this paper is to determine the trend of the relative improvement in Location Distance Error (LDE), in the presence of sensor position and timing errors, as the number of sensors (N) increases. The statistical metrics used are the mean, 50th, 95th, and 99th percentile LDE.

Analysis is based on Monte Carlo simulations of randomly generated geometries based on parameterized configurations of an emitter and the sensors, where the sensors may be immersed in the same search area with the emitter or standoff in an adjacent area. It is shown that configurations consisting of three or four sensors have significant percentages of intrinsically bad geometries that may have large LDE values even in error-free cases; based on these findings, a minimum of five sensors should be used for ground-based or airborne sensor configurations.

Several sensor pairing methods based on combining either all pairs, disjoint pairs, or linearly independent pairs are compared on the basis of their mean LDE values. It is found that the all pairs method consistently provides the smallest LDE.

This paper determines the sensitivity of LDE to sensor altitude and position and timing error conditions. For a given number of sensors in an immersed or standoff configuration, it is shown that each of the LDE statistical metrics is approximately scale-invariant to the ratio of

Approved for Public Release; distribution unlimited; AFRL-2021-0842

the altitude to the search area side length and there is an optimal ratio for each statistical metric. Various regression models are developed to relate LDE statistical metrics to the number of sensors and the specific configurations; the simplest regression models show that the double logarithm of each of the LDE statistical metrics is closely estimated by a linear function of the double logarithm of the number of sensors.

The problem of determining the relative improvement in the LDE statistical metrics, for a given configuration and error conditions, can be framed as estimating the ratio of an LDE statistical metric for N sensors to that LDE statistical metric for five sensors. Based on the main data set used in this paper, this "Improvement Ratio" can be closely estimated by a simple reciprocal approximation w_{RA}/N for $N \geq 6$, where w_{RA} varies from 2.50 to 5.96 over the full set of LDE statistical metrics for the configurations and error conditions considered. Based on an ensemble data set that used a wider set of error conditions, compared to the baseline of five sensors, the mean LDE falls off roughly as the ratios $4.5/N$ and $4.8/N$ for $N \geq 6$ for immersed and standoff sensors, respectively.

While the general approach used here assumes that geometries are completely random within the specifications for the configurations, this paper also determines the improvement in LDE achieved using the simple rule of enforcing minimum separation between the sensors.

Contents

1 Introduction

This paper addresses the problem of locating a radio frequency (RF) emitter on the ground using a set of sensors. [1] The sensors may be stationary or they may be in motion. They may be on the ground or airborne. [2] The sensors are networked and processing is done in a centralized manner using all of the available measurements.

Such problems arise in military applications where it is necessary to locate an adversarial RF transmitter. This problem also applies to civilian operations such as search-and-rescue. It is assumed in this paper is that a variable number of sensors can be deployed over a relatively small area of interest and the number of sensors can be controlled to provide a desired degree of geolocation accuracy. The configurations, [3] characteristics, and parameters used in this paper are not based any actual military or civilian systems or scenarios.

Commonly used techniques for locating an RF emitter include Time-of-Arrival (ToA), Time-Difference-of-Arrival (TDoA), Angle-of-Arrival (AoA), Frequency-Difference-of-Arrival (FDoA), and Received Signal Strength (RSS), as well as hybrids of these approaches [Montminy (2007)] [Sadaphal (2005)]. It is known that techniques based on time measurements are far more accurate than those based on measuring angles or signal strengths [Sadaphal (2005)] so AoA and RSS techniques were not used in this work. FDoA requires the emitter to be moving and ToA requires time synchronization with the emitter, and since the scenarios considered in this paper assume an uncooperative emitter which can be stationary, TDoA is the only technique considered here.

[1] The terms "locate" and "geolocate" are used interchangeably in this paper. The terms "location" and "position" refer synonymously to the placement of the emitter and sensors, although "location" will generally be used in connection with the emitter and "position" in connection with the sensors. The terms "ground" and "surface" are used interchangeably and refer to zero altitude.

[2] The ground-based sensors may be pre-positioned and stationary or may be on vehicles in motion. Airborne sensors may be on manned aircraft or hosted on drones as part of an Unmanned Aircraft System (UAS). Sensors that are not on the ground may of course be mounted on buildings or towers, but for brevity will be referred to as being "airborne."

[3] A "configuration" is a parameterized template for the placement of the emitter and sensors and a "geometry" is a specific, randomly generated instance of a configuration.

RF TDoA measures the difference in the time of arrival of a signal propagating at the speed of light from an emitter at pairs of sensors. In two-dimensional (2D) space, the locus of points that have the same TDoA form a hyperbola. In three-dimensional space (3D), the points form a hyperboloid. Since the TDoA solution method used in these investigations operates in 3D space even when the sensors are at ground level, the term "hyperboloid" is used throughout this paper. The two sensors are the foci of the hyperboloid. Ideally, the emitter would be found at the intersection of the hyperboloids on the surface defined by multiple pairs of sensors. Thus, TDoA-based systems are referred to as "hyperbolic location" systems [Torrieri (1984)].

Several practical issues arise in using TDoA measurements to locate the emitter. One issue is that measurement errors are inevitable in any actual system. Causes of such errors are inaccuracies in sensor position determination and time synchronization between pairs of sensors [Gholami (2013)] [Qu (2012)] [Wang (2013)]. Another issue, intrinsic to the geometry of the problem, is that there may be multiple valid solutions where all the hyperboloids intersect. [4] Even when a single solution may exist in principle, hyperboloids may intersect at small angles and thus even minor position or timing errors may cause numerical solutions to converge to incorrect results [Kaune (2012)].

The figure-of-merit used in this paper to express the accuracy of TDoA geolocation is **the distance between the estimated location of the emitter and its true location**, referred to in this paper as the **Location Distance Error (LDE)**. [5] The primary statistical metric used is the *mean* LDE. Other related statistical metrics used are the *50th percentile (50%ile)* or median LDE, the *95th percentile (95%ile)* LDE, and the *99th percentile (99%ile)* LDE. [6]

In the 2D case, where the emitter and sensors are lying in a plane, a minimum of three (that is, $N = 3$) sensors are needed to uniquely locate an

[4] Even when the hyperboloids do not intersect exactly, they may converge closely enough that the specific TDoA solution method cannot distinguish between the correct solution and other possible solutions.

[5] All distances in this paper are Euclidean or "Manhattan" distances calculated using the Pythagorean Theorem.

[6] The term "percentile" does not have a single mathematical definition. In this paper, percentiles are calculated using the "nearest rank" method and are not interpolated. The median of a set of values is given by the 50%ile value. For the large sets of data used in this paper, the specific algorithm used to calculate percentiles makes almost no difference.

emitter. However, some intrinsically bad geometries may require additional sensors. For example, if the sensors are collinear (that is, positioned in a straight line), then there are valid solutions on either side of the line of sensors; at least one additional sensor that is not collinear may be required to resolve the ambiguity of the emitter location. Another problem occurs when two or more sensors are clustered together: foci that are close to each other create small baselines for the hyperboloids and effectively reduce the number of sensors to the number of distinct clusters. [7]

Studies have addressed the problem of optimizing sensor positions to minimize LDE [Hamdollahzadeh (2016)] [Huie (2014)]. However, even when sensor positions are optimized, small numbers of sensors may be confounded by poor emitter locations which, of course, are unknown and not controllable. Regardless of any optimizations, geolocation accuracy suffers whenever an emitter is collinear with two sensors.

Sensors that are in motion are constantly changing their geometries and, in general, cannot be guaranteed to maintain desirable geometries for geolocation. This paper does not assume that geometries are optimal, but instead uses Monte Carlo simulation to derive LDE statistical metrics over large numbers of randomly generated geometries of emitters and sensors. However, this paper briefly assesses in an appendix the benefits of the simple optimization rule of enforcing a minimum xy separation between sensors to avoid small baselines.

TDoA analyses usually involve discussion of error ellipses, Geometric Dilution of Precision (GDoP), and the Cramér-Rao Lower Bound (CRLB) [Chen (2013)] [Ho (2007)] [Huie (2014)] [Qu (2012)] [Sadaphal (2005)] [Torrieri (1984)]. However, these concepts do not apply in the Monte Carlo situation where the figure-of-merit is the LDE obtained over large numbers of randomly generated geometries.

Some previous work has considered fixed numbers of sensors (such as six, eight, or ten) or sought to minimize the number of sensors to provide adequate LDE. Some studies have addressed the improvement of LDE in the

[7] For example, if there are four sensors but two are clustered closely together, then the geometry is little more effective than if it had only three spatially separated sensors. This paper uses only TDoA as the geolocation technique, but a hybrid approach that includes other means, such as the use of a high-gain antenna to resolve AoA of an emitter signal, could resolve location ambiguity [Torrieri (1984)].

2D case gained by, say, using four sensors rather than the absolute minimum of three. (See, for example, [Chen (2013)] [Huie (2014)] [Sadaphal (2005)].) However, there do not appear to have been any systematic studies of the reduction of LDE specifically as a function of the number of sensors.

Thus, **the central question addressed in this paper is to determine the trend of the relative improvement of the LDE statistical metrics as the number of sensors increases**. The approach is to observe how the LDE statistical metrics vary with the number of randomly placed sensors used to geolocate a randomly placed emitter for several sensor/emitter configurations in the presence of sensor position and timing errors.

The answers to the central question are developed as follows.

To demonstrate the motivation for this work, examples of the geolocation challenges created by sensor position and timing errors are given in Section 2. Major aspects of this work are outlined here, and provide a preview for further assumptions and details of the model that are are discussed in Section 4.

Section 3 summarizes the nomenclature, terms, and abbreviations used in this paper.

Section 4 expands on the brief overview of the method given in Section 2. This section describes how parameterized configurations of emitter and sensors are converted into randomly generated geometries and simulated. Sensor position and timing error conditions are defined. The 2D grid search-based TDoA solution method is described as well as the optimization techniques that were found to improve run times and accuracy. Justification is given for a "flat earth model" over the distances considered in this work.

Several methods are used in the literature for combining TDoA measurements at pairs of sensors. Section 5 compares three such methods and shows that the "all pairs" method gives superior geolocation accuracy, albeit at a high computational cost for configurations with large numbers of sensors.

The geolocation challenges created by bad sensor and emitter geometries, in the absence of sensor position or timing errors, are addressed in Section 6.

A major finding is that a minimum of five sensors should be used to avoid potentially large LDE even in error-free cases.

Section 7 shows how LDE varies with the number of sensors as a function of the nominal altitude of the sensors and the size of the search area that contains the emitter.

Section 8 describes the general approach for using linear regression models to estimate LDE. Section 9 develops linear regression models for fixed configurations of nominal altitude and search area side lengths, where the double logarithms of LDE statistical metrics are shown to be linear functions of the double logarithms of the number of sensors. Section 10 generalizes the linear regression models given in Section 9 so that LDE can be estimated for any nominal altitude or search area size within the limits of the Main Data Set used in this paper.

The central question of determining the trend of the relative improvement of the LDE statistical metrics as the number of sensors increases is directly addressed in Section 11 by defining the Improvement Ratios for LDE statistical metrics. These ratios are shown to be estimated well by power-law linear regression models that are far simpler than the double logarithm models developed for the LDE statistical metrics themselves.

Section 12 uses the envelope of the Improvement Ratios for the entire Main Data Set and develops power-law bounds for the envelope and its mean, as a function of the number of sensors. The power-law estimates are simplified further by expressing them as approximations in terms of the reciprocal of the number of sensors.

Section 13 determines the sensitivity of the models used in this paper to variations in the parameters for altitude and error conditions. Additional data sets are generated using wider ranges of error conditions in Section 14 and expanded power-law estimates and reciprocal approximations are developed for these data.

Following the Conclusions presented in Section 15, two appendices present results that are outside the assumptions of the main stream of this work.

Appendix A studies the distributions of timing difference that result from the assumption of Gaussian distributions of sensor timing error and position error. While the timing difference errors at pairs of sensors are Gaussian due to the Gaussian *timing errors*, the same is not true for the timing difference errors that result from Gaussian *position errors*.

The main results of this paper are not based on the assumption that geometries are designed to be optimal, but instead derives LDE statistical metrics based on randomly generated geometries of emitters and sensors. However, Appendix B assesses the benefits of the simple optimization rule of enforcing a minimum xy separation between sensors to avoid small baselines.

2 Examples of Location Distance Error

This section provides motivation for the TDoA LDE problem. More properly, this material should have followed Section 4 where details of the configurations and resulting geometries, error conditions, TDoA solution method, and graphing technique are provided. It is presented early in the paper to motivate the basic problem of LDE due to position and timing errors in TDoA geolocation. In advance of the in-depth explanations given in Section 4, the situations considered in this section are outlined briefly as follows. The situations described in this section are a subset of the Main Data Set described in Section 4.3.

For the examples in this section, the emitter is located at a randomly selected location on the ground in a square search area that is 1 km on a side (parameter $side = 1{,}000$ m). The sensors are randomly placed, and are either **immersed** on or above the square area that contains the emitter or **standoff** on or above a square area adjacent to the area that contains the emitter. The sensors are either all on the ground (parameter $alt = 0$ m) or all located at mean altitudes of 100 m with a standard deviation of 5 m (parameters $alt = 100$ m and $\sigma_{alt} = 5$ m). In the error-free case, these presumed positions and the time-of-arrival measurements are correct.

In the case of errors, the presumed positions of the sensors are not the true positions. Each sensor has a **position error** [8] about the presumed position with a Gaussian distribution with zero mean and a standard deviation of 10 m; the true position is unknown to the TDoA solution method.

The sensors also have **timing errors**, where there is a time drift with a Gaussian distribution with zero mean and standard deviation of 30 ns with respect to the global clock. The assumptions of zero mean Gaussian distributions of errors and the independence of position errors and timing errors are common in the relevant literature; see, for example, [Ho (2007)] [Qu (2012)] [Wang (2013)].

For the TDoA solution method used in this paper, the location estimate is the point in the search area that minimizes the sum of squared errors (SSE) between the measured TDoA values and those obtained for candidate

[8] The position error is restricted to the 2D xy plane when the sensors are on the ground and it extends in 3D when the sensors are at non-zero altitudes.

points tested using a 2D grid search; in this section, all pairwise TDoA measurements are used to locate the emitter. As shown later, the performance and quality of any TDoA solution method depends greatly on the specific algorithm and parameters used to solve for an estimated location of the emitter based on the TDoA measurements.

Due to graphing limitations, only configurations involving three or four sensors are considered in this section. Only the xy coordinates of the sensor positions are shown in the graphs; that is, the points plotted on the graphs are the 2D projections of their positions on the ground. The sensors are shown at their presumed positions rather than their true positions.

All of the examples shown in this section were chosen such that they had zero LDE in the error-free case so as to demonstrate the deleterious effects of position errors and timing errors. The issue of error-free cases having non-zero LDE is discussed in Section 6.

The first set of examples used in this section involves three sensors.

Figure 1 shows an error-free case with three sensors on the ground and immersed with the emitter. The three hyperboloids created by the three pairwise TDoA measurements intersect at a single point in the search area; that same point (marked by a green square) provides the minimum SSE and is the correct location of the emitter.

Figure 2 shows the same geometry in the case of errors. The three hyperboloids have shifted and the point that provides the minimum SSE (marked by a red square) has LDE of 283.45 m from the correct location.

Figure 3 shows an error-free case with three sensors at mean altitudes of 100 m with standard deviation of 5 m and immersed with the emitter. [9] The point in the search area that minimizes the SSE is again the correct location.

Figure 4 shows the same geometry in the case of errors. The point that minimizes the SSE has LDE of 168.14 m from the correct location.

[9] The three specific altitudes generated by the simulator in this case with these parameters were 92.65 m, 96.99 m, and 103.25 m.

Figure 5 shows an error-free case with three sensors on the ground, but the sensors are now standoff from the emitter in a 1 km $\times$ 1 km area adjacent to the search area. The point in the search area that minimizes the SSE is again the correct location.

Figure 6 shows the same geometry in the case of errors. The point that minimizes the SSE has LDE of 483.34 m from the correct location.

Figure 7 shows the same error-free standoff geometry of three sensors as in Figure 5 but at mean altitudes of 100 m with standard deviation of 5 m. [10] The point in the search area that minimizes the SSE is the correct location.

Figure 8 shows the same geometry in the case of errors. The point that minimizes the SSE has LDE of 517.49 m from the correct location.

The next set of examples used in this section involves four sensors.

Figure 9 shows an error-free case with four sensors on the ground and immersed with the emitter. Note that the six hyperboloids created by the six pairwise TDoA measurements intersect at a single point in the search area. That point provides the minimum SSE and is the correct location of the emitter.

Figure 10 shows the same geometry in the case of errors. The six hyperboloids have shifted and no longer intersect at a single point. The point that provides the minimum SSE has LDE of 101.90 m from the correct location.

Figure 11 shows the same error-free standoff geometry of four sensors as in Figure 9 but at mean altitudes of 100 m with standard deviation of 5 m. The point in the search area that minimizes the SSE is the correct location.

Figure 12 shows the same geometry in the case of errors. The point that minimizes the SSE has LDE of 80.25 m from the correct location.

These examples have demonstrated how position and timing errors can cause erroneous TDoA location estimates. The examples used in this sec-

[10] That is to say, the xy coordinates were the same as in Figure 5 but the specific altitudes generated by the simulator in this case were 110.67 m, 103.43 m, and 93.14 m.

tion had LDE values of zero in the error-free cases, but it should be noted that poor geometries may still result in non-zero LDE values for location estimates. Later sections will quantify LDE, as a function of the number of sensors, to mitigate position and timing errors as well as poor geometries.

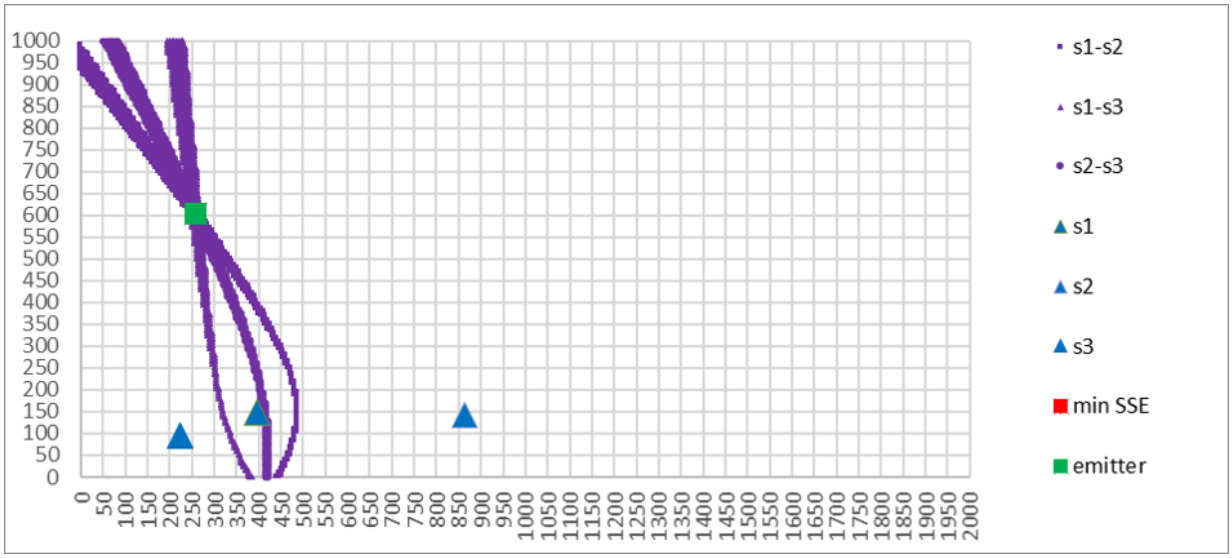

Figure 1: The hyperboloids intersect at a single point that has the smallest SSE and is the correct position of the emitter. Parameters: $N = 3$ immersed sensors, $side = 1{,}000$ m, $alt = 0$ m, error-free.

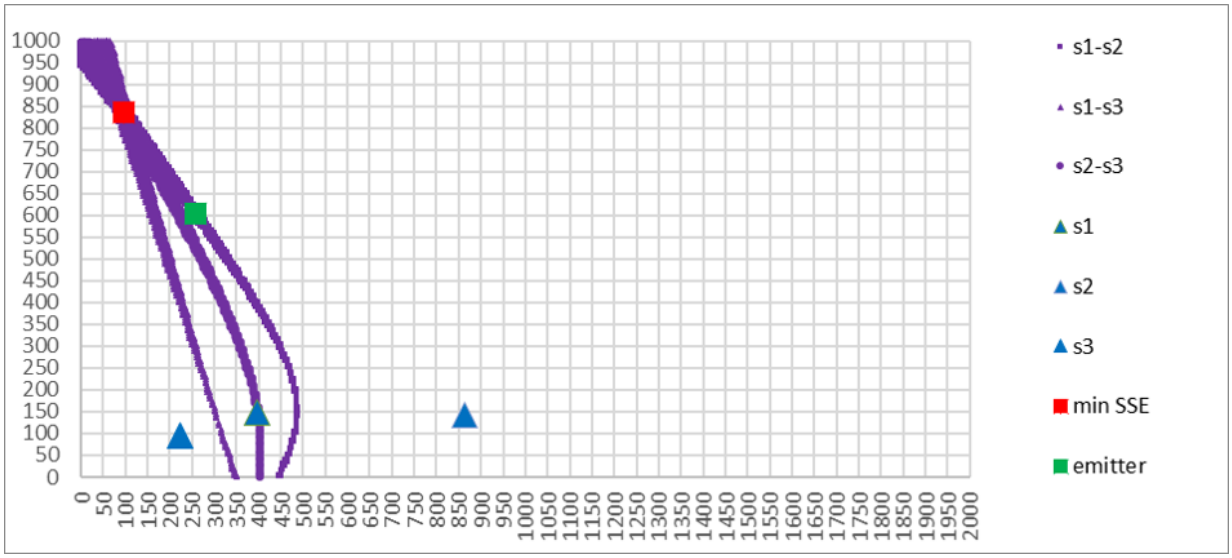

Figure 2: In the same geometry as shown in Figure 1 but with position and timing errors, the hyperboloids have shifted so that the point that has the minimum SSE is 283 m from the true position of the emitter. Parameters: $N = 3$ immersed sensors, $side = 1{,}000$ m, $alt = 0$ m, with errors.

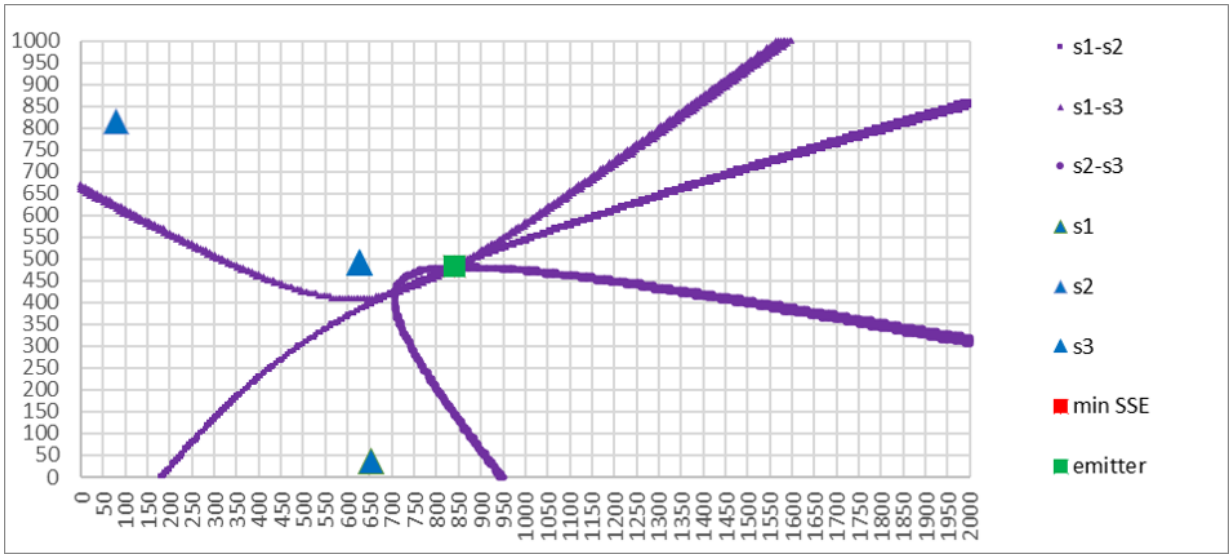

Figure 3: The hyperboloids intersect at a single point that has the smallest SSE and is the correct position of the emitter. Parameters: $N = 3$ immersed sensors, $side$ = 1,000 m, alt = 100 m, error-free.

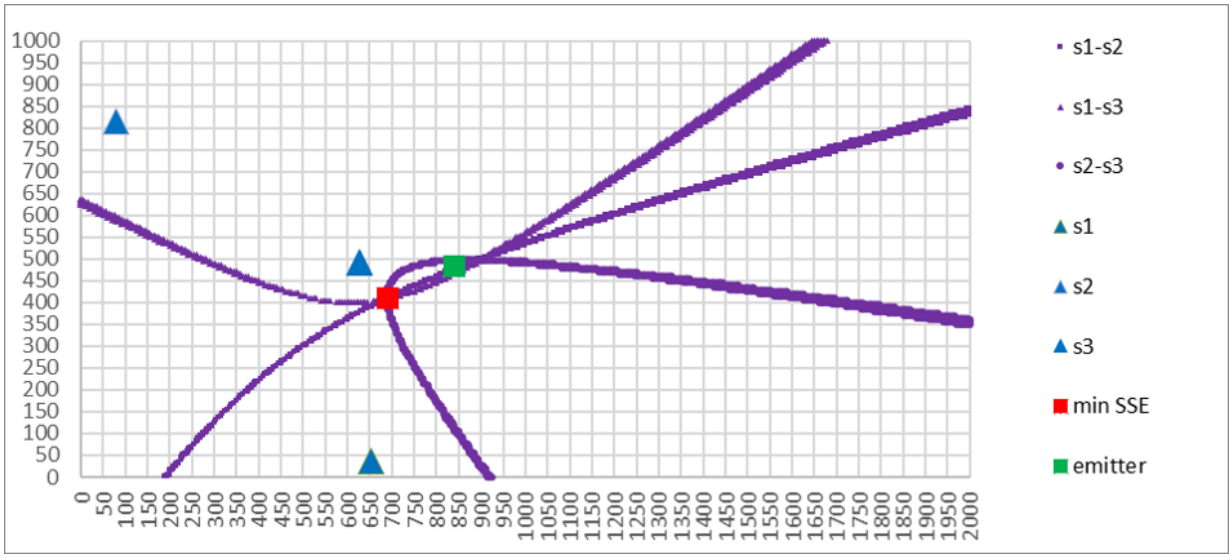

Figure 4: In the same geometry as shown in Figure 3 but with position and timing errors, the hyperboloids have shifted so that the point that has the minimum SSE is 168 m from the true position of the emitter. Parameters: $N = 3$ immersed sensors, $side$ = 1,000 m, alt = 100 m, with errors.

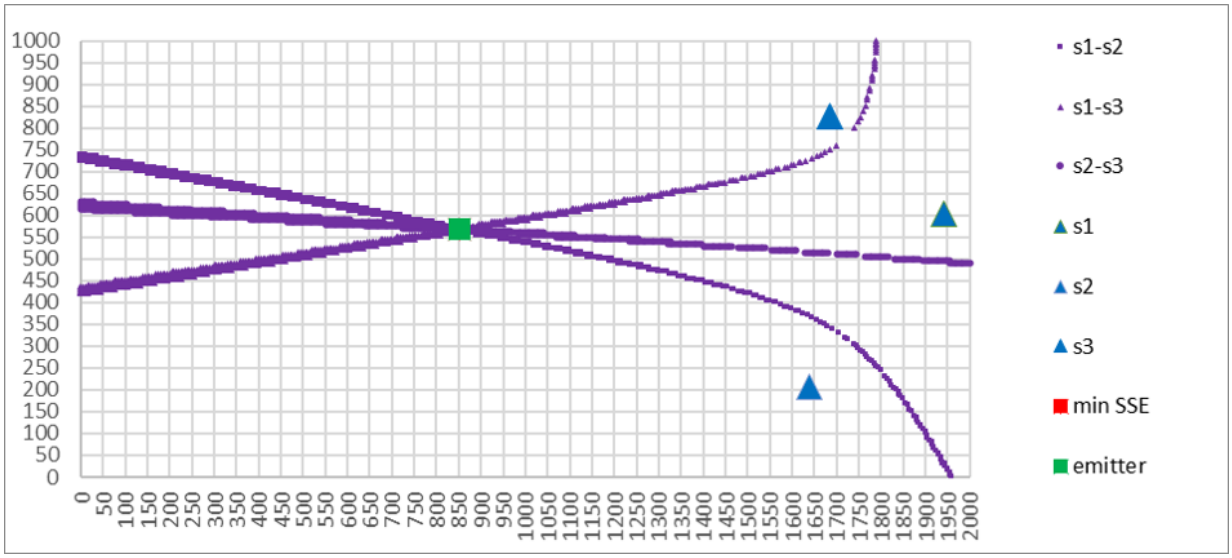

Figure 5: The hyperboloids intersect at a single point that has the smallest SSE and is the correct position of the emitter. Parameters: $N = 3$ standoff sensors, $side$ = 1,000 m, alt = 0 m, error-free.

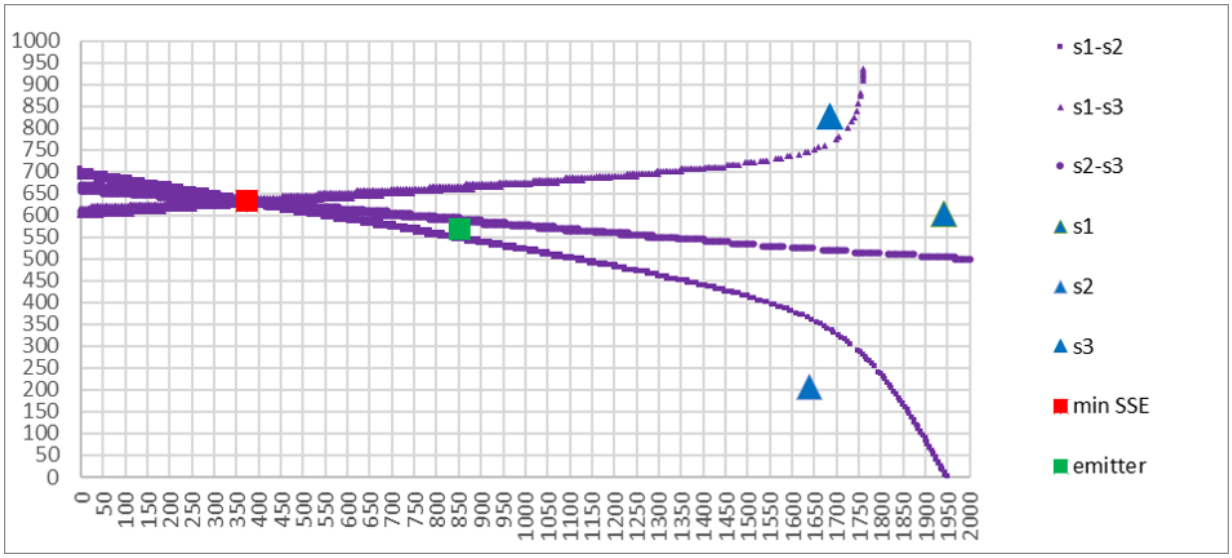

Figure 6: In the same geometry as shown in Figure 5 but with position and timing errors, the hyperboloids have shifted so that the point that has the minimum SSE is 483 m from the true position of the emitter. Parameters: $N = 3$ standoff sensors, $side$ = 1,000 m, alt = 0 m, with errors.

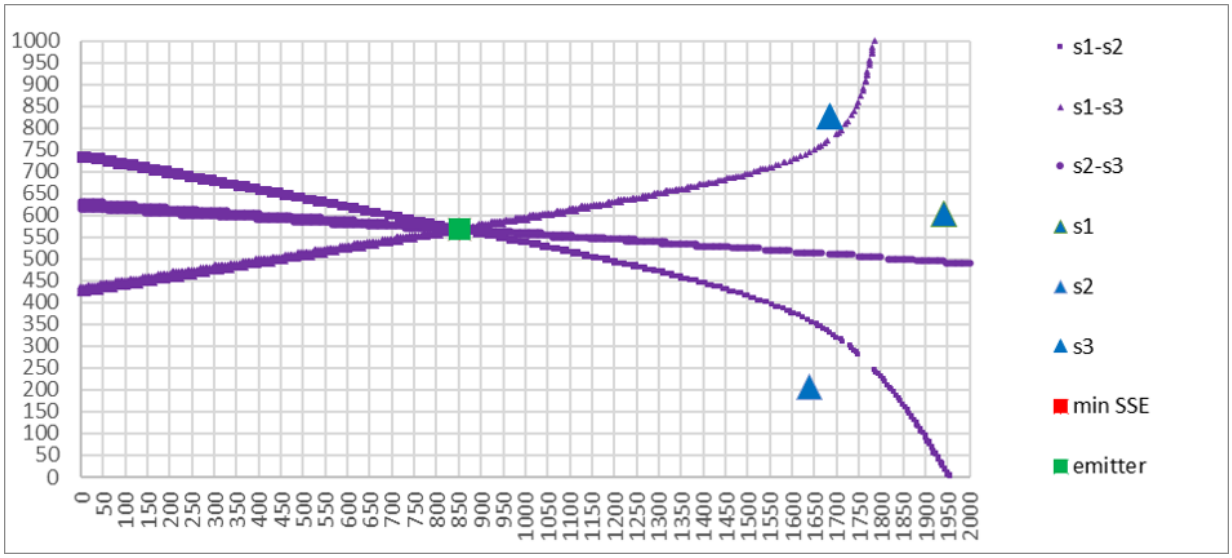

Figure 7: The hyperboloids intersect at a single point that has the smallest SSE and is the correct position of the emitter. Parameters: $N = 3$ standoff sensors, $side$ = 1,000 m, alt = 100 m, error-free.

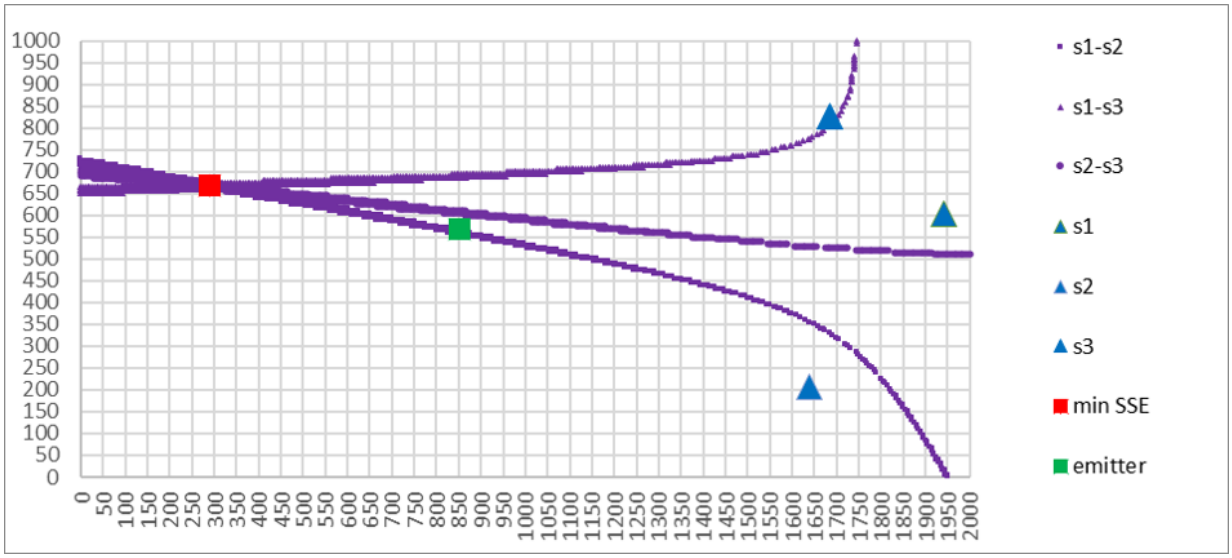

Figure 8: In the same geometry as shown in Figure 7 but with position and timing errors, the hyperboloids have shifted so that the point that has the minimum SSE is 517 m from the true position of the emitter. Parameters: $N = 3$ standoff sensors, $side$ = 1,000 m, alt = 100 m, with errors.

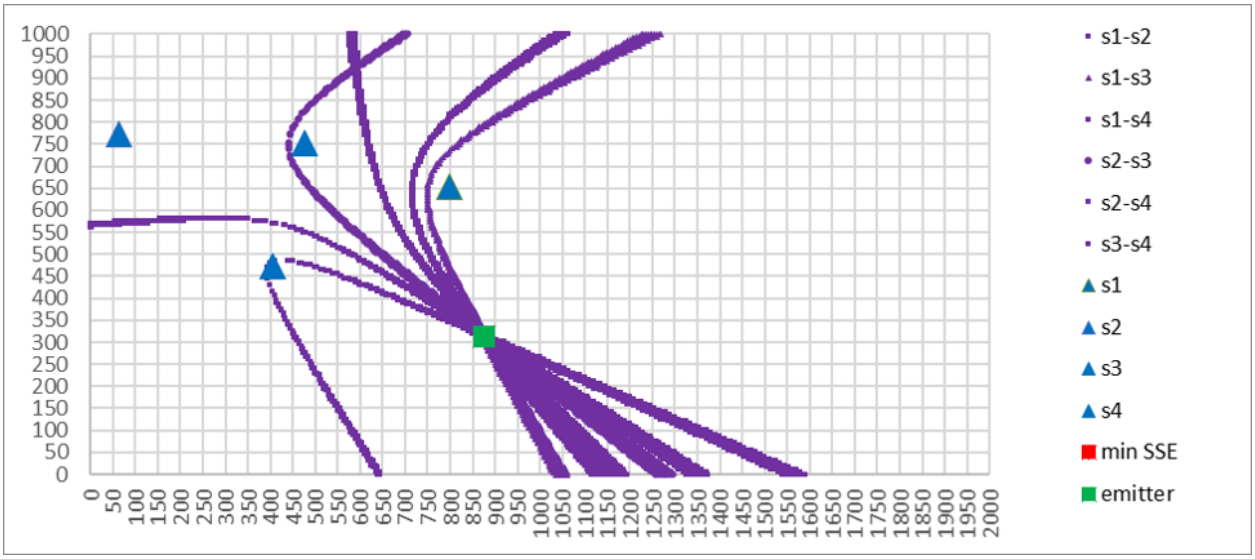

Figure 9: The hyperboloids intersect at a single point that has the smallest SSE and is the correct position of the emitter. Parameters: $N = 4$ immersed sensors, $side = 1{,}000$ m, $alt = 0$ m, error-free.

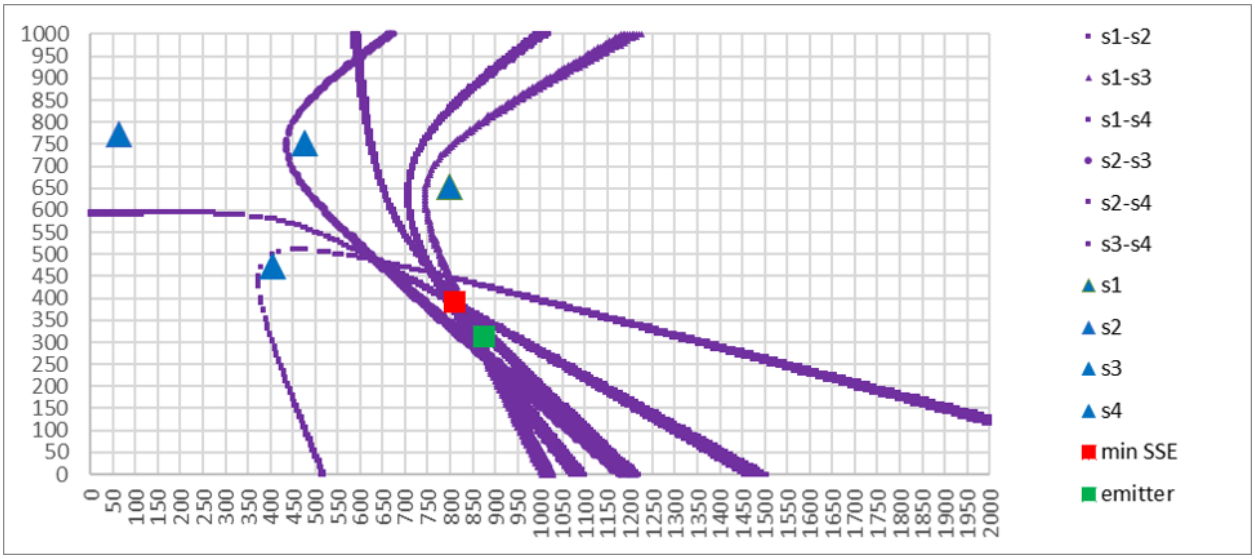

Figure 10: In the same geometry as shown in Figure 9 but with position and timing errors, the hyperboloids have shifted so that the point that has the minimum SSE is 102 m from the true position of the emitter. Parameters: $N = 4$ immersed sensors, $side = 1{,}000$ m, $alt = 0$ m, with errors.

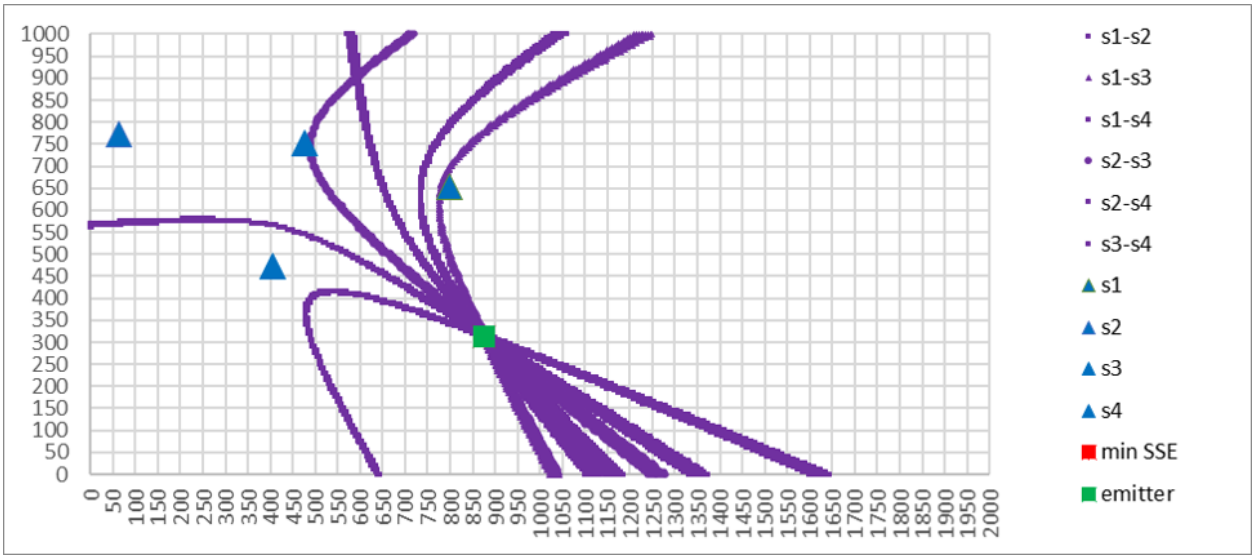

Figure 11: The hyperboloids intersect at a single point that has the smallest SSE and is the correct position of the emitter. Parameters: $N = 4$ immersed sensors, $side$ = 1,000 m, alt = 100 m, error-free.

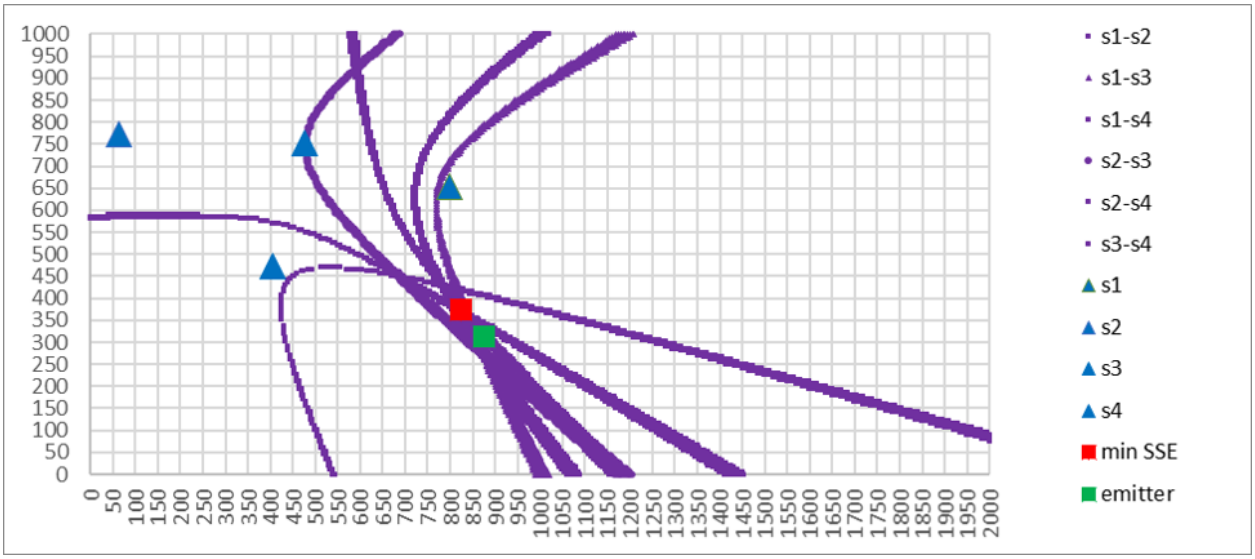

Figure 12: In the same geometry as shown in Figure 11 but with position and timing errors, the hyperboloids have shifted so that the point that has the minimum SSE is 80 m from the true position of the emitter. Parameters: $N = 4$ immersed sensors, $side$ = 1,000 m, alt = 100 m, with errors.

3 Nomenclature

The following terms, abbreviations, and symbols are used in this paper. They are listed roughly in the order in which they are introduced.

Long phrases used for the figures-of-merit are defined in the list below and again at the end of the list for additional clarification.

Terms and other critical concepts are bolded in the text at the point where they are defined.

Acronyms represent both the singular or plural forms; for example, "LDE" stands for both "Location Distance Error" and "Location Distance Errors."

Distances are given in meters unless otherwise specified. Time is specified in seconds or nanoseconds. A distance or time that is stated as "zero" or "0" is understood to be 0 m or 0 ns, respectively.

Units are bound to the names of the quantities. For example, if a value for an altitude is assigned as "$alt = 100$ m," then that value is later stated as "*alt*" and not "*alt* meters" or "*alt* m." Distances are always used in units of meters even when specified in kilometers or centimeters and time is always used in units of seconds even when specified in nanoseconds.

$\ln x$, $\ln(x)$ – Natural logarithm of x; the logarithm base e, where $e = 2.71828182845\ldots$. All logarithms used in this paper are natural logs.

$\ln\ln x$, $\ln(\ln(x))$ – Double logarithm of x.

$\exp(x)$, e^x – Exponential function of x.

$\exp(\exp(x))$, e^{e^x} – Double exponential function of x.

m, km, cm – Meters, kilometers, centimeters.

sec, ns – Seconds, nanoseconds.

rad, $^\circ$ – Radians, degrees.

c – Speed of light. The rounded value of 3×10^8 m/sec is used in this paper as it is close enough for practical purposes to the actual speed of propagation of electromagnetic radiation in air or vacuum.

%ile – Percentile of a set of values. For example, "95th percentile" is written as "95%ile." Percentiles are calculated using the "nearest rank" method and the median is given by the 50%ile value.

"Unknown" – Information is designated as "unknown" when the simulation does not provide it to the TDoA solution method.

ToA – Time-of-Arrival.

TDoA – Time-Difference-of-Arrival.

AoA – Angle-of-Arrival.

FDoA – Frequency-Difference-of-Arrival.

RSS – Received Signal Strength.

2D – Two-dimensional, with coordinates (x, y).

3D – Three-dimensional, with coordinates (x, y, z).

LDE – Location Distance Error. This is the fundamental figure-of-merit for geolocation accuracy used in this paper. All other figures-of-merit are based on the LDE.

LDE statistical metrics – The mean, 50%ile (median), 95%ile, or 99%ile LDE, for a given configuration and set of error conditions, based on a set of simulations.

CRLB – Cramér-Rao Lower Bound.

GDoP – Geometric Dilution of Precision.

N – Number of sensors.

alt – Mean altitude of all sensors in a configuration.

σ_{alt} – Standard deviation about the mean altitude. The value $\sigma_{alt} = alt/20$ (or 5% of alt) is used in all simulations unless otherwise specified. Thus, the coefficient of variation σ_{alt}/alt was 0.05.

Nominal altitude – "Nominal altitude of alt" is shorthand for "mean altitude of alt with the specified standard deviation σ_{alt}." The variation in nominal altitude is not an error condition but rather an aspect of the randomly generated geometry for a configuration.

$side$ – Search area side length.

σ_{pos} – Standard deviation of sensors' position errors.

σ_{time} – Standard deviation of sensors' timing errors.

Standard error conditions – The standard values for position and timing error conditions used for all simulations are $\sigma_{pos} = 10$ m and $\sigma_{time} = 30$ ns unless otherwise specified.

Main Data Set – The set of configurations that is the basis for most of the analyses in this paper. It consists of 4,840 configurations that use the "Standard Error Conditions." Results are based on 10,000 simulations (of randomly generated geometries) per configuration. It is described in detail in Section 4.3.

LIP – Linearly Independent Pairs sensor pairing method.

LIP n – LIP that uses sensor n (out of N sensors) as the reference sensor.

RF – Radio Frequency.

SEM – Spherical Earth Model.

FEM – Flat Earth Model.

θ – Earth central angle between the sensor and emitter.

ϕ – Angle of the sensor above earth horizon from the location of the emitter.

r – Slant range from sensor to emitter for SEM.

r' – Slant range from sensor to emitter for FEM.

s – Surface distance from the point directly below the sensor (for both SEM and FEM) to the emitter.

s_{hor} – Surface distance of the horizon from the point directly below the sensor.

R – Earth radius (mean equatorial): 6,378,137 m.

i – Sensor index in the range 1 to N. "Sensor i" means "sensor with index i."

t'_i – Timing error (or time drift or time skew), with respect to the global clock, for sensor i.

(x_i, y_i, z_i) – Presumed or intended position of sensor i, which is correct in an error-free case but erroneous in the case of position error.

(x'_i, y'_i, z'_i) – The true (but unknown) position of sensor i.

(x'_e, y'_e, z'_e) – The true (but unknown) location of the emitter. Coordinate z'_e is 0 because the emitter is on the ground.

(x_e, y_e, z_e) – A candidate emitter location: a grid point to be tested by the TDoA solution method. Coordinate z_e is assigned the value 0 because the emitter is assumed to be on the ground.

d_i – Distance from a candidate emitter location to the presumed position of sensor i.

d'_i – Distance from the true location of the emitter to the true position of sensor i.

$\Delta t_{i,j}$	– Presumed TDoA between sensors with indices i and j from a candidate emitter location based on presumed positions with no timing errors.
$\Delta t'_{i,j}$	– Measured (true TDoA) between sensors with indices i and j based on true positions and timing errors.
$(\widehat{x}_e, \widehat{y}_e, \widehat{z}_e)$	– Estimated location of emitter obtained by the TDoA solution method. LDE is the Euclidean distance between the estimated location of the emitter $(\widehat{x}_e, \widehat{y}_e, \widehat{z}_e)$ and its true location (x'_e, y'_e, z'_e).
SSE	– Sum of the squared errors.
Longfellow Event	– The event where local minima for SSE created by a bad geometry of emitter and sensors cause estimated emitter locations to be either very close or very far from the correct emitter location (see Section 6.1).
K	– Initial grid step divisor for the grid search-based TDoA solution method.
ss_p	– Step size in the x and y directions in pass p for the grid search-based TDoA solution method.
C	– Coverage factor for the grid search-based TDoA solution method: on step p, a square with sides $\pm Css_{p-1}$ around the center point has a coverage factor of C.
R^2	– Coefficient of determination: a commonly used measure of goodness-of-fit of a linear regression. It describes how much of the variation in the output variable is explained by the linear regression model. R^2 values range from 0 to 1, where closer to 1 is a better fit [MathWorks (2020)]. ("R^2 " used in linear regression is not to be confused with "R^2" to denote the square of the earth's radius.)
MAPE	– Mean Absolute Percentage Error: a measure of the predictive or forecasting power of a statistical model. MAPE is the average of the absolute values of the percentage errors of the model's predicted values for the output variable with respect to the true or measured values of the output variable [Kim (2016)].
Raw variables	– Configuration parameters such as N, $side$, or alt.
Transformed variables	– Functions of raw variables such as $\ln N$, $\ln \ln N$, $side^2$, $1/alt$, or replacing alt by $alt + 0.001$ m (to avoid division by zero).

Combined variables – Functions that combine raw or transformed variables such as $alt/side$ or $alt/side^2$.

y – Output variable for linear regression models. Can represent values such as an LDE statistical metric or an Improvement Ratio for an LDE statistical metric.

v – Number of input variables to a linear regression model. The number of input variables includes the raw, transformed, or combined variables.

x_i – The v input variables to a linear regression model are x_1, x_2, x_3, $\ldots x_v$. The variables are raw, transformed, or combined.

w_i – Weights for weighted sum representing a linear regression model. The $v + 1$ weights are w_0, w_1, w_2, $\ldots w_v$, where w_i is the weight for input variable x_i.

w'_i – Weights used in the first stage of the two-stage process described in Section 10.1.

Improvement Ratio – For a given configuration and set of error conditions, the Improvement Ratio for an LDE statistical metric is the ratio of the LDE statistical metric for that configuration with $N \geq 5$ sensors relative to the LDE statistical metric for the same configuration with five sensors. It is defined to be 1.0 for five sensors.

Ballpark Estimate – Estimates of the Improvement Ratio for an LDE statistical metric based on the envelope of all of the values of that ratio.

Reciprocal Approximation – An approximation for an Improvement Ratio for an LDE statistical metric expressed as w_{RA}/N.

w_{RA} – Weight for Reciprocal Approximation for the Improvement Ratio of an LDE statistical metric.

N_{equiv} – Equivalent number of sensors for minimum xy separation, defined as the number of sensors that yield the same mean LDE *without* enforcing a minimum xy separation as is achieved *with* a minimum xy separation.

The LDE is the figure-of-merit for geolocation accuracy in this paper. The LDE, its statistical metrics, and other metrics based on it are summarized again below.

Location Distance Error (LDE): The Euclidean distance of the estimated location of the emitter to the true location of the emitter.

LDE statistical metric: The mean, 50%ile (median), 95%ile, or 99%ile LDE, for a given configuration and set of error conditions, based on a set of simulations.

Improvement Ratio for an LDE statistical metric: For a given configuration, this is the ratio of the LDE statistical metric for that configuration with $N \geq 5$ sensors relative to the LDE statistical metric for the same configuration with five sensors. It is defined to be 1.0 for configurations with five sensors.

Ballpark Estimate of the Envelope of Improvement Ratio for an LDE statistical metric: This is a descriptive statistic for the envelope of the Improvement Ratios, for a complete data set (such as the Main Data Set) and a given LDE statistical metric. The Ballpark Estimates are the Minimum, Mean, or Maximum of the Improvement Ratio for that LDE statistical metric for N sensors.

Reciprocal Approximation: A simple reciprocal relationship with respect to N that approximates the power-law linear regression model fit for an Improvement Ratio.

4 Model

The underlying model used in this paper is described. Parameterized configurations of emitter and sensors are converted into randomly generated geometries and simulated. Sensor position and timing error conditions are defined. The 2D grid search-based TDoA solution method is presented as well as the optimization techniques necessary to obtain results with reasonable run times as well as improve the geolocation accuracy. The validity of a "flat earth model" is shown for the configurations used in this paper. The generation of random variates is discussed.

4.1 Simulations

Three factors are specified in the simulations: the **configuration**, the **error conditions**, and the **TDoA solution method**. Each instance of a simulation consists of a geometry based on the specified configuration which is then perturbed by a set of error conditions, subject to the simulation parameters as described below. The geometries and error conditions are generated randomly for each simulation. The simulation results are then processed according to the specific TDoA solution method. LDE statistical metrics are derived for a large number of simulations for each geometry, set of error conditions, and TDoA solution method.

If not otherwise specified, the number of simulations performed for each configuration was 10,000.

4.1.1 Configurations

The **configuration** is a parameterized template that describes the placement of the emitter and sensors. The parameters are the number of sensors (N), the size of the square search area that contains the emitter ($side \times side$), whether the sensors are immersed with the emitter or standoff from the emitter, and a mean value (alt) and standard deviation (σ_{alt}) for the altitude of the sensors. For the specified configuration, each simulation creates a randomly generated instance referred to as a **geometry**.

An approximation based on a flat earth model (FEM) is used. [11] The "xy-plane" represents coordinates on the surface or a plane parallel with the surface, and the "z-axis" represents the altitude above the ground.

Each simulation starts with an emitter on the ground that is randomly placed in the xy-plane of an area comprised of a square with sides of length $side$ where $side$ varies from 1,000 m (1 km) to 10,000 m (10 km).

Next, N sensors are randomly placed in an xy-plane that is either **immersed** with the emitter (meaning on or above the same square area where the emitter is located) or **standoff** from the emitter (meaning on or above an adjacent square area of the same size). The simulations vary N from 3 to 24 sensors. Unlike the emitters that are always on the ground in this model, sensors can have a z-axis displacement. Each simulation is given a single mean altitude alt for all of the N sensors. If the specified altitude is 0 m, then all the sensors are on the ground; if the specified mean altitude is greater than 0 m, then the z value of each sensor is given by a Gaussian distribution with the given mean value and standard deviation σ_{alt}. [12]

In most of the configurations used in this paper, the sensors' mean altitude alt varies from 100 m to 1,000 m and σ_{alt} is assigned the value $alt/20$ or 5% of alt. Sensitivity to the value of σ_{alt} is explored in Section 13.1 and it is found that LDE does not depend greatly on the value of this parameter.

[11] See Section 4.2 for justification of the flat earth approximation in this situation.

[12] If the calculated value of z is less than zero, then it is set to 0 m. How this condition is handled makes no practical difference because there is essentially no chance that a negative z value could occur for the values of alt and σ_{alt} used in this paper.

The phrase "**nominal altitude of** *alt*" for a configuration is understood to be shorthand for a "mean altitude of *alt* with the specified standard deviation σ_{alt}."

Note that the variation of the nominal altitude about the mean altitude due to σ_{alt} is not an error condition but rather part of the randomly generated geometry for a specified configuration.

For sensor i, the sensor coordinates (x_i, y_i, z_i) are used by the TDoA solution method to geolocate the emitter. These **presumed** or intended positions of the sensors are the only positions known to the TDoA solution method. Furthermore, the TDoA solution method assumes the sensors have no time synchronization error with respect to the global clock. When true, these conditions are referred to as the **error-free case**.

4.1.2 Error Conditions for Sensor Position and Timing

The next factor, the **error conditions**, specify how the true simulated conditions differ from the presumed conditions. This is referred to as the **case of errors.** The error conditions involve position errors and timing errors.

There are many factors that contribute to TDoA measurement errors; notably, these factors include low signal-to-noise ratios (SNR) [Huie (2014)] [Montminy (2007)] as well as non-line-of-sight propagation, multipath propagation, and synchronization errors [El Gemayel (2014)]. It is assumed in this work that all of the TDoA measurement issues can be lumped together and accounted for in terms of the standard deviations of the position and timing errors as outlined below.

The true sensor positions in the case of errors are derived from the presumed sensor positions by introducing offsets to the presumed coordinates generated as described in Section 4.1.1. **Position errors** have a magnitude given by the absolute value of a Gaussian distribution with zero mean and a given standard deviation σ_{pos}. For sensors on the ground, the angle of the position error is uniformly distributed from 0° to 360° in the xy-plane. For sensors with non-zero nominal altitudes, the angle of the position error is uniformly distributed with respect to the three axes. The true (but unknown) position for sensor i is denoted by (x'_i, y'_i, z'_i).

In addition to position errors, the error conditions include **timing errors**. Instead of assuming that each sensor is perfectly time-synchronized to a global clock, this model simulates a Gaussian distribution with zero mean time drift or time skew and a specified standard deviation σ_{pos}, expressed in seconds or nanoseconds. For sensor i, the time drift with respect to the global clock is denoted by t'_i. Timing errors are added to the measured or true times-of-arrival at the sensors, so a negative value of t'_i means that sensor i reports an arrival time that is earlier than the actual time (implying the distance from the emitter is less than the true distance), while a positive value of t'_i means that sensor i reports an arrival time that is later than the actual time (implying the distance from the emitter is greater than the true distance).

As stated in Section 4.1.1, the TDoA solution method uses only the presumed sensor positions and assumes zero time drift, but the simulated time

measurements provided to the TDoA solution method are based on the true (but unknown) sensor positions and measurements that include timing errors. [13] In the case of errors, each simulation of a geometry assigns a set of position and timing errors that holds for all of the pairwise TDoA measurements for the duration of that simulation. For example, suppose sensor i has a presumed position of (x_i, y_i, z_i) = (700 m, 300 m, 100 m) but actually has a true (but unknown) position of (x_i', y_i', z_i') = (705 m, 315 m, 97 m) and a time drift of t_i' = -5 ns. That true position and the perturbed time measurement apply for all of the TDoA measurements involving sensor i during that simulation, but the TDoA solution method obtains its geolocation estimate based on the erroneous presumed position and no knowledge of the time drift.

Most results obtained in this paper in the case of errors are based on simulations with error conditions where independent position error standard deviation σ_{pos} = 10 m and timing error standard deviation σ_{time} = 30 ns together are introduced. The data resulting from these simulations are referred to as the "Main Data Set" and these values of σ_{pos} and σ_{time} are referred to as the "Standard Error Conditions"; they are discussed in Section 4.3. These values were chosen to be reasonable but independent of any actual military or civilian systems or scenarios. They were also chosen to be somewhat commensurate in impact, as 10 m of distance is roughly equivalent to 30 ns at the speed of light c.

In Section 13.2, the model is tested for sensitivity to ranges of values of σ_{pos} and σ_{time} as well as introduction of position and timing errors separately.

The relationships between position error, distance error, distance difference error, timing error, and timing difference error are discussed in Appendix A.

[13] The decision to select the presumed position and perturb the true position according to the random distribution was somewhat arbitrary, and was decided in favor of this approach so that the presumed position was always within the specified immersed or standoff area; otherwise, the presumed position could fall outside that area. In retrospect, it might have been better to have designed the simulation to select the true position and vary the presumed position as that would have presented an opportunity to construct a set of experiments to measure the sensitivity of LDE to position and timing errors for a fixed position.

4.1.3 TDoA Solution Method: Sensor Pairing and 2D Emitter Location Estimation by Grid Search

The third factor, the **TDoA solution method**, specifies how the TDoA measurements from sensor pairs are processed. The TDoA solution method consists of two components: the **sensor pairing** that determines how the sensors pairs are handled and **emitter location estimation**.

It is shown in this section that the performance and quality of any TDoA solution method depends greatly on the specific algorithm and parameters used to solve for an estimated location of the emitter based on the TDoA measurements.

Sensor Pairing Method

Ideally, N sensors would yield $N-1$ linearly independent pairs that could be solved algebraically for a unique solution, if one existed [Hamdollahzadeh (2016)] [Smith (1987)]. In that case it would be sufficient to select one sensor arbitrarily as the reference sensor and use the pairwise TDoAs between that sensor and the other $N-1$ sensors. In this paper, the "linearly independent pairs" sensor pairing method is referred to as **LIP**. More specifically, with sensors numbered arbitrarily as $n = 1, 2, 3, \ldots N$, the method that uses sensor n [Wang (2013)] as the reference is referred to here as **LIP** n. Under ideal conditions (meaning the error-free case), the choice of reference sensor should matter little if at all. Under non-ideal conditions (the case of errors) however, the choice of reference sensor can greatly affect the quality of the location estimate as the sensor chosen as the reference might have the greatest position error or timing error. This paper explores how the LIP geolocation estimates vary with the choice of reference sensor under position and timing error conditions. The computational effort to obtain an estimate of the emitter location using LIP sensor pairing increases linearly with the number of sensors.

To improve noise immunity [Smith (1987)], sensor pairing involving more than $N-1$ pairs have been proposed. The upper bound is that of **all pairs** sensor pairing, where all $N(N-1)/2$ pairwise combinations of TDoA measurements are used. The computational effort to obtain an estimate of the emitter location using all pairs sensor pairing increases quadratically with the number of sensors.

Finally, N sensors (where N is even) can be paired as $N/2$ **disjoint pairs** [Hu (2006)] [Huie (2014)]. This may provide some noise immunity advantage due to the fact that a single sensor with large position error or timing error may not contaminate many TDoA measurements. In this paper, without loss of generality, the disjoint sensor pairs are assumed to be assigned consecutively according to the arbitrary sensor indices. That is, the pairs are sensors 1 and 2, 3 and 4, 5 and 6, and so on. Having fewer pairs of data to process (relative even to LIP) reduces the amount of computation to obtain a location estimate; the computational effort to obtain an estimate of the emitter location using disjoint pairs sensor pairing increases linearly with the number of sensors. Also, time synchronization is simplified in that a global clock is not needed since only pairs of sensors rather than all N of the sensors must be synchronized.

This paper compares the geolocation performance of the LIP and disjoint sensors pairing methods to the all pairs method in Section 5.

Grid Search for 2D Emitter Location Estimation

Closed-form algebraic solutions and gradient descent solutions have been proposed for TDoA geolocation [Chan (1994)] [Smith (1987)]. However, none were suitable for the situations pursued in this investigation. A primary reason was that these techniques cannot deal readily with the over-specified case where all pairs of sensors are used. Furthermore, the situation is complicated by the need to optimize solutions involving sensors located in 3D space rather than the simpler case of 2D. The only emitter location estimation method applicable to the configurations and error conditions studied here was also the one that seems to be the most commonly used in the literature: a *grid search* [Chen (2013)] [Huie (2014)] [Zhang (2019)].

In general, grid search-based methods involve stepping through points in a search area of interest and choosing the estimated location of the emitter to be a point that minimizes a selected cost function. A common cost function is the *sum of squared errors (SSE)* [14] between the measured TDoA values and those obtained for candidate points in the search area [Chen (2013)] [Huie (2014)] [Ho (2007)] [Kaune (2012)] [Montminy (2007)] [Zhang (2019)]. [15]

The true (but unknown) location of the emitter is denoted by (x'_e, y'_e, z'_e). Because the emitter is assumed to be on the ground, z'_e is taken to be 0. [16] The goal is to find an **estimated** location $(\widehat{x_e}, \widehat{y_e}, \widehat{z_e})$ (where $\widehat{z_e} = 0$) that has the smallest possible LDE from the true emitter location.

When calculating the TDoA between two sensors, it is irrelevant as to the order of subtraction as long as that order is used consistently throughout the solution process. For simplicity, the implementations used in this paper used the values for the sensor with the smaller index as the minuend and the values for the sensor with the larger index as the subtrahend.

[14] Equivalently, the optimized cost function can be mean squared errors (MSE) and root mean squared errors (RMSE). This cost function is known to be able to achieve the CRLB in the error-free case [Ho (2007)].

[15] Even the closed-form and gradient descent TDoA solutions require a good guess for their initial condition to avoid local minima for their cost functions. Thus, implicitly, their implementations usually begin with a grid search.

[16] The z coordinates of the emitter are always on the ground in the configurations considered in this paper, but they are retained in the discussion for consistency with the sensor coordinates which can be at any altitude.

The distance from the true location of the emitter to the true position of sensor i is

$$d'_i = \sqrt{(x'_i - x'_e)^2 + (y'_i - y'_e)^2 + (z'_i - z'_e)^2} \tag{1}$$

and, for a candidate emitter location (x_e, y_e, z_e), the distance to the presumed position of sensor i is

$$d_i = \sqrt{(x_i - x_e)^2 + (y_i - y_e)^2 + (z_i - z_e)^2} \ . \tag{2}$$

Using (1) and (2), the **distance error** for sensor i is given by

$$d_i - d'_i \ . \tag{3}$$

For each simulated geometry, the **measured** (that is, the **true TDoA**) is determined using the true sensor positions [17] and timing errors for each pair of sensors with indices i and j as

$$\Delta t'_{i,j} = (d'_i/c + t'_i) - (d'_j/c + t'_j) \tag{4}$$

where the set of pairs is determined by the specified sensor pairing method (all pairs, LIP, or disjoint pairs).

The TDoA **timing difference error** due to timing errors for the pair of sensors i and j is given by

$$t'_i - t'_j \ . \tag{5}$$

The **distance difference error** due to the two position errors for the pair of sensors i and j is given by

$$(d_i - d'_i) - (d_j - d'_j) \ . \tag{6}$$

The associated **timing difference error** that results from that distance difference error due to the speed of light is given by

$$\frac{(d_i - d'_i) - (d_j - d'_j)}{c} \ . \tag{7}$$

[17] This assumes line-of-sight signal propagation at the speed of light c.

The TDoA solution method is provided with the measured or true TDoA values $\Delta t'_{i,j}$ obtained by the simulation using (4), but does not know the true distances or timing errors.

The grid search-based method attempts to find a candidate emitter location in the specified search area that minimizes the SSE between the true TDoAs and those that would result if the emitter were in fact at that location. For a grid point (x_e, y_e, z_e) tested as a candidate emitter location, the presumed TDoA for each pair of sensors i and j is calculated based on the presumed sensor positions and without knowledge of timing errors as

$$\Delta t_{i,j} = (d_i/c) - (d_j/c) \ . \tag{8}$$

In **all pairs** sensor pairing, where each sensor is paired with every other sensor, the estimated emitter location is the coordinate set $(\widehat{x_e}, \widehat{y_e}, \widehat{z_e})$ (where $\widehat{z_e} = 0$) that minimizes the SSE given by

$$\sum_{i=1}^{N-1} \sum_{j=i+1}^{N} (\Delta t_{i,j} - \Delta t'_{i,j})^2 \ . \tag{9}$$

In **LIP** n sensor pairing, where sensor n is paired with each of the other $N-1$ sensors, the estimated emitter location is the coordinate set $(\widehat{x_e}, \widehat{y_e}, \widehat{z_e})$ (where $\widehat{z_e} = 0$) that minimizes the SSE given by

$$\sum_{\substack{i=1 \\ i \neq n}}^{N} (\Delta t_{i,n} - \Delta t'_{i,n})^2 \ . \tag{10}$$

In **disjoint pairs** sensor pairing, where the sensor pairs are grouped by consecutive indices, the estimated emitter location is the coordinate set $(\widehat{x_e}, \widehat{y_e}, \widehat{z_e})$ (where $\widehat{z_e} = 0$) that minimizes the SSE given by

$$\sum_{i=1}^{N/2} (\Delta t_{2i-1,2i} - \Delta t'_{2i-1,2i})^2 \ . \tag{11}$$

Once the TDoA solution method has obtained its best estimated location for the emitter $(\widehat{x_e}, \widehat{y_e}, \widehat{z_e})$, **the LDE for that method is determined with respect to the true emitter location as**

$$\sqrt{(\widehat{x_e} - x'_e)^2 + (\widehat{y_e} - y'_e)^2 + (\widehat{z_e} - z'_e)^2} \ . \tag{12}$$

As mentioned in the Introduction, the LDE statistical metrics calculated for a given configuration and set of error conditions are the mean, 50%ile or median, 95%ile, and 99%ile for a set of simulated randomly generated geometries.

Grid search-based methods suffer from several potential issues. The quality of a geolocation estimate is related to the number of candidate grid points tested, but the computational effort to find a solution increases with the number of points. Grid solutions may select a local minimum rather than find the global minimum. Finally, a grid search cannot resolve the ambiguity between equally valid solutions created by a bad geometry [18] [19] such as when all sensors are collinear. The last two issues are shared by other emitter location estimation methods as well.

A great deal of the effort involved in the study outlined in this paper was expended on implementing a grid search that was both fast and accurate. Several heuristics were tested over ranges of parameters and a set was chosen that gave the most overall consistently reliable performance.

A **fine grid search** phase was performed for each instance of a given geometry and set of error conditions. This search consisted of a series of passes involving finer and finer grids over smaller and smaller areas to find a point in the search area that effectively minimized the SSE. Let $p = 1, 2, 3, \ldots$ denote the index of the pass and let ss_p represent the length of the step size in the x and y directions in pass p. An initial grid step divisor K determined the first pass step size where $ss_1 = side/K$. For example, for a search area with $side$ = 1,000 m and $K = 100$, the step size for the first pass was $ss_1 = side/K = 10$ so the (x, y) values tested in the first pass are all of the pairs of values 0 m, 10 m, 20 m, ... 1,000 m for a total of 101^2 points.

In the subsequent passes $p = 2, 3, 4, \ldots$, the new step size was the previous step size divided by 10: $ss_p = ss_{p-1}/10$. The point found to have the smallest SSE in pass $p-1$ was the center of the searched area in pass p.

[18] See the examples presented in Section 6 such as Figure 20 and Figure 21.

[19] The grid search method implemented for this work was designed to find only a single solution that minimized or closely minimized the SSE. With additional effort, however, a grid search could identify multiple points in distinct regions of the search area as a set of candidate solutions that provides the smallest SSE.

Optimizing the Grid Search

Experiments were conducted to determine a good value for K. Values of K from 10 to 5,000 were tested; the number of points and thus the computational effort grew with the square of K. Surprisingly, larger values of K did not always give better results. Overall, a value of $K = 100$ gave the most consistently good results.

The fact that the TDoA solution method performed well with the smaller value of K indicates that the grid search-based method was not confounded by the multiple local minima for the SSE values. However, the fact that it was not infallible shows how dependent the results are on the specific TDoA solution method and its parameters.

On pass p, it should have been sufficient to search a square that was $\pm ss_{p-1}$ around the center point with the new step size ss_p. However, it was observed in many cases that smaller LDE values could be achieved by searching a larger area around the center point of a pass. Let a square with sides $\pm Css_{p-1}$ around the center point be defined to have a **coverage factor** of C. Trials showed that the best trade off between run time and the quality of the results were obtained using a coverage factor $C = 4$; this is to say that, on pass p, the search area around the center point was a square with sides $\pm 4ss_{p-1}$ or $8ss_{p-1}$.

The fine grid search phase ended after the first pass p where ss_p was less than 1 cm.

The fine grid search was extremely slow for the larger values of N and K, so two related algorithmic speed-ups were used.

The first speed-up was an elementary optimization that bounded the TDoA SSE calculations by terminating the summation of the squared errors in (9), (10), or (11) whenever it exceeded the smallest SSE value found so far. For example, for $N = 10$ with all pairs sensor pairing, there are $5 \times 9 = 45$ pairs of TDoA measurements; if, after summing only a few squared-error values in (9) for a given point, the sum were greater than the current minimum SSE, then that point would be abandoned since the remaining unevaluated squared-error pairs could only make the total SSE value for that point larger. The second speed-up was to introduce a **coarse grid search** phase to get an initial estimate of the global minimum SSE

value prior to the fine grid search. Referring to the coarse grid search phase as pass $p = 0$, a good coarse grid step value was found to be $ss_0 = side/10$; this provided nearly the maximum speed-up over the ranges of N used in these experiments.

After extensive experimentation, the **standard heuristics set** selected for the TDoA solution were to use a coarse grid search before the fine grid search, initial grid step divisor $K = 100$, and coverage factor $C = 4$.

The results and CPU run times achieved using the standard heuristics set were the basis for comparison to those obtained using simulations using all combinations of no coarse grid search, $K = 5{,}000$, and $C = 1$. Sets of 1,000 simulations were run with various numbers of sensors and search area side lengths, $alt = 100$ m, $\sigma_{alt} = 5$ m, and the Standard Error Conditions of $\sigma_{pos} = 10$ m position error and $\sigma_{time} = 30$ ns timing error. For a few combinations of parameters, some comparisons to the standard heuristics set are as follows: [20]

- $N = 3$ sensors, $side = 1{,}000$ m:
  - No coarse grid search, $K = 5{,}000$, $C = 1$: CPU time increased by 665X, while mean and 95%ile LDE both decreased by 2%.
  - Coarse grid search, $K = 5{,}000$, $C = 4$: CPU time increased by 527X, while mean and 95%ile LDE both decreased by 2%.
- $N = 12$ sensors, $side = 1{,}000$ m:
  - No coarse grid search, $K = 5{,}000$, $C = 1$: CPU time increased by 267X, while mean and 95%ile LDE had no change.
  - Coarse grid search, $K = 100$, $C = 1$: mean LDE increased by 7% and 95%ile LDE increased by 3%.
- $N = 12$ sensors, $side = 10{,}000$ m:
  - No coarse grid search, $K = 5{,}000$, $C = 1$: CPU time increased by 241X, while mean and 95%ile LDE had no change.

[20] The terms "increased by" and "decreased by" are used in two ways in this paper, depending on the scale of the change. To avoid ambiguity, the following examples are provided. "Increased by 10X" means to multiply the original value by 10; for large changes, this is more useful than the equivalent statement "increased by 900%." "Increased by 2%" is equivalent to but more natural than "increased by 1.02X." "Decreased by 2%" is more natural than saying "decreased by 0.98X."

  - Coarse grid search, $K = 100$, $C = 1$: mean LDE increased by 3.60X and 95%ile LDE increased by 2.47X.

- $N = 24$ sensors, $side = 1{,}000$ m:
  - No coarse grid search, $K = 5{,}000$, $C = 1$: CPU time increased by 267X, while mean and 95%ile LDE had no change.
  - Coarse grid search, $K = 100$, $C = 1$: mean LDE increased by 13% and 95%ile LDE increased by 11%.

- $N = 24$ sensors, $side = 10{,}000$ m:
  - No coarse grid search, $K = 5{,}000$, $C = 1$: CPU time increased by 244X, while mean and 95%ile LDE both increased by 1%.
  - Coarse grid search, $K = 100$, $C = 1$: mean LDE increased by 5.80X and 95%ile LDE increased by 3.98X.

Observations on the Grid Search

A lesson-learned during the process of exploring, implementing, and tuning the TDoA solution methods was that results depend heavily on the specific algorithms and parameters of the algorithms. No single approach performed best under all conditions of the random geometries created for the configurations used in this paper.

Because of the assumption that the emitter is on the ground, it was sufficient to implement the 2D grid search as described above. It would be possible to do a 3D grid search as well, but at a substantial computational cost. Pass 1 of the fine grid search alone would grow roughly as K^3 instead of the K^2 cost incurred by the 2D search. The run time for subsequent phases would grow substantially as well.

It would be interesting to determine how the issues with LDE associated with bad geometries would manifest in the 3D case. One immediate concern would be the ambiguity of the emitter location being below or above the thin plane of airborne sensors.

4.2 Flat Earth Model

The calculations in this paper are simplified by ignoring the curvature of the earth over the region of interest. Effectively, the configuration is an approximation based on a flat earth model (FEM) rather than a spherical earth model (SEM). [21] For airborne sensors, the most critical factor is that the emitter-to-sensor slant range calculated using the FEM has negligible error from the "true" slant range obtained from the SEM. For ground-based sensors, a justification for the FEM requires that the assumption of emitter-to-sensor line-of-sight paths is not violated by exceeding the horizon with respect to the sensors.

[21] Of course, even the more faithful assumption of a spherical earth is still a simplification.

4.2.1 Airborne Sensor Slant Range

Figure 13a shows an arc representing the surface of the earth in the SEM. R is the standard value of the mean equatorial radius of the earth (6,378,137 m); it is assumed here that the RF wavelengths are short enough that the actual earth radius can be used rather than the commonly used value of $4/3\,R$ for longer-wavelength RF line-of-sight calculations [Holleman (2012)]. [22] The altitude of a sensor above the surface is denoted by alt. The scale of alt in Figure 13a is exaggerated in comparison with the magnitudes of the altitudes considered in this paper. The emitter is located at surface distance s from the point directly below the sensor. The central angle θ is the angle between the sensor and the emitter. When the value of θ is in radians, s is given by the fraction of the circumference of the earth subtended by θ as

$$s = \frac{\theta}{2\pi} \times 2\pi R = \theta R \tag{13}$$

and so

$$\theta = \frac{s}{R} \text{ rad} \ . \tag{14}$$

The slant range r from the sensor to the emitter can be found using the Law of Cosines as

$$r^2 = R^2 + (R + alt)^2 - 2(R)(R + alt)\cos\theta \tag{15}$$

where cos() takes its argument in radians.

Thus, for given values of alt and s, the slant range r is

$$r = \sqrt{R^2 + (R + alt)^2 - 2(R)(R + alt)\cos\frac{s}{R}} \ . \tag{16}$$

Figure 13b shows a representation of a sensor at altitude alt above a flat earth with an emitter located at surface distance s from the point directly below the sensor. The slant range r' in this case is given by the Pythagorean Theorem as

$$r = \sqrt{alt^2 + s^2} \ . \tag{17}$$

[22] Thus, "line-of-sight" is purely geometrical. This is often referred to as "optical line-of-sight."

Now it remains to be seen how the two slant ranges r and r' differ over the areas and configurations of interest in this paper.

Consider the case where the sensors are immersed with the emitter, meaning they are over the same square area where the emitter is assumed to be located. For a square that is 1,000 m on a side, the maximum diagonal surface distance is 1,000 $\sqrt{2}$ = 1,414 m. Applying (16) and (17), the differences in slant range between SEM and FEM ($r - r'$) for alt = 100 m and alt = 1,000 m are 1 cm and 9 cm, respectively. For a square that is 10,000 m on a side, the maximum diagonal surface distance is 10,000 $\sqrt{2}$ = 14,142 m. Applying (16) and (17), the differences in slant range between SEM and FEM for alt = 100 m and alt = 1,000 m are 11 cm and 1.1 m, respectively.

Now consider the case where the sensors are standoff, meaning the sensors are located over a square area adjacent to the square area where the emitter is assumed to be located. For two squares that are 1,000 m on a side, the maximum diagonal surface distance is 1,000 $\sqrt{2}$ = 2,236 m. Applying (16) and (17), the differences in slant range between SEM and FEM for alt = 100 m and alt = 1,000 m are 2 cm and 16 cm, respectively. For squares that are 10,000 m on a side, the maximum diagonal surface distance is 10,000 $\sqrt{2}$ = 22,361 m. Applying (16) and (17), the differences in slant range between SEM and FEM for alt = 100 m and alt = 1,000 m are 16 cm and 1.74 m, respectively.

Later sections will obtain LDE values that are much greater than these differences in slant range between the SEM and the FEM. Thus, for the parameters used in this paper, the FEM appears to be adequate for configurations where the sensors are not on the ground.

The next section addresses the FEM in the context of sensors on the ground.

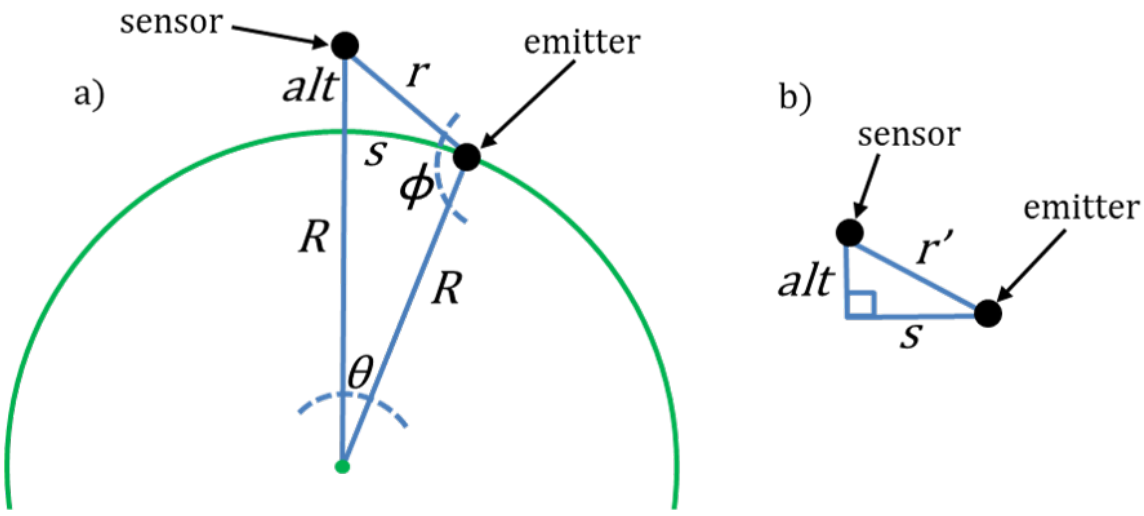

Figure 13: a. Spherical Earth Model (SEM). b. Flat Earth Model (FEM).

4.2.2 Horizon

Since signal propagation is assumed to be line-of-sight, the issue of the horizon must be considered. In the FEM, there is no notion of a horizon. Therefore, it must be determined under what conditions the horizon can be neglected in the FEM. As mentioned earlier, the actual earth radius R can be used rather than the value of $4/3\,R$ that is commonly used for RF line-of-sight calculations; using R as the earth radius provides the worst-case values for the horizon.

In Figure 13a, ϕ is the angle of the sensor above the horizon from the location of the emitter. When ϕ forms a right angle ($\pi/2$ rad), the emitter is at the intersection of the surface of the earth and a line from the sensor that is tangent to the surface; thus, the emitter is at the horizon from the viewpoint of the sensor.

By the Pythagorean Theorem,

$$r = \sqrt{(R + alt)^2 - R^2} \quad . \tag{18}$$

The Law of Sines states that

$$\frac{\sin \frac{\pi}{2}}{R + alt} = \frac{\sin \theta}{r} \quad . \tag{19}$$

Solving (19) for θ and substituting θ into (13) yields s_{hor}, the surface distance of the horizon from the point directly below the sensor as a function of alt, as

$$s_{hor} = R \arcsin \frac{\sqrt{(R + alt)^2 - R^2}}{R + alt} \tag{20}$$

where arcsin() returns the angle in radians.

The minimum sensor altitudes required by (20) to achieve horizons sufficient for strict line-of-sight visibility for the configurations noted above are:

Immersed:	$s_{hor} \geq$ 1,414 m	requires $alt \geq$ 16 cm
	$s_{hor} \geq$ 14,142 m	requires $alt \geq$ 15.68 m
Standoff:	$s_{hor} \geq$ 2,236 m	requires $alt \geq$ 39 cm
	$s_{hor} \geq$ 22,361 m	requires $alt \geq$ 39.20 m

All of these altitudes are less than the smallest non-zero nominal altitude of 100 m used in the simulations described in this paper. Thus, in the case of airborne sensors, the line-of-sight limitation of the horizon can be safely neglected in the FEM.

4.2.3 Ground-Level Sensing

When the sensors are on the ground, algebraically the horizon is at zero distance from the sensor. This is a consequence of (20) which says s_{hor} is 0 m when alt is 0 m. While this paper does not address any specific parameters of actual RF geolocation systems, the fact that ground-based systems exist is *prima facie* evidence that the mathematical concept of a zero-distance horizon is not a limiting factor.

One reason for this is that the receiving antenna for a "ground-level" sensor may be at some small distance above the ground and the same can be true of the transmitting antenna for the emitter; this creates non-zero horizons for both the sensors and the emitter.

Consider the case where the antennas for an emitter and a sensor both are located at a small distance alt above the ground. There is then an emitter-to-sensor line-of-sight path between a sensor and an emitter at a distance that is $2s_{hor}$ (that is, two "horizons") for a given value of alt.

For the SEM, the antenna heights required by (20) to achieve a line-of-sight distance of $2s_{hor}$ for the immersed and standoff configurations noted above are:

Immersed:	$2s_{hor} \geq$ 1,414 m	requires $alt \geq$ 4 cm
	$2s_{hor} \geq$ 14,142 m	requires $alt \geq$ 3.92 m
Standoff:	$2s_{hor} \geq$ 2,236 m	requires $alt \geq$ 10 cm
	$2s_{hor} \geq$ 22,361 m	requires $alt \geq$ 9.80 m

The smaller areas considered in this paper (that is, squares with sides of 1,000 m and slightly larger) require only minuscule values of alt to achieve line-of-sight paths. Whether the values of alt required to provide line-of-sight connectivity for the larger areas addressed in this paper (search area squares with sides up to 10,000 m and standoff sensors) are in fact practical is not a concern of this paper.

With the understanding that "ground-level" sensing is understood to include cases where the antennas for the emitter and the sensors are at small heights above the actual surface of the earth, this section has established that the horizon determined by the SEM is not a limiting factor in the FEM.

4.3 Parameters for Configurations and Simulations

Section 4.1.1 gave details as to how each simulation generates a geometry of an emitter and N sensors for a given area. Section 4.1.2 described the process for introducing position and timing errors into the geometries and simulation process. This section summarizes the parameters used to specify the configurations and control the simulations.

- Configuration:
  - Number of sensors N.
  - Mean altitude alt and its standard deviation σ_{alt}.
  - Side length *side* for the square search area assumed to contain the emitter.
  - Sensors are either *immersed* in the same area as the emitter or *standoff* in an adjacent area of the same size.
- Error Conditions:
  - Sensor position error standard deviation σ_{pos}.
  - Sensor timing error standard deviation σ_{time}.
- TDoA Solution Method:
  - Sensor pairing: all pairs, disjoint pairs, or LIP n.
  - Emitter location estimation by grid search.

The **Main Data Set** [23] is the collection of data that are the basis for most of the analyses in this paper. It is based on 4,840 configurations consisting of all of the combinations of numbers of sensors ranging from $N = 3$ to 24 (immersed and standoff) with mean altitudes $alt = 0$ m to 1,000 m (in steps of 100 m), $\sigma_{alt} = alt/20$ (or 5% of alt), and search area side lengths $side = 1{,}000$ m to 10,000 m (in steps of 1,000 m).

All configurations in the Main Data Set use the **Standard Error Conditions** [24] of $\sigma_{pos} = 10$ m and $\sigma_{time} = 30$ ns.

The TDoA solution method used for the Main Data Set is all pairs sensor pairing.

[23] Capitalization is used to help identify this phrase as a single term.
[24] Capitalization is used to help identify this phrase as a single term.

Results are based on 10,000 simulations of randomly generated geometries per configuration.

Smaller sets of simulations are used to explore specific aspects of the problem and these data are distinguished where applicable from those of the Main Data Set. In particular, Section 13 considers values of σ_{alt} other than $alt/20$ and error conditions wider than the Standard Error Conditions.

4.4 Random Numbers and Gaussian Distributions

Uniformly distributed random numbers used in these simulations were produced using the "ran2" random number generator given by [Press (2002)]. Press et al. made the following bold statement: "We think that, within the limits of its floating-point precision, ran2 provides perfect random numbers; a practical definition of "perfect" is that we will pay $1,000 to the first reader who convinces us otherwise (by finding a statistical test that ran2 fails in a nontrivial way, excluding the ordinary limitations of a machine's floating-point representation)." Nineteen years after that statement was made, there does not appear yet to have been a payoff against this challenge.

Values for the Gaussian (Normal) distribution were generated using the Box-Muller Transformation [Weisstein (2019a)] from the uniform random distribution produced by ran2.

The central question addressed in this paper is "How does geolocation accuracy improve as the number of sensors increases?" This question is framed as the problem of estimating the marginal improvement in geolocation accuracy obtained by sequentially adding sensors to an existing geometry. Similarly, it was desirable that every set contained the same 10,000 geometries (including good and bad), the only differences being the geometries stretched in scale with the sides of the areas and nominal altitudes of the sensors. Thus, ***each set used the same random seed***. While using the same seed for each set of simulations ordinarily would violate the norms of Monte Carlo simulation, this was necessary to ensure that each set was identical to every other set *except* for the change in the relevant parameters.

To achieve the repeatable incremental addition of sensors to the previous geometries, in each simulation all the sensor positions were initially generated up to the maximum number of sensors to be used, and they were included sequentially as the simulation progressed with increasing values of N.

4.5 Graphing

The graphs of the intersections of the TDoA hyperboloids with the surface were generated in a spread sheet as follows, using an approach similar to the grid search-based method for finding the emitter location. Graphs were generated only for geometries involving $N = 3$ and 4 sensors.

Using all pairs sensor pairing, for three sensors there were three pairs of measurements and for four sensors there were six pairs of measurements. For a given pair of sensors i and j, the spread sheet calculated the measured or true TDoA with respect to the emitter location for the true positions of the sensors due to their position errors and included the timing error offsets; this is the value denoted by $\Delta t'_{i,j}$ obtained from (4).

The spread sheet enumerated points of a grid representing candidate emitter locations on the ground (x_e, y_e, z_e) (where $z_e = 0$) in a 1 km $\times$ 2 km area; the left half of the area represented the search area for the emitter and the immersed sensor region and the right half represented the standoff sensor region. The x and y step sizes were 5 m. [25] For each (x_e, y_e, z_e) point in this grid, the value $\Delta t_{i,j}$ was obtained from (8) using the presumed positions of sensors i and j and without knowledge of timing errors.

With the step size of 5 m, the spread sheet's simulated grid contained 80,601 points. For sensors i and j, the value $|\Delta t_{i,j} - \Delta t'_{i,j}|$ was calculated and the points with the smallest 1% of that value were plotted; this represented the locus of points on the surface for which the TDoA based on the presumed positions of those two sensors matched the measured TDoA.

This process was repeated for each pair of sensors (three pairs for three sensors and six pairs for four sensors) to generate the intersections of the TDoA hyperboloids with the surface.

The graphs of the points with the "small SSE values" shown in Section 6 were generated in a similar manner. Recall that, for all pairs sensor pairing, the estimated emitter location on the ground $(\widehat{x_e}, \widehat{y_e}, \widehat{z_e})$ (where $\widehat{z_e} = 0$) is the coordinate set that minimizes the SSE given by (9). The points plotted

[25] As described in Section 4.1.3, the grid search continues until the step size is smaller than 1 cm, but the step size of 5 m was used in the graphing process to keep the size of the spread sheet and the formula update time manageable.

as “small SSE” are the points on the simulated grid that yield the smallest 0.1% of the SSE values calculated using (9).

5 Sensitivity to Sensor Pairing Method

Three approaches for sensor pairing were discussed in Section 4.1.3. It was observed that the computational effort incurred using the disjoint pairs and LIP methods grows linearly with the number of sensors while that incurred by all pairs sensor pairing grows as N^2. This section briefly addresses how the choice of sensor pairing method impacts the LDE determined using (12).

Sets of 10,000 simulations per configuration were performed to generate the data for these examples, where the configurations had the sensors immersed with the emitter in a 1 km $\times$ 1 km area with the Standard Error Conditions of $\sigma_{pos} = 10$ m position error and $\sigma_{time} = 30$ ns timing error.

The figure-of-merit used for these comparisons was the mean LDE.

5.1 Comparing Disjoint Sensor Pairing to All Pairs Sensor Pairing

Figure 14 shows the mean LDE for sensors on the ground, with number of sensors $3 \leq N \leq 24$ for all pairs sensor pairing and $4 \leq N \leq 24$ (only even values) for disjoint pairs. It is clear that the mean LDE for disjoint pairs sensor pairing was never less than that of all pairs: the ratio for disjoint pairs sensor pairing to all pairs mean LDE varied from 2.05 to 1.44 for these simulated results.

Another way of looking at the data presented in Figure 14 is to observe that six sensors combined as disjoint pairs yielded only slightly smaller mean LDE than four sensors combined as all pairs. Eight sensors in disjoint pairs performed about as well as five sensors combined as all pairs, and ten sensors in disjoint pairs performed about as well as seven sensors combined as all pairs.

Figure 15 shows the mean LDE for the same geometries and position and timing errors as for Figure 14, but where the sensors were at nominal altitudes of 100 m. The mean LDE at this altitude was less than that for sensors on the ground, but otherwise the trends were practically the same as for configurations with the sensors on the ground. The ratio of the mean LDE for disjoint pairs sensor pairing to all pairs varied from 2.13 to 1.45 for these simulated results.

As was the case in Figure 14, Figure 15 shows that six sensors combined as disjoint pairs yielded only slightly smaller mean LDE than four sensors combined as all pairs, eight sensors in disjoint pairs performed about as well as five sensors combined as all pairs, and ten sensors in disjoint pairs performed about as well as seven sensors combined as all pairs.

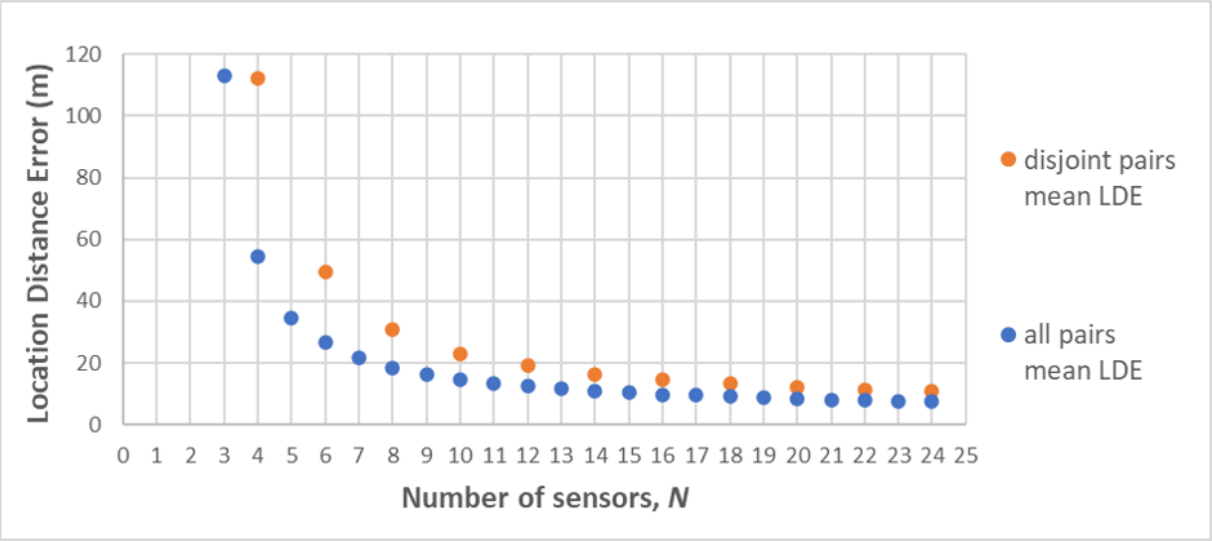

Figure 14: Comparing sensor pairing methods: All pairs vs. disjoint pairs showing mean LDE for $3 \leq N \leq 24$ immersed sensors (only even values of N for disjoint pairs). Parameters: $side$ = 1,000 m, alt = 0 m, with errors.

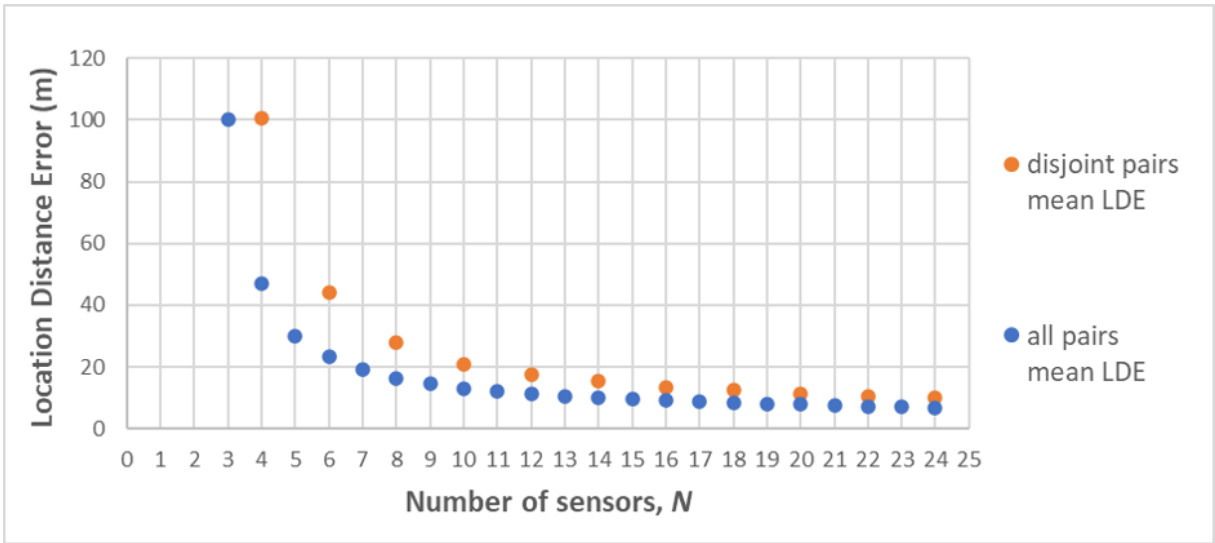

Figure 15: Comparing sensor pairing methods: All pairs vs. disjoint pairs showing mean LDE for $3 \leq N \leq 24$ immersed sensors (only even values of N for disjoint pairs). Parameters: $side$ = 1,000 m, alt = 100 m, with errors.

5.2 Comparing LIP Sensor Pairing to All Pairs Sensor Pairing

The performance of LIP sensor pairing was compared to that of all pairs sensor pairing using a different approach from that in Section 5.1 in order to more precisely understand the sensitivity of LIP n to the choice of n, the index of the reference sensor. For a given configuration, 50 experiments consisting of randomly generated geometries with position and timing errors were created and the LDE for each was obtained for LIP n over the range of $1 \leq n \leq N$.

Figure 16 shows the results for $N = 8$ immersed sensors on the ground. This figure is a scatter plot of the LDE for all pairs sensor pairing and each of the N individual LDE values for the LIP n emitter location estimates. [26] Figure 17 shows the ratios of all of the LIP n LDE values to the all pairs LDE for the same experiments. [27] Not only was there wide variation in LDE over the values of n but, for any given experiment, the LIP n LDE values were predominantly worse than those for all pairs.

One measure of the performance of the sensor pairing methods is the mean LDE. For the 50 geometries with position and timing errors that were simulated and summarized in Figure 16 and Figure 17, the mean LDE for LIP n (over all n) was 18.49 m and for all pairs the mean LDE was 15.57 m; the *ratio of these averages* was 1.19 which indicates that mean LDE for LIP n appears to trend higher than that for all pairs. However, the effect of sensor pairing is better gauged by looking at the *average of the ratios* for the 50 experiments which was 1.43.

Figure 18 and Figure 19 were generated for the same geometries and position and timing errors as for Figure 16 and Figure 17 but where the sensors were at nominal altitudes of 100 m. Again, the LIP n LDE values tended to be worse than those for all pairs. The mean LDE for LIP n (over all n) was 17.77 m and for all pairs the mean LDE was 14.52; the ratio of

[26] For example, the fifth experiment ("Exper 5") resulted in an all pairs LDE of 62.84 m, while the LDE values for LIP n ($1 \leq n \leq 8$) were 32.36 m, 54.12 m, 60.39 m, 63.67 m, 64.02 m, 65.58 m, 66.02 m, and 73.06 m, respectively. Thus, for five of the eight choices of n, the LIP n LDE was higher than that achieved by all pairs sensor pairing.

[27] Note that the logarithmic scale for the ratios is necessary to visualize the individual values, but it causes the eye to exaggerate the impact of the values that are less than one and understate the values that are greater than one.

the averages was 1.22 and the average of the ratios for the 50 experiments was 1.44.

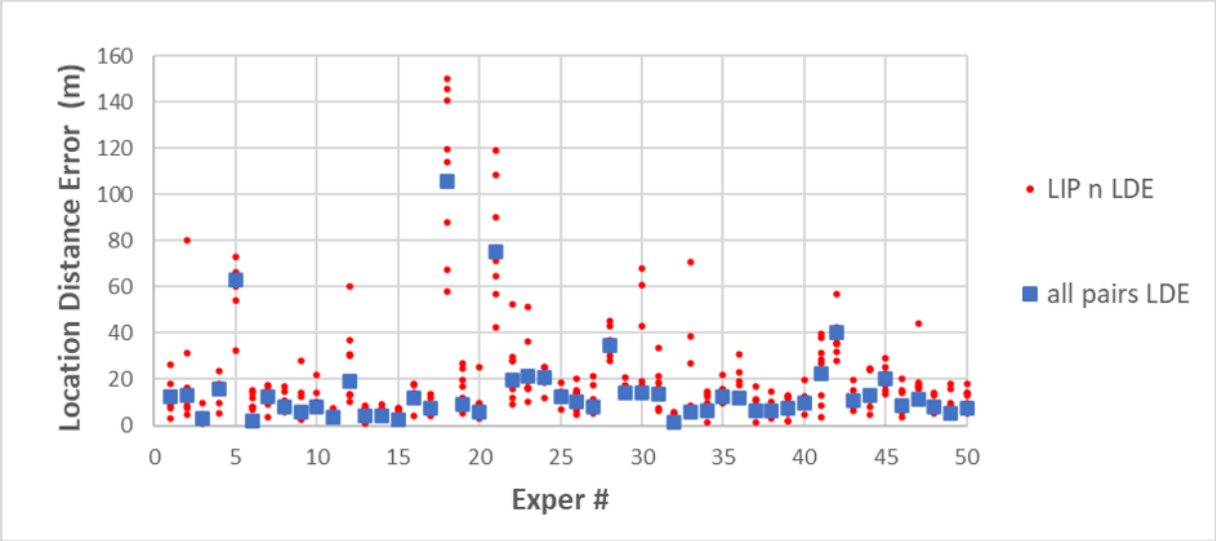

Figure 16: Comparing sensor pairing methods: All pairs vs. LIP n for sensors on the ground for 50 experiments. For each experiment, blue dot shows all pairs LDE, red dots show LDE for LIP 1, LIP 2, ... LIP 8. Parameters: $N = 8$ immersed sensors, $side = 1{,}000$ m, $alt = 0$ m, with errors.

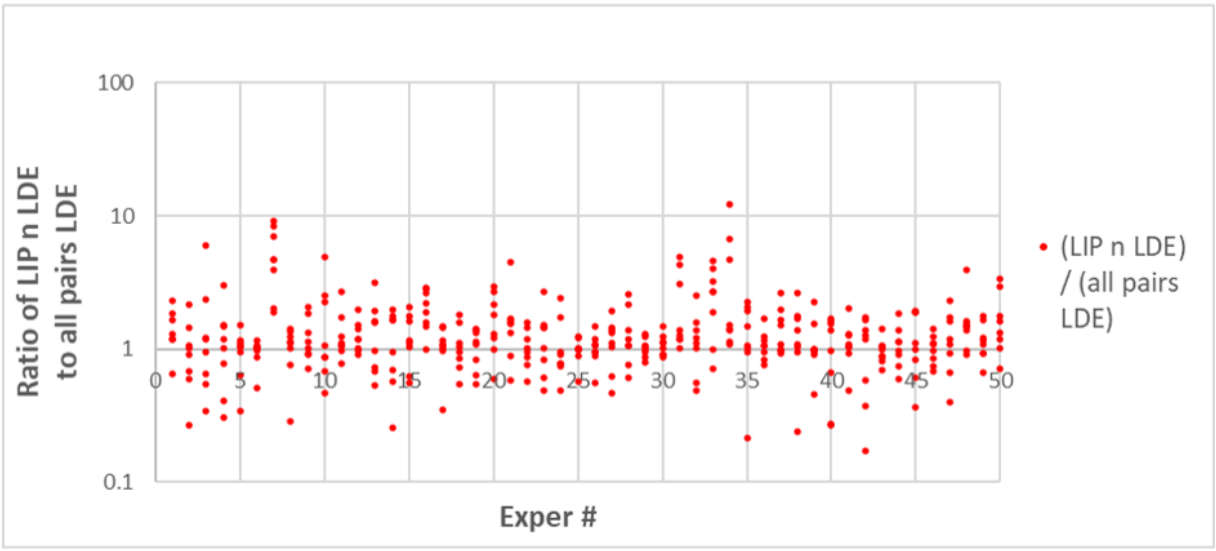

Figure 17: Comparing sensor pairing methods: All pairs vs. LIP n for same experiments summarized in Figure 16. For each experiment, plot shows ratios of LIP 1, LIP 2, ... LIP 8 LDE to all pairs LDE. Ratio scale is logarithmic.

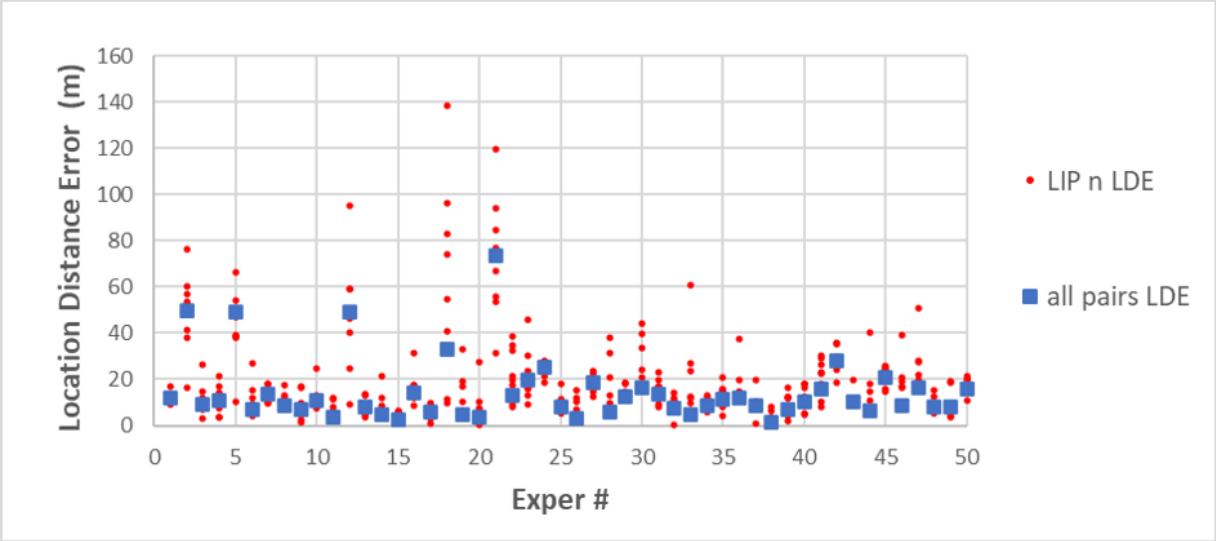

Figure 18: Comparing sensor pairing methods: All pairs vs. LIP n for sensors at nominal altitudes of 100 m for 50 experiments. For each experiment, blue dot shows all pairs LDE, red dots show LDE for LIP 1, LIP 2, ... LIP 8. Parameters: $N = 8$ immersed sensors, $side = 1{,}000$ m, $alt = 100$ m, with errors.

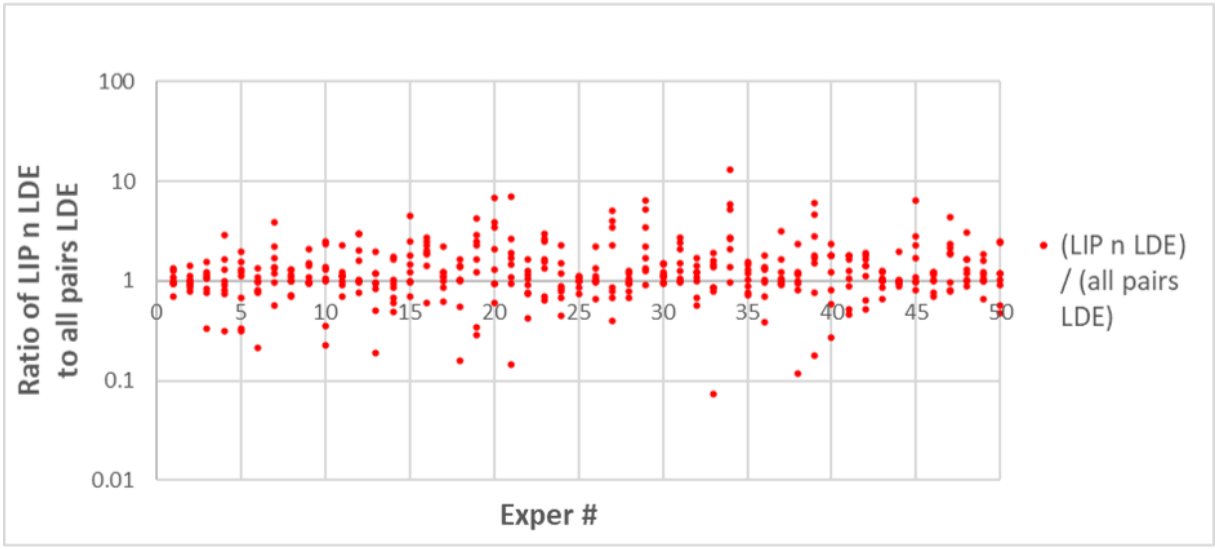

Figure 19: Comparing sensor pairing methods: All pairs vs. LIP n for same experiments summarized in Figure 18. For each experiment, plot shows ratios of LIP 1, LIP 2, ... LIP 8 LDE to all pairs LDE. Ratio scale is logarithmic.

5.3 Choice of Sensor Pairing Method

It is unnecessary to analyze additional configurations, error conditions, or LDE statistical metrics to conclude that all pairs sensor pairing provides consistently smaller LDE values than disjoint pairs and strongly tends to provide smaller LDE values than LIP n. If the goal is to achieve the best possible LDE values, then it is clear that all pairs sensor pairing is to be preferred over the other two methods. However, the considerably smaller computational effort, especially for larger values of N, may make the other two sensor pairings more attractive when the degradation in LDE is acceptable. This may be in the case when the TDoA geolocation function is being performed in real time by computationally challenged systems. In addition, disjoint pairs may be the only option in cases where a global clock synchronization is not available but pairwise timing synchronization is possible.

Due to the generally smaller and more consistent LDE values achieved using all pairs sensor pairing compared to the other two methods, that method only is used for the remainder of this paper.

6 Intrinsically Bad Geometries

Section 2 gave several examples of geometries that demonstrated non-zero LDE in the case of position and timing errors. All of those examples were selected such that the TDoA solution method described in Section 4.1.3 yielded zero LDE in the error-free case. It is shown in this section that certain geometries inherently have non-zero LDE, even without the introduction of errors, and this is a significant issue when only small numbers of sensors are employed.

These results depend on the specific TDoA solution method used, as was shown in Section 4.1.3. One challenge to finding the best estimate of the emitter location is that there may be multiple valid solutions where all the hyperboloids intersect. When the hyperboloids do not intersect exactly, they may converge closely enough that the TDoA solution method cannot distinguish between the single best solution and other possible solutions. Even when a single solution may exist, hyperboloids may intersect at small angles and thus even minor position or timing errors may cause numerical solutions to converge to incorrect results [Kaune (2012)].

All of the examples used in this section are error-free cases that have non-zero LDE values solely due to their geometries and the specific TDoA solution method used in this paper. Thus, the sensors' presumed positions are the same as their true positions.

It is demonstrated here that a major factor that contributes to non-zero LDE in the error-free case is that of *collinearity*. When sensors are collinear or even simply close to being collinear, or the random position of the emitter happens to be collinear with sensors, there is side-to-side location ambiguity as to where the minimum SSE value will be found due to multiple local minima. In these events, it may be practically a "coin flip" as to whether the estimated location of the emitter will be exactly correct or drastically wrong. Unfortunately, examples that follow show that determining *a priori* when collinearity or other geometric factors are an issue is problematic.

6.1 Longfellow Events

Figure 20 shows an error-free case with $N = 3$ sensors on the ground and immersed with the emitter. The three sensors are nearly collinear. The grid search found an estimated location of the emitter (marked with the red square) that was 979.20 m from the correct location (marked with the green square). Figure 21 shows the same geometry with 0.1% of the smallest SSE values overlaid on the plot (marked with brown shading). The two distinct patches of brown shading indicate side-to-side ambiguity in emitter location (that is, local SSE minima), within the limitations of the TDoA solution method used, and thus led to a drastically wrong estimate of the emitter location.

The phenomenon where a seemingly arbitrary "coin flip" makes the difference between being either very close to a correct solution or very distant from it is reminiscent of the verse from a famous poem by Henry Wadsworth Longfellow [Longfellow (1904)], reportedly about his daughter:

> There was a little girl
> Who had a little curl
> Right in the middle of her forehead.
> When she was good,
> She was very very good
> But when she was bad
> She was horrid.

In this paper, such events are called **Longfellow Events** to avoid the implication that simple randomness is their cause or that their probability of occurrence might be near 1/2.

Longfellow Events cause the grid search-based method used in this paper to slightly *underestimate* the LDE statistical metrics. This is because the grid search is constrained to a fixed area (1 km $\times$ 1 km in the examples considered in this section), so a minimum SSE value that falls outside the search area will not be found and the grid search fortuitously finds the correct location of the emitter without the potential penalty of the Longfellow Event. For example, imagine that the emitter and three sensors shown in Figure 20 were shifted to the left by 150 m but their relative positions were

unchanged. The SSE value currently marked with the red square would be outside the search area and so the grid search would report the correct emitter location as the estimated location. Thus, the LDE would be underestimated compared to a search that was not constrained to the specified 1 km $\times$ 1 km search area.

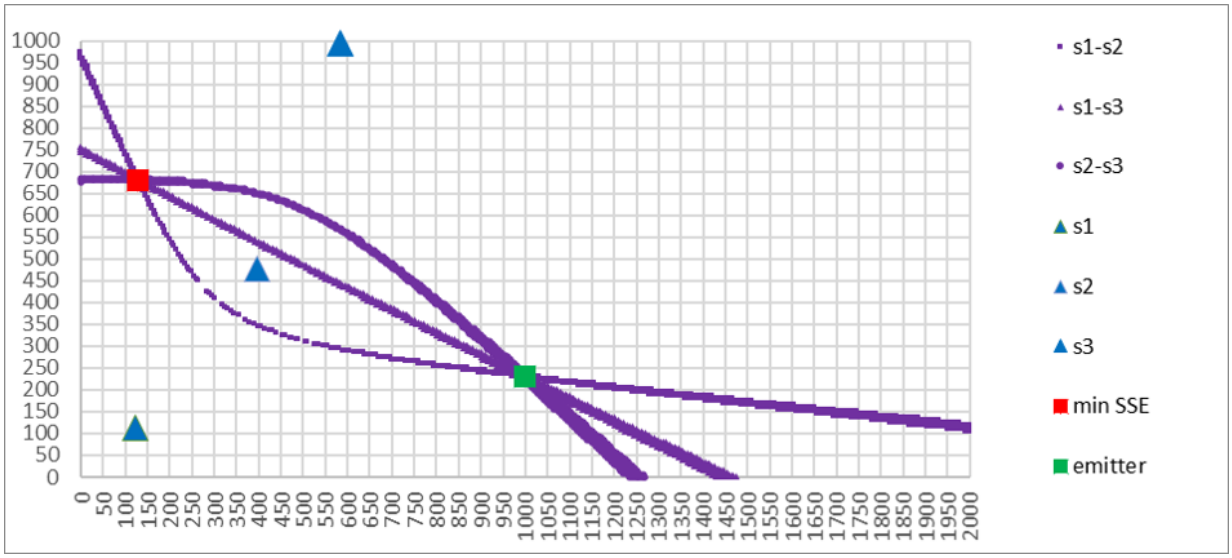

Figure 20: Three immersed sensors on the ground that are nearly collinear, without position or timing errors, where the point that has the minimum SSE is 979 m from the true position of the emitter. Parameters: $N = 3$ immersed sensors, $side = 1{,}000$ m, $alt = 0$ m, error-free.

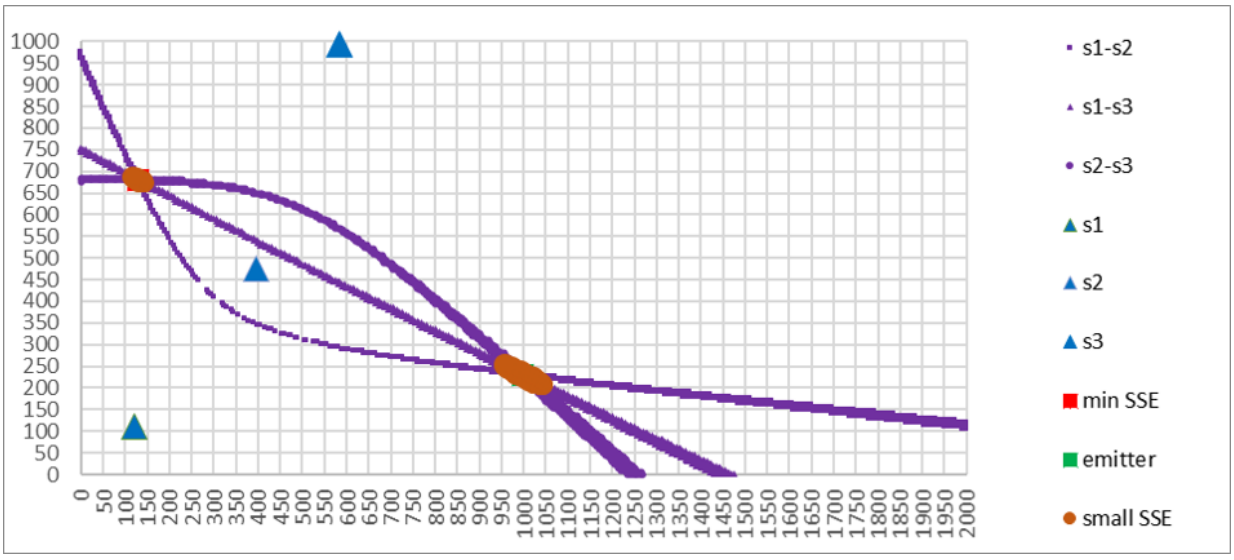

Figure 21: Same geometry as in Figure 20 showing 0.1% of the smallest SSE values overlaid on the plot (marked with brown shading). Parameters: $N = 3$ immersed sensors, $side = 1{,}000$ m, $alt = 0$ m, error-free.

6.2 Longfellow Events Decrease with the Number of Sensors

Figure 22 shows an error-free case with $N = 3$ sensors at nominal altitudes of 100 m and immersed with the emitter. The LDE is 286.34 m. Figure 23 shows the same geometry with 0.1% of the smallest SSE values overlaid on the plot. In this case, the apparent issue with the geometry is that the emitter is collinear with two of the sensors. Since the location of the emitter is unknown to the TDoA solution method, there is no way to anticipate or mitigate the situation other than by the presence of additional sensors.

Figure 24 shows an error-free case with three sensors on the ground and standoff from the emitter. Figure 25 shows the same geometry with 0.1% of the smallest SSE values overlaid on the plot. The LDE is 962.24 m. The apparent issue in this case was that the correct emitter location was close to being collinear with a pair of sensors and the grid search found the minimum SSE value at a distant point and erroneously placed the location estimate so that it was close to being collinear with the sensors.

Geolocation estimates are often poor when only three sensors are used. Figure 26 shows a histogram of LDE values for 10,000 simulations of error-free cases with three immersed sensors on the ground. For that set of simulations, 86.82% of the LDE values were zero, an additional 4.67% were less than or equal 20 m, an additional 0.92% were less than or equal 40 m, and 7.59% were greater than 40 m. The largest LDE value was 1,082.73 m.

Figure 27 shows a histogram of LDE values for 10,000 simulations of error-free cases with three immersed sensors at nominal altitudes of 100 m. For that set of simulations, 89.11% of the LDE values were zero, an additional 3.55% were less than or equal 20 m, an additional 0.73% were less than or equal 40 m, and 6.61% were greater than 40 m. The largest LDE value was 1,104.63 m.

Figure 28 shows a histogram of LDE values for 10,000 simulations of error-free cases with three standoff sensors on the ground. For that set of simulations, 78.61% of the LDE values were zero, an additional 13.50% were less than or equal 20 m, an additional 1.93% were less than or equal 40 m, and 5.96% were greater than 40 m. The largest LDE value was 1,024.90 m.

Figure 29 shows a histogram of LDE values for 10,000 simulations of error-free cases with three standoff sensors at nominal altitudes of 100 m. For that set of simulations, 80.63% of the LDE values were zero, an additional 12.42% were less than or equal 20 m, an additional 1.59% were less than or equal 40 m, and 5.36% were greater than 40 m. The largest LDE value was 1,000.62 m.

Figure 30 shows an error-free case with four immersed sensors on the ground. The LDE is 85.78 m. Figure 31 shows the same geometry with 0.1% of the smallest SSE values overlaid on the plot.

Figure 32 shows an error-free case with four immersed sensors at nominal altitudes of 100 m. The LDE is 382.37 m. Figure 33 shows the same geometry with 0.1% of the smallest SSE values overlaid on the plot.

LDE values in the error-free case grow smaller as the number of sensors increases. Figure 34 shows a histogram of LDE values for 10,000 simulations of error-free cases with four immersed sensors on the ground. For that set of simulations, 99.10% of the LDE values were zero, an additional 0.54% were less than or equal 20 m, an additional 0.03% were less than or equal 40 m, and 0.33% were greater than 40 m. The largest LDE value was 788.74 m.

Figure 35 shows a histogram of LDE values for 10,000 simulations of error-free cases with four immersed sensors at nominal altitudes of 100 m. For that set of simulations, 99.42% of the LDE values were zero, an additional 0.38% were less than or equal 20 m, an additional 0.03% were less than or equal 40 m, and 0.17% were greater than 40 m. The largest LDE value was 805.62 m.

The histograms for four standoff sensors on the ground and at nominal altitudes of 100 m showed similar reductions in the percent of non-zero LDE values.

LDE values rapidly decrease with increasing N. This is shown for five immersed sensors on the ground in Figure 36 and at nominal altitudes of 100 m in Figure 37. The results for six immersed sensors on the ground are given in Figure 38 and at nominal altitudes of 100 m in Figure 39. Additional decrease in LDE values is shown for seven immersed sensors on the ground in Figure 40 and at nominal altitudes of 100 m in Figure 41. The reductions in LDE for standoff sensors were on similar scales.

For immersed or standoff sensors on the ground or at nominal altitudes of 100 m, the largest percentage of geometries with non-zero LDE was 21.39% for $N = 3$, 6.20% for $N = 4$, 2.65% for $N = 5$, 1.39% for $N = 6$, 0.75% for $N = 7$, and 0.50% for $N = 8$.

These results show that the fraction of non-zero LDE values in error-free cases and, perhaps more importantly, the fraction of large LDE values, continues to drop as the number of sensors increases.

Based on these observations, it is recommended that a **minimum of five sensors** [28] be used, regardless of altitude or whether they are immersed with or standoff from the search area for the emitter. This avoids the issue of large percentages of grossly wrong geolocation estimates due to Longfellow Events even when sensors do not experience position or timing errors.

[28] Using more sensors would reduce LDE, but this number of sensors seems like a reasonable compromise between geolocation accuracy and the complexity and cost of implementation.

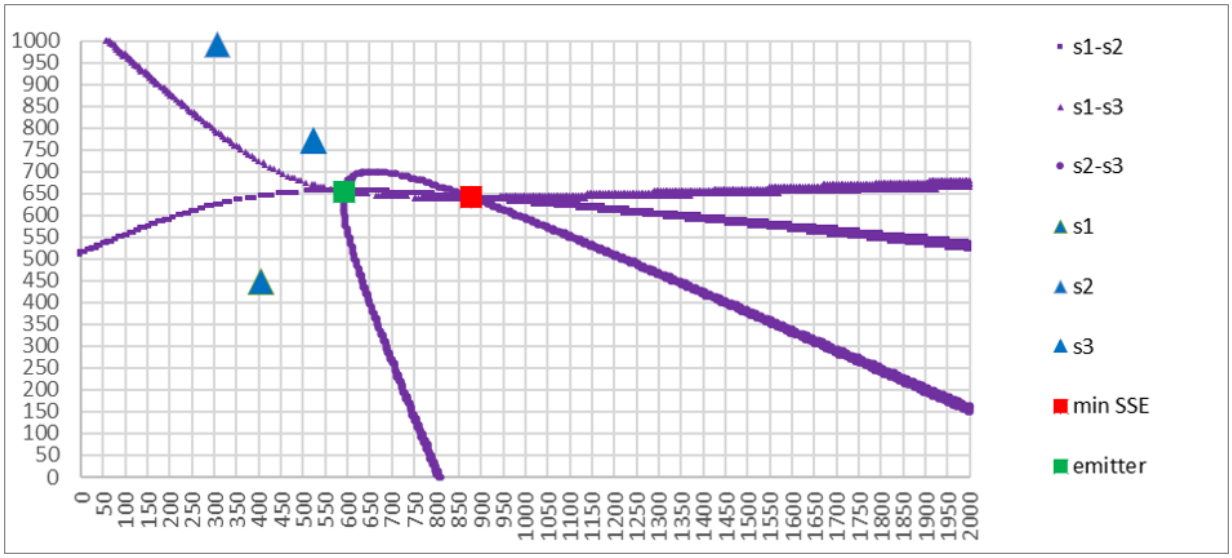

Figure 22: Three immersed sensors at nominal altitudes of 100 m, without position or timing errors, where the point that has the minimum SSE is 286 m from the true position of the emitter. Parameters: $N = 3$ immersed sensors, $side$ = 1,000 m, alt = 100 m, error-free.

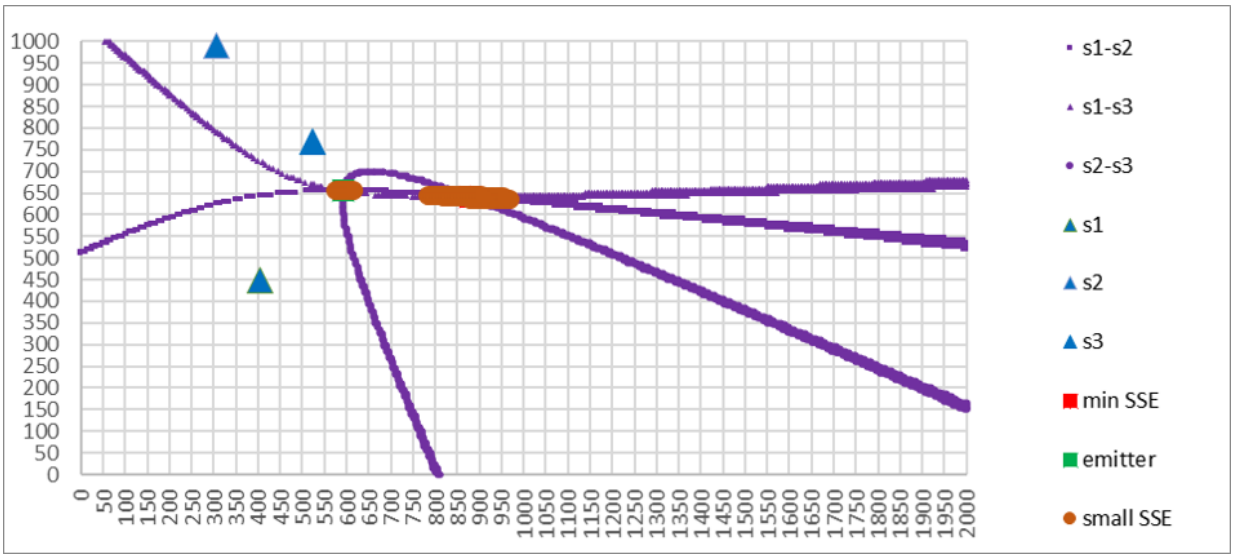

Figure 23: Same geometry as in Figure 22 showing 0.1% of the smallest SSE values overlaid on the plot (marked with brown shading). Parameters: $N = 3$ immersed sensors, $side$ = 1,000 m, alt = 100 m, error-free.

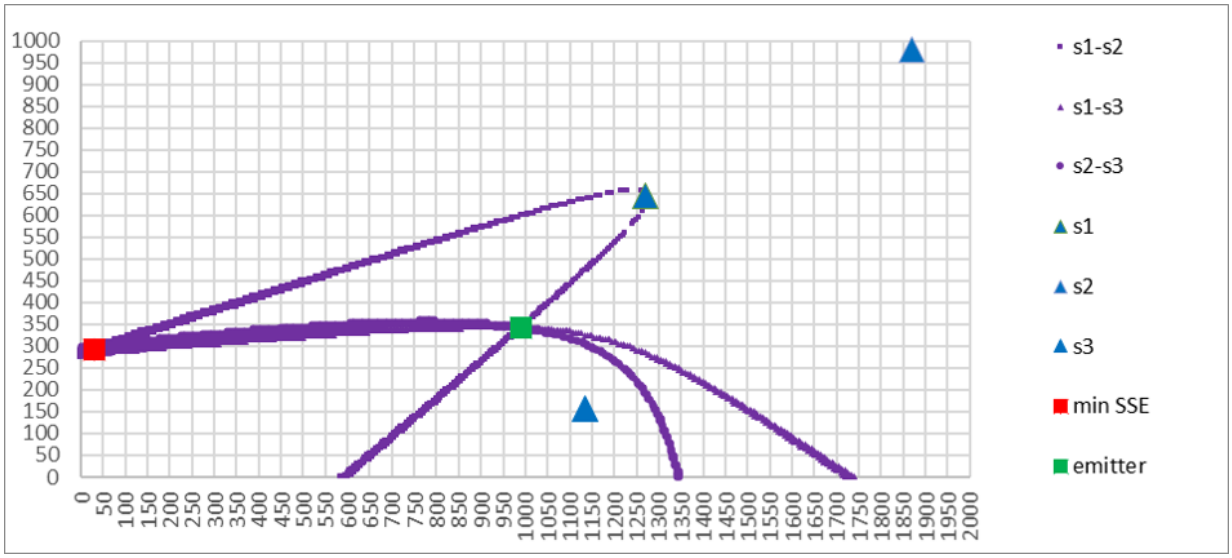

Figure 24: Three standoff sensors that are on the ground, without position or timing errors, where the point that has the minimum SSE is 962 m from the true position of the emitter. Parameters: $N = 3$ standoff sensors, $side$ = 1,000 m, alt = 0 m, error-free.

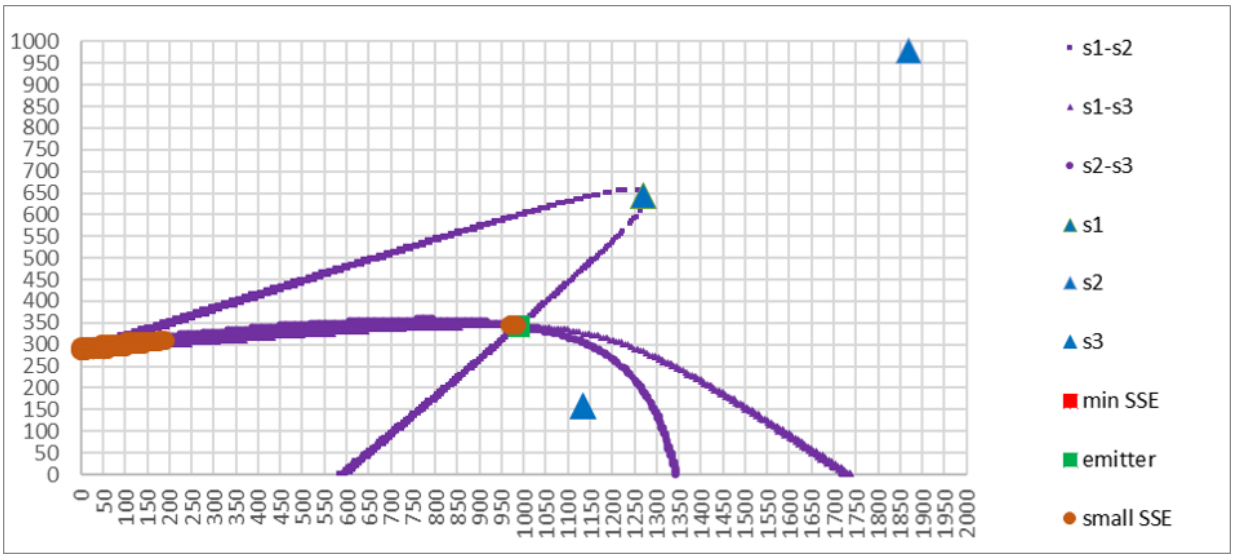

Figure 25: Same geometry as in Figure 24 showing 0.1% of the smallest SSE values overlaid on the plot (marked with brown shading). Parameters: $N = 3$ standoff sensors, $side$ = 1,000 m, alt = 0 m, error-free.

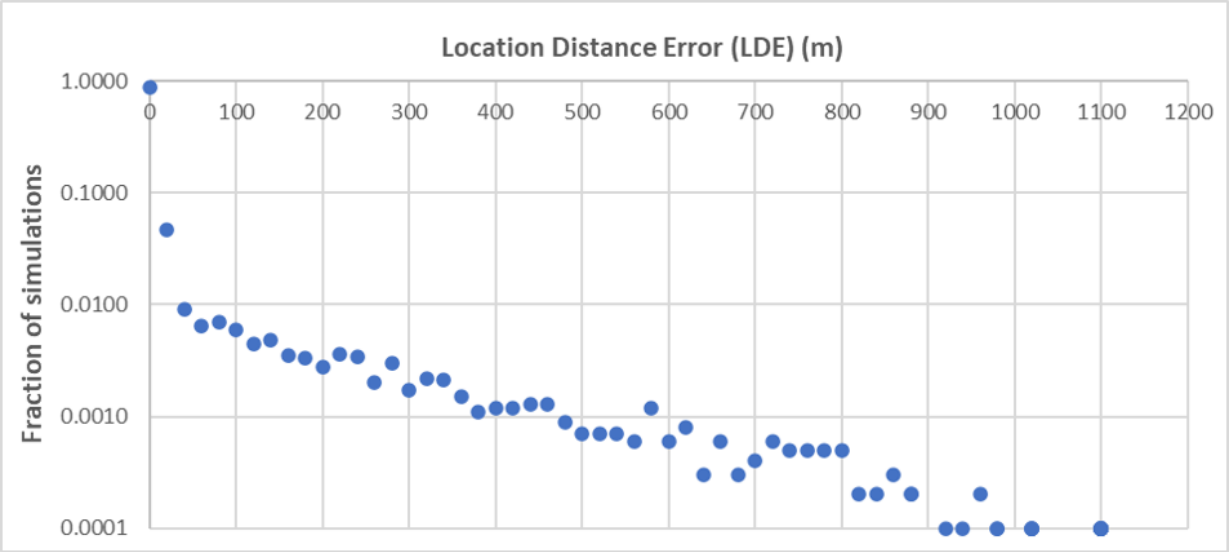

Figure 26: Three immersed sensors on the ground: histogram of LDE obtained from 10,000 simulations. Parameters: $N = 3$ immersed sensors, $side$ = 1,000 m, alt = 0 m, error-free.

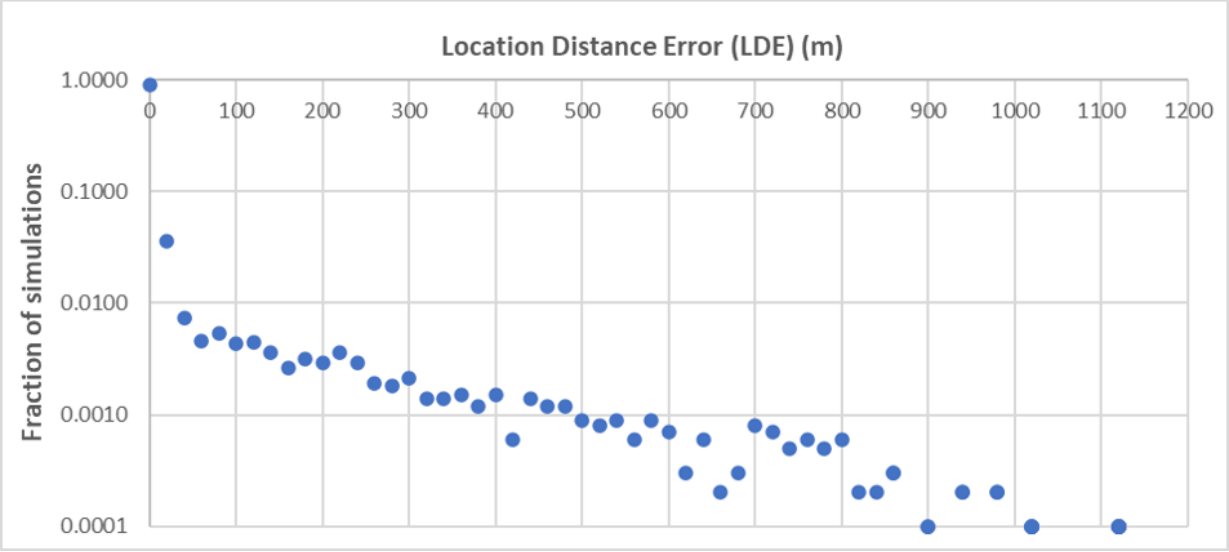

Figure 27: Three immersed sensors at nominal altitudes of 100 m: histogram of LDE obtained from 10,000 simulations. Parameters: $N = 3$ immersed sensors, $side$ = 1,000 m, alt = 100 m, error-free.

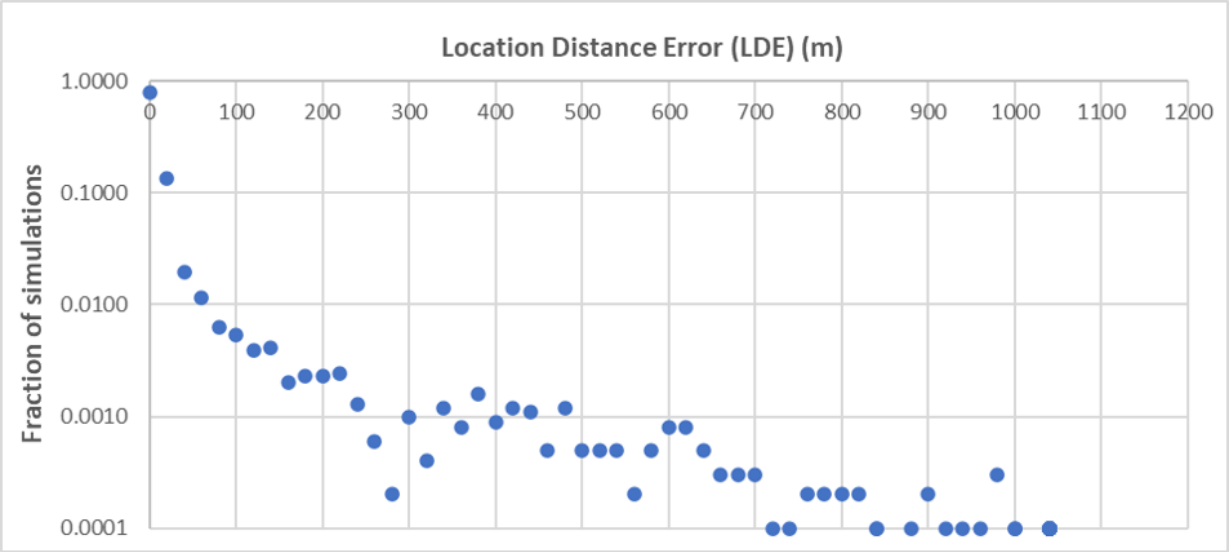

Figure 28: Three standoff sensors on the ground: histogram of LDE obtained from 10,000 simulations. Parameters: $N = 3$ standoff sensors, $side$ = 1,000 m, alt = 0 m, error-free.

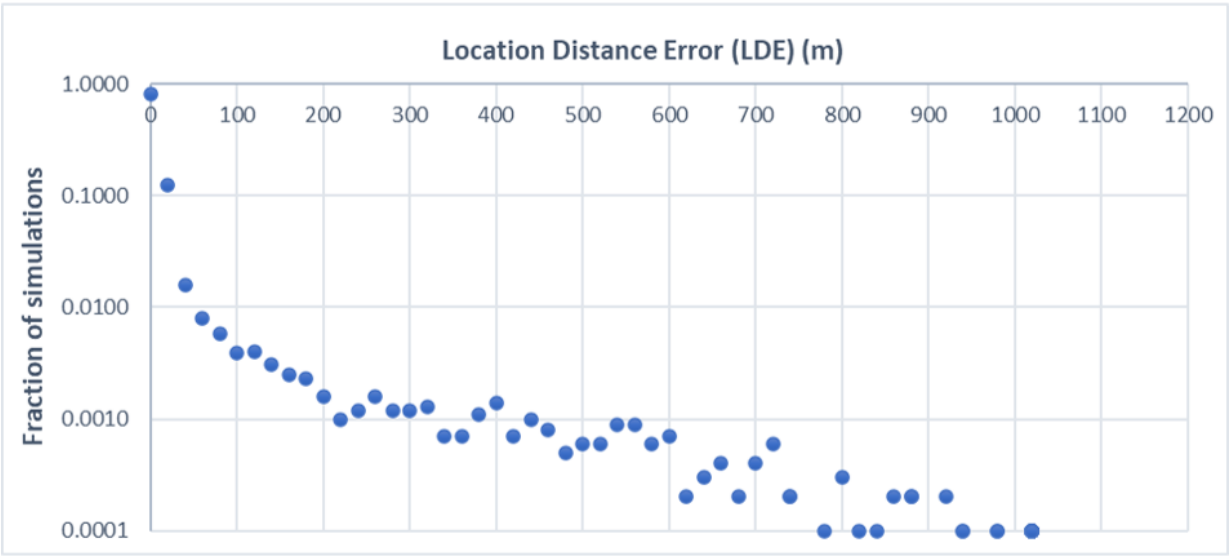

Figure 29: Three standoff sensors at nominal altitudes of 100 m: histogram of LDE obtained from 10,000 simulations. Parameters: $N = 3$ standoff sensors, $side$ = 1,000 m, alt = 100 m, error-free.

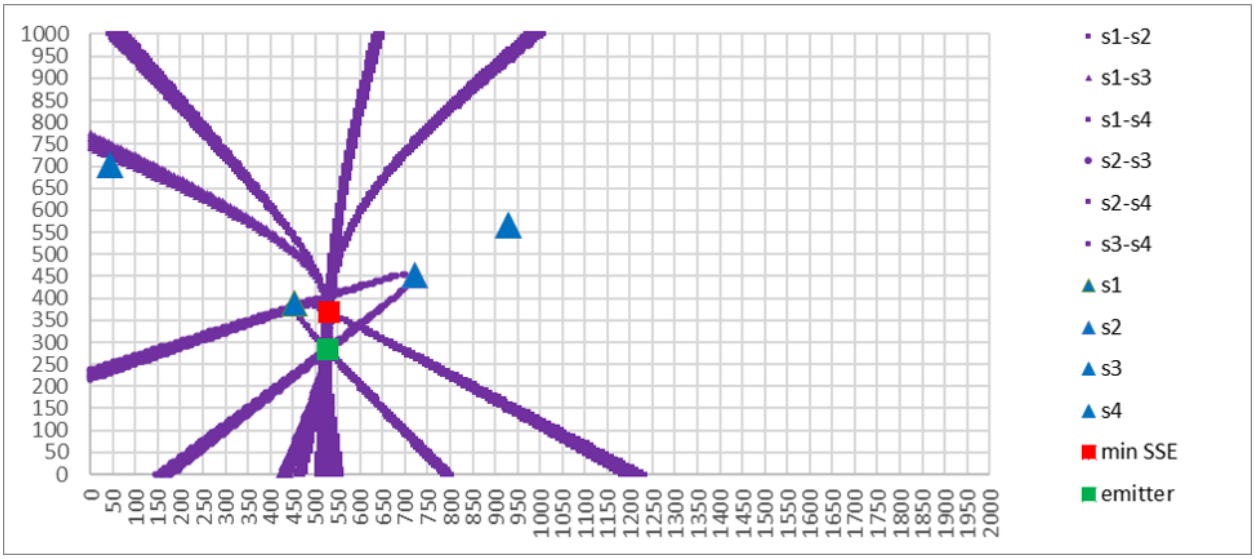

Figure 30: Four immersed sensors on the ground, without position or timing errors, where the point that has the minimum SSE is 86 m from the true position of the emitter. Parameters: $N = 4$ immersed sensors, $side$ = 1,000 m, alt = 0 m, error-free.

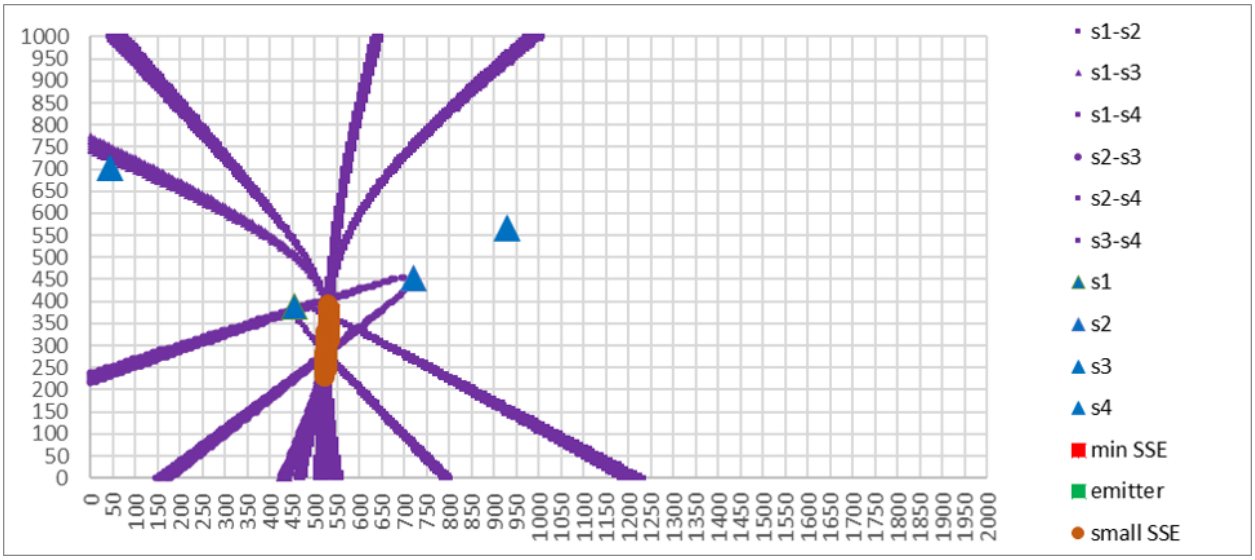

Figure 31: Same geometry as in Figure 30 showing 0.1% of the smallest SSE values overlaid on the plot (marked with brown shading). Parameters: $N = 4$ immersed sensors, $side$ = 1,000 m, alt = 0 m, error-free.

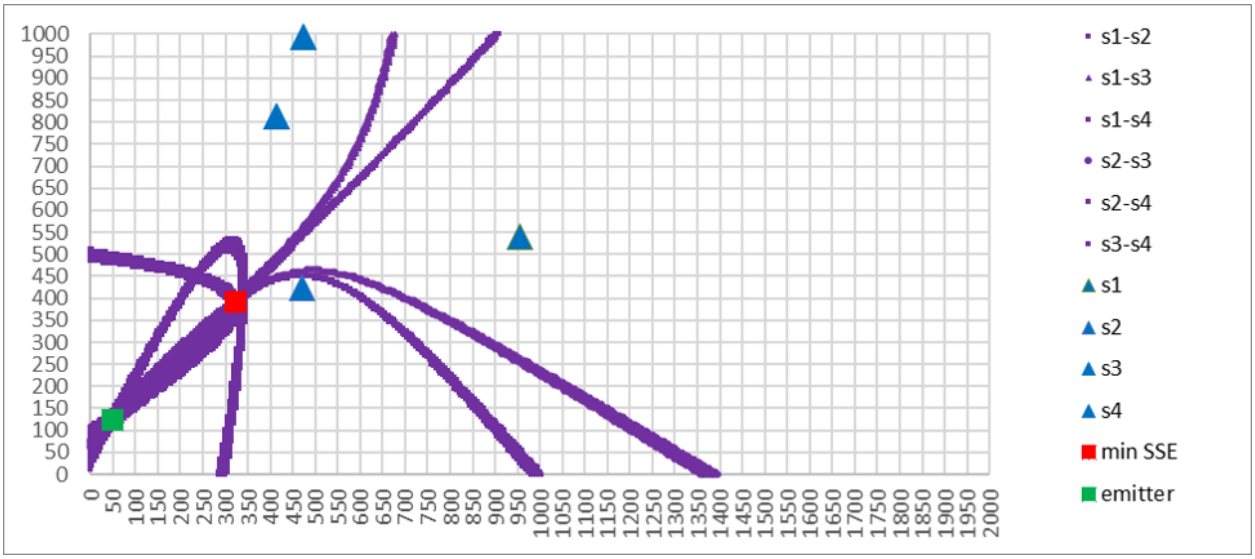

Figure 32: Four immersed sensors at nominal altitudes of 100 m, without position or timing errors, where the point that has the minimum SSE is 382 m from the true position of the emitter. Parameters: $N = 4$ immersed sensors, $side$ = 1,000 m, alt = 100 m, error-free.

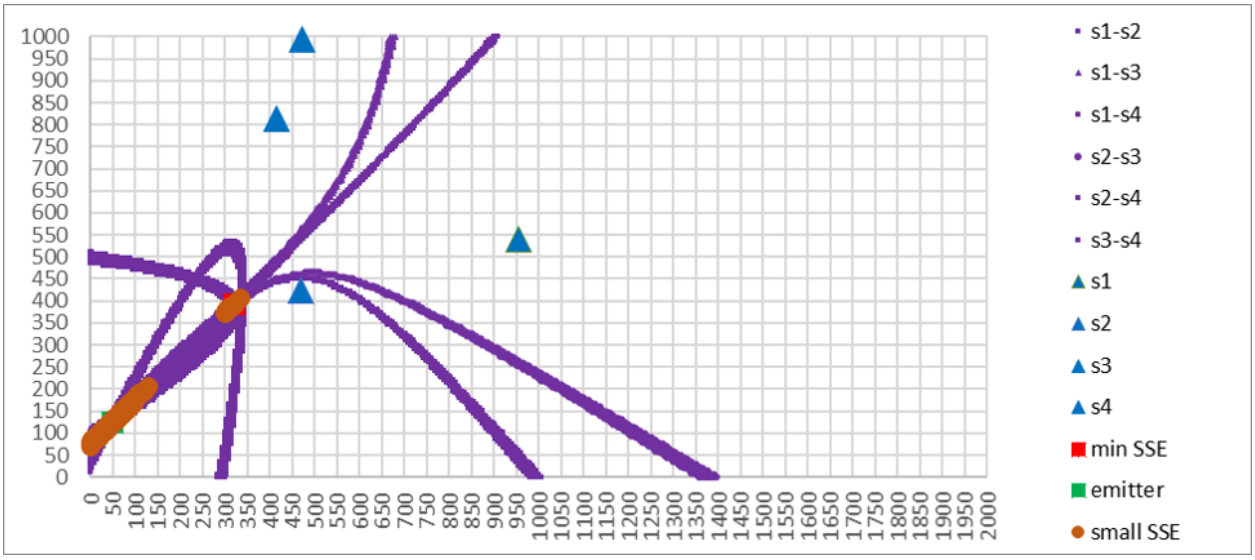

Figure 33: Same geometry as in Figure 32 showing 0.1% of the smallest SSE values overlaid on the plot (marked with brown shading). Parameters: $N = 4$ immersed sensors, $side$ = 1,000 m, alt = 100 m, error-free.

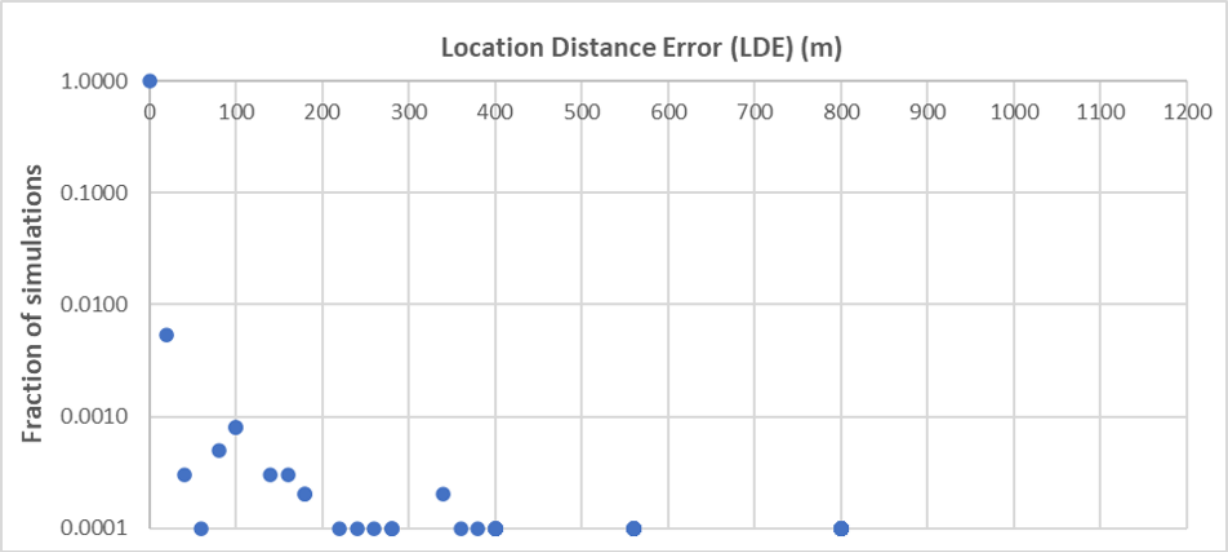

Figure 34: Four immersed sensors on the ground: histogram of LDE obtained from 10,000 simulations. Parameters: $N = 4$ immersed sensors, $side$ = 1,000 m, alt = 0 m, error-free.

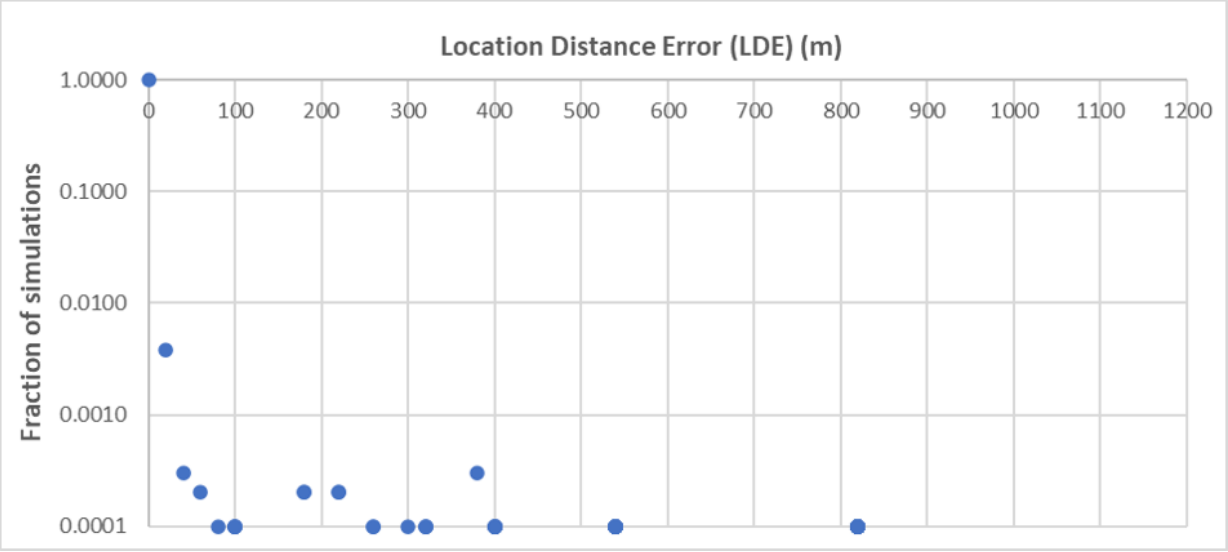

Figure 35: Four immersed sensors at nominal altitudes of 100 m: histogram of LDE obtained from 10,000 simulations. Parameters: $N = 4$ immersed sensors, $side$ = 1,000 m, alt = 100 m, error-free.

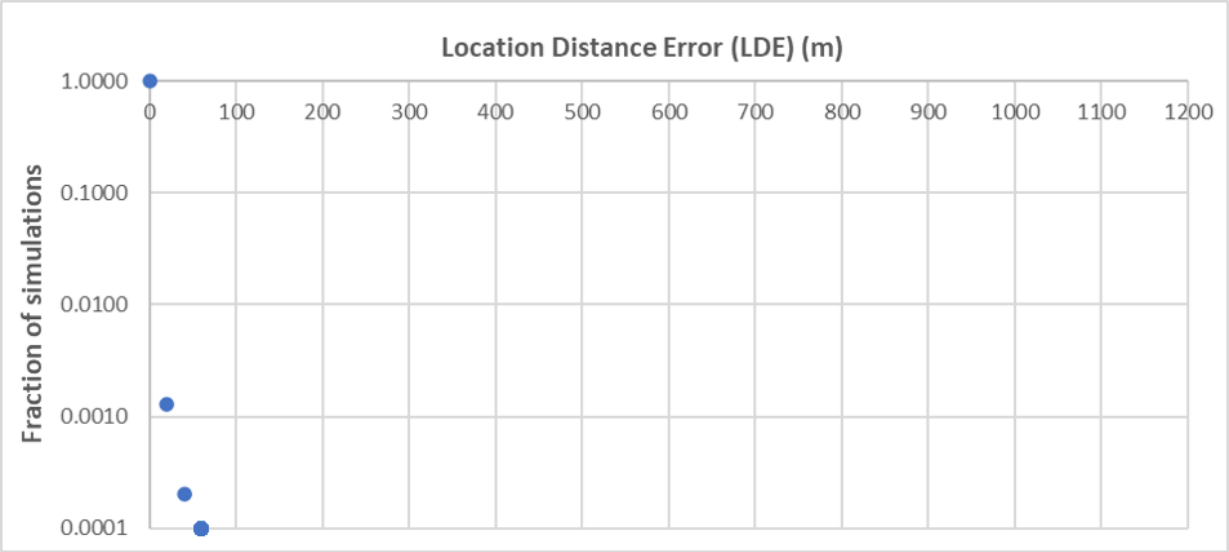

Figure 36: Five immersed sensors on the ground: histogram of LDE obtained from 10,000 simulations. Parameters: $N = 5$ immersed sensors, $side$ = 1,000 m, alt = 0 m, error-free.

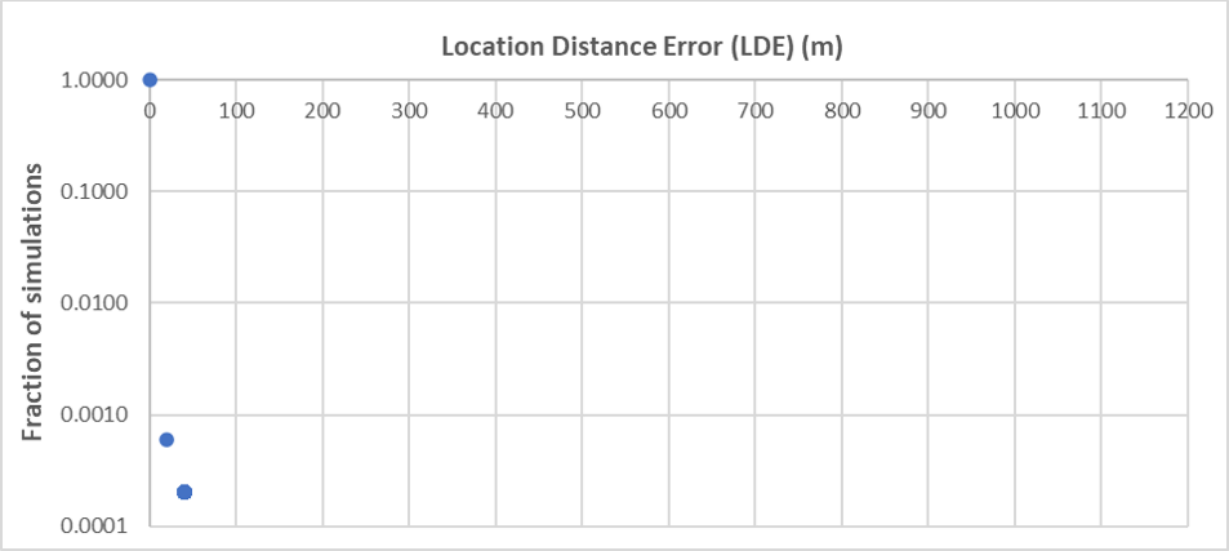

Figure 37: Five immersed sensors at nominal altitudes of 100 m: histogram of LDE obtained from 10,000 simulations. Parameters: $N = 5$ immersed sensors, $side$ = 1,000 m, alt = 100 m, error-free.

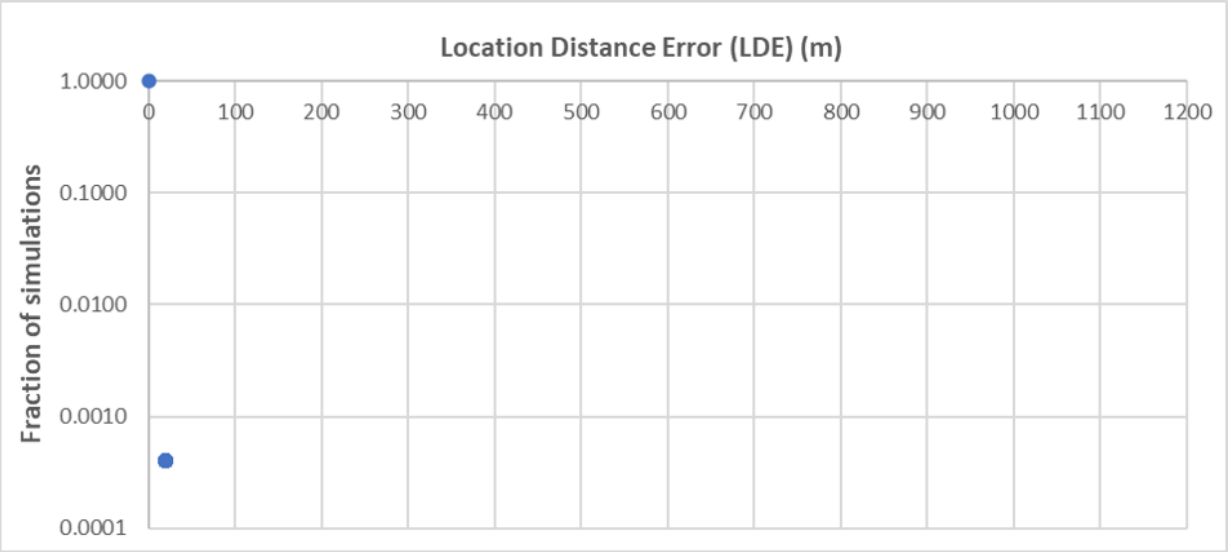

Figure 38: Six immersed sensors on the ground: histogram of LDE obtained from 10,000 simulations. Parameters: $N = 6$ immersed sensors, $side$ = 1,000 m, alt = 0 m, error-free.

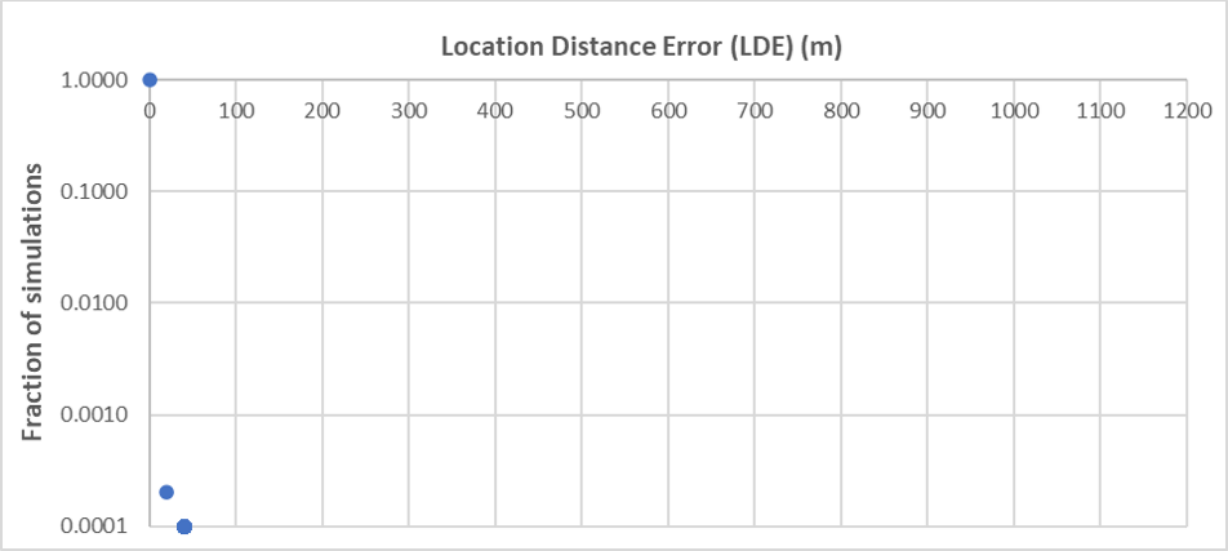

Figure 39: Six immersed sensors at nominal altitudes of 100 m: histogram of LDE obtained from 10,000 simulations. Parameters: $N = 6$ immersed sensors, $side$ = 1,000 m, alt = 100 m, error-free.

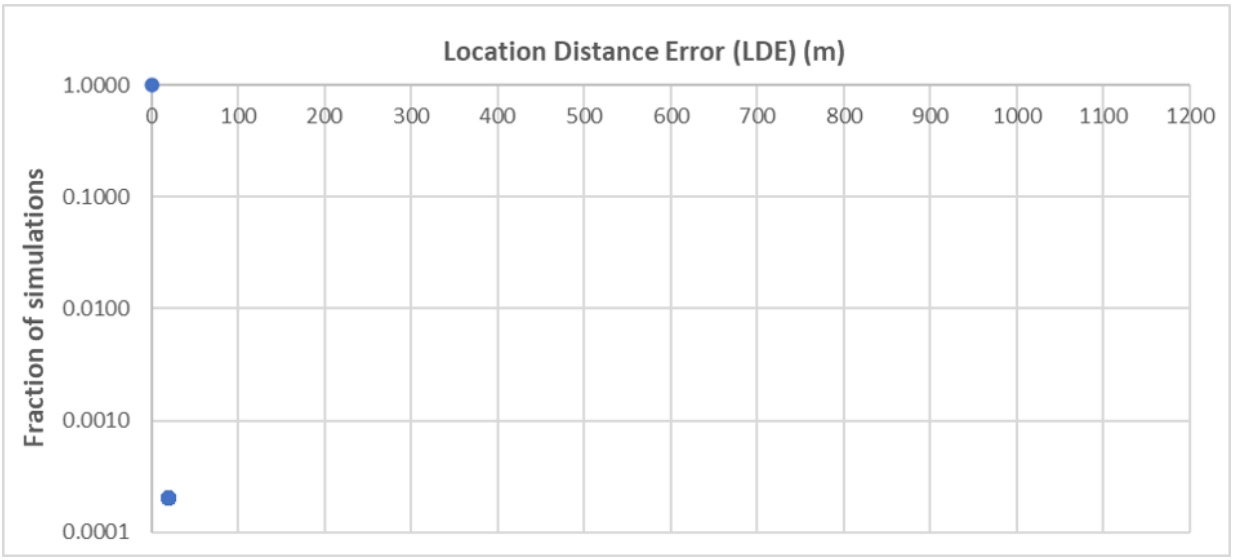

Figure 40: Seven immersed sensors on the ground: histogram of LDE obtained from 10,000 simulations. Parameters: $N = 7$ immersed sensors, $side$ = 1,000 m, alt = 0 m, error-free.

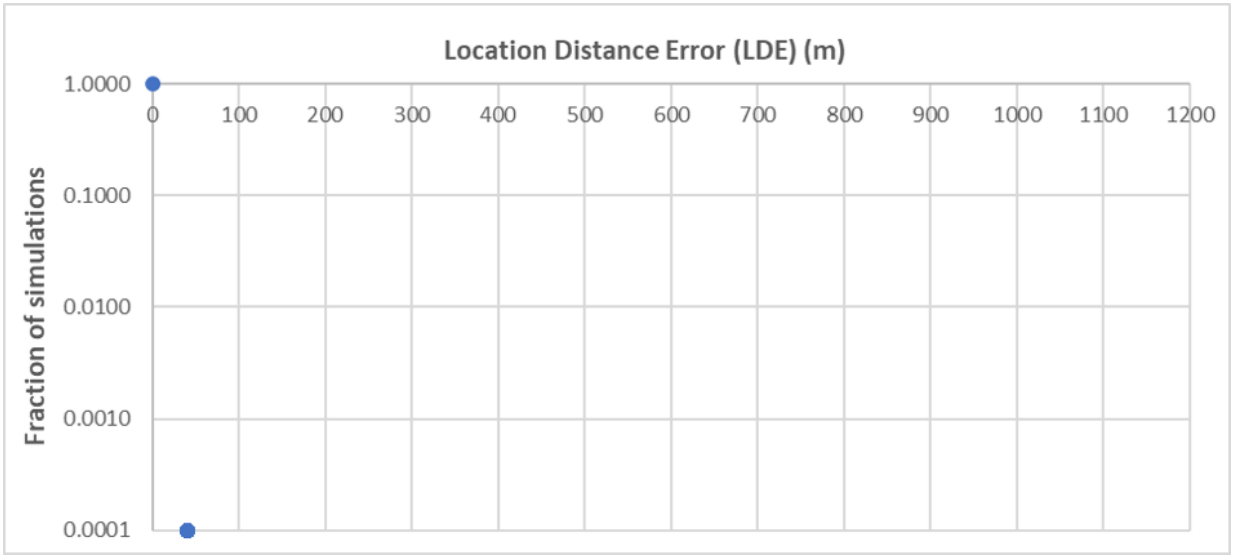

Figure 41: Seven immersed sensors at nominal altitudes of 100 m: histogram of LDE obtained from 10,000 simulations. Parameters: $N = 7$ immersed sensors, $side$ = 1,000 m, alt = 100 m, error-free.

7 Location Distance Error as a Function of Altitude and Search Area Side Length for a Given Number of Sensors

This section explores the relationship between altitude, search area side length, and LDE. It is observed here that LDE varies with the nominal altitude *alt* and the search area side length *side* and, to some degree, LDE is approximately scale-invariant with respect to the ratio of those parameters.

The curves are also approximately convex as a function of the ratio $alt/side$ for each of the four LDE statistical metrics. Thus, there is an "interesting" optimal altitude that minimizes LDE for a given number of sensors and any search area side length; the solution is "interesting" in the sense that the optimal altitude is not necessarily at an extreme value and there appears to be a single optimal value within the resolution of the statistics of the data.

The data used in this section resulted from configurations that varied *side* from 1,000 m to 10,000 m (in steps of 1,000 m) with the Standard Error Conditions of $\sigma_{pos} = 10$ m position error and $\sigma_{time} = 30$ ns timing error. These configurations differed from all other data sets used in this paper in that the nominal altitudes varied over a wider range. The other configurations varied *alt* only up to 1,000 m, whereas the configurations used in this section varied *alt* from 0 m to *side* (in steps of $side/20$) for immersed sensors and from 0 m to $2 \times side$ (in steps of $side/10$) for standoff sensors (with $\sigma_{alt} = alt/20$); thus, the configurations used a total of 21 altitudes per value of *side*.

Due to the long run times required for the large number of configurations, only 1,000 simulations of each configuration were performed.

Figure 42 shows the four LDE statistical metrics used in this paper for $N = 5$ immersed sensors as a function of the ratio $alt/side$. Even though the values for each statistical metric show some scattering, [29] particularly at the

[29] "Scattering" is meant in the following sense. For a given N, ten combinations of *alt* and *side* are simulated that have the same $alt/side$ ratio. "No scattering" would mean that the ten values of an LDE statistical metric at a particular ratio would overlap and appear as a single point. "Scattering" thus indicates visual divergence of the points at a particular ratio.

smaller ratios, the trends are clear that the four statistical metrics decrease with the ratio to minimum values and then increase. Figure 43 shows the same immersed situation but only for the mean and 95%ile LDE. Even with the scattering of LDE values for a given ratio, there are indications that there is some degree of scale-invariance of LDE with respect to the ratio $alt/side$. Even with the scattering of values, the convexity of the curves is clear in Figure 42 for all four of the LDE statistical metrics and even more obvious in Figure 43 for the mean and 95%ile LDE.

The minimum for the mean LDE was at approximately $alt/side = 0.20$. The minima occurred at approximately $alt/side$ ratios of 0.05, 0.40, and 0.65 for the 50%ile, 95%ile, and 99%ile LDE, respectively. The term "approximately" is used because the precision of these ratios is limited by the small number of step sizes of alt. In addition, the curves are relatively flat around their minima, so small amounts of random variation in the measured LDE may cause the observed minima to shift from their actual values.

Figure 44 shows the four LDE statistical metrics for $N = 5$ standoff sensors, where similar dependence on the ratio $alt/side$ can be observed. The minima occurred at approximately $alt/side$ ratios of 1.20, 1.00, 1.20, and 1.50 for the mean, 50%ile, 95%ile, and 99%ile LDE, respectively. Figure 45 shows the same standoff situation but only for the mean and 95%ile LDE.

Figure 46 and Figure 47 show the mean and 95%ile LDE for $N = 10$ immersed and standoff sensors, respectively. There is less scattering of LDE at the lower values of the $alt/side$ ratio. This trend continues as the number of sensors increases as shown in Figure 48 and Figure 49 for $N = 15$ immersed and standoff sensors as well as in Figure 50 and Figure 51 for $N = 20$ immersed and standoff sensors. Figure 52 and Figure 53 show all four of the LDE statistical metrics for $N = 20$ immersed and standoff sensors.

The full sets of values of the $alt/side$ ratios that provided the minima for the four LDE statistical metrics are given in Table 1 for immersed sensors and Table 2 for standoff sensors.

For immersed sensors, the mean and 50%ile metrics appeared to be better at smaller ratios of altitude to search area side length, approximately in the range of 0.15 to 0.20. The 95%ile and 99%ile LDE values were better at larger $alt/side$ ratios, but still only approximately in the range of 0.15 to 0.65.

Standoff sensor configurations performed better at larger ratios. The mean and 50%ile metrics were minimized at ratios approximately in the range of 0.90 to 1.20, while the 95%ile and 99%ile LDE values were minimized at ratios approximately in the range of 1.20 to 1.70.

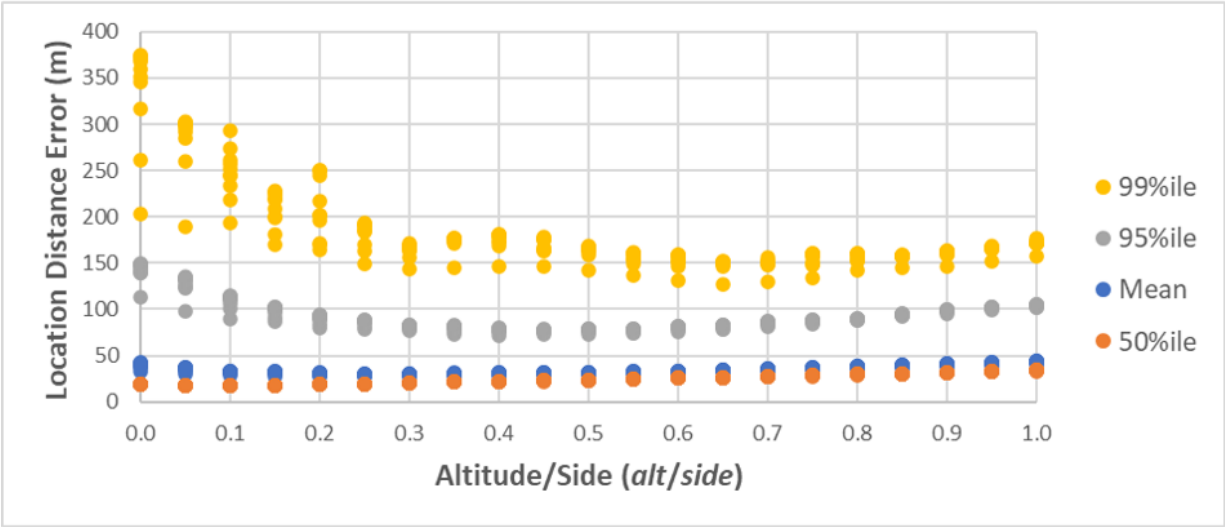

Figure 42: For five immersed sensors with errors, the mean, 50%ile, 95%ile, and 99%ile LDE statistical metrics are shown as a function of the ratio $alt/side$. See text for ranges of alt and $side$.

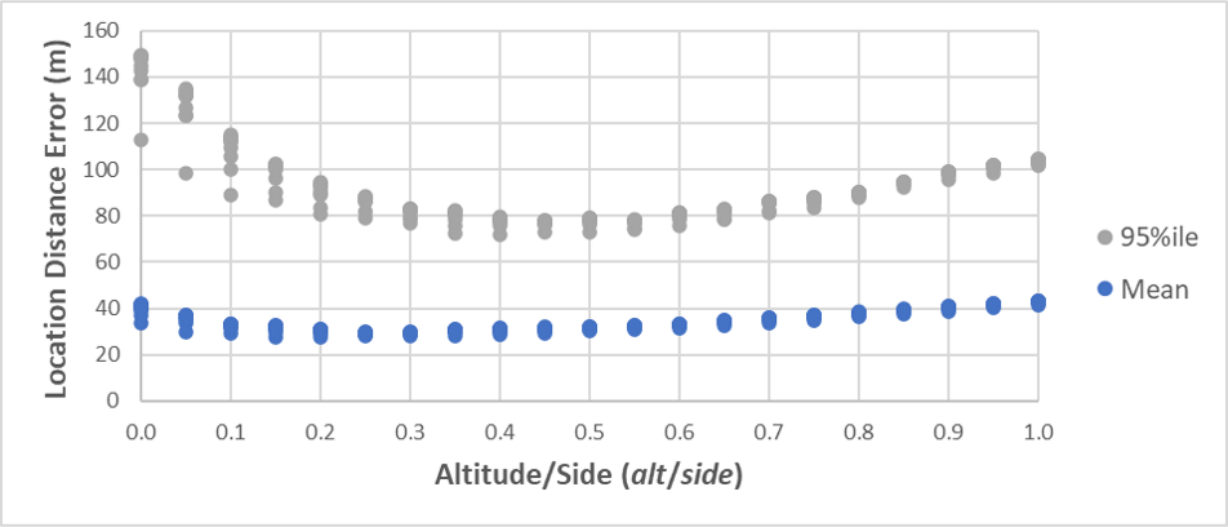

Figure 43: For five immersed sensors, only the mean and 95%ile LDE statistical metrics are shown as a function of the ratio $alt/side$. Otherwise, configurations and conditions are the same as for Figure 42.

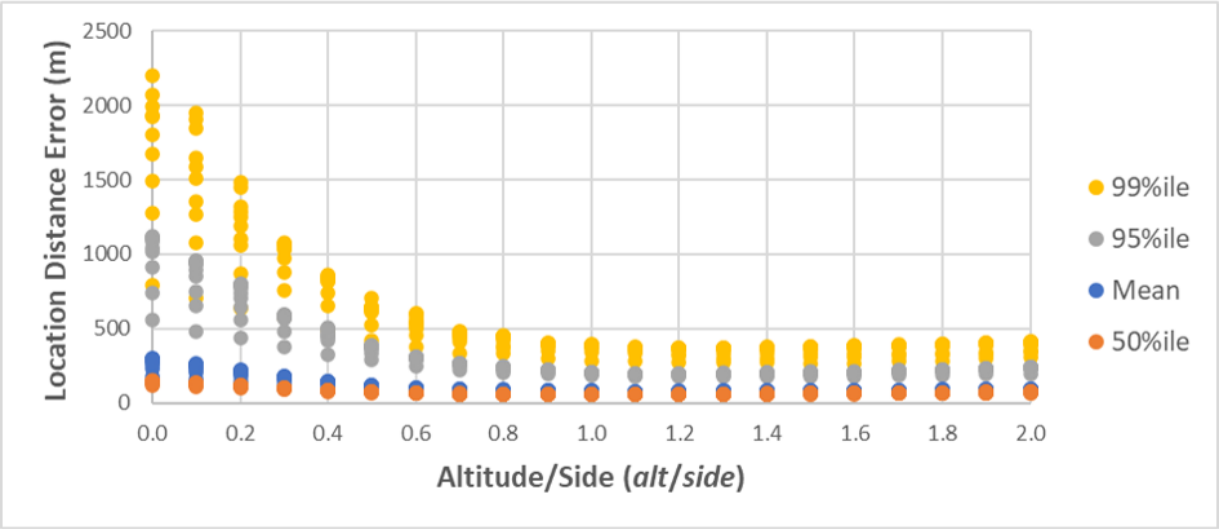

Figure 44: For five standoff sensors with errors, the mean, 50%ile, 95%ile, and 99%ile LDE statistical metrics are shown as a function of the ratio $alt/side$. See text for ranges of alt and $side$.

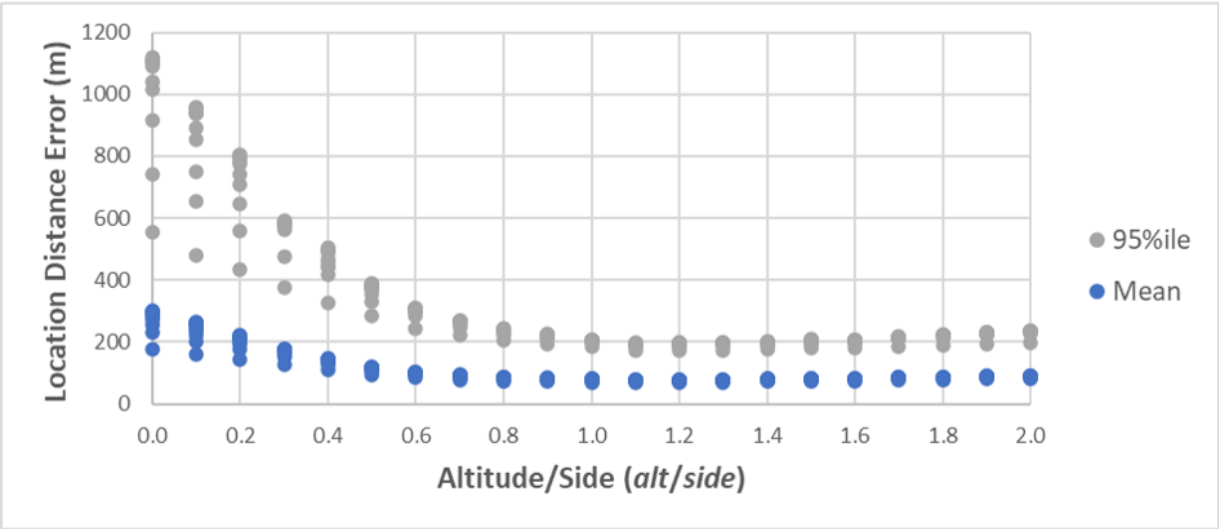

Figure 45: For five standoff sensors, only the mean and 95%ile LDE statistical metrics are shown as a function of the ratio $alt/side$. Otherwise, configurations and conditions are the same as for Figure 44.

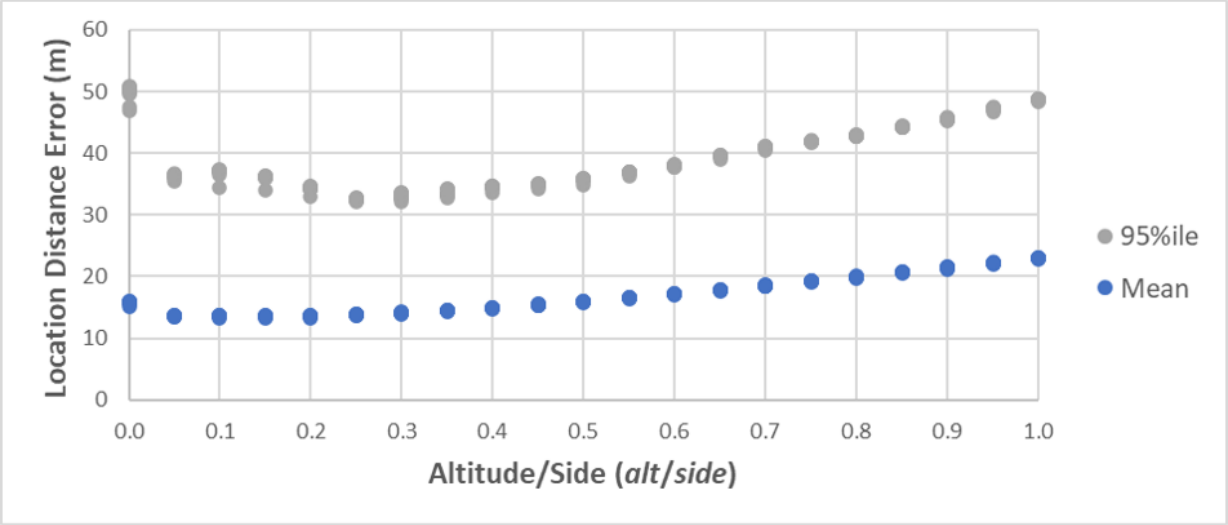

Figure 46: For ten immersed sensors with errors, the mean and 95%ile LDE statistical metrics are shown as a function of the ratio $alt/side$. See text for ranges of alt and $side$.

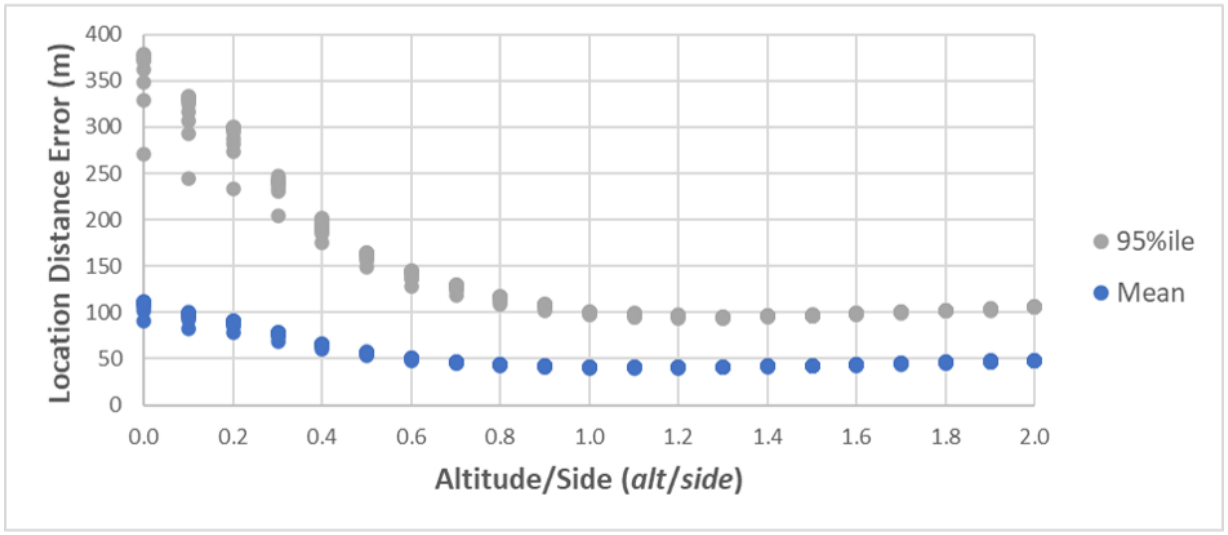

Figure 47: For ten standoff sensors with errors, the mean and 95%ile LDE statistical metrics are shown as a function of the ratio $alt/side$. See text for ranges of alt and $side$.

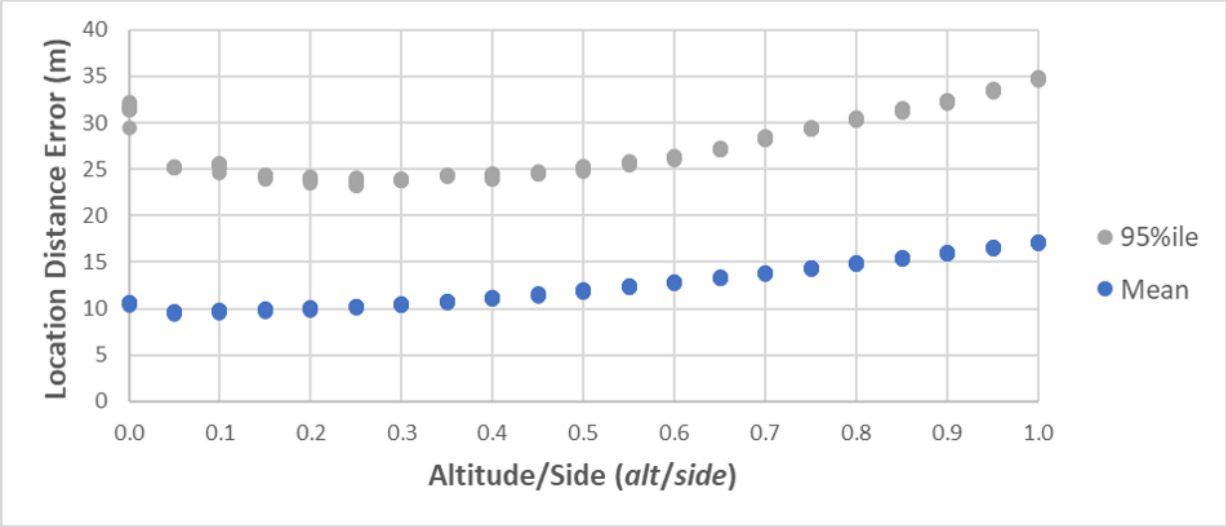

Figure 48: For 15 immersed sensors with errors, the mean and 95%ile LDE statistical metrics are shown as a function of the ratio $alt/side$. See text for ranges of alt and $side$.

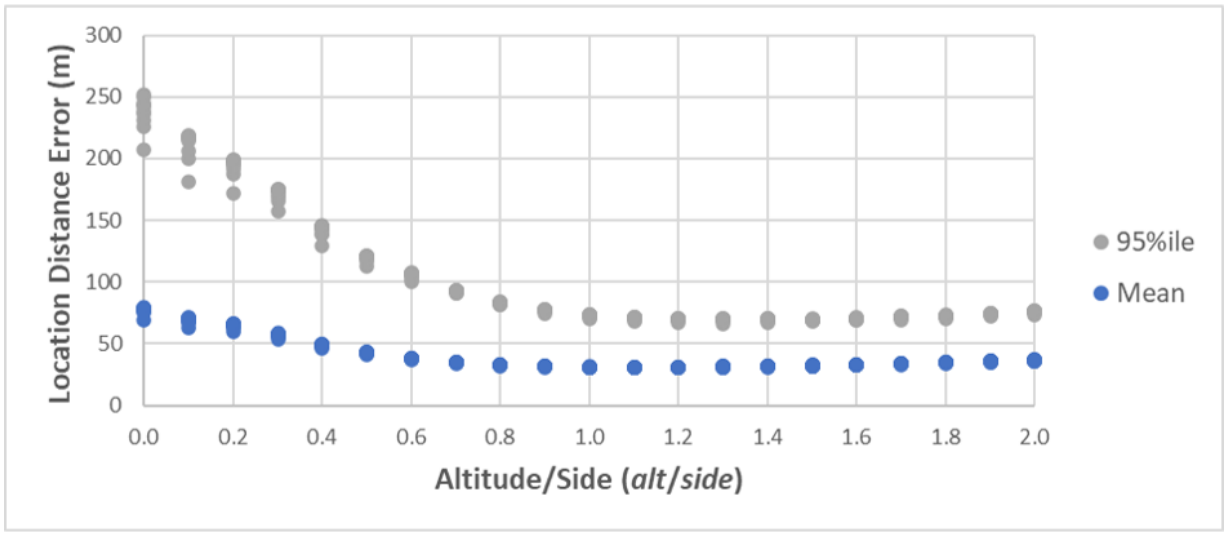

Figure 49: For 15 standoff sensors with errors, the mean and 95%ile LDE statistical metrics are shown as a function of the ratio $alt/side$. See text for ranges of alt and $side$.

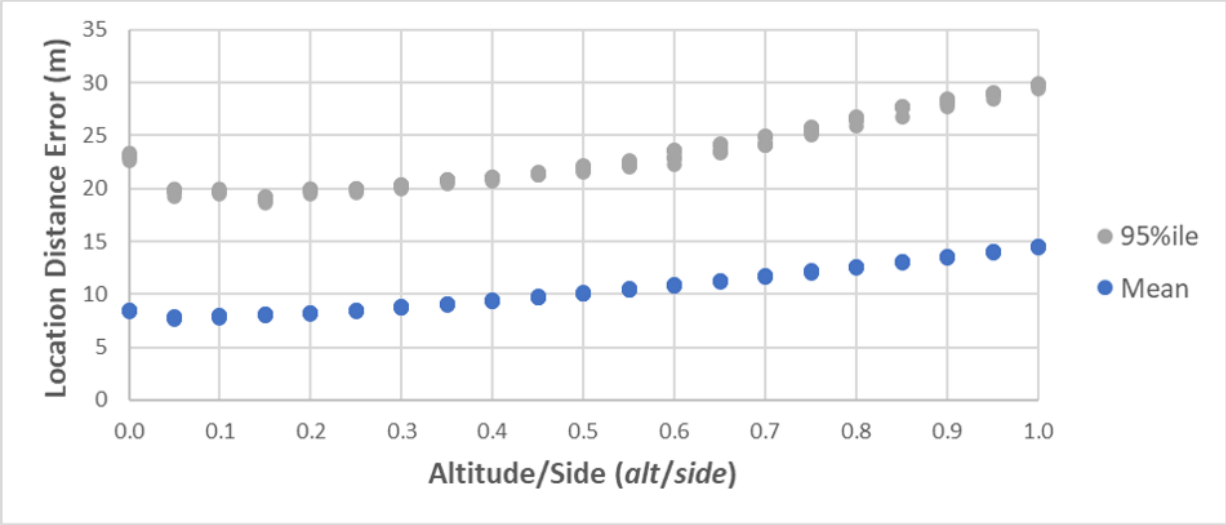

Figure 50: For 20 immersed sensors with errors, the mean and 95%ile LDE statistical metrics are shown as a function of the ratio $alt/side$. See text for ranges of alt and $side$.

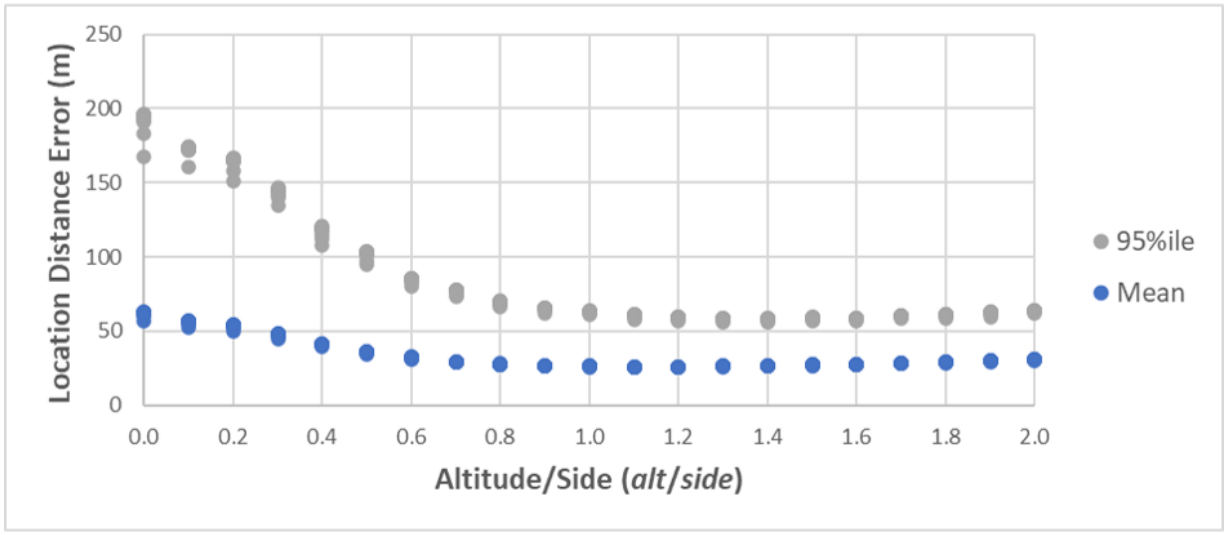

Figure 51: For 20 standoff sensors with errors, the mean and 95%ile LDE statistical metrics are shown as a function of the ratio $alt/side$. See text for ranges of alt and $side$.

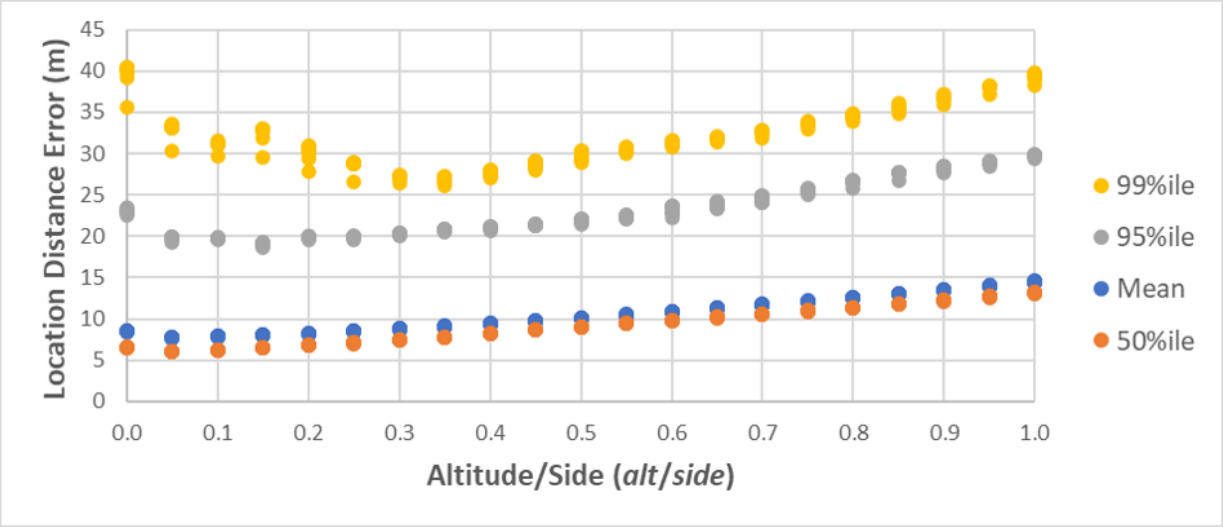

Figure 52: For 20 immersed sensors with errors, the mean, 50%ile, 95%ile, and 99%ile LDE metrics are shown as a function of the ratio $alt/side$. See text for ranges of alt and $side$.

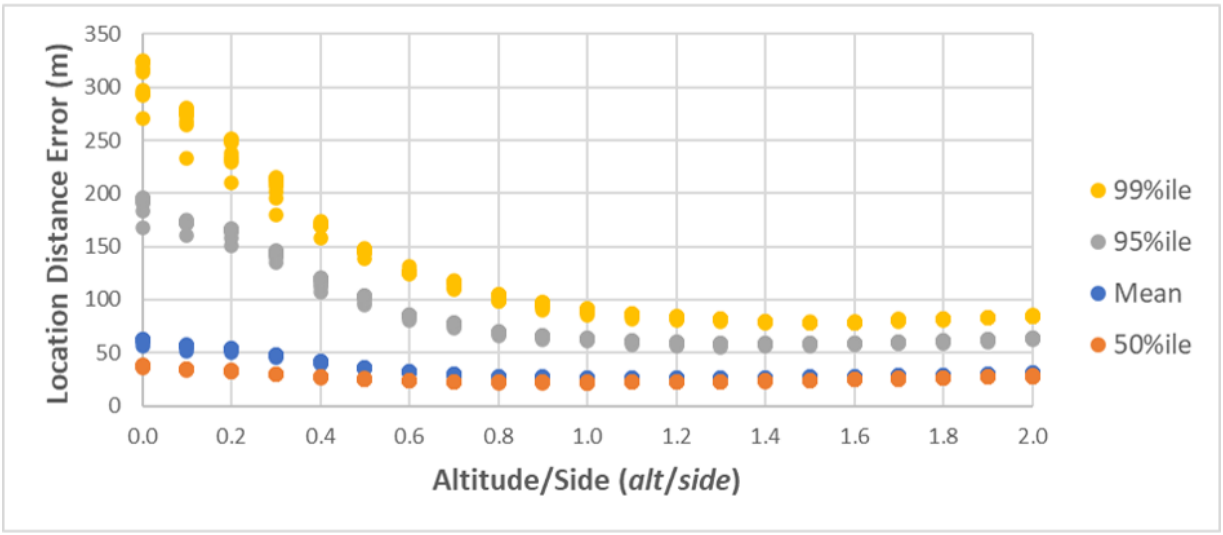

Figure 53: For 20 standoff sensors with errors, the mean, 50%ile, 95%ile, and 99%ile LDE statistical metrics are shown as a function of the ratio $alt/side$. See text for ranges of alt and $side$.

Table 1: Values of the *alt*/*side* ratios that provided the minima for the mean, 50%ile, 95%ile, and 99%ile LDE statistical metrics for immersed sensors.

N	*alt*/*side* **for min 50%ile**	*alt*/*side* **for min Mean**	*alt*/*side* **for min 95%ile**	*alt*/*side* **for min 99%ile**
3	0.25	0.30	0.35	0.55
4	0.10	0.40	0.40	0.60
5	0.05	0.20	0.40	0.65
6	0.05	0.25	0.40	0.40
7	0.05	0.20	0.30	0.35
8	0.05	0.15	0.25	0.40
9	0.05	0.15	0.25	0.30
10	0.05	0.15	0.30	0.60
11	0.05	0.05	0.25	0.40
12	0.05	0.05	0.15	0.45
13	0.05	0.05	0.20	0.40
14	0.05	0.05	0.20	0.45
15	0.05	0.05	0.25	0.30
16	0.05	0.05	0.15	0.40
17	0.05	0.05	0.25	0.35
18	0.05	0.05	0.15	0.40
19	0.05	0.05	0.15	0.35
20	0.05	0.05	0.15	0.35
21	0.05	0.05	0.05	0.35
22	0.05	0.05	0.15	0.25
23	0.05	0.05	0.10	0.15
24	0.05	0.05	0.20	0.40

Table 2: Values of the *alt/side* ratios that provided the minima for the mean, 50%ile, 95%ile, and 99%ile LDE statistical metrics for standoff sensors.

N	*alt/side* **for min 50%ile**	*alt/side* **for min Mean**	*alt/side* **for min 95%ile**	*alt/side* **for min 99%ile**
3	1.00	1.20	1.10	1.60
4	1.10	1.20	1.20	1.20
5	1.00	1.20	1.20	1.50
6	0.90	1.10	1.20	1.40
7	0.90	1.10	1.30	1.30
8	0.90	1.10	1.50	1.50
9	0.90	1.10	1.20	1.40
10	0.90	1.10	1.30	1.50
11	1.00	1.10	1.40	1.60
12	0.90	1.10	1.30	1.50
13	0.90	1.10	1.30	1.60
14	0.90	1.10	1.40	1.70
15	0.90	1.10	1.30	1.70
16	0.90	1.10	1.30	1.50
17	1.00	1.10	1.40	1.30
18	0.90	1.10	1.40	1.60
19	0.80	1.10	1.40	1.40
20	0.90	1.10	1.30	1.50
21	1.00	1.10	1.30	1.50
22	0.90	1.10	1.40	1.70
23	1.00	1.10	1.30	1.40
24	1.00	1.10	1.40	1.60

8 Linear Regression-Based Approximations for Location Distance Error

This section applies linear regression to the results of simulations to gain insight into how LDE statistical metrics improve with increasing numbers of sensors N. Approximations of the LDE statistical metrics as functions of N are obtained for the configurations and error conditions addressed in this paper.

The primary tool used here is linear regression to find models of each of the LDE statistical metrics with respect to the configuration parameters. It is multivariate and is applied the raw and transformed versions of the LDE statistical metrics over sets of input variables consisting of the raw and transformed versions of those variables as well as combinations of those variables. Thus, it is able to uncover certain nonlinear relationships between an output variable and the set of input variables upon which it depends.

8.1 Linear Regression Models and Weighted Sums

The general form of the linear regression model is outlined as follows. In the context of linear regression in this paper, the symbols x and y represent the input and output variables for a statistical model rather than coordinate positions. The symbol y refers to an output variable and x_1, x_2, x_3, $\ldots x_v$ refer to the inputs to a multivariate model with v input variables.

Consider the case of linear regression for an output variable y with respect to a single input variable x_1 (thus, $v = 1$). The slope-intercept formula for a straight line can be written as

$$y = w_0 + w_1 x_1 \tag{21}$$

where w_1 represents the slope of the line and w_0 represents the y-axis intercept of the line. [30] A linear regression of an ordered list of output values y (the dependent variable) as a function of an ordered list of input values x_1 (the independent variable) yields the weights w_1 and w_0 where the weighted sum $y = w_0 + w_1 x_1$ represents the "best straight line" for the relationship between the x_1 values and the y values.

Linear regression can be performed with respect to any number of input variables. With v input variables, linear regression generates $v + 1$ weights w_i, where $i = 0, 1, 2, \ldots v$. These weights are used in a weighted sum to produce the "best hyperplane" $y = w_0 + w_1 x_1 + w_2 x_2 + w_3 x_3 + \ldots + w_v x_v$.

As noted above, linear regression can be performed over raw and transformed versions of variables as well as their combinations. For example, if the candidate model were believed to be power-law,

$$\begin{aligned} y &= \exp(w_0 + w_1 \ln x_1) \\ &= e^{w_0} x_1^{w_1} \quad , \end{aligned} \tag{22}$$

then the linear regression would be performed over the transformed variables $\ln x_1$ and $\ln y$. The resulting statistical model would fit w_0 and w_1 in the expression $\ln y = w_0 + w_1 \ln x_1$ or $y = e^{w_0} {x_1}^{w_1}$ resulting in (22).

[30] The reason for writing the slope-intercept with the intercept first will become clear when applied to multiple input variables.

If it were believed that y^2 might be quadratic polynomial in x_1 and linear with respect to $1/x_2$ and x_1x_2, then linear regression would be performed over the set of input variables x_1^2, x_1, $1/x_2$, x_1x_2 (thus, $v = 4$), and y^2; the resulting model with its $v+1 = 5$ weights would be $y^2 = w_0 + w_1x_1^2 + w_2x_1 + w_3/x_2 + w_4x_1x_2$. [31]

[31] This example is cavalier with its association between the indices of the raw, transformed, and combined versions of the x_i variables and the w_i weights of the linear regression model, but their application should be clear. It seems that this is more clear than to generate more nomenclature and symbols for variables.

8.2 Shotgun Approach to Building Linear Regression Models

The linear regression models presented here were generated for the LDE statistical metrics obtained from 10,000 simulations for each configuration and error conditions using (12) with what can be called a "shotgun approach." The raw configuration parameters N, alt, and $side$ along with transformed versions and combinations of these parameters were explored to determine the variables that had the most significance in the linear regressions. Transformations included logarithm, double logarithm, square, and reciprocal. Among the various combinations used were ratios such as $alt/side$, $(alt/side)^2$, and $side^2/alt$. Note that, since alt could be zero, one millimeter was added to avoid division by zero when alt appeared as the denominator. [32]

The shotgun approach began with a multivariate linear regression in Microsoft Excel spread sheets that first included all of the raw, transformed, and combined input variables that were considered, and then sequentially eliminated variables and combinations that were found to have weights close to zero.

The goodness-of-fit of the linear regression models was determined by their R^2 values. Once a set of candidate linear regression models with the highest or nearly highest R^2 values was obtained, that set was narrowed based on the models' predictive or forecasting power where that factor was determined using **Mean Absolute Percentage Error (MAPE)**. [33]

Models that provided minimum or close to minimum MAPE values were preferred. In addition, it was desired to obtain models that were parsimonious in that they required the smallest possible number of significant input variables while achieving nearly minimum MAPE.

Finally, additional subjective criteria guided the statistical model exploration among several linear regression models that were still viable candidates. These selection criteria included minimizing the **maximum absolute percentage error** and reducing the sizes of the tails of histograms of the percentage error.

[32] That is, the transformed value of altitude $alt + 0.001$ m was used instead of alt.
[33] See definitions of R^2 and MAPE in Section 3.

As noted in Section 6, a minimum of five sensors should be used to avoid a significant fraction of grossly wrong geolocation estimates due to Longfellow Events. Thus, it seemed it should be reasonable to disregard the LDE data for three and four sensors and develop the linear regression models for configurations and error conditions with $N = 5$ to 24 sensors. However, after experimentation the surprising result was observed that the linear regression models gave smaller MAPE for $N = 5$ to 24 sensors when the LDE data for three and four sensors were included, even though the models gave very poor results for the configurations with three and four sensors. The reason for this was unclear but, in any case, the linear regression models reported in this paper were built in this way with the exception of the linear regression models for the "Ballpark Estimates" developed in Section 12.2.

While the final models for the four LDE statistical metrics differed in the specific values of the linear regression weights of the variables, in no case did any one of the LDE statistical metrics require a different set of input variables to achieve a significant improvement in R^2 or MAPE. Thus, all the weighted sums had the same form.

9 Estimating Location Distance Error for Fixed Configurations of Altitude and Search Area Side Length

This section explores four directions. The first is the form of the linear regression model that best fits the LDE data in the Main Data Set. The second is the behavior of LDE for large numbers of sensors to determine whether there is asymptotic behavior at a level greater than zero LDE. The third is to determine whether the number of simulations performed have sufficiently small error bounds to yield results that are statistically significant. Finally, linear regression models are obtained for the simplest case, that of estimating LDE as a function of the number of sensors for specific configurations with fixed nominal altitude and search area side length.

9.1 Linear Regression Models with Double Logarithm Transformations

With some exploration of simulation results in the Main Data Set, it was determined that, for a given altitude and search area side length and sensors both immersed and standoff from the emitter, **the double logarithm of all four LDE statistical metrics varied as a linear function of the double logarithm of the number of sensors**. That is, if the output variable y represents the mean, 50%ile, 95%ile, or 99%ile LDE, then, for a given configuration and error conditions, there exist linear regression weights w_0 and w_1 such that the expression

$$\ln\ln y = w_0 + w_1 \ln\ln N \tag{23}$$

is a good approximation. Expression (23) can be solved for y and expressed as the forms

$$\begin{aligned} y &= \exp(\exp(w_0 + w_1 \ln\ln N)) \\ &= e^{e^{w_0 + w_1 \ln\ln N}} \\ &= e^{e^{w_0} \ln^{w_1} N} \end{aligned} \tag{24}$$

but the alternate expressions in (24) probably do not provide any insight beyond that already apparent in (23).

9.2 LDE and Its Error Bounds for Very Large Numbers of Sensors

Sets of configurations were simulated where the number of sensors ranged from $N = 3$ to 100 with $side$ = 1,000 m and alt = 0 m and 300 m. The Standard Error Conditions of $\sigma_{pos} = 10$ m position error and $\sigma_{time} = 30$ ns timing error were used.

Due to the long run times resulting from quadratic growth with N, only 1,000 simulations of each configuration were performed.

Figure 54 shows the mean and 95%ile LDE for immersed sensors on the ground. In addition, the ±3 standard error bounds [34] around the mean are shown. Figure 55 shows the same results plotted as the double logarithms for N and the mean and 95%ile LDE. It is clear that with 1,000 simulations per configuration the ±3 standard error bounds are extremely tight about the mean LDE for each value of N. Also, the double logarithm plot on both axes demonstrates the very nearly linear decrease in mean and 95%ile LDE with respect to N for those transformed variables. A slight bending of both curves can be observed starting around the value of 1.2 for $\ln \ln N$, which corresponds to $N = 28$ sensors but, as this paper develops models for up to only 24 sensors, this indicates that linearity of the double logarithm relationships can safely be assumed.

Figure 56 and Figure 57 show the results for standoff sensors on the ground for the same parameters as above. Again, the ±3 standard error bounds are extremely tight about the mean LDE and both the mean and 95%ile LDE show linear decrease with increasing N.

Similar behavior is shown for immersed sensors at nominal altitudes of 300 m as shown in Figure 58 and Figure 59 for immersed sensors and in Figure 60 and Figure 61 for standoff sensors.

Most of the results presented in this paper are based on 10,000 simulations per configuration, so the tightness of the ±3 standard error bounds for the results from only 1,000 simulations per configuration support the

[34] The statistical term "standard error" refers to the standard deviation of a set of samples divided by the square root of the number of samples [Altman (2015)] [Weisstein (2019b)]. This term is not to be confused with the term "Standard Error Conditions" as defined in this paper.

statistical validity of this approach. They also indicate that the linearity of the relationship between double logarithm transformations of the LDE statistical metrics and the number of sensors holds for the parameter ranges of interest. Finally, there is no indication of convergence to an asymptotic LDE greater than zero; thus, more sensors are always better than fewer.

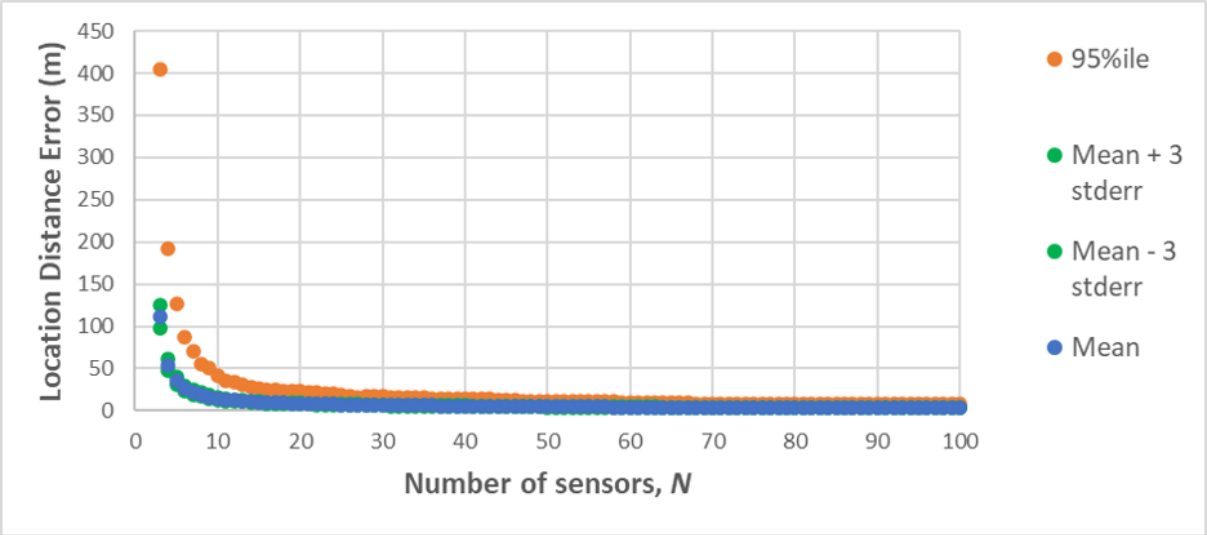

Figure 54: Mean and 95%ile LDE, with ±3 standard error bounds around the mean LDE. Parameters: $N = 3$ to 100 immersed sensors, $side$ = 1,000 m, alt = 0 m, with errors.

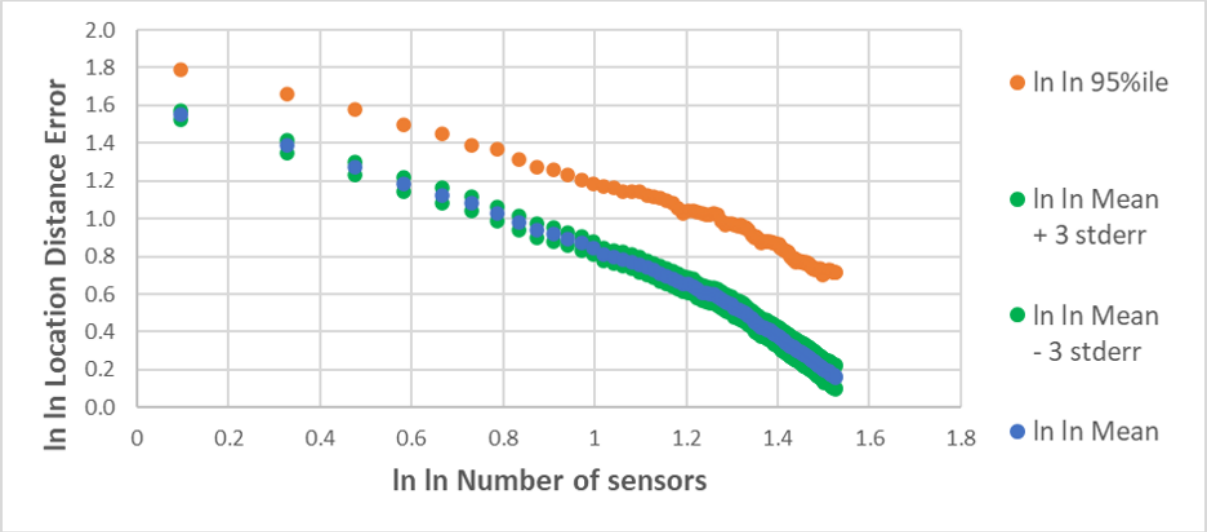

Figure 55: Configurations and conditions are the same as for Figure 54. The values plotted are for the double logarithms of N and LDE.

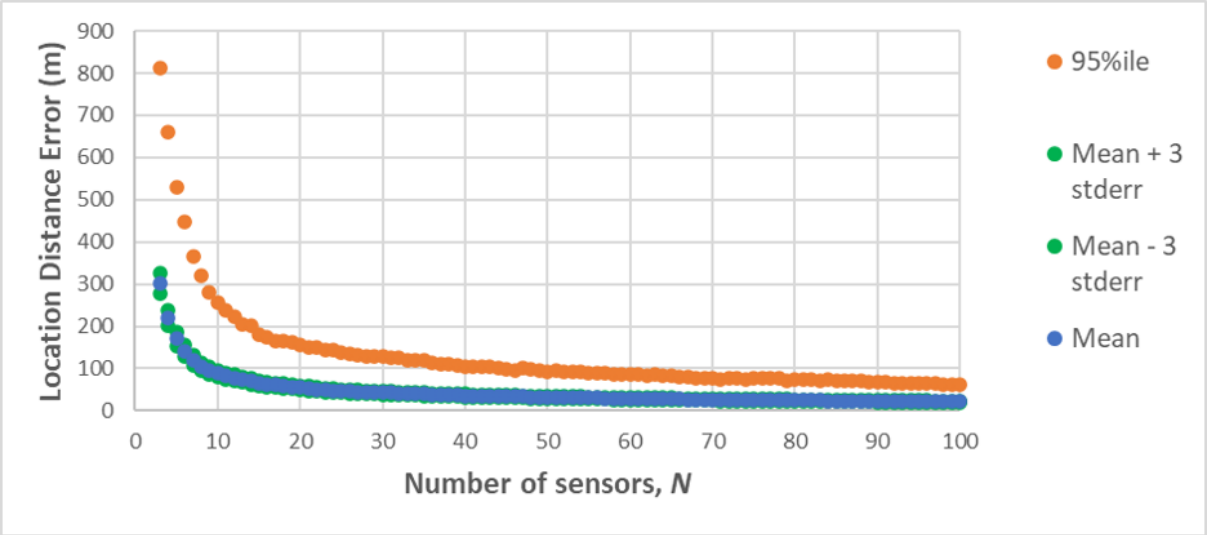

Figure 56: Mean and 95%ile LDE, with ±3 standard error bounds around the mean LDE. Parameters: $N = 3$ to 100 standoff sensors, $side$ = 1,000 m, alt = 0 m, with errors.

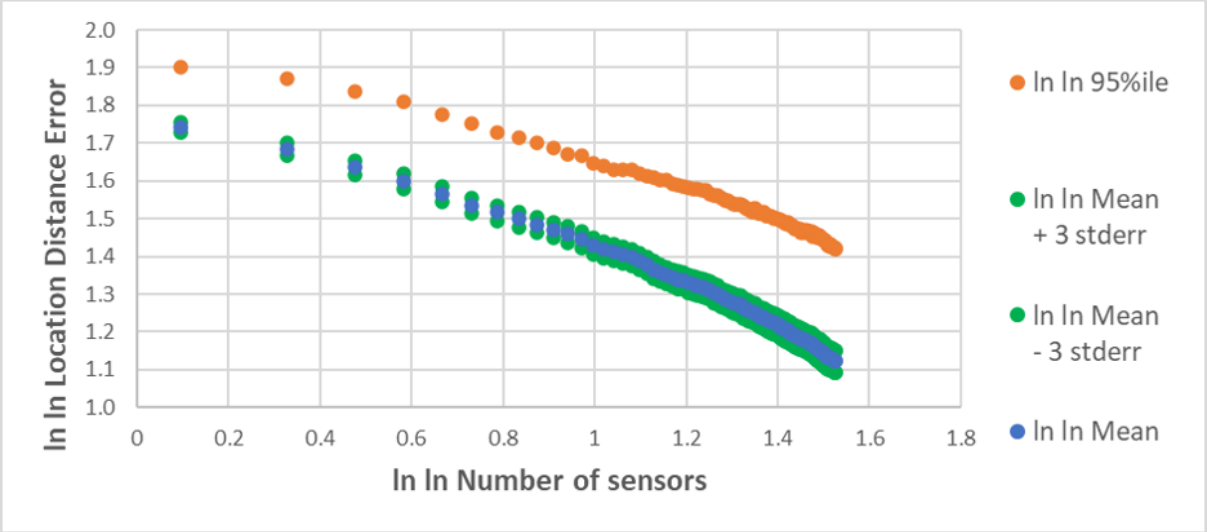

Figure 57: Configurations and conditions are the same as for Figure 56. The values plotted are for the double logarithms of N and LDE.

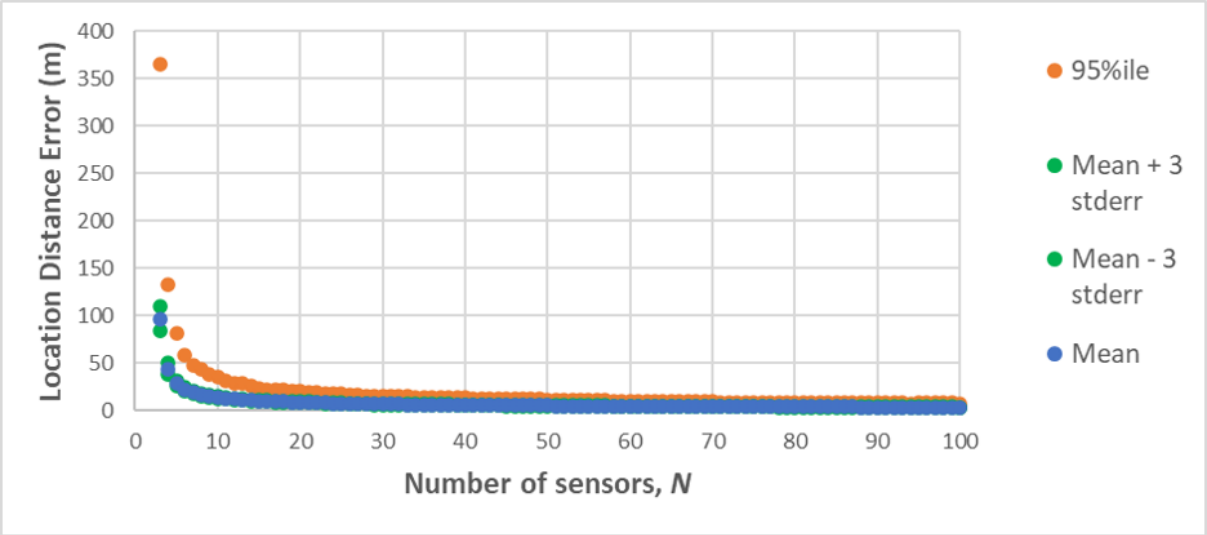

Figure 58: Mean and 95%ile LDE, with ±3 standard error bounds around the mean LDE. Parameters: $N = 3$ to 100 immersed sensors, $side$ = 1,000 m, alt = 300 m, with errors.

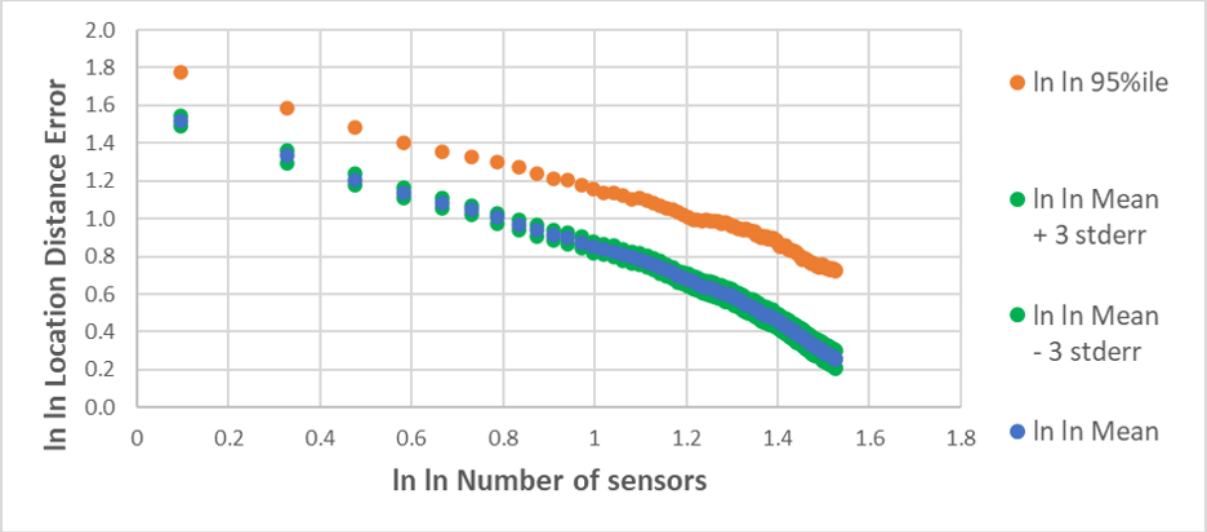

Figure 59: Configurations and conditions are the same as for Figure 58. The values plotted are for the double logarithms of N and LDE.

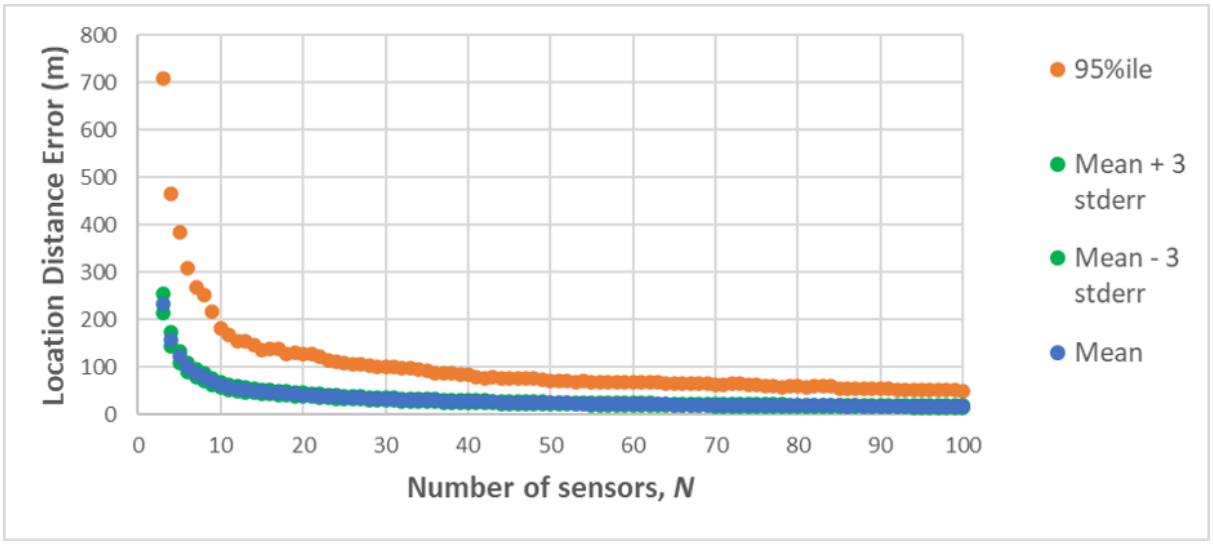

Figure 60: Mean and 95%ile LDE, with ±3 standard error bounds around the mean LDE. Parameters: $N = 3$ to 100 standoff sensors, $side = 1{,}000$ m, $alt = 300$ m, with errors.

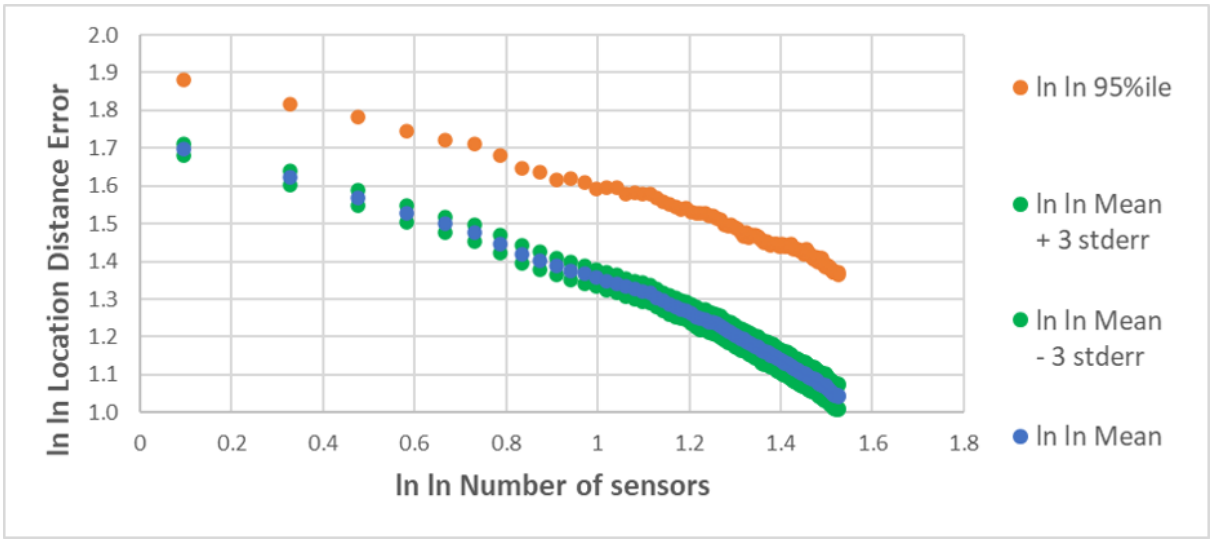

Figure 61: Configurations and conditions are the same as for Figure 60. The values plotted are for the double logarithms of N and LDE.

9.3 Linear Regression Models for Fixed Configurations of Altitude and Search Area Side Length

This section explores the linearity of the double logarithm relationships between the four LDE statistical metrics and the number of sensors, with the appropriate weights, as expressed in (23). All of the results presented in this section are based on the Main Data Set as described in Section 4.3.

The linear regression models are developed for specific configurations with fixed nominal altitude and search area length. These models are generalized in Section 10.1.

Figure 62 shows the four LDE statistical metrics on linear scales for immersed sensors at $alt = 0$ m for $side = 1{,}000$ m with the Standard Error Conditions of $\sigma_{pos} = 10$ m position error and $\sigma_{time} = 30$ ns timing error; Figure 63 shows the same results on double logarithm scales. All four curves show linearity after the double logarithm transformations. The linear regression equations resulting from Microsoft Excel are shown on the plot, along with the associated R^2 coefficients of determination. In the notation of this paper, Figure 63 shows, for example, that the double logarithm of the mean LDE is approximately $1.6528 - 0.8154 \ln\ln N$ and the double logarithm of the 95%ile LDE is approximately $1.8918 - 0.6940 \ln\ln N$. In both of these cases, the R^2 values are nearly unity (0.9984 and 0.9985, respectively) signifying excellent goodness-of-fit of the regression models.

Figure 64 and Figure 65 show the simulation results for standoff sensors on the ground and otherwise the same configurations and error conditions as above. Again, the R^2 values are nearly unity showing good statistical fit of the linear regression for the transformed variables. Note the shallower slope of the regression lines in Figure 65 compared to Figure 63; this shows that, even though the LDE statistical metrics decrease with increasing numbers of sensors that are both immersed and standoff, the decrease for standoff sensors is much slower than for immersed sensors.

Figure 66 and Figure 67 show the simulation results for immersed sensors at $alt = 300$ m and otherwise the same configurations and error conditions as above and Figure 68 and Figure 69 show the simulation results for standoff sensors at $alt = 300$ m and otherwise the same configurations and error conditions as above. The same trends noted above are observed here.

The results outlined in Figure 62 through Figure 69 are systematically expanded upon in Table 3 through Table 14. These tables present the linear regression weights w_0 and w_1 derived for (23), which is the linear approximation for the double logarithm of the four LDE statistical metrics with respect to the double logarithm of the number of immersed and standoff sensors. The tables are valid for the numbers of sensors, the altitudes, search area side lengths, and error conditions represented in the Main Data Set. All results are based on 10,000 simulations per configuration. Due to formatting constraints in LaTeX, separate tables were provided for the *side* ranges 1,000 m to 4,000 m, 5,000 m to 8,000 m, and 9,000 m to 10,000 m. The mean and 95%ile LDE linear regression weights are shown together and the 50%ile and 99%ile linear regression weights are shown together.

For example, Table 3 shows the linear regression weights for mean and 95%ile LDE linear regression weights for immersed sensors in search areas with $side$ = 1,000 m to 4,000 m. The first line of the table is for alt = 0 m and $side$ = 1,000 m. The linear regression weights w_0 and w_1 reported for the regression lines for those LDE statistical metrics on that line are the same as those shown in Figure 63 for the same configurations and error conditions.

A quick scan of the R^2 columns in Table 3 through Table 14 show that the minimum R^2 for any LDE statistical metric is 0.9880 for immersed sensors and 0.9532 for standoff sensors; only 3.07% of the combined set of R^2 values are below 0.99. This indicates an excellent goodness-of-fit for the linear relationship expressed in (23).

Table 3 through Table 14 and (23) are applied as follows.

For example, consider the problem of estimating the mean LDE for the configuration of N = 8 immersed sensors with alt = 300 m and $side$ = 5,000 m; denote the value of that statistical metric by y. For the mean LDE, Table 4 provides the weights w_0 = 1.7593 and w_1 = -0.9498. These weights are substituted into (23) to obtain $\ln\ln y = 1.7593 - 0.9498 \ln\ln 8 = 1.0640$. Solving for y, the estimate for the mean LDE based on linear regressions for this configuration is 18.13 m.

For comparison, the measured mean LDE resulting from 10,000 simulations of this configuration was 17.64 m, so the error of the linear regression estimate for the mean LDE relative to the measured value was 2.81%. [35]

The predictive power of these individual regression models was found to be excellent. As noted in Section 6, a minimum of five sensors should be used to avoid a significant fraction of grossly wrong geolocation estimates due to Longfellow Events. For $N = 5$ to 24 sensors, the four LDE statistical metrics were calculated using the linear regression weights tabulated for each *alt* and *side* and compared to the results of the 10,000 simulations of those configurations and error conditions. For immersed sensors, the MAPE values were 2.18%, 3.20%, 1.96%, and 3.82% for the mean, 50%ile, 95%ile, and 99%ile LDE, respectively. For standoff sensors, the MAPE values were 1.08%, 1.69%, 1.43%, and 2.47% for the same statistical metrics. This demonstrated that the regression models based on specific configurations had good predictive power for the decrease in LDE as a result of increasing the number of sensors.

The linear regression models presented in this section are point solutions for the central question posed in this paper. Section 10.1 uses these tabulated values as the first stage of a two-stage linear regression model that arrives at a generalized set of expressions for the relationship between the number of sensors and the LDE statistical metrics.

[35] The error calculations given in this paper are generally those derived from the spread sheet calculations of the linear regression models. The error for the estimate of "18.13 m" relative to the measured value of 17.64 m would be 2.78%, but the error was calculated on the basis of the value "18.13485 m" in the spread sheet.

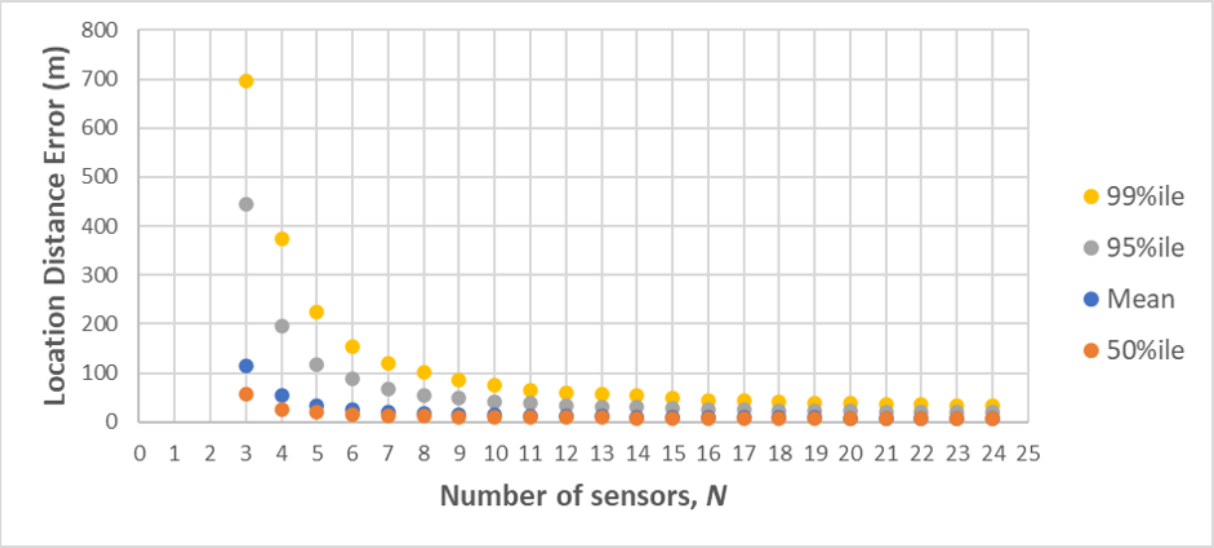

Figure 62: Mean, 50%ile, 95%ile, and 99%ile LDE. Parameters: N = 3 to 24 immersed sensors, *side* = 1,000 m, *alt* = 0 m, with errors.

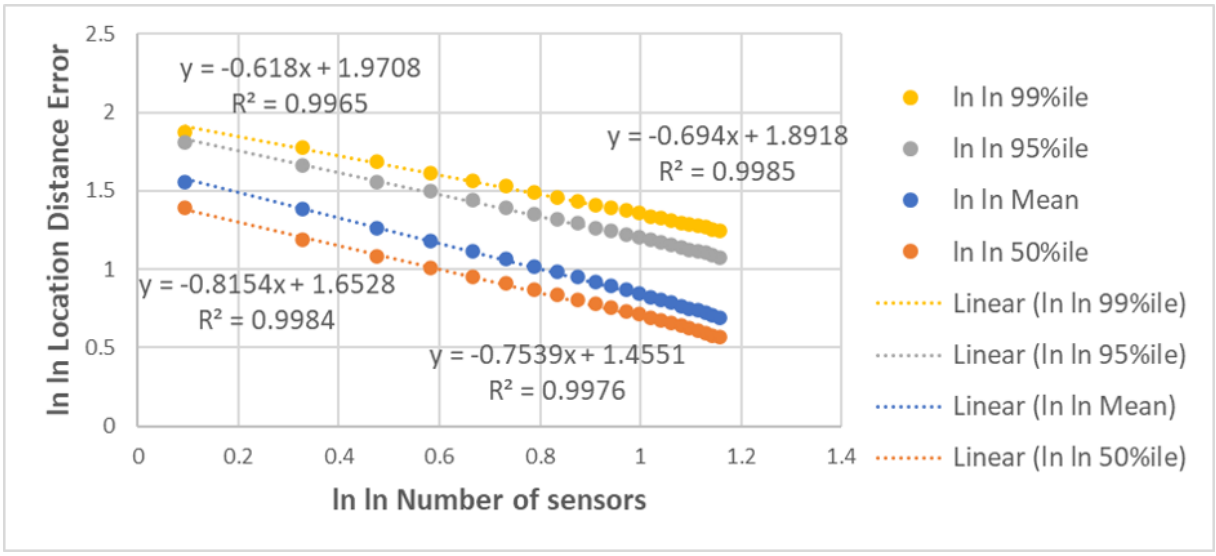

Figure 63: Configurations and conditions are the same as for Figure 62. The values plotted are for the double logarithms of N and LDE. Linear regression trend lines for the double logarithm transformations are shown.

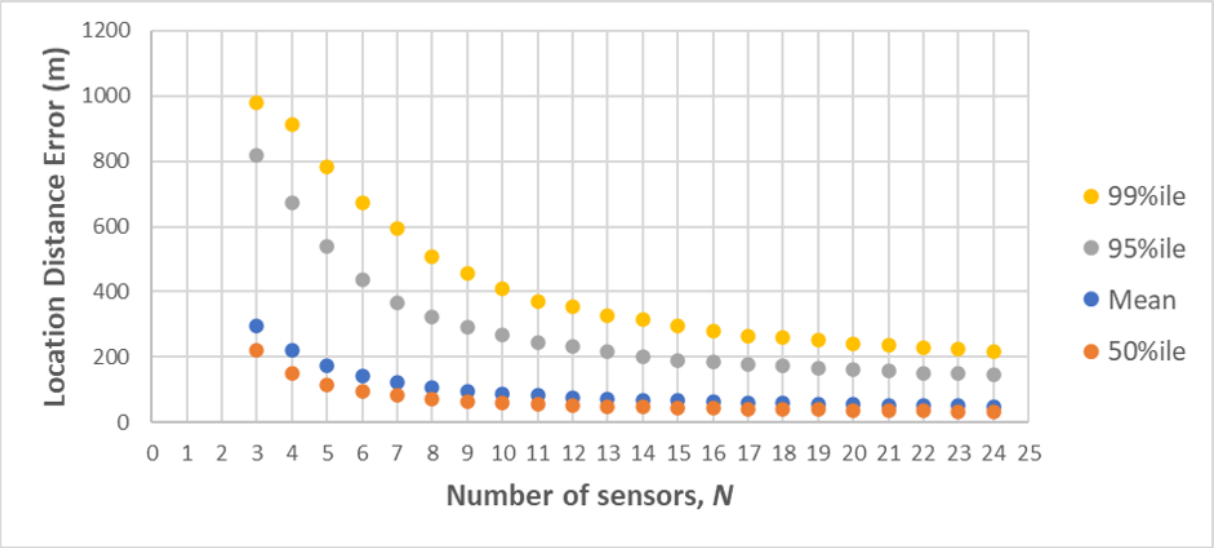

Figure 64: Mean, 50%ile, 95%ile, and 99%ile LDE. Parameters: $N = 3$ to 24 standoff sensors, $side = 1{,}000$ m, $alt = 0$ m, with errors.

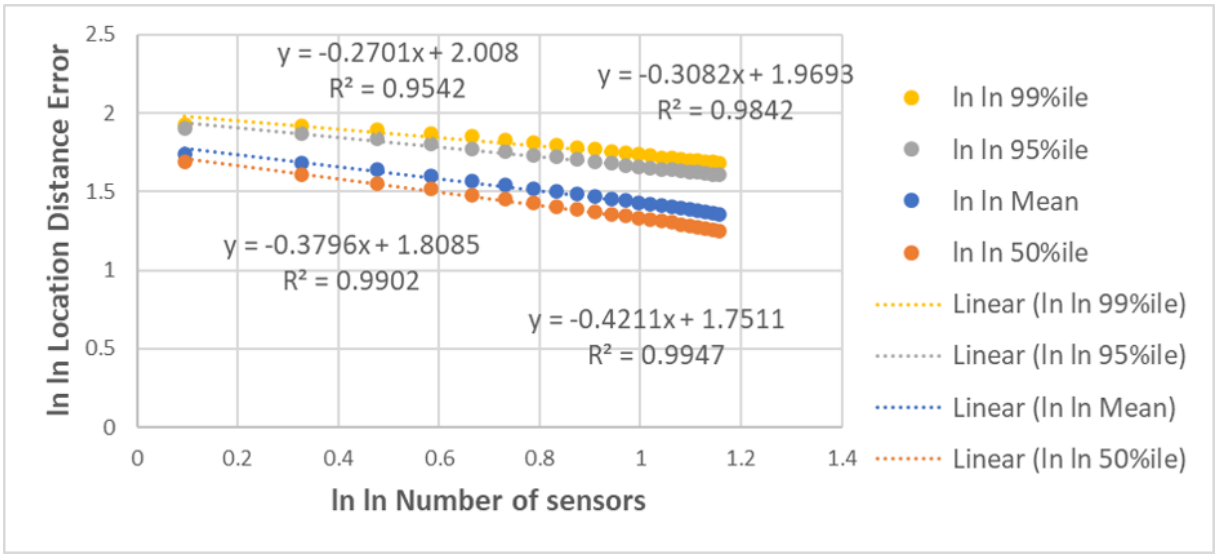

Figure 65: Configurations and conditions are the same as for Figure 64. The values plotted are for the double logarithms of N and LDE. Linear regression trend lines for the double logarithm transformations are shown.

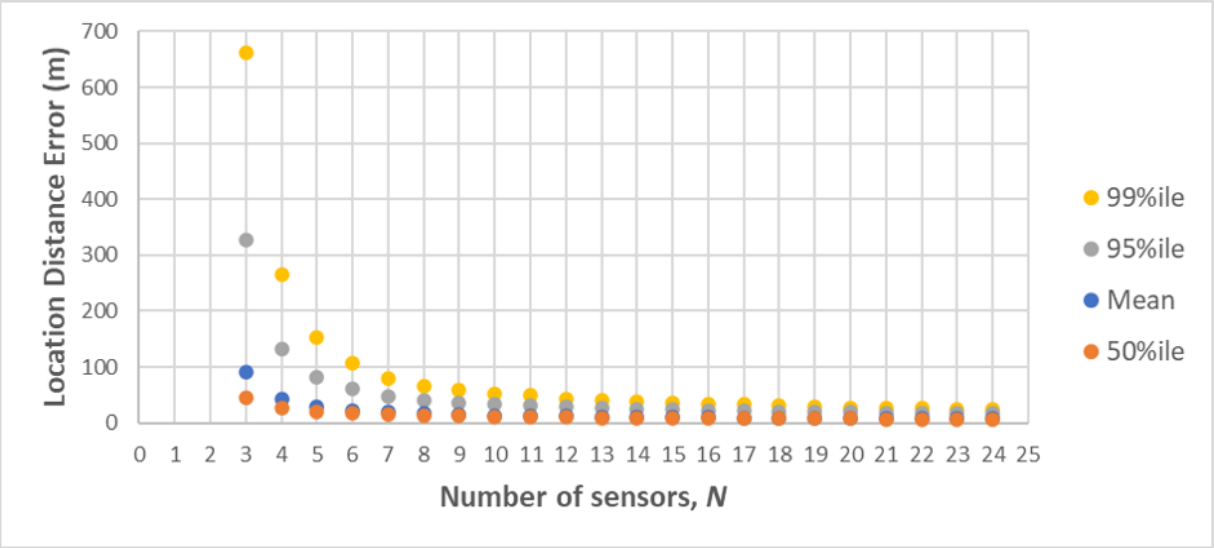

Figure 66: Mean, 50%ile, 95%ile, and 99%ile LDE. Parameters: N = 3 to 24 immersed sensors, *side* = 1,000 m, *alt* = 300 m, with errors.

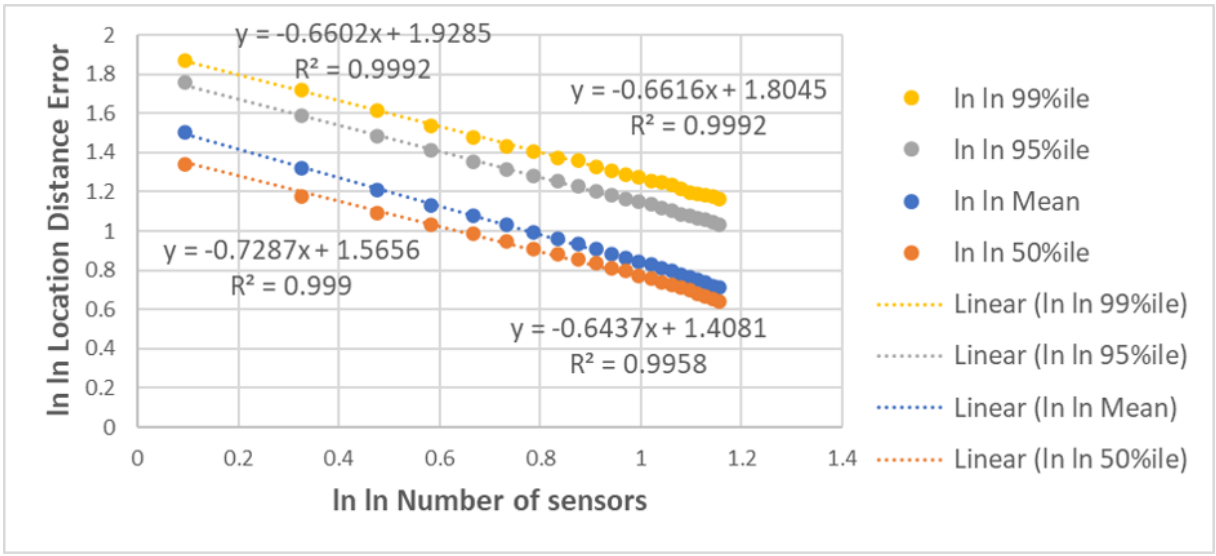

Figure 67: Configurations and conditions are the same as for Figure 66. The values plotted are for the double logarithms of N and LDE. Linear regression trend lines for the double logarithm transformations are shown.

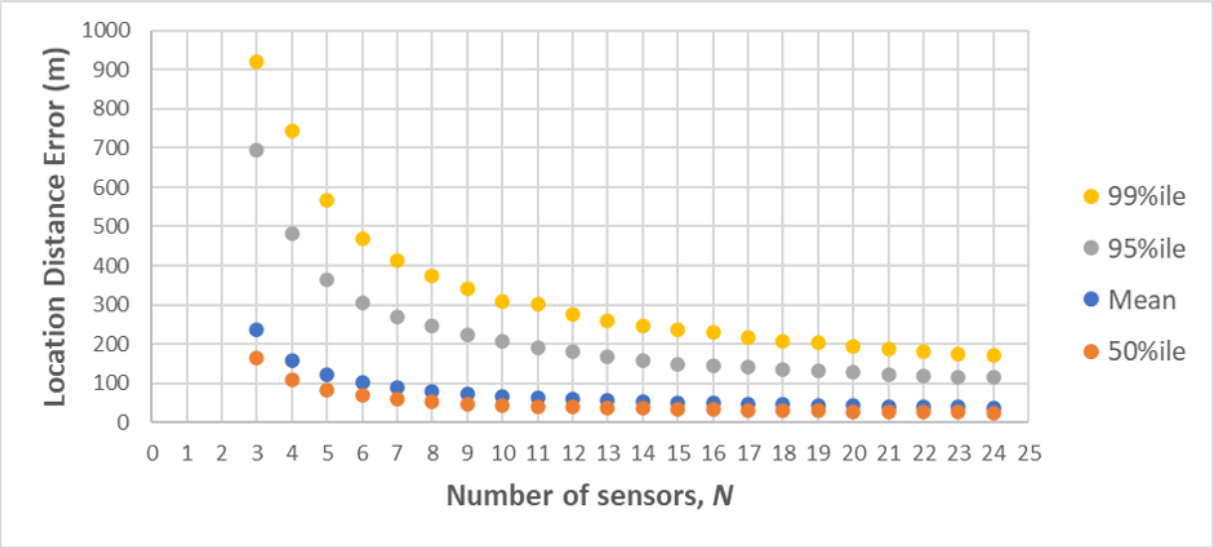

Figure 68: Mean, 50%ile, 95%ile, and 99%ile LDE. Parameters: N = 3 to 24 standoff sensors, $side$ = 1,000 m, alt = 300 m, with errors.

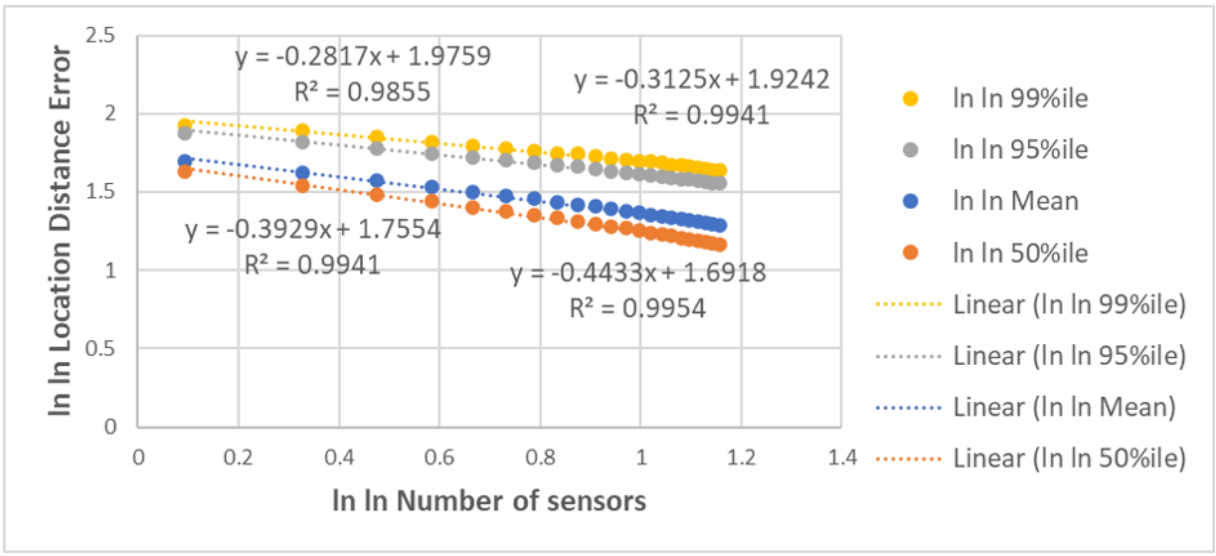

Figure 69: Configurations and conditions are the same as for Figure 68. The values plotted are for the double logarithms of N and LDE. Linear regression trend lines for the double logarithm transformations are shown.

Table 3: Linear regression models for immersed sensors for individual *alt* and *side*: Mean and 95%ile LDE for *side* = 1,000 m to 4,000 m.

alt **(m)**	*side* **(m)**		**Mean** $\ln\ln N$ w_1	**Mean** w_0	**Mean** R^2		**95%ile** $\ln\ln N$ w_1	**95%ile** w_0	**95%ile** R^2
0	1000		-0.8154	1.6528	0.9984		-0.6940	1.8918	0.9985
100	1000		-0.8141	1.6165	0.9988		-0.7016	1.8598	0.9993
200	1000		-0.7716	1.5875	0.9991		-0.6857	1.8305	0.9997
300	1000		-0.7287	1.5656	0.9990		-0.6616	1.8045	0.9992
400	1000		-0.6939	1.5570	0.9987		-0.6415	1.7917	0.9979
500	1000		-0.6663	1.5584	0.9983		-0.6222	1.7864	0.9965
600	1000		-0.6405	1.5624	0.9981		-0.6057	1.7875	0.9954
700	1000		-0.6187	1.5699	0.9981		-0.5886	1.7900	0.9956
800	1000		-0.5993	1.5787	0.9981		-0.5770	1.7978	0.9957
900	1000		-0.5819	1.5881	0.9981		-0.5627	1.8034	0.9956
1000	1000		-0.5663	1.5977	0.9981		-0.5493	1.8095	0.9955
0	2000		-0.8728	1.7188	0.9995		-0.7455	1.9544	0.9996
100	2000		-0.8943	1.6987	0.9995		-0.7653	1.9386	0.9996
200	2000		-0.8671	1.6762	0.9994		-0.7517	1.9177	0.9994
300	2000		-0.8410	1.6551	0.9990		-0.7411	1.8987	0.9987
400	2000		-0.8174	1.6383	0.9985		-0.7325	1.8832	0.9980
500	2000		-0.7914	1.6212	0.9980		-0.7192	1.8660	0.9976
600	2000		-0.7697	1.6102	0.9975		-0.7051	1.8522	0.9962
700	2000		-0.7485	1.6013	0.9972		-0.6915	1.8406	0.9955
800	2000		-0.7294	1.5955	0.9967		-0.6786	1.8321	0.9943
900	2000		-0.7126	1.5927	0.9963		-0.6671	1.8266	0.9934
1000	2000		-0.6975	1.5920	0.9960		-0.6547	1.8219	0.9921
0	3000		-0.9030	1.7519	0.9995		-0.7744	1.9854	0.9993
100	3000		-0.9316	1.7370	0.9994		-0.7989	1.9760	0.9993
200	3000		-0.9118	1.7200	0.9992		-0.7872	1.9605	0.9989
300	3000		-0.8927	1.7039	0.9990		-0.7777	1.9457	0.9984
400	3000		-0.8731	1.6876	0.9987		-0.7686	1.9312	0.9979
500	3000		-0.8567	1.6748	0.9980		-0.7628	1.9196	0.9968
600	3000		-0.8404	1.6629	0.9973		-0.7545	1.9069	0.9961
700	3000		-0.8228	1.6509	0.9967		-0.7474	1.8963	0.9951
800	3000		-0.8088	1.6433	0.9959		-0.7393	1.8871	0.9940
900	3000		-0.7918	1.6335	0.9955		-0.7279	1.8763	0.9936
1000	3000		-0.7775	1.6270	0.9950		-0.7156	1.8650	0.9931
0	4000		-0.9222	1.7725	0.9992		-0.7910	2.0033	0.9985
100	4000		-0.9557	1.7618	0.9991		-0.8168	1.9960	0.9985
200	4000		-0.9427	1.7507	0.9988		-0.8124	1.9893	0.9978
300	4000		-0.9262	1.7362	0.9984		-0.8020	1.9750	0.9975
400	4000		-0.9110	1.7233	0.9981		-0.7934	1.9623	0.9972
500	4000		-0.8973	1.7120	0.9977		-0.7883	1.9530	0.9966
600	4000		-0.8807	1.6979	0.9973		-0.7803	1.9409	0.9954
700	4000		-0.8692	1.6892	0.9967		-0.7755	1.9320	0.9949
800	4000		-0.8567	1.6800	0.9958		-0.7694	1.9226	0.9938
900	4000		-0.8449	1.6722	0.9952		-0.7635	1.9142	0.9928
1000	4000		-0.8311	1.6630	0.9947		-0.7553	1.9043	0.9928

Table 4: Linear regression models for immersed sensors for individual *alt* and *side*: Mean and 95%ile LDE for *side* = 5,000 m to 8,000 m.

alt **(m)**	*side* **(m)**		**Mean** $\ln\ln N$ w_1	**Mean** w_0	**Mean** R^2		**95%ile** $\ln\ln N$ w_1	**95%ile** w_0	**95%ile** R^2
0	5000		-0.9366	1.7876	0.9987		-0.8041	2.0172	0.9973
100	5000		-0.9729	1.7794	0.9986		-0.8298	2.0102	0.9972
200	5000		-0.9621	1.7701	0.9984		-0.8237	2.0025	0.9971
300	5000		-0.9498	1.7593	0.9980		-0.8181	1.9943	0.9965
400	5000		-0.9364	1.7475	0.9975		-0.8106	1.9834	0.9959
500	5000		-0.9253	1.7381	0.9971		-0.8076	1.9770	0.9955
600	5000		-0.9115	1.7263	0.9969		-0.7969	1.9634	0.9954
700	5000		-0.9006	1.7172	0.9965		-0.7933	1.9566	0.9941
800	5000		-0.8905	1.7091	0.9957		-0.7903	1.9496	0.9931
900	5000		-0.8789	1.6999	0.9951		-0.7854	1.9420	0.9924
1000	5000		-0.8683	1.6920	0.9946		-0.7789	1.9326	0.9925
0	6000		-0.9493	1.8008	0.9981		-0.8136	2.0276	0.9962
100	6000		-0.9849	1.7915	0.9981		-0.8388	2.0203	0.9961
200	6000		-0.9776	1.7853	0.9978		-0.8361	2.0160	0.9959
300	6000		-0.9690	1.7780	0.9973		-0.8323	2.0106	0.9952
400	6000		-0.9573	1.7677	0.9969		-0.8243	2.0000	0.9950
500	6000		-0.9465	1.7583	0.9966		-0.8177	1.9905	0.9945
600	6000		-0.9365	1.7498	0.9961		-0.8168	1.9867	0.9940
700	6000		-0.9254	1.7401	0.9959		-0.8111	1.9788	0.9937
800	6000		-0.9156	1.7319	0.9953		-0.8043	1.9692	0.9925
900	6000		-0.9042	1.7221	0.9950		-0.7993	1.9610	0.9922
1000	6000		-0.8956	1.7152	0.9944		-0.7972	1.9560	0.9915
0	7000		-0.9576	1.8096	0.9976		-0.8214	2.0358	0.9952
100	7000		-0.9959	1.8027	0.9974		-0.8469	2.0289	0.9950
200	7000		-0.9913	1.7989	0.9972		-0.8465	2.0273	0.9949
300	7000		-0.9805	1.7892	0.9968		-0.8403	2.0197	0.9946
400	7000		-0.9735	1.7833	0.9962		-0.8371	2.0146	0.9937
500	7000		-0.9633	1.7743	0.9958		-0.8322	2.0074	0.9934
600	7000		-0.9535	1.7658	0.9957		-0.8250	1.9977	0.9929
700	7000		-0.9468	1.7601	0.9948		-0.8265	1.9967	0.9922
800	7000		-0.9368	1.7515	0.9945		-0.8215	1.9892	0.9919
900	7000		-0.9263	1.7423	0.9944		-0.8143	1.9799	0.9915
1000	7000		-0.9174	1.7347	0.9941		-0.8074	1.9711	0.9912
0	8000		-0.9667	1.8189	0.9969		-0.8288	2.0437	0.9939
100	8000		-1.0059	1.8127	0.9968		-0.8553	2.0376	0.9934
200	8000		-1.0001	1.8077	0.9967		-0.8528	2.0342	0.9938
300	8000		-0.9926	1.8010	0.9963		-0.8510	2.0313	0.9933
400	8000		-0.9860	1.7955	0.9958		-0.8472	2.0261	0.9926
500	8000		-0.9775	1.7878	0.9954		-0.8422	2.0190	0.9923
600	8000		-0.9678	1.7793	0.9953		-0.8360	2.0106	0.9922
700	8000		-0.9601	1.7726	0.9947		-0.8326	2.0050	0.9915
800	8000		-0.9547	1.7683	0.9940		-0.8329	2.0033	0.9908
900	8000		-0.9459	1.7605	0.9935		-0.8286	1.9968	0.9906
1000	8000		-0.9377	1.7535	0.9934		-0.8238	1.9902	0.9902

Table 5: Linear regression models for immersed sensors for individual *alt* and *side*: Mean and 95%ile LDE for *side* = 9,000 m and 10,000 m.

alt **(m)**	*side* **(m)**		**Mean** $\ln\ln N$ w_1	**Mean** w_0	**Mean** R^2		**95%ile** $\ln\ln N$ w_1	**95%ile** w_0	**95%ile** R^2
0	9000		-0.9740	1.8264	0.9963		-0.8357	2.0509	0.9930
100	9000		-1.0131	1.8200	0.9963		-0.8604	2.0429	0.9925
200	9000		-1.0107	1.8181	0.9959		-0.8616	2.0434	0.9920
300	9000		-1.0033	1.8115	0.9957		-0.8572	2.0381	0.9923
400	9000		-0.9963	1.8055	0.9953		-0.8534	2.0331	0.9919
500	9000		-0.9907	1.8007	0.9946		-0.8519	2.0302	0.9908
600	9000		-0.9822	1.7931	0.9946		-0.8445	2.0211	0.9912
700	9000		-0.9728	1.7846	0.9944		-0.8423	2.0166	0.9908
800	9000		-0.9666	1.7794	0.9937		-0.8392	2.0116	0.9901
900	9000		-0.9604	1.7740	0.9930		-0.8366	2.0073	0.9900
1000	9000		-0.9510	1.7657	0.9926		-0.8326	2.0013	0.9898
0	10000		-0.9800	1.8325	0.9958		-0.8409	2.0563	0.9921
100	10000		-1.0195	1.8264	0.9957		-0.8656	2.0482	0.9916
200	10000		-1.0175	1.8249	0.9955		-0.8661	2.0483	0.9916
300	10000		-1.0125	1.8206	0.9953		-0.8641	2.0455	0.9914
400	10000		-1.0041	1.8130	0.9950		-0.8597	2.0402	0.9912
500	10000		-1.0011	1.8108	0.9942		-0.8594	2.0386	0.9900
600	10000		-0.9937	1.8041	0.9937		-0.8550	2.0326	0.9897
700	10000		-0.9854	1.7967	0.9936		-0.8486	2.0246	0.9897
800	10000		-0.9777	1.7898	0.9933		-0.8457	2.0199	0.9895
900	10000		-0.9738	1.7866	0.9923		-0.8475	2.0195	0.9880
1000	10000		-0.9660	1.7797	0.9922		-0.8422	2.0128	0.9885

Table 6: Linear regression models for immersed sensors for individual *alt* and *side*: 50%ile and 99%ile LDE for *side* = 1,000 m to 4,000 m.

alt **(m)**	*side* **(m)**		**50%ile** $\ln\ln N$ w_1	**50%ile** w_0	**50%ile** R^2		**99%ile** $\ln\ln N$ w_1	**99%ile** w_0	**99%ile** R^2
0	1000		-0.7539	1.4551	0.9976		-0.6180	1.9708	0.9965
100	1000		-0.7445	1.4248	0.9965		-0.6494	1.9599	0.9981
200	1000		-0.6864	1.4099	0.9959		-0.6630	1.9474	0.9983
300	1000		-0.6437	1.4081	0.9958		-0.6602	1.9285	0.9992
400	1000		-0.6108	1.4150	0.9959		-0.6470	1.9114	0.9984
500	1000		-0.5866	1.4277	0.9962		-0.6465	1.9147	0.9968
600	1000		-0.5630	1.4398	0.9960		-0.6332	1.9112	0.9959
700	1000		-0.5446	1.4548	0.9959		-0.6231	1.9148	0.9948
800	1000		-0.5291	1.4705	0.9960		-0.6106	1.9173	0.9951
900	1000		-0.5138	1.4842	0.9962		-0.6002	1.9225	0.9952
1000	1000		-0.4999	1.4971	0.9962		-0.5885	1.9272	0.9957
0	2000		-0.7703	1.4741	0.9974		-0.6918	2.0580	0.9985
100	2000		-0.7928	1.4555	0.9971		-0.7034	2.0423	0.9988
200	2000		-0.7602	1.4429	0.9969		-0.7130	2.0370	0.9992
300	2000		-0.7267	1.4311	0.9965		-0.7120	2.0221	0.9988
400	2000		-0.6985	1.4240	0.9964		-0.7251	2.0189	0.9985
500	2000		-0.6731	1.4195	0.9962		-0.7183	2.0013	0.9978
600	2000		-0.6512	1.4181	0.9960		-0.7154	1.9910	0.9967
700	2000		-0.6331	1.4202	0.9963		-0.7037	1.9760	0.9960
800	2000		-0.6176	1.4239	0.9962		-0.6983	1.9684	0.9949
900	2000		-0.6055	1.4304	0.9964		-0.6969	1.9675	0.9935
1000	2000		-0.5938	1.4369	0.9965		-0.6934	1.9651	0.9928
0	3000		-0.7768	1.4814	0.9972		-0.7287	2.0983	0.9991
100	3000		-0.8053	1.4638	0.9970		-0.7404	2.0864	0.9987
200	3000		-0.7856	1.4551	0.9971		-0.7383	2.0762	0.9989
300	3000		-0.7647	1.4483	0.9970		-0.7395	2.0679	0.9988
400	3000		-0.7412	1.4392	0.9966		-0.7385	2.0598	0.9984
500	3000		-0.7204	1.4327	0.9965		-0.7437	2.0541	0.9974
600	3000		-0.7026	1.4289	0.9966		-0.7470	2.0459	0.9972
700	3000		-0.6843	1.4248	0.9963		-0.7468	2.0368	0.9962
800	3000		-0.6695	1.4235	0.9963		-0.7452	2.0292	0.9947
900	3000		-0.6547	1.4221	0.9962		-0.7419	2.0211	0.9942
1000	3000		-0.6425	1.4232	0.9964		-0.7351	2.0112	0.9927
0	4000		-0.7810	1.4859	0.9969		-0.7509	2.1231	0.9989
100	4000		-0.8137	1.4707	0.9969		-0.7673	2.1155	0.9987
200	4000		-0.8026	1.4666	0.9969		-0.7658	2.1103	0.9985
300	4000		-0.7828	1.4565	0.9971		-0.7643	2.1020	0.9981
400	4000		-0.7678	1.4517	0.9968		-0.7612	2.0916	0.9980
500	4000		-0.7497	1.4445	0.9965		-0.7597	2.0846	0.9973
600	4000		-0.7336	1.4392	0.9965		-0.7572	2.0747	0.9969
700	4000		-0.7188	1.4349	0.9965		-0.7632	2.0716	0.9958
800	4000		-0.7053	1.4319	0.9965		-0.7685	2.0690	0.9951
900	4000		-0.6913	1.4288	0.9964		-0.7709	2.0645	0.9947
1000	4000		-0.6788	1.4260	0.9964		-0.7689	2.0573	0.9938

Table 7: Linear regression models for immersed sensors for individual *alt* and *side*: 50%ile and 99%ile LDE for *side* = 5,000 m to 8,000 m.

alt **(m)**	*side* **(m)**		**50%ile** $\ln\ln N$ w_1	**50%ile** w_0	**50%ile** R^2		**99%ile** $\ln\ln N$ w_1	**99%ile** w_0	**99%ile** R^2
0	5000		-0.7841	1.4890	0.9968		-0.7700	2.1425	0.9988
100	5000		-0.8175	1.4734	0.9967		-0.7865	2.1359	0.9981
200	5000		-0.8092	1.4699	0.9966		-0.7856	2.1323	0.9981
300	5000		-0.7958	1.4633	0.9969		-0.7830	2.1257	0.9978
400	5000		-0.7821	1.4580	0.9970		-0.7775	2.1146	0.9974
500	5000		-0.7701	1.4542	0.9968		-0.7776	2.1092	0.9968
600	5000		-0.7553	1.4483	0.9965		-0.7714	2.0977	0.9967
700	5000		-0.7417	1.4433	0.9965		-0.7713	2.0929	0.9961
800	5000		-0.7297	1.4397	0.9965		-0.7744	2.0888	0.9945
900	5000		-0.7186	1.4370	0.9965		-0.7784	2.0855	0.9943
1000	5000		-0.7068	1.4337	0.9966		-0.7800	2.0817	0.9934
0	6000		-0.7860	1.4910	0.9967		-0.7819	2.1551	0.9985
100	6000		-0.8196	1.4749	0.9967		-0.7989	2.1490	0.9975
200	6000		-0.8142	1.4732	0.9966		-0.7994	2.1479	0.9973
300	6000		-0.8061	1.4702	0.9966		-0.7997	2.1446	0.9971
400	6000		-0.7929	1.4632	0.9969		-0.7955	2.1358	0.9963
500	6000		-0.7810	1.4583	0.9969		-0.7920	2.1285	0.9964
600	6000		-0.7711	1.4555	0.9967		-0.7880	2.1200	0.9953
700	6000		-0.7597	1.4512	0.9965		-0.7857	2.1131	0.9954
800	6000		-0.7479	1.4466	0.9964		-0.7811	2.1049	0.9943
900	6000		-0.7364	1.4423	0.9964		-0.7850	2.1032	0.9944
1000	6000		-0.7271	1.4400	0.9964		-0.7879	2.1006	0.9932
0	7000		-0.7865	1.4916	0.9968		-0.7931	2.1665	0.9978
100	7000		-0.8219	1.4767	0.9966		-0.8120	2.1625	0.9966
200	7000		-0.8163	1.4744	0.9966		-0.8119	2.1614	0.9965
300	7000		-0.8109	1.4726	0.9964		-0.8085	2.1549	0.9964
400	7000		-0.8009	1.4675	0.9968		-0.8103	2.1541	0.9960
500	7000		-0.7910	1.4634	0.9968		-0.8039	2.1435	0.9950
600	7000		-0.7808	1.4593	0.9968		-0.7996	2.1358	0.9949
700	7000		-0.7722	1.4567	0.9967		-0.7982	2.1308	0.9936
800	7000		-0.7626	1.4532	0.9965		-0.7927	2.1214	0.9934
900	7000		-0.7516	1.4485	0.9964		-0.7922	2.1173	0.9926
1000	7000		-0.7423	1.4452	0.9963		-0.7936	2.1149	0.9929
0	8000		-0.7879	1.4928	0.9967		-0.8017	2.1758	0.9970
100	8000		-0.8241	1.4784	0.9965		-0.8224	2.1737	0.9957
200	8000		-0.8190	1.4763	0.9966		-0.8182	2.1679	0.9957
300	8000		-0.8140	1.4740	0.9966		-0.8205	2.1679	0.9959
400	8000		-0.8078	1.4718	0.9966		-0.8189	2.1639	0.9953
500	8000		-0.7981	1.4667	0.9968		-0.8151	2.1573	0.9942
600	8000		-0.7887	1.4628	0.9968		-0.8114	2.1507	0.9939
700	8000		-0.7810	1.4601	0.9966		-0.8079	2.1441	0.9935
800	8000		-0.7729	1.4573	0.9967		-0.8051	2.1379	0.9927
900	8000		-0.7646	1.4546	0.9966		-0.8046	2.1342	0.9921
1000	8000		-0.7551	1.4503	0.9963		-0.8018	2.1281	0.9915

Table 8: Linear regression models for immersed sensors for individual *alt* and *side*: 50%ile and 99%ile LDE for *side* = 9,000 m and 10,000 m.

alt **(m)**	*side* **(m)**		**50%ile** $\ln\ln N$ w_1	**50%ile** w_0	**50%ile** R^2		**99%ile** $\ln\ln N$ w_1	**99%ile** w_0	**99%ile** R^2
0	9000		-0.7876	1.4928	0.9967		-0.8080	2.1826	0.9964
100	9000		-0.8248	1.4789	0.9966		-0.8284	2.1798	0.9951
200	9000		-0.8220	1.4785	0.9965		-0.8284	2.1788	0.9945
300	9000		-0.8161	1.4752	0.9966		-0.8252	2.1742	0.9946
400	9000		-0.8114	1.4737	0.9964		-0.8267	2.1730	0.9947
500	9000		-0.8039	1.4700	0.9969		-0.8245	2.1690	0.9941
600	9000		-0.7955	1.4659	0.9969		-0.8213	2.1628	0.9930
700	9000		-0.7883	1.4634	0.9969		-0.8167	2.1558	0.9929
800	9000		-0.7807	1.4603	0.9967		-0.8130	2.1491	0.9921
900	9000		-0.7738	1.4582	0.9966		-0.8110	2.1440	0.9914
1000	9000		-0.7670	1.4561	0.9965		-0.8084	2.1389	0.9906
0	10000		-0.7889	1.4940	0.9966		-0.8152	2.1902	0.9959
100	10000		-0.8253	1.4793	0.9965		-0.8336	2.1848	0.9942
200	10000		-0.8222	1.4783	0.9966		-0.8349	2.1856	0.9937
300	10000		-0.8178	1.4760	0.9966		-0.8326	2.1823	0.9937
400	10000		-0.8136	1.4743	0.9964		-0.8331	2.1805	0.9941
500	10000		-0.8096	1.4736	0.9966		-0.8348	2.1802	0.9935
600	10000		-0.8013	1.4688	0.9968		-0.8308	2.1748	0.9924
700	10000		-0.7930	1.4649	0.9968		-0.8266	2.1673	0.9917
800	10000		-0.7866	1.4626	0.9969		-0.8222	2.1608	0.9915
900	10000		-0.7801	1.4602	0.9967		-0.8193	2.1554	0.9904
1000	10000		-0.7737	1.4581	0.9967		-0.8165	2.1500	0.9901

Table 9: Linear regression models for standoff sensors for individual *alt* and *side*: Mean and 95%ile LDE for *side* = 1,000 m to 4,000 m.

alt **(m)**	*side* **(m)**		**Mean** $\ln\ln N$ w_1	**Mean** w_0	**Mean** R^2		**95%ile** $\ln\ln N$ w_1	**95%ile** w_0	**95%ile** R^2
0	1000		-0.3796	1.8085	0.9902		-0.3082	1.9693	0.9842
100	1000		-0.3959	1.8000	0.9890		-0.3210	1.9645	0.9826
200	1000		-0.3906	1.7804	0.9909		-0.3151	1.9482	0.9876
300	1000		-0.3929	1.7554	0.9941		-0.3125	1.9242	0.9941
400	1000		-0.4052	1.7335	0.9963		-0.3282	1.9096	0.9967
500	1000		-0.4193	1.7144	0.9977		-0.3456	1.8954	0.9987
600	1000		-0.4337	1.7008	0.9985		-0.3635	1.8830	0.9993
700	1000		-0.4447	1.6904	0.9989		-0.3805	1.8742	0.9989
800	1000		-0.4528	1.6835	0.9991		-0.3947	1.8679	0.9981
900	1000		-0.4584	1.6795	0.9991		-0.4089	1.8659	0.9974
1000	1000		-0.4612	1.6772	0.9991		-0.4189	1.8630	0.9973
0	2000		-0.4359	1.8812	0.9964		-0.3692	2.0488	0.9946
100	2000		-0.4543	1.8762	0.9961		-0.3848	2.0471	0.9947
200	2000		-0.4499	1.8695	0.9958		-0.3813	2.0421	0.9944
300	2000		-0.4443	1.8584	0.9962		-0.3748	2.0321	0.9953
400	2000		-0.4385	1.8435	0.9967		-0.3679	2.0185	0.9964
500	2000		-0.4354	1.8276	0.9974		-0.3643	2.0043	0.9983
600	2000		-0.4363	1.8128	0.9981		-0.3631	1.9900	0.9992
700	2000		-0.4387	1.7975	0.9986		-0.3647	1.9765	0.9992
800	2000		-0.4435	1.7838	0.9991		-0.3700	1.9653	0.9988
900	2000		-0.4485	1.7705	0.9993		-0.3757	1.9535	0.9981
1000	2000		-0.4545	1.7593	0.9993		-0.3859	1.9462	0.9976
0	3000		-0.4642	1.9153	0.9985		-0.4004	2.0867	0.9975
100	3000		-0.4826	1.9103	0.9986		-0.4159	2.0841	0.9985
200	3000		-0.4803	1.9073	0.9984		-0.4138	2.0811	0.9980
300	3000		-0.4762	1.9014	0.9982		-0.4105	2.0770	0.9977
400	3000		-0.4712	1.8931	0.9982		-0.4047	2.0690	0.9981
500	3000		-0.4661	1.8831	0.9984		-0.3992	2.0599	0.9981
600	3000		-0.4620	1.8723	0.9986		-0.3953	2.0506	0.9989
700	3000		-0.4579	1.8600	0.9988		-0.3912	2.0394	0.9995
800	3000		-0.4567	1.8491	0.9990		-0.3885	2.0287	0.9996
900	3000		-0.4575	1.8388	0.9992		-0.3877	2.0185	0.9992
1000	3000		-0.4579	1.8272	0.9993		-0.3884	2.0091	0.9987
0	4000		-0.4822	1.9363	0.9993		-0.4202	2.1093	0.9986
100	4000		-0.5007	1.9313	0.9995		-0.4366	2.1071	0.9994
200	4000		-0.4996	1.9298	0.9993		-0.4354	2.1055	0.9993
300	4000		-0.4967	1.9261	0.9993		-0.4338	2.1035	0.9992
400	4000		-0.4932	1.9211	0.9993		-0.4293	2.0980	0.9991
500	4000		-0.4888	1.9143	0.9993		-0.4238	2.0911	0.9992
600	4000		-0.4845	1.9068	0.9993		-0.4188	2.0839	0.9992
700	4000		-0.4800	1.8981	0.9993		-0.4143	2.0760	0.9993
800	4000		-0.4769	1.8898	0.9994		-0.4110	2.0687	0.9997
900	4000		-0.4740	1.8808	0.9995		-0.4096	2.0620	0.9998
1000	4000		-0.4711	1.8710	0.9994		-0.4050	2.0516	0.9997

Table 10: Linear regression models for standoff sensors for individual *alt* and *side*: Mean and 95%ile LDE for *side* = 5,000 m to 8,000 m.

alt **(m)**	*side* **(m)**		**Mean** $\ln\ln N$ w_1	**Mean** w_0	**Mean** R^2		**95%ile** $\ln\ln N$ w_1	**95%ile** w_0	**95%ile** R^2
0	5000		-0.4952	1.9511	0.9996		-0.4342	2.1250	0.9986
100	5000		-0.5140	1.9462	0.9998		-0.4499	2.1223	0.9994
200	5000		-0.5130	1.9451	0.9998		-0.4497	2.1218	0.9994
300	5000		-0.5117	1.9432	0.9997		-0.4483	2.1200	0.9996
400	5000		-0.5089	1.9395	0.9997		-0.4468	2.1181	0.9994
500	5000		-0.5049	1.9343	0.9997		-0.4416	2.1121	0.9995
600	5000		-0.5013	1.9289	0.9997		-0.4370	2.1064	0.9996
700	5000		-0.4974	1.9226	0.9997		-0.4324	2.1000	0.9997
800	5000		-0.4937	1.9159	0.9997		-0.4281	2.0934	0.9998
900	5000		-0.4903	1.9089	0.9997		-0.4258	2.0882	0.9999
1000	5000		-0.4872	1.9016	0.9997		-0.4212	2.0804	0.9998
0	6000		-0.5051	1.9623	0.9997		-0.4442	2.1361	0.9986
100	6000		-0.5236	1.9569	0.9999		-0.4595	2.1329	0.9993
200	6000		-0.5225	1.9557	0.9999		-0.4588	2.1321	0.9993
300	6000		-0.5222	1.9550	0.9999		-0.4580	2.1310	0.9994
400	6000		-0.5201	1.9524	0.9999		-0.4576	2.1302	0.9995
500	6000		-0.5170	1.9485	0.9999		-0.4545	2.1266	0.9995
600	6000		-0.5138	1.9442	0.9999		-0.4508	2.1223	0.9996
700	6000		-0.5105	1.9394	0.9999		-0.4466	2.1173	0.9996
800	6000		-0.5078	1.9349	0.9999		-0.4437	2.1131	0.9997
900	6000		-0.5043	1.9291	0.9999		-0.4392	2.1067	0.9999
1000	6000		-0.5010	1.9230	0.9999		-0.4366	2.1019	0.9998
0	7000		-0.5135	1.9715	0.9996		-0.4527	2.1454	0.9980
100	7000		-0.5317	1.9658	0.9998		-0.4671	2.1411	0.9987
200	7000		-0.5313	1.9654	0.9998		-0.4670	2.1411	0.9989
300	7000		-0.5301	1.9639	0.9999		-0.4662	2.1400	0.9990
400	7000		-0.5291	1.9625	0.9998		-0.4651	2.1387	0.9992
500	7000		-0.5272	1.9601	0.9999		-0.4642	2.1373	0.9993
600	7000		-0.5240	1.9562	0.9999		-0.4602	2.1330	0.9994
700	7000		-0.5211	1.9523	0.9999		-0.4583	2.1304	0.9995
800	7000		-0.5182	1.9482	0.9999		-0.4555	2.1271	0.9996
900	7000		-0.5160	1.9444	0.9999		-0.4537	2.1240	0.9996
1000	7000		-0.5123	1.9389	0.9999		-0.4480	2.1168	0.9996
0	8000		-0.5203	1.9789	0.9995		-0.4605	2.1537	0.9975
100	8000		-0.5382	1.9729	0.9997		-0.4730	2.1477	0.9983
200	8000		-0.5380	1.9726	0.9997		-0.4732	2.1478	0.9983
300	8000		-0.5369	1.9714	0.9997		-0.4733	2.1478	0.9984
400	8000		-0.5357	1.9698	0.9998		-0.4710	2.1455	0.9986
500	8000		-0.5350	1.9688	0.9998		-0.4703	2.1445	0.9988
600	8000		-0.5326	1.9660	0.9998		-0.4693	2.1431	0.9990
700	8000		-0.5301	1.9627	0.9998		-0.4667	2.1401	0.9990
800	8000		-0.5272	1.9590	0.9999		-0.4640	2.1367	0.9991
900	8000		-0.5242	1.9549	0.9999		-0.4616	2.1339	0.9993
1000	8000		-0.5215	1.9509	0.9999		-0.4592	2.1306	0.9993

Table 11: Linear regression models for standoff sensors for individual *alt* and *side*: Mean and 95%ile LDE for *side* = 9,000 m and 10,000 m.

alt **(m)**	*side* **(m)**		**Mean** $\ln\ln N$ w_1	**Mean** w_0	**Mean** R^2		**95%ile** $\ln\ln N$ w_1	**95%ile** w_0	**95%ile** R^2
0	9000		-0.5261	1.9853	0.9992		-0.4660	2.1596	0.9969
100	9000		-0.5438	1.9789	0.9995		-0.4784	2.1533	0.9977
200	9000		-0.5435	1.9786	0.9996		-0.4782	2.1533	0.9977
300	9000		-0.5425	1.9775	0.9996		-0.4784	2.1535	0.9979
400	9000		-0.5421	1.9769	0.9996		-0.4779	2.1528	0.9980
500	9000		-0.5405	1.9749	0.9996		-0.4758	2.1506	0.9982
600	9000		-0.5393	1.9734	0.9996		-0.4748	2.1494	0.9984
700	9000		-0.5375	1.9711	0.9997		-0.4748	2.1491	0.9984
800	9000		-0.5349	1.9679	0.9997		-0.4726	2.1463	0.9984
900	9000		-0.5326	1.9648	0.9998		-0.4697	2.1428	0.9986
1000	9000		-0.5297	1.9610	0.9998		-0.4663	2.1390	0.9989
0	10000		-0.5314	1.9909	0.9990		-0.4705	2.1646	0.9964
100	10000		-0.5486	1.9841	0.9993		-0.4831	2.1586	0.9972
200	10000		-0.5487	1.9842	0.9993		-0.4836	2.1591	0.9970
300	10000		-0.5480	1.9834	0.9994		-0.4831	2.1585	0.9971
400	10000		-0.5472	1.9824	0.9994		-0.4825	2.1578	0.9973
500	10000		-0.5457	1.9806	0.9994		-0.4813	2.1565	0.9975
600	10000		-0.5448	1.9794	0.9994		-0.4809	2.1559	0.9977
700	10000		-0.5434	1.9777	0.9995		-0.4795	2.1544	0.9980
800	10000		-0.5417	1.9755	0.9995		-0.4780	2.1526	0.9981
900	10000		-0.5391	1.9724	0.9996		-0.4758	2.1500	0.9980
1000	10000		-0.5375	1.9700	0.9996		-0.4745	2.1480	0.9981

Table 12: Linear regression models for standoff sensors for individual *alt* and *side*: 50%ile and 99%ile LDE for *side* = 1,000 m to 4,000 m.

alt **(m)**	*side* **(m)**		**50%ile** $\ln\ln N$ w_1	**50%ile** w_0	**50%ile** R^2		**99%ile** $\ln\ln N$ w_1	**99%ile** w_0	**99%ile** R^2
0	1000		-0.4211	1.7511	0.9947		-0.2701	2.0080	0.9542
100	1000		-0.4439	1.7407	0.9933		-0.2794	2.0049	0.9532
200	1000		-0.4382	1.7175	0.9941		-0.2722	1.9886	0.9685
300	1000		-0.4433	1.6918	0.9954		-0.2817	1.9759	0.9855
400	1000		-0.4464	1.6635	0.9973		-0.3049	1.9676	0.9902
500	1000		-0.4493	1.6404	0.9974		-0.3296	1.9618	0.9945
600	1000		-0.4489	1.6230	0.9971		-0.3527	1.9567	0.9971
700	1000		-0.4464	1.6105	0.9968		-0.3742	1.9531	0.9980
800	1000		-0.4426	1.6022	0.9968		-0.3920	1.9503	0.9985
900	1000		-0.4384	1.5976	0.9967		-0.4066	1.9482	0.9985
1000	1000		-0.4350	1.5960	0.9968		-0.4210	1.9494	0.9984
0	2000		-0.4582	1.7979	0.9983		-0.3506	2.1104	0.9727
100	2000		-0.4771	1.7868	0.9978		-0.3595	2.1081	0.9728
200	2000		-0.4770	1.7831	0.9978		-0.3533	2.0998	0.9752
300	2000		-0.4728	1.7721	0.9981		-0.3455	2.0891	0.9806
400	2000		-0.4678	1.7554	0.9977		-0.3407	2.0778	0.9865
500	2000		-0.4660	1.7383	0.9978		-0.3379	2.0655	0.9930
600	2000		-0.4695	1.7250	0.9980		-0.3400	2.0556	0.9969
700	2000		-0.4679	1.7070	0.9986		-0.3471	2.0476	0.9978
800	2000		-0.4675	1.6904	0.9989		-0.3563	2.0396	0.9986
900	2000		-0.4672	1.6752	0.9987		-0.3665	2.0322	0.9979
1000	2000		-0.4653	1.6613	0.9986		-0.3774	2.0251	0.9978
0	3000		-0.4739	1.8169	0.9991		-0.3869	2.1545	0.9834
100	3000		-0.4916	1.8052	0.9989		-0.3959	2.1528	0.9861
200	3000		-0.4909	1.8032	0.9988		-0.3941	2.1507	0.9850
300	3000		-0.4896	1.7989	0.9987		-0.3888	2.1444	0.9854
400	3000		-0.4865	1.7912	0.9987		-0.3829	2.1357	0.9895
500	3000		-0.4826	1.7812	0.9988		-0.3760	2.1263	0.9912
600	3000		-0.4789	1.7693	0.9984		-0.3721	2.1173	0.9944
700	3000		-0.4774	1.7580	0.9985		-0.3675	2.1072	0.9966
800	3000		-0.4790	1.7481	0.9986		-0.3685	2.1006	0.9984
900	3000		-0.4788	1.7366	0.9986		-0.3694	2.0931	0.9992
1000	3000		-0.4760	1.7224	0.9990		-0.3694	2.0842	0.9989
0	4000		-0.4830	1.8277	0.9995		-0.4118	2.1844	0.9872
100	4000		-0.4989	1.8139	0.9992		-0.4206	2.1816	0.9907
200	4000		-0.4982	1.8129	0.9991		-0.4200	2.1809	0.9898
300	4000		-0.4980	1.8114	0.9990		-0.4164	2.1767	0.9888
400	4000		-0.4974	1.8080	0.9989		-0.4117	2.1712	0.9910
500	4000		-0.4941	1.8017	0.9989		-0.4068	2.1642	0.9938
600	4000		-0.4908	1.7943	0.9991		-0.4043	2.1600	0.9944
700	4000		-0.4879	1.7861	0.9988		-0.3981	2.1510	0.9952
800	4000		-0.4853	1.7770	0.9985		-0.3954	2.1446	0.9963
900	4000		-0.4838	1.7684	0.9986		-0.3922	2.1367	0.9975
1000	4000		-0.4819	1.7583	0.9987		-0.3911	2.1302	0.9986

Table 13: Linear regression models for standoff sensors for individual *alt* and *side*: 50%ile and 99%ile LDE for *side* = 5,000 m to 8,000 m.

alt **(m)**	*side* **(m)**		**50%ile** $\ln\ln N$ w_1	**50%ile** w_0	**50%ile** R^2		**99%ile** $\ln\ln N$ w_1	**99%ile** w_0	**99%ile** R^2
0	5000		-0.4881	1.8336	0.9995		-0.4305	2.2052	0.9904
100	5000		-0.5029	1.8192	0.9993		-0.4418	2.2046	0.9934
200	5000		-0.5039	1.8197	0.9992		-0.4414	2.2039	0.9926
300	5000		-0.5033	1.8185	0.9991		-0.4398	2.2021	0.9921
400	5000		-0.5034	1.8172	0.9991		-0.4352	2.1971	0.9922
500	5000		-0.5013	1.8129	0.9990		-0.4302	2.1913	0.9939
600	5000		-0.4993	1.8084	0.9991		-0.4272	2.1867	0.9954
700	5000		-0.4963	1.8027	0.9991		-0.4237	2.1815	0.9962
800	5000		-0.4939	1.7963	0.9990		-0.4192	2.1754	0.9959
900	5000		-0.4909	1.7890	0.9989		-0.4158	2.1694	0.9972
1000	5000		-0.4896	1.7823	0.9986		-0.4147	2.1646	0.9977
0	6000		-0.4917	1.8380	0.9995		-0.4454	2.2218	0.9924
100	6000		-0.5062	1.8234	0.9993		-0.4566	2.2200	0.9949
200	6000		-0.5065	1.8234	0.9992		-0.4559	2.2192	0.9944
300	6000		-0.5069	1.8232	0.9992		-0.4563	2.2197	0.9935
400	6000		-0.5072	1.8227	0.9991		-0.4527	2.2160	0.9941
500	6000		-0.5055	1.8197	0.9991		-0.4486	2.2110	0.9946
600	6000		-0.5045	1.8170	0.9991		-0.4449	2.2066	0.9952
700	6000		-0.5026	1.8132	0.9990		-0.4418	2.2021	0.9963
800	6000		-0.5011	1.8091	0.9991		-0.4385	2.1974	0.9975
900	6000		-0.4978	1.8030	0.9992		-0.4349	2.1924	0.9979
1000	6000		-0.4956	1.7974	0.9991		-0.4318	2.1875	0.9977
0	7000		-0.4942	1.8412	0.9994		-0.4577	2.2350	0.9937
100	7000		-0.5089	1.8269	0.9993		-0.4699	2.2342	0.9956
200	7000		-0.5092	1.8270	0.9992		-0.4690	2.2334	0.9956
300	7000		-0.5091	1.8263	0.9991		-0.4668	2.2309	0.9954
400	7000		-0.5089	1.8257	0.9991		-0.4649	2.2290	0.9955
500	7000		-0.5092	1.8251	0.9991		-0.4635	2.2273	0.9954
600	7000		-0.5080	1.8226	0.9990		-0.4592	2.2226	0.9957
700	7000		-0.5069	1.8200	0.9990		-0.4566	2.2192	0.9965
800	7000		-0.5048	1.8164	0.9990		-0.4517	2.2131	0.9975
900	7000		-0.5039	1.8132	0.9990		-0.4507	2.2109	0.9981
1000	7000		-0.5019	1.8090	0.9991		-0.4474	2.2065	0.9984
0	8000		-0.4954	1.8429	0.9993		-0.4681	2.2461	0.9944
100	8000		-0.5106	1.8290	0.9992		-0.4796	2.2449	0.9958
200	8000		-0.5108	1.8290	0.9991		-0.4800	2.2452	0.9957
300	8000		-0.5115	1.8294	0.9990		-0.4766	2.2418	0.9964
400	8000		-0.5114	1.8287	0.9991		-0.4743	2.2393	0.9964
500	8000		-0.5117	1.8286	0.9990		-0.4755	2.2406	0.9959
600	8000		-0.5108	1.8269	0.9990		-0.4728	2.2374	0.9954
700	8000		-0.5095	1.8245	0.9990		-0.4694	2.2335	0.9968
800	8000		-0.5086	1.8221	0.9989		-0.4642	2.2277	0.9974
900	8000		-0.5066	1.8191	0.9989		-0.4623	2.2249	0.9980
1000	8000		-0.5055	1.8158	0.9989		-0.4586	2.2201	0.9983

Table 14: Linear regression models for standoff sensors for individual *alt* and *side*: 50%ile and 99%ile LDE for *side* = 9,000 m and 10,000 m.

alt **(m)**	*side* **(m)**		**50%ile** $\ln\ln N$ w_1	**50%ile** w_0	**50%ile** R^2		**99%ile** $\ln\ln N$ w_1	**99%ile** w_0	**99%ile** R^2
0	9000		-0.4969	1.8449	0.9993		-0.4766	2.2552	0.9951
100	9000		-0.5124	1.8311	0.9990		-0.4869	2.2528	0.9965
200	9000		-0.5126	1.8312	0.9990		-0.4882	2.2540	0.9961
300	9000		-0.5129	1.8313	0.9990		-0.4835	2.2492	0.9972
400	9000		-0.5133	1.8310	0.9989		-0.4839	2.2495	0.9969
500	9000		-0.5124	1.8300	0.9990		-0.4809	2.2464	0.9969
600	9000		-0.5129	1.8299	0.9989		-0.4820	2.2474	0.9961
700	9000		-0.5123	1.8284	0.9990		-0.4788	2.2437	0.9962
800	9000		-0.5109	1.8261	0.9988		-0.4758	2.2403	0.9971
900	9000		-0.5104	1.8242	0.9988		-0.4727	2.2365	0.9979
1000	9000		-0.5086	1.8215	0.9989		-0.4714	2.2345	0.9983
0	10000		-0.4981	1.8465	0.9992		-0.4837	2.2625	0.9957
100	10000		-0.5140	1.8329	0.9990		-0.4937	2.2597	0.9971
200	10000		-0.5139	1.8328	0.9990		-0.4943	2.2605	0.9969
300	10000		-0.5143	1.8330	0.9990		-0.4923	2.2585	0.9969
400	10000		-0.5145	1.8328	0.9989		-0.4908	2.2567	0.9970
500	10000		-0.5143	1.8322	0.9989		-0.4892	2.2551	0.9967
600	10000		-0.5147	1.8322	0.9989		-0.4894	2.2552	0.9966
700	10000		-0.5143	1.8313	0.9989		-0.4897	2.2555	0.9964
800	10000		-0.5142	1.8303	0.9988		-0.4863	2.2514	0.9965
900	10000		-0.5121	1.8274	0.9988		-0.4825	2.2473	0.9975
1000	10000		-0.5117	1.8258	0.9987		-0.4805	2.2447	0.9982

10 Estimating Location Distance Error as a Function of Altitude and Search Area Side Length

This section generalizes the results of Section 9.3 for individual configurations of given altitude and search area side length to arrive at expressions that estimate the LDE statistical metrics over *all* simulated altitudes and search area side lengths. Again, the method used is linear regression over a set of transformed variables and various combinations of those variables.

The initial attempts to find linear regression models for LDE statistical metrics were based on direct application to the set of input variables and their transformations and combinations. However, those approaches resulted in expressions that had twice or greater MAPE than that achieved by the method described below in this section. In addition, the expressions that provided the smallest MAPE were different for the various LDE statistical metrics and for immersed and standoff sensors in the sense that the expressions were functions of different sets of input variables. The expressions also had greater worst-case MAPE. Therefore, after much experimentation, linear regression directly over the set of input variables was abandoned in favor of the following approach.

10.1 Generalizing the Linear Regression Models Developed for Fixed Configurations

A **two-stage linear regression model** was used to obtain estimates of the four LDE statistical metrics. The *first stage* has already been described: it was the procedure given in Section 9.3 that produced Table 3 through Table 14, which list the linear regression weights w_0 and w_1 for the weighted sum for the double logarithm of the LDE statistical metrics as a function of the double logarithm of the number of sensors as expressed in (23).

The *second stage* was another pair of linear regressions that estimated the weights w_0 and w_1 as weighted sums of the sets of input variables based on altitude and search area side length. It is worth stating again that, unlike the direct approach outlined above, the same set of variables in weighted sums (with different weights) gave nearly optimal MAPE across the four LDE statistical metrics and for immersed and standoff sensors. The shotgun approach described in Section 8.2 found that the best linear regression models of w_0 and w_1 had $v = 5$ significant input variables: $alt/side$, $1/alt$, $1/side$, $1/side^2$, and $alt/side^2$. Thus, there are $v + 1 = 6$ weights in each the weighted sums for w_0 and w_1 for each of the LDE statistical metrics, denoted by w'_0, w'_1, w'_2, w'_3, w'_4, w'_5.

These weights for immersed sensors are given in Table 15. The MAPE achieved by these linear regression models for $N = 5$ to 24 were 2.33%, 2.01%, 3.79%, and 4.69% and the largest percentage errors were 14.30%, 9.31%, 20.51%, and 22.58% for the mean, 50%ile, 95%ile, and 99%ile LDE, respectively; the worst R^2 for those four linear regression models was 0.8959. The weights for standoff sensors are given in Table 16. The MAPE achieved by these linear regression models for $N = 5$ to 24 were 2.43%, 2.61%, 2.94%, and 3.54% and the largest percentage errors were 15.31%, −13.70%, 18.01%, and 23.35% for the mean, 50%ile, 95%ile, and 99%ile LDE, respectively; the smallest R^2 for any linear regression model was 0.9764.

These weights are used as follows. In Table 15 for immersed sensors or Table 16 for standoff sensors, there are two rows for each of the LDE statistical metrics; let the LDE statistical metric be represented by the output variable y. The first row lists the w'_0, w'_1, w'_2, w'_3, w'_4, w'_5 weights for the expression for w_0 and the second row lists the w'_0, w'_1, w'_2, w'_3, w'_4, w'_5 weights for the expression for w_1. Using the weights from the corresponding row for

w_0 or w_1, the linear regression estimate for the weights w_0 and w_1 are given by: [36]

$$w_0 = w_0' + w_1' \frac{alt}{side} + w_2' \frac{1}{alt + 0.001} + w_3' \frac{1}{side} + w_4' \frac{1}{side^2} + w_5' \frac{alt}{side^2} \quad (25)$$

$$w_1 = w_0' + w_1' \frac{alt}{side} + w_2' \frac{1}{alt + 0.001} + w_3' \frac{1}{side} + w_4' \frac{1}{side^2} + w_5' \frac{alt}{side^2} \quad (26)$$

The estimated linear regression weights w_0 and w_1 are then used in (23) to obtain the estimate of the LDE statistical metric represented by the output variable y as a function of the number of sensors N.

[36] As noted in Section 8.2, a millimeter was added to the altitude *alt* to avoid division by zero when *alt* appeared as the denominator; thus, the transformed value $alt + 0.001$ m was used instead of *alt*.

Table 15: Linear regression models for immersed sensors, based on shotgun approach as functions of *alt* and *side*, for mean, 50%ile, 95%ile, and 99%ile LDE.

LDE	w_i	w'_0	w'_1	w'_2	w'_3	w'_4	w'_5
Mean	w_0	1.8619	-5.3677×10^{-1}	1.0873×10^{-5}	-3.9855×10^{2}	1.3623×10^{5}	5.0824×10^{2}
Mean	w_1	−1.0566	6.2847×10^{-1}	4.1311×10^{-5}	3.8009×10^{2}	-1.5350×10^{5}	-3.4133×10^{2}
50%ile	w_0	1.4859	-2.4263×10^{-1}	2.0301×10^{-5}	-6.2005×10^{1}	-2.1106×10^{4}	3.2277×10^{2}
50%ile	w_1	−0.8421	6.6214×10^{-1}	3.8413×10^{-5}	6.7325×10^{1}	2.3593×10^{4}	-3.8132×10^{2}
95%ile	w_0	2.0853	-4.8795×10^{-1}	6.3765×10^{-6}	-3.4933×10^{2}	1.1160×10^{5}	4.2128×10^{2}
95%ile	w_1	−0.8967	3.0668×10^{-1}	3.0214×10^{-5}	3.1799×10^{2}	-1.3927×10^{5}	-1.3033×10^{2}
99%ile	w_0	2.2256	-3.7335×10^{-1}	2.9147×10^{-6}	-4.3234×10^{2}	1.5763×10^{5}	3.3242×10^{2}
99%ile	w_1	−0.8609	5.2166×10^{-2}	2.1083×10^{-5}	3.8667×10^{2}	-1.8934×10^{5}	7.1724×10^{0}

Table 16: Linear regression models for standoff sensors, based on shotgun approach as functions of *alt* and *side*, for mean, 50%ile, 95%ile, and 99%ile LDE.

LDE	w_i	w'_0	w'_1	w'_2	w'_3	w'_4	w'_5
Mean	w_0	2.0281	-3.1295×10^{-1}	-5.2250×10^{-6}	-3.6449×10^{2}	1.4236×10^{5}	1.6165×10^{2}
Mean	w_1	−0.5782	1.6218×10^{-1}	1.7738×10^{-5}	3.2424×10^{2}	-1.2837×10^{5}	-2.4539×10^{2}
50%ile	w_0	1.8626	-2.7988×10^{-1}	5.7116×10^{-7}	-1.5297×10^{2}	3.7051×10^{4}	1.0113×10^{2}
50%ile	w_1	−0.5277	7.5116×10^{-2}	1.8956×10^{-5}	1.1361×10^{2}	-2.9788×10^{4}	-7.3787×10^{1}
95%ile	w_0	2.2044	-2.8498×10^{-1}	-6.3793×10^{-6}	-3.7504×10^{2}	1.3953×10^{5}	1.6075×10^{2}
95%ile	w_1	−0.5180	1.8181×10^{-1}	1.3979×10^{-5}	3.4433×10^{2}	-1.2544×10^{5}	-2.9617×10^{2}
99%ile	w_0	2.3141	-2.8758×10^{-1}	-5.6204×10^{-6}	-5.2354×10^{2}	2.1414×10^{5}	2.2034×10^{2}
99%ile	w_1	−0.5364	1.9332×10^{-1}	7.5542×10^{-6}	4.8418×10^{2}	-2.0102×10^{5}	-3.6142×10^{2}

10.2 Applying the Two-Stage Linear Regression Models

Table 15 and Table 16, (25) and (26), and finally (23) and (24) are applied in the two-stage linear regression model as follows. The same example used in Section 9.3 is used here.

Consider the problem of estimating the mean LDE for the configuration of $N = 8$ immersed sensors with $alt = 300$ m and $side = 5{,}000$ m; denote the value of that statistical metric by y. In the first step, for the mean LDE, Table 15 provides the weights w'_0, w'_1, w'_2, w'_3, w'_4, w'_5 in the "w_0" row to obtain $w_0 = 1.7616$ from (25) and the weights w'_0, w'_1, w'_2, w'_3, w'_4, w'_5 from the "w_1" row to obtain $w_1 =$ -0.9531 from (26). In the second stage, the weights w_0 and w_1 are substituted into (23) to obtain $\ln \ln y = 1.7616 - 0.9531 \ln \ln 8 = 1.0637$. Solving for y as (24), the linear regression estimate for the mean LDE for this configuration is 18.12 m.

For comparison, the measured linear regression weights listed in Table 4 resulting from 10,000 simulations of this configuration are $w_0 = 1.7593$ and $w_1 =$ -0.9498 as noted in the example involving this configuration in Section 9.3.

The measured mean LDE for this configuration was 17.64 m, so the error of the two-stage linear regression model estimate for the mean LDE relative to the measured value was 2.75%.

Compared to the candidate linear regression models developed directly over the set of input variables, the two-stage linear regression model produced linear regression estimates of the four LDE statistical metrics that better matched the convex shape of the LDE curves (noted in Section 7) as a function of altitude for a given number of sensors and search area side length. The plots of the LDE statistical metrics shown in Section 7 were functions of the $alt/side$ ratio, but here the plots are shown as a function of alt for a given value of $side$ so as to better observe the tightness of the LDE estimates without scattering.

The linear regression estimates obtained using the two-stage linear regression model were applied to the data used in Section 7. The two-stage linear regression estimates were based on sets of 10,000 simulations per configuration where the altitude was varied from 0 m to 1,000 m (in steps of 100 m). The data used in Section 7 were obtained using a different random

seed, were based on 1,000 simulations per configuration, and the altitudes were incremented in steps of 10% of the range from 0 m to *side* for immersed sensors and $2 \times side$ for standoff sensors. Thus, the demonstration of the effectiveness of the two-stage linear regression model involved a different set of data from that for which the linear regressions were obtained. The results are shown in Figure 70 through Figure 85. As in Section 7, the four LDE statistical metrics are plotted as functions of the $alt/side$ ratio, but in this case the linear regression estimates are shown in addition to the measured results from the simulations. Note that only the results for altitudes from 0 m to 1,000 m are shown as the linear regression models are valid for only that range. To avoid the issue of Longfellow Events, only configurations of five and more sensors are considered.

Figure 70 shows the four LDE statistical metrics for five immersed sensors as a function of the $alt/side$ ratio. The superimposing of eight sets of points makes the plot difficult to read, but the only important observation is the fact that the plotted points for the linear regression estimates track closely or are covered by those for the measured results. For clarity, Figure 71 shows the same comparison but only for the mean and 95%ile LDE.

The same situations for standoff sensors are shown in Figure 72 for the four LDE statistical metrics and in Figure 73 for the mean and 95%ile LDE. The same close tracking of the measured and estimated LDE statistical metrics are observed over the plotted range of $alt/side$ ratios.

Most encouraging is the fact that the two-stage linear regression model is able to reproduce the convex behavior of the LDE statistical metrics with respect to the $alt/side$ ratio, which other candidate linear regression approaches did not accomplish.

The comparisons continue in Figure 74 and Figure 75 for $N = 10$ immersed sensors and Figure 76 and Figure 77 for $N = 10$ standoff sensors, in Figure 78 and Figure 79 for $N = 15$ immersed sensors and Figure 80 and Figure 81 for $N = 15$ standoff sensors, and in Figure 82 and Figure 83 for $N = 20$ immersed sensors and Figure 84 and Figure 85 for $N = 20$ standoff sensors. It can be observed that the close tracking of the measured LDE statistical metrics and their linear regression estimates only improve with increasing numbers of sensors.

The two-stage linear regression model generalized the extensive sets of weights listed in Table 3 through Table 14 into a few equations. It is unfortunate that the double logarithm relationships between the LDE statistical metrics and the number of sensors expressed in (23) provide little intuitive feeling for the trends of those relationships. The next section provides a set of simpler power-law approximations based on an alternate approach.

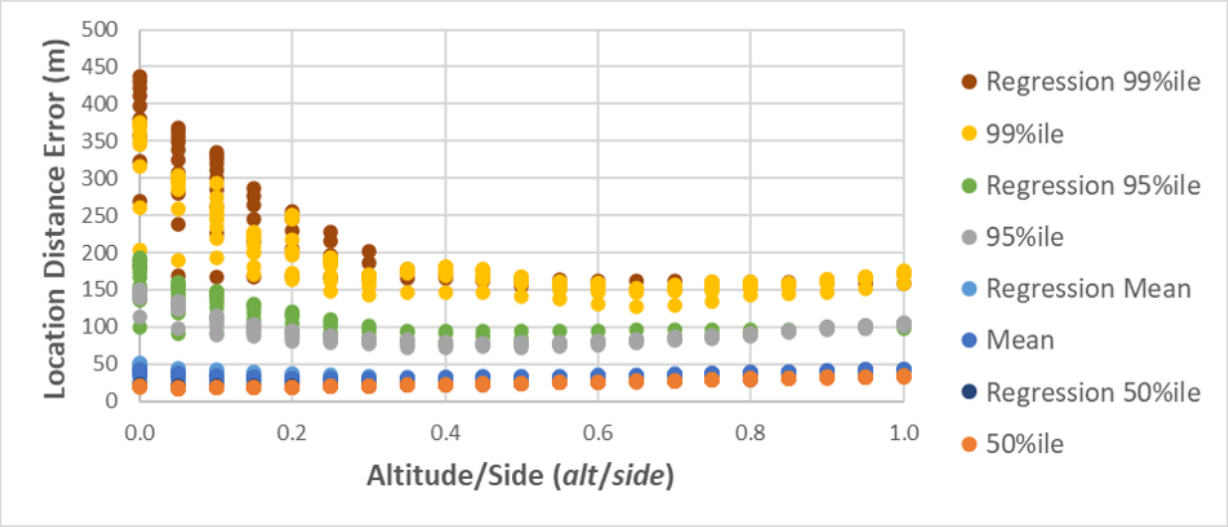

Figure 70: For five immersed sensors, the mean, 50%ile, 95%ile, and 99%ile LDE statistical metrics are shown as a function of the ratio $alt/side$. See text for ranges of alt and $side$. With errors.

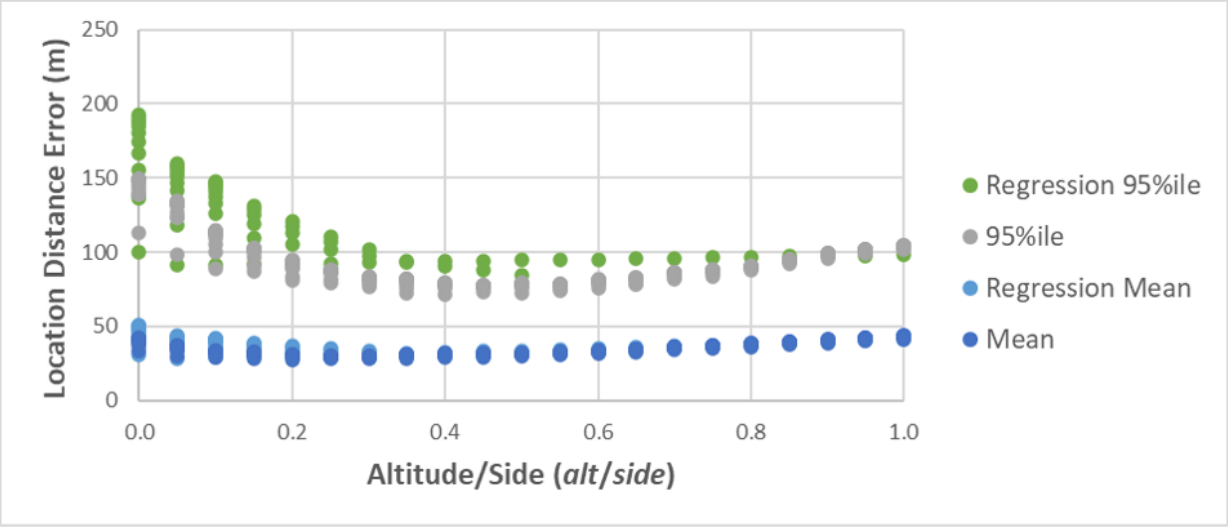

Figure 71: For five immersed sensors, only the mean and 95%ile LDE statistical metrics are shown as a function of the ratio $alt/side$. See text for ranges of alt and $side$. With errors.

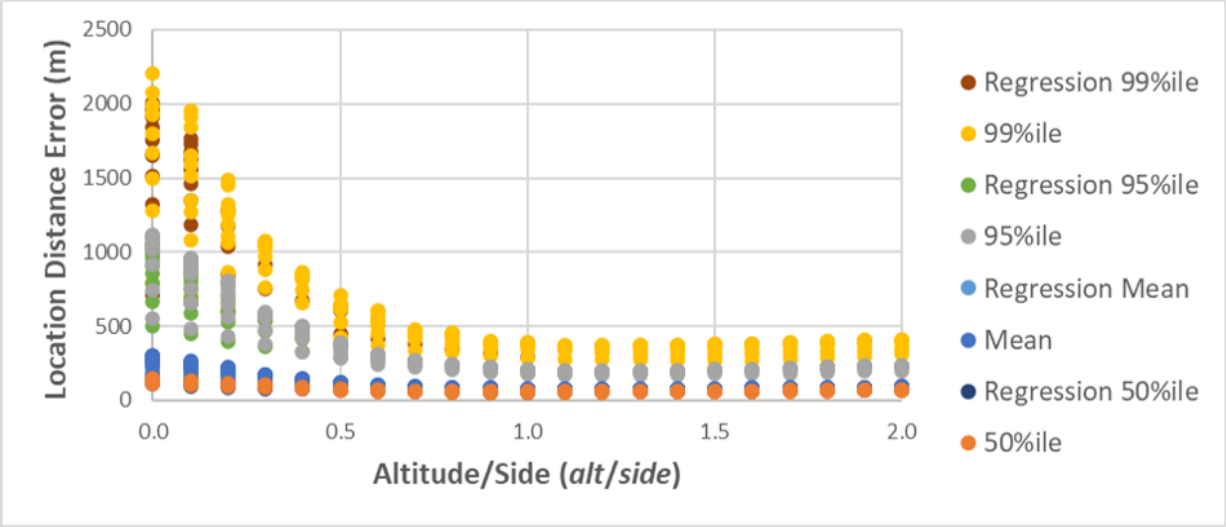

Figure 72: For five standoff sensors, the mean, 50%ile, 95%ile, and 99%ile LDE statistical metrics are shown as a function of the ratio $alt/side$. See text for ranges of alt and $side$. With errors.

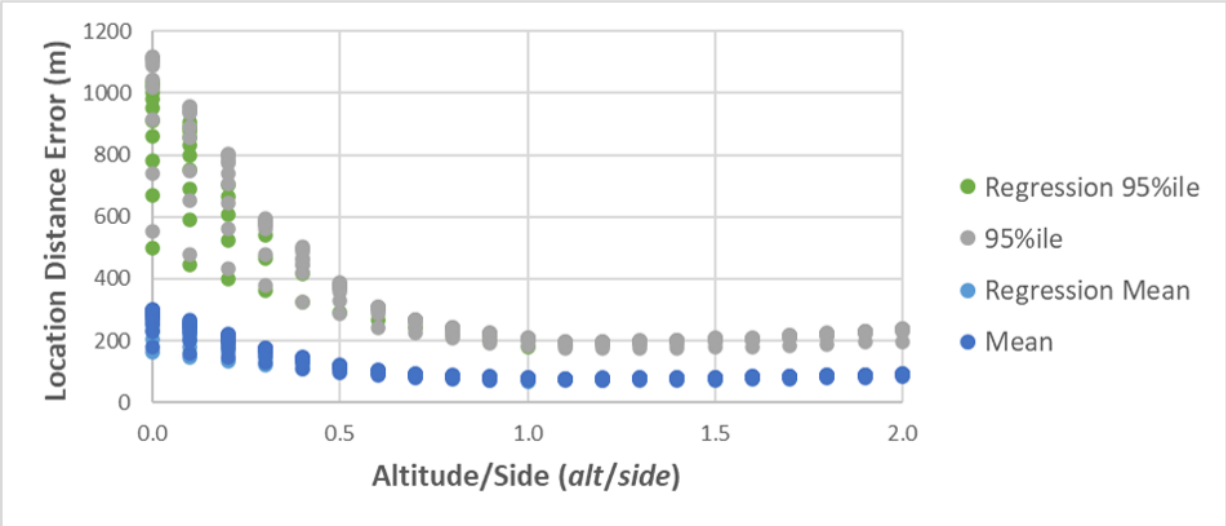

Figure 73: For five standoff sensors, only the mean and 95%ile LDE statistical metrics are shown as a function of the ratio $alt/side$. See text for ranges of alt and $side$. With errors.

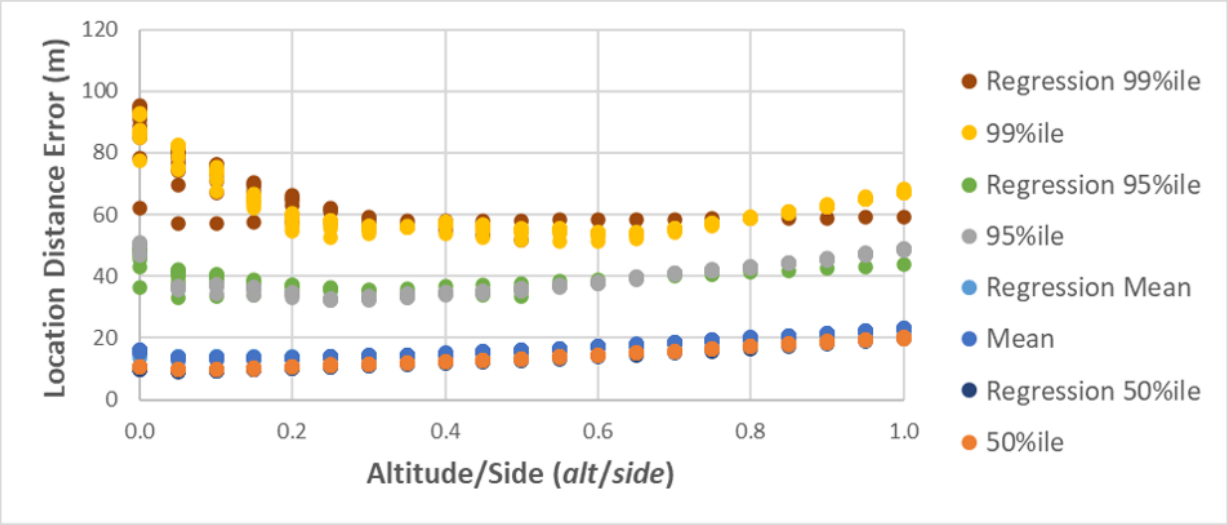

Figure 74: For ten immersed sensors, the mean, 50%ile, 95%ile, and 99%ile LDE statistical metrics are shown as a function of the ratio $alt/side$. See text for ranges of alt and $side$. With errors.

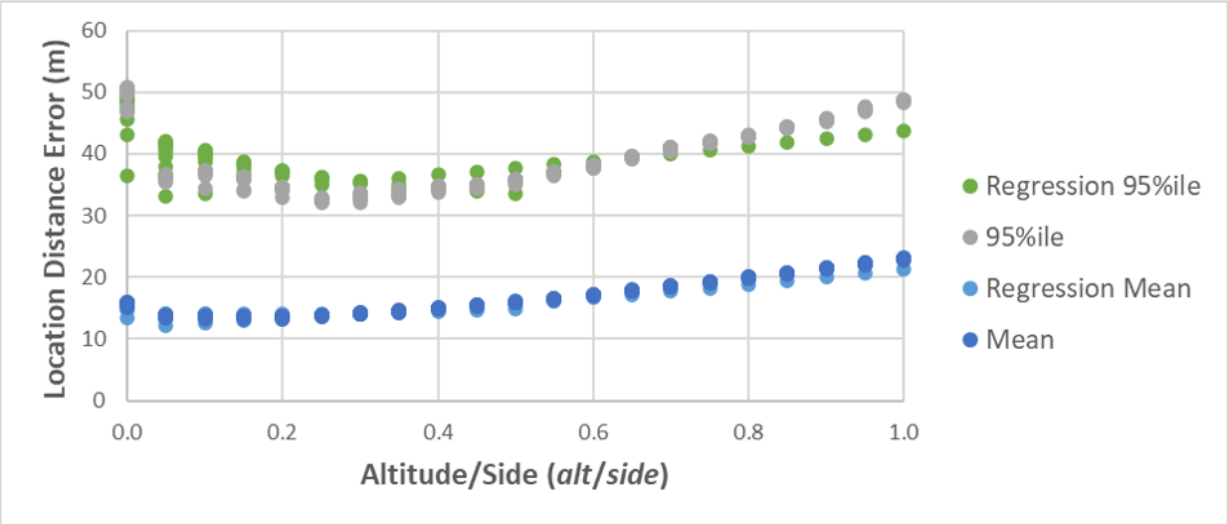

Figure 75: For ten immersed sensors, only the mean and 95%ile LDE statistical metrics are shown as a function of the ratio $alt/side$. See text for ranges of alt and $side$. With errors.

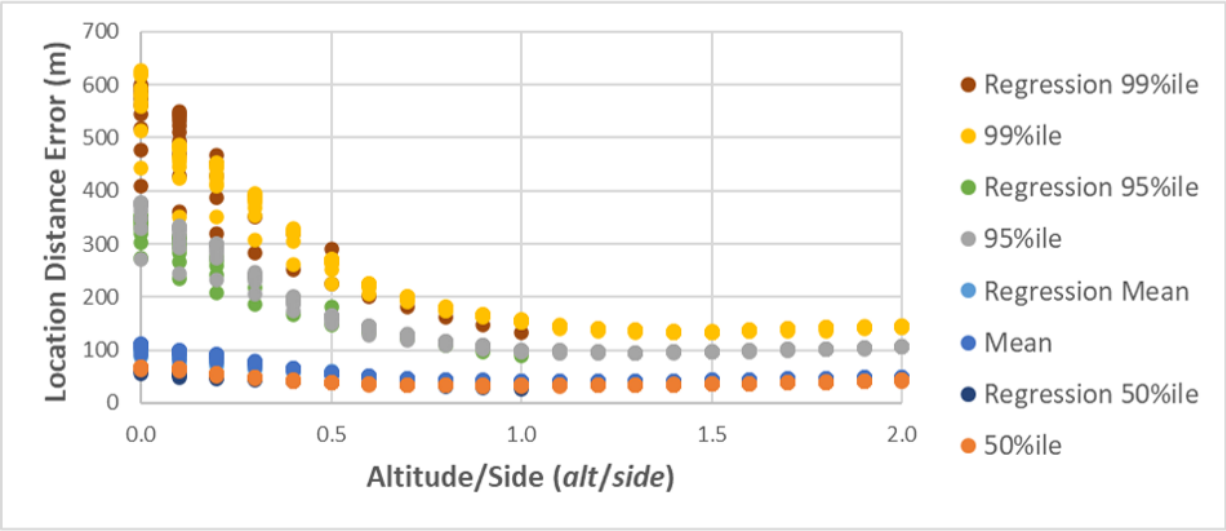

Figure 76: For ten standoff sensors, the mean, 50%ile, 95%ile, and 99%ile LDE statistical metrics are shown as a function of the ratio $alt/side$. See text for ranges of alt and $side$. With errors.

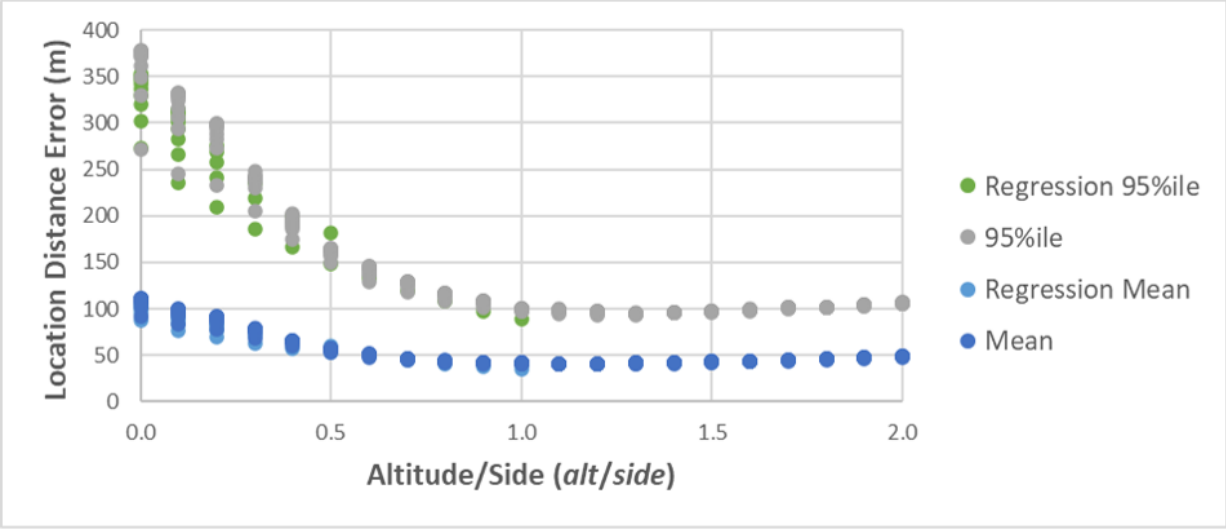

Figure 77: For ten standoff sensors, only the mean and 95%ile LDE statistical metrics are shown as a function of the ratio $alt/side$. See text for ranges of alt and $side$. With errors.

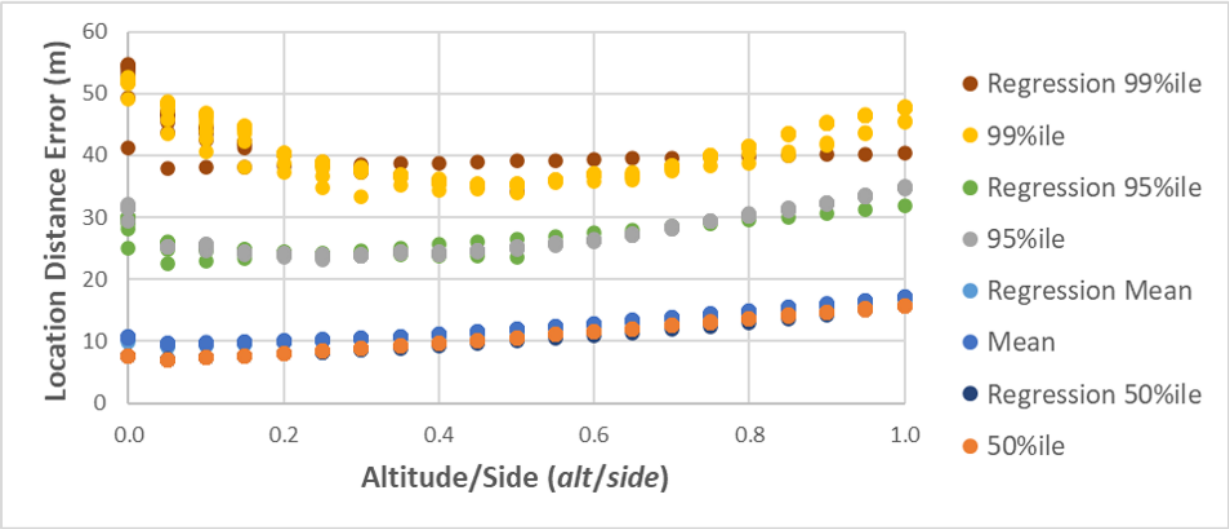

Figure 78: For 15 immersed sensors, the mean, 50%ile, 95%ile, and 99%ile LDE statistical metrics are shown as a function of the ratio $alt/side$. See text for ranges of alt and $side$. With errors.

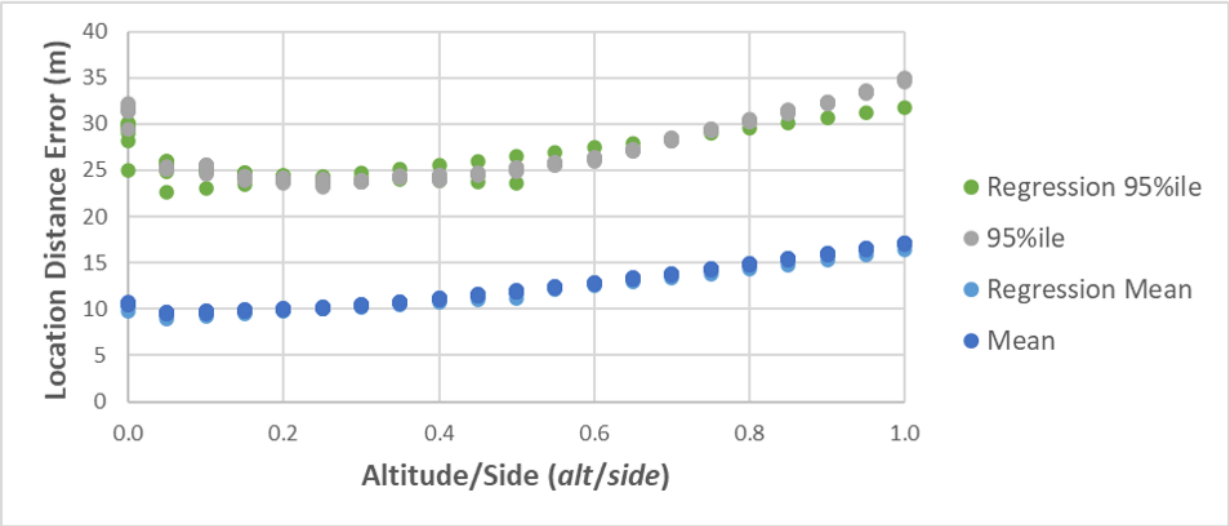

Figure 79: For 15 immersed sensors, only the mean and 95%ile LDE statistical metrics are shown as a function of the ratio $alt/side$. See text for ranges of alt and $side$. With errors.

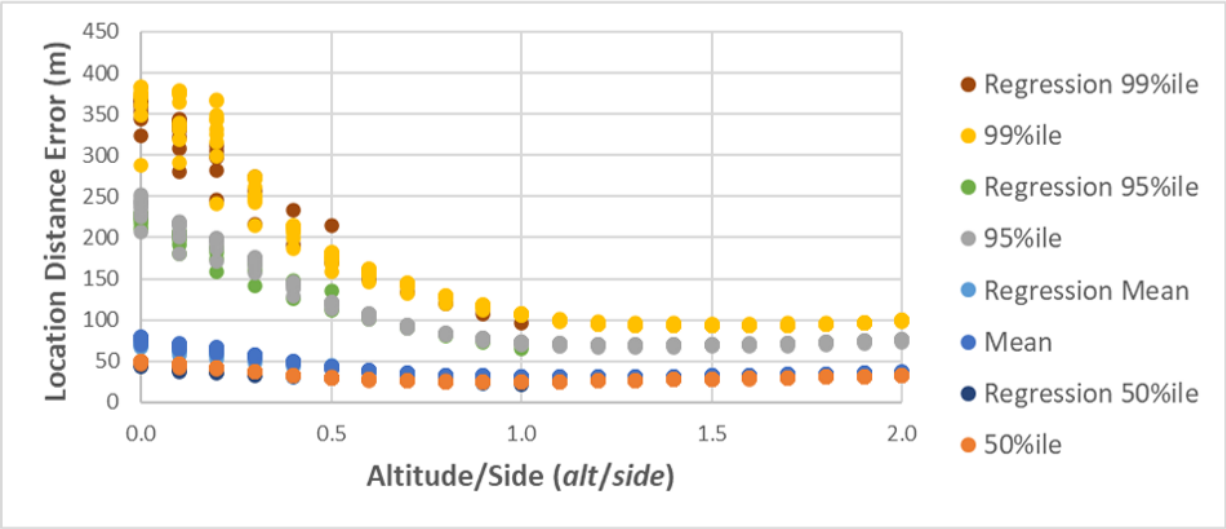

Figure 80: For 15 standoff sensors, the mean, 50%ile, 95%ile, and 99%ile LDE statistical metrics are shown as a function of the ratio $alt/side$. See text for ranges of alt and $side$. With errors.

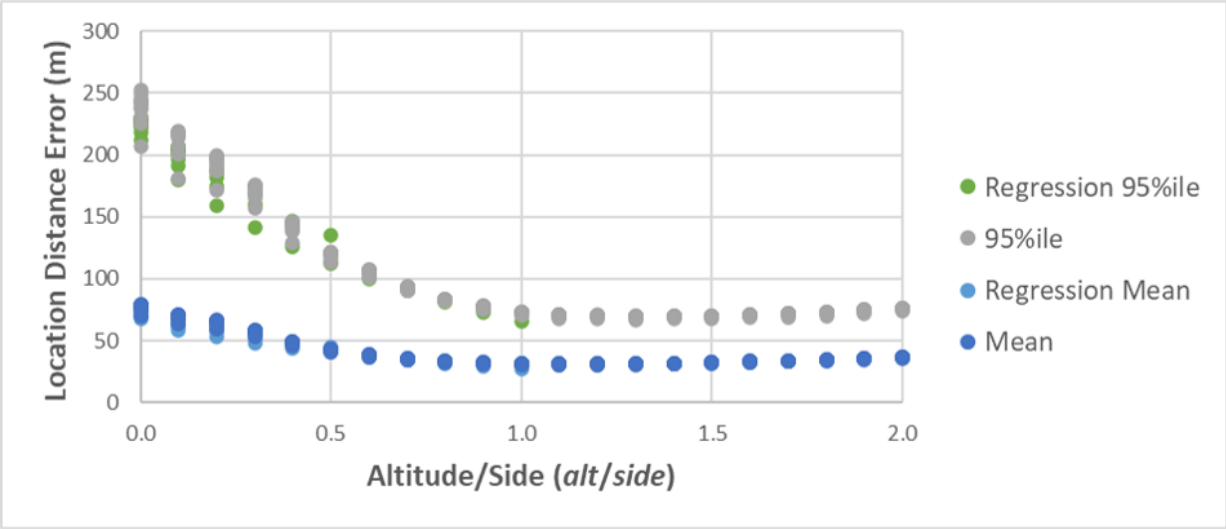

Figure 81: For 15 standoff sensors, only the mean and 95%ile LDE statistical metrics are shown as a function of the ratio $alt/side$. See text for ranges of alt and $side$. With errors.

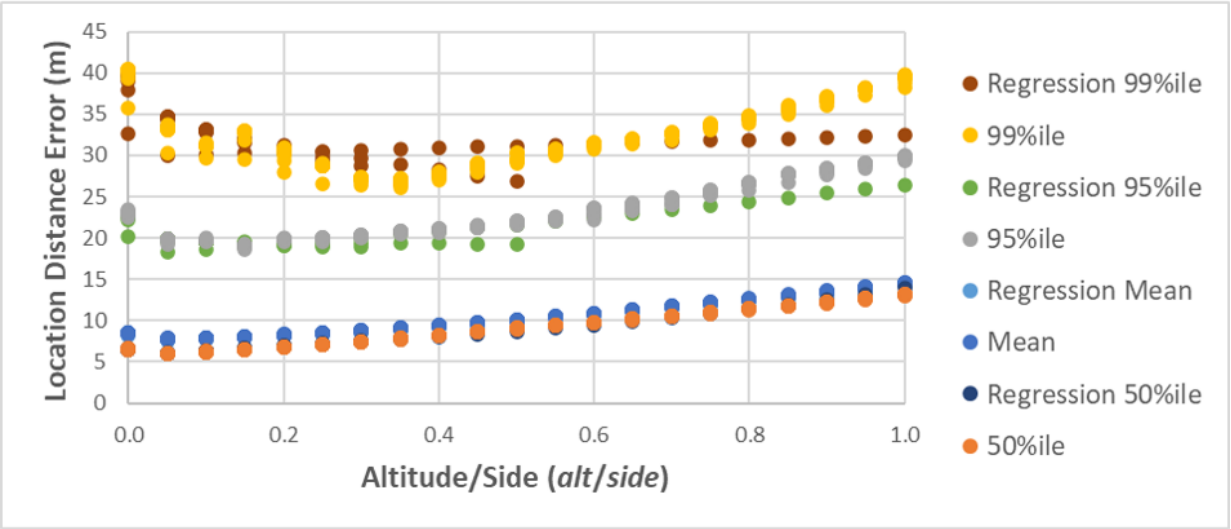

Figure 82: For 20 immersed sensors, the mean, 50%ile, 95%ile, and 99%ile LDE statistical metrics are shown as a function of the ratio $alt/side$. See text for ranges of alt and $side$. With errors.

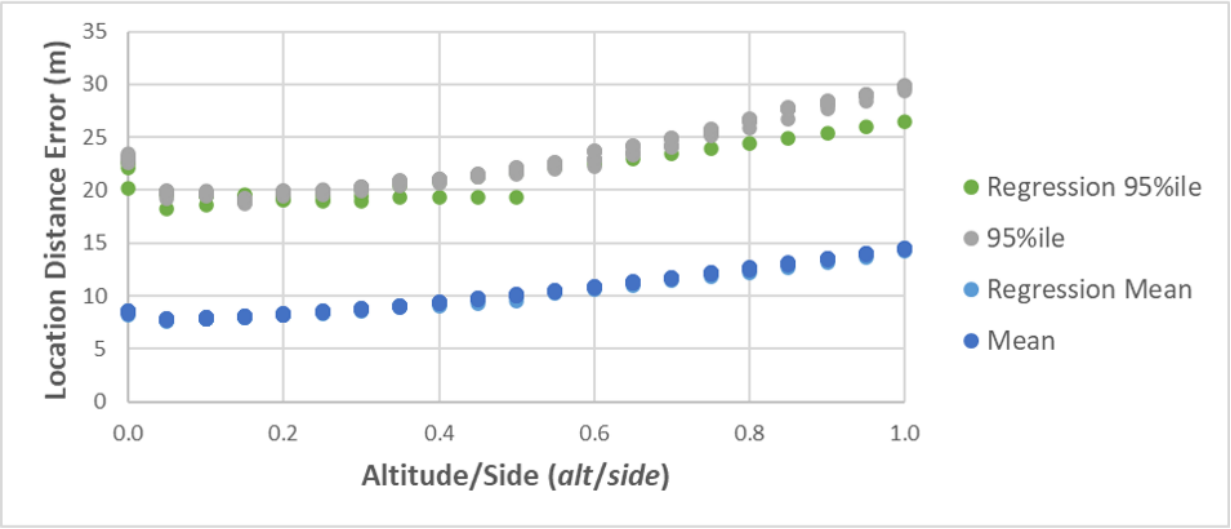

Figure 83: For 20 immersed sensors, only the mean and 95%ile LDE statistical metrics are shown as a function of the ratio $alt/side$. See text for ranges of alt and $side$. With errors.

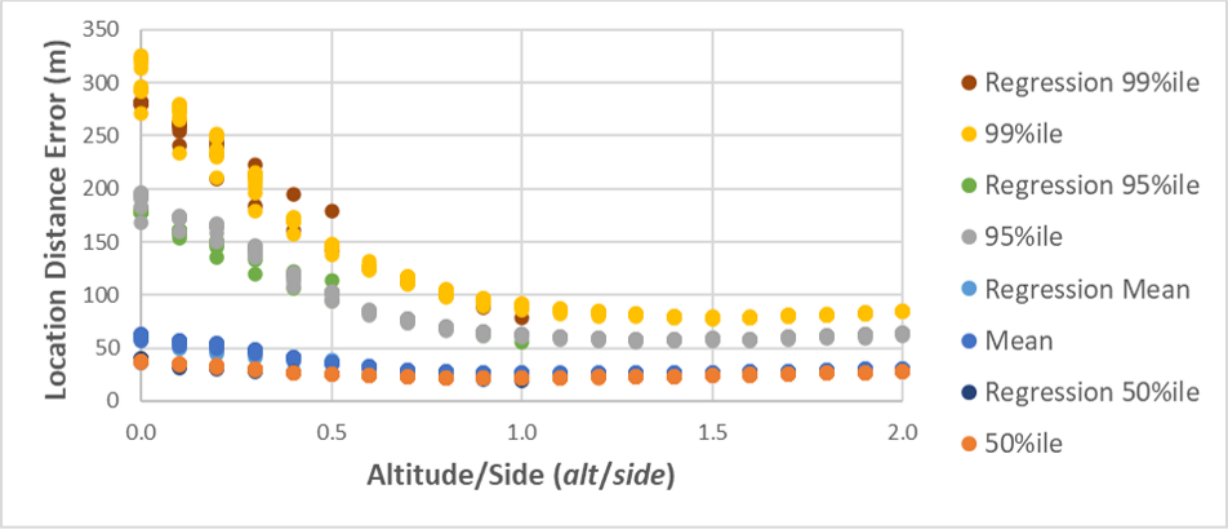

Figure 84: For 20 standoff sensors, the mean, 50%ile, 95%ile, and 99%ile LDE statistical metrics are shown as a function of the ratio $alt/side$. See text for ranges of alt and $side$. With errors.

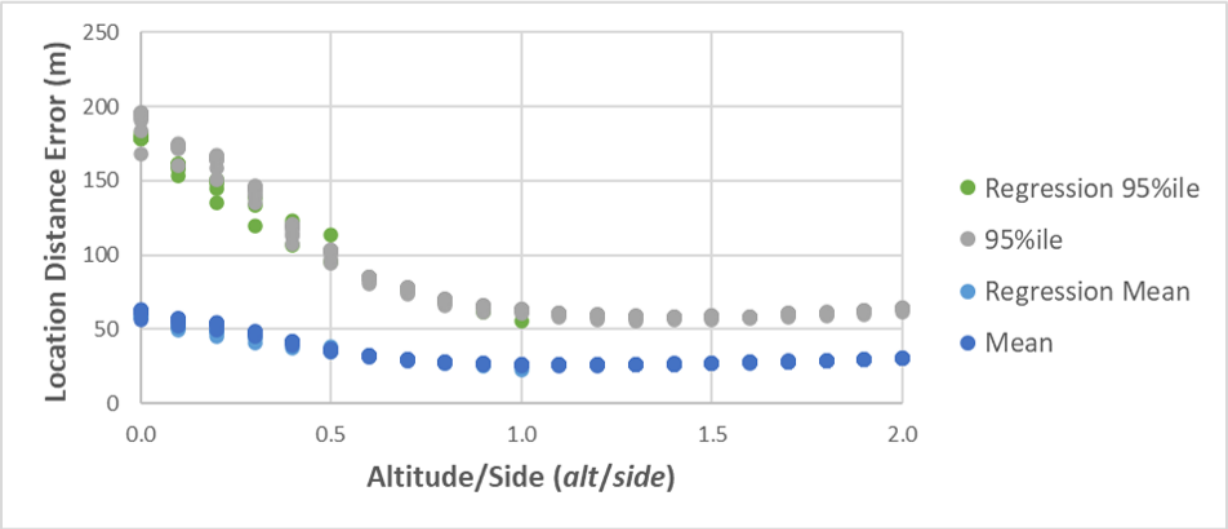

Figure 85: For 20 standoff sensors, only the mean and 95%ile LDE statistical metrics are shown as a function of the ratio $alt/side$. See text for ranges of alt and $side$. With errors.

11 Improvement Ratio for Location Distance Error

Prior to this section, attention has focused on estimating the values of an LDE statistical metric of interest (the mean, 50%ile, 95%ile, or 99%ile) for two values of N (the number of sensors) and comparing them. The challenges in developing the linear regression models were to maximize R^2 and minimize MAPE to produce the best estimates of the LDE statistical metrics for a given configuration, altitude, search area side length, and error conditions.

This section seeks to answer directly the central question of the relative improvement in LDE as the number of sensors increases. The key idea is to work directly with the *ratio of an LDE statistical metric of interest with respect to a reference value*, as a function of N, rather than the value of the LDE statistical metric itself. Because Longfellow Events can be disregarded for configurations involving five or more sensors, that reference value is the LDE statistical metric with five sensors. The approach then consists of obtaining, for a configuration of N sensors, the ratio of the LDE statistical metric with N sensors to the reference value at five sensors.

11.1 Improvement Ratio for an LDE Statistical Metric

For a given configuration and set of error conditions, the term "**Improvement Ratio for the Mean LDE for N sensors**" [37] means "**the ratio of the mean LDE for that configuration with N sensors relative to the mean LDE for the same configuration with five sensors**," where the mean LDE is obtained by simulating 10,000 geometries per configuration in the case of the Main Data Set.

For example, if the mean LDE for a specific configuration [38] with eight sensors were 18.14 m and the mean LDE for the same configuration with five sensors were 34.46 m, then the Improvement Ratio for the Mean LDE for eight sensors would be $18.14/34.46 = 0.5264$.

The terms "**Improvement Ratio for the 50%ile LDE for N sensors**," "**Improvement Ratio for the 95%ile LDE for N sensors**," and "**Improvement Ratio for the 99%ile LDE for N sensors**" are defined similarly for the other LDE statistical metrics. Thus, if y represents an LDE statistical metric, **the Improvement Ratio for y for N sensors** for a given configuration and error conditions is given by

$$\frac{y \text{ for that configuration with } N \text{ sensors}}{y \text{ for that configuration with 5 sensors}} \tag{27}$$

with the convention that, even when approximated, the Improvement Ratio is defined to be 1.0 for $N = 5$ and approximations are used only for $N \geq 6$.

[37] Capitalization is used to help identify this long phrase as a single term.

[38] This configuration has immersed sensors on the ground in a search area with $side$ = 1,000 m with the Standard Error Conditions of σ_{pos} = 10 m position error and σ_{time} = 30 ns timing error. These mean LDE values are based on 10,000 simulations per configuration.

11.2 Power-Law Linear Regression Model for the Improvement Ratio

It was observed that the power-law (22) linear regression models, with the input variable x_1 replaced b y N, provided excellent fits for the Improvement Ratios for the configurations used in this paper.

Contrary to the experience with the linear regression models for the LDE statistical metrics as noted in Section 10.1, the best linear regression model fits for the Improvement Ratios were obtained using the data for five and more sensors (and not including the data for three and four sensors). Again, as noted in that section, the reasons for this are unclear. The power-law fit for five sensors, however, is not close to the actual value of 1.0 for the Improvement Ratio for five sensors and so (as noted in Section 11.1) it is defined to be exactly 1.0 for five sensors.

Thus, the **power-law** for an Improvement Ratio y can be defined in terms of N and the linear regression weights in a manner similar to that of (24) as

$$\begin{aligned} y &= \exp(w_0 + w_1 \ln N) \\ &= e^{w_0} N^{w_1} \end{aligned} \tag{28}$$

for $N \geq 6$, and $y = 1$ for five sensors.

To be completely forthcoming, the power-law fit was not quite the optimal linear regression model. The best fit in all cases appeared to be an exponential function of the double logarithm of the number of sensors (that is, the logarithm of an LDE statistical metric y was a linear function of the double logarithm of the number of sensors N). However, the improvements in R^2 and MAPE were so slight that the increased complexity of the exponential function of the double logarithm did not warrant their use. [39]

[39] It is also not clear why the "logarithm of the Improvement Ratios as a linear function of the logarithm of N" (that is, the power-law) and the "logarithm of Improvement Ratios as a linear function of the double logarithm of N" linear regression model fits were considerably better than the "double logarithm of the LDE statistical metrics as a linear function of the double logarithm of N" as observed in Section 9.1. Since the denominator in the Improvement Ratio for an LDE statistical metric is a constant with respect to N,

Figure 86 shows the Improvement Ratio for the Mean LDE for immersed sensors on the ground in a search area with $side = 1{,}000$ m with the Standard Error Conditions. The Improvement Ratio for $N = 8$ sensors is 0.5264, as was calculated in the example above. The trend line for a power-law fit, $y = 3.7354\, N^{-0.921}$, is shown on that plot and it can be seen that R^2 is nearly unity.

Figure 87, Figure 88, and Figure 89 show the Improvement Ratios for several other configurations, and the power-law is seen to provide good fits.

For the mean LDE for all of the configurations in the Main Data Set, MAPE for the power-law approximation was 4.75% when calculated for $N \geq 6$ immersed sensors. The maximum absolute percentage error for any configuration was 11.05% and the minimum R^2 was 0.9669. Fits were similarly good for the other LDE statistical metrics and for standoff configurations. [40]

The sets of w_0 (or e^{w_0}) and w_1 weights for the power-law linear regression model (28) could have been tabulated for each specific configuration as was done in Section 9.3 or generalized linear regression models could have been developed using the shotgun approach as was done in Section 10.1. However, good approximations of the Improvement Ratio are obtained by using the LDE linear regression models of Section 9.3 or Section 10.1.

For a given configuration, one of those linear regression models can be used to get an estimate of a desired LDE statistical metric for N sensors and for five sensors, and ratio of those values provides an estimate of the Improvement Ratio. Using the linear regression models of Section 9.3, for all configurations with $N \geq 6$ immersed sensors, MAPE was 7.6% and the maximum absolute percentage error for any configuration was 14.56%. For standoff sensors, MAPE was 1.75% and the maximum absolute percentage error for any configuration was 10.69%.

---

the overall shape of the Improvement Ratio should follow the overall shape of the specific LDE statistical metric. It is possible that the values of the LDE statistical metric for five and more sensors may be modeled better by the power-law. This might be the basis for future statistical exploration.

[40] MAPE would have been even smaller if it were calculated for $N \geq 5$ sensors using the definition that the Improvement Ratio is 1.0 for $N = 5$.

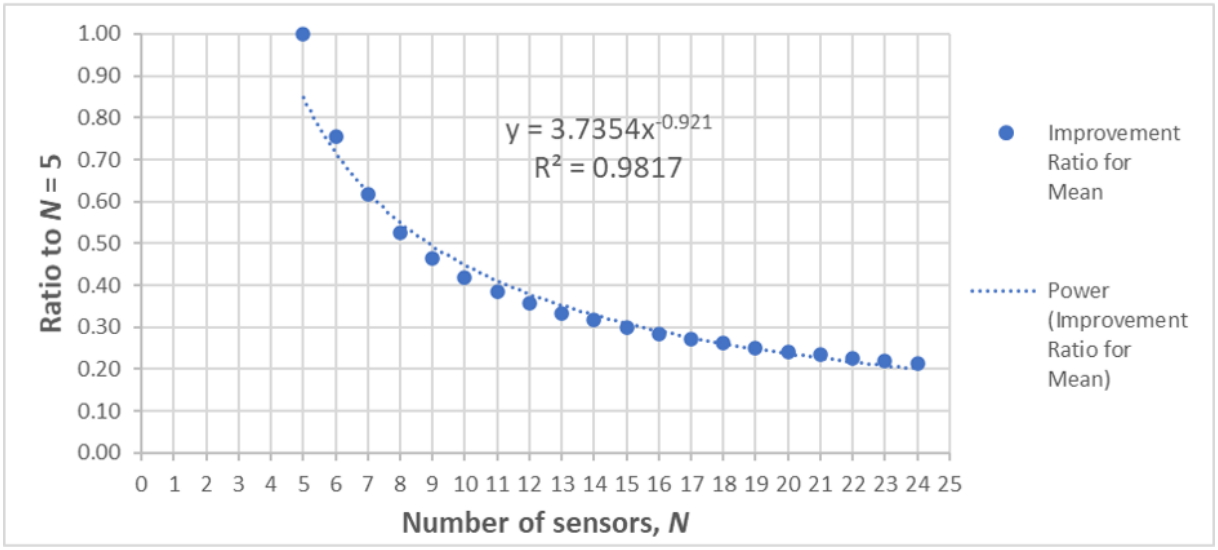

Figure 86: Improvement Ratio for the Mean LDE and its power-law trend line for immersed sensors. Parameters: *side* = 1,000 m, *alt* = 0 m, with errors.

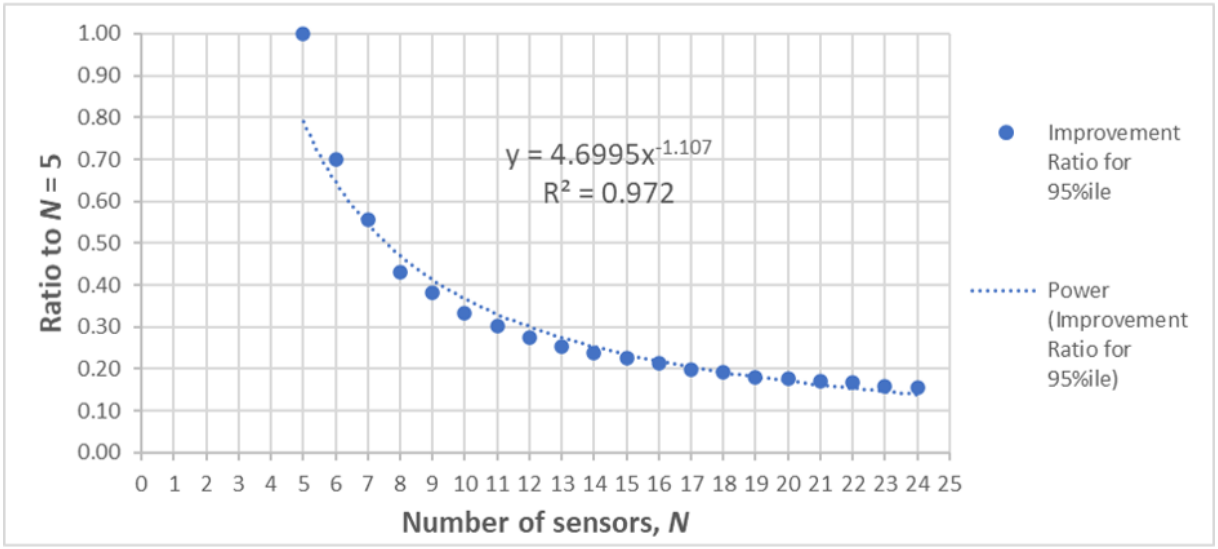

Figure 87: Improvement Ratio for the 95%ile LDE and its power-law trend line for immersed sensors. Parameters: *side* = 5,000 m, *alt* = 7,000 m, with errors.

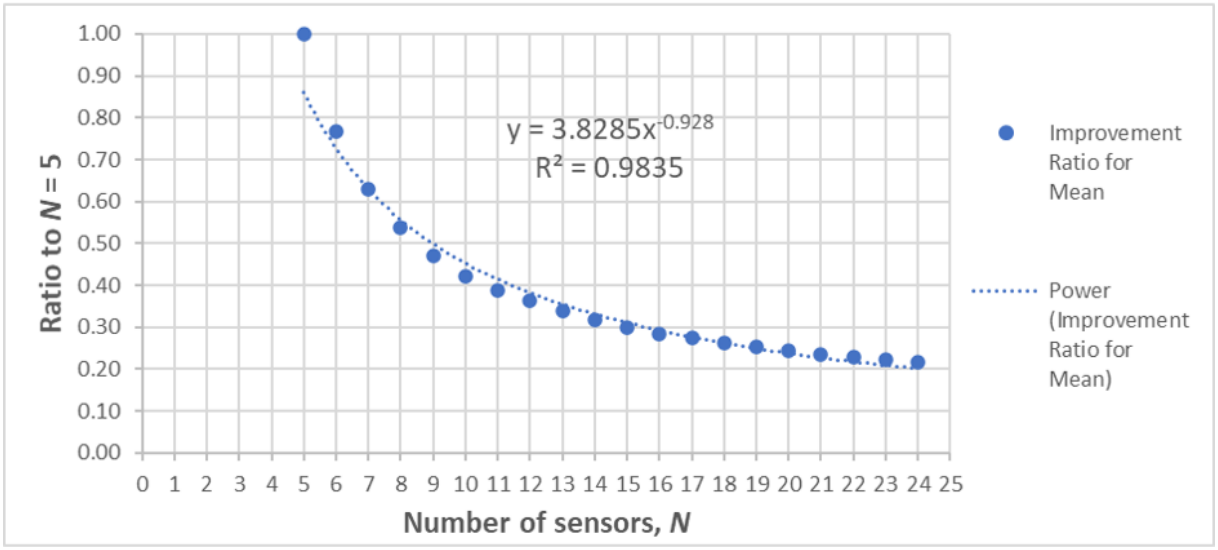

Figure 88: Improvement Ratio for the Mean LDE and its power-law trend line for standoff sensors. Parameters: $side$ = 3,000 m, alt = 300 m, with errors.

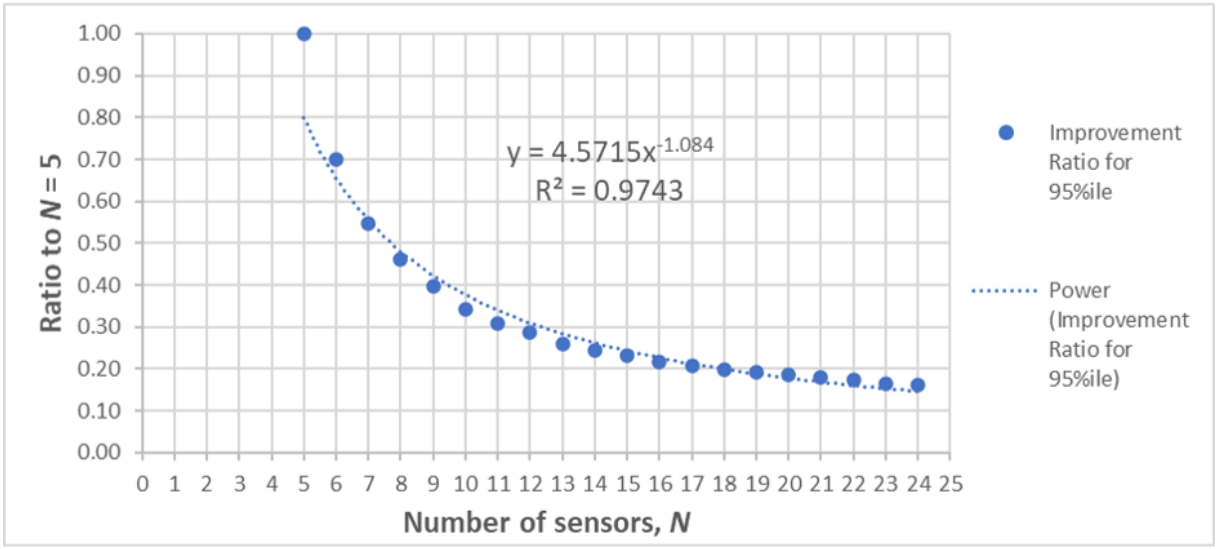

Figure 89: Improvement Ratio for the 95%ile LDE and its power-law trend line for standoff sensors. Parameters: $side$ = 8,000 m, alt = 500 m, with errors.

11.3 Reciprocal Approximations for the Improvement Ratio

Averaging over all of the configurations in the Main Data Set, the value of w_1 in the power-law fit for the Improvement Ratio hovered around negative one. For immersed sensors, w_1 averaged -0.9360, -0.7073, -1.1194, and -1.2761 for the mean, 50%ile, 95%ile, and 99%ile LDE, respectively, although the w_1 values for specific configurations ranged from -0.6322 to -1.4269. For standoff sensors, w_1 averaged -0.9291, -0.8203, -0.9981, and -1.1339 for the mean, 50%ile, 95%ile, and 99%ile LDE, respectively, and the w_1 values for specific configurations ranged from -0.6458 to -1.2959.

The fact that the averaged w_1 weights were close to negative one suggested that (28) might be approximated by a simple reciprocal function of N for these statistics. That is, the estimate of an Improvement Ratio for an LDE statistical metric, denoted by y, given by (28) as a function of two weights w_0 and w_1, might itself be estimated by the simpler **Reciprocal Approximation** [41] that is a function of a single weight [42] w_{RA} as

$$y = \frac{w_{RA}}{N} \quad . \tag{29}$$

for $N \geq 6$, and $y = 1$ for five sensors.

Since the MAPE curve as a function of w_{RA} is convex, the value of w_{RA} that minimizes MAPE over all of the configurations in the Main Data Set (for a given LDE statistical metric and for immersed or standoff sensors) for (29) is easily found. [43] For each of the four LDE statistical metrics, Table 17 gives the weights that minimized the MAPE for all configurations as well as the worst-case percentage error for any N for any configuration.

For example, if y is the Improvement Ratio for the Mean LDE for immersed sensors, then the value of w_{RA} the Reciprocal Approximations given in Table 17 is 4.07; thus, (29) yields $y = 4.07/N$ which has a MAPE of 10.92% over all configurations in the Main Data Set with $N \geq 6$. If y is the

[41] Capitalization is used to help identify this phrase as a single term.

[42] The term "weight" is used for w_{RA} for consistency, although the more general term "coefficient" might be more appropriate.

[43] Unlike the methods used to obtain the linear regression model weights for other estimates in this paper, the process of finding a good value of w_{RA} for the Reciprocal Approximations by minimizing MAPE is not linear regression.

Improvement Ratio for the 95%ile LDE for standoff sensors, the Reciprocal Approximation yields $y = 3.80/N$ which has a MAPE of 11.56% over all configurations in the Main Data Set with $N \geq 6$.

Table 17: Reciprocal Approximation weights w_{RA} for immersed and standoff sensors, based on Main Data Set, for mean, 50%ile, 95%ile, and 99%ile LDE.

Sensor Pairing	**LDE Statistical Metric**	w_{RA}	**MAPE**	**Max Percentage Error**
Immersed:	Mean	4.07	10.92%	-45.02%
	50%ile	5.96	12.13%	-31.02%
	95%ile	3.20	11.96%	-46.34%
	99%ile	2.50	15.29%	-44.64%
Standoff:	Mean	4.28	10.70%	-43.40%
	50%ile	5.16	9.23%	-37.71%
	95%ile	3.80	11.56%	-48.99%
	99%ile	3.00	18.09%	-58.57%

12 Ballpark Estimates and Reciprocal Approximations of the Envelope of the Improvement Ratio

The key idea of the previous section was to use the Improvement Ratio as the figure-of-merit for the decrease of an LDE statistical metric as the number of sensors increases. The previous section applied the Improvement Ratios and their Reciprocal Approximations to configurations with specific values of *alt* and *side*.

This section introduces another key idea where all configurations in the Main Data Set are considered at once using the **envelope** of an LDE statistical metric.

12.1 Envelope of the Improvement Ratio

The approach used here is to produce estimates of relative performance based on the statistics for an *envelope of the Improvement Ratio for an LDE statistical metric* **for all of the configurations and error conditions** in the Main Data Set (separately for immersed and standoff sensors), rather than considering the configurations individually. Figure 90 plots the Improvement Ratios for the Mean LDE for $N = 5$ to 24 immersed sensors for all of the configurations and error conditions represented in the Main Data Set. Each point in the envelope represents the Improvement Ratio for the Mean LDE resulting from 10,000 simulated geometries for a configuration with N sensors and a specific combination of altitude and search area side length. Similarly, Figure 91 plots the Improvement Ratios for the Mean LDE for $N = 5$ to 24 standoff sensors.

The surprisingly narrow width of the envelopes over the range of N prompted exploration of the descriptive statistics that describe the envelopes. These **Ballpark Estimates** [44] bound the envelope of the complete Main Data Set, for a given number of sensors, rather than try to pin down the LDE for a specific configuration and error conditions.

[44] Capitalization is used to help identify this phrase as a single term.

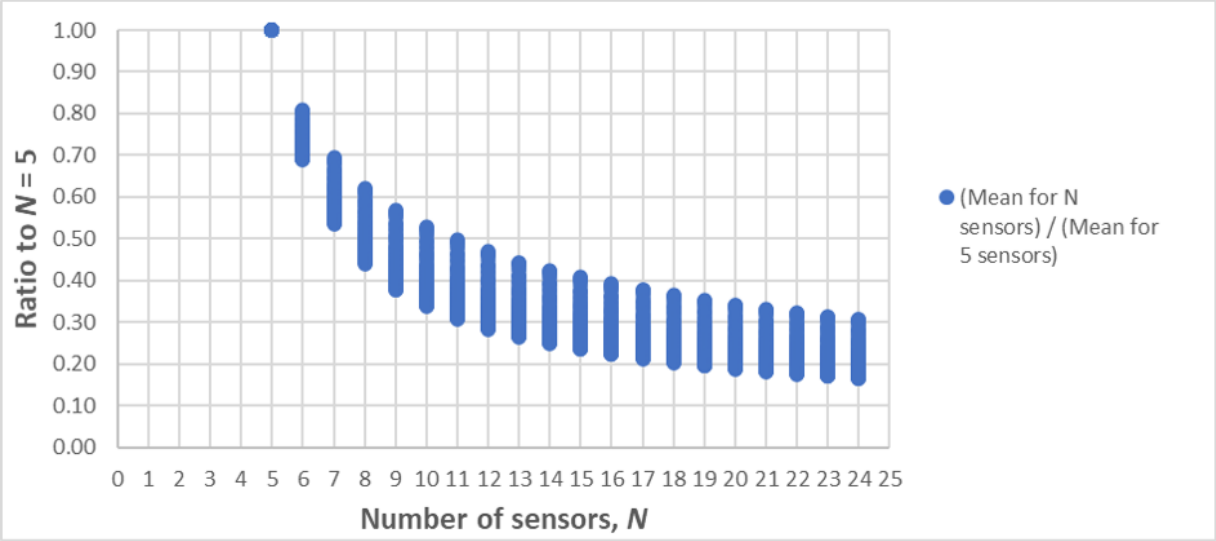

Figure 90: Envelope of all of the Improvement Ratios for the Mean LDE in the Main Data Set for immersed sensors.

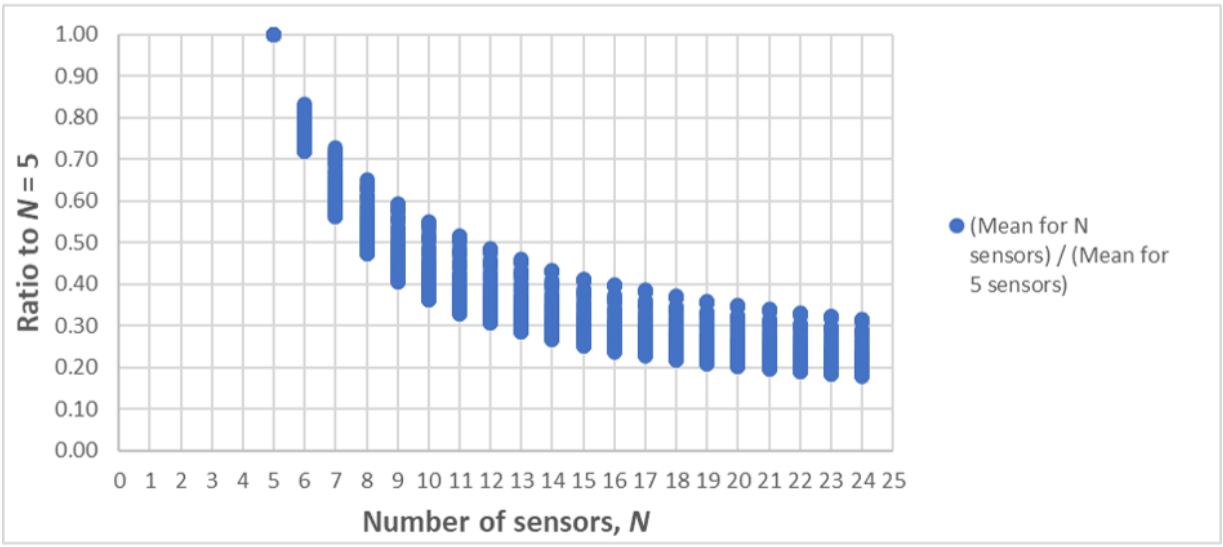

Figure 91: Envelope of all of the Improvement Ratios for the Mean LDE in the Main Data Set for standoff sensors.

12.2 Ballpark Estimates of the Statistics for the Envelope of the Improvement Ratio

For each of the four Improvement Ratios for an LDE statistical metric, linear regression models are obtained for descriptive statistics for the envelopes for N sensors. The envelope for the Improvement Ratios for the Mean LDE at N sensors, for example, is described using linear regression models for these descriptive statistics: the ***Minimum* of the Improvement Ratios for the Mean LDE**, the ***Mean* of the Improvement Ratios for the Mean LDE**, and the ***Maximum* of the Improvement Ratios for the Mean LDE**. [45] These descriptive statistics are obtained for a vertical slice through the envelope at a given value of N.

Thus, based on the envelope of the Improvement Ratios, the complete set of combinations of the descriptive statistics for the Improvement Ratios [46] for the statistical metrics is:

$$\left\{ \begin{array}{c} \text{Minimum} \\ \text{Mean} \\ \text{Maximum} \end{array} \right\} \text{ of the Improvement Ratios for the } \left\{ \begin{array}{c} \text{Mean} \\ \text{50\%ile} \\ \text{95\%ile} \\ \text{99\%ile} \end{array} \right\} \text{ LDE}$$

$$\text{for } N \left\{ \begin{array}{c} \text{immersed} \\ \text{standoff} \end{array} \right\} \text{ sensors, with respect to five sensors.}$$

Figure 92 shows the linear regression models for the statistics for the envelope of the Improvement Ratios for the Mean LDE for immersed sensors plotted in Figure 90. For numbers of sensors $N = 5$ to 24, the points plotted are the Minimum, Mean, and Maximum of the Improvement Ratios for the Mean LDE for *any* configuration and error conditions in the Main Data Set with N sensors.

Just as the Improvement Ratios for the LDE statistical metrics were modeled adequately using a power-law function of the number of sensors, it was found that the descriptive statistics for the *envelopes* of the Improvement Ratios for the LDE statistical metrics also were described

[45] Capitalization is used to help identify these long phrases as single terms.

[46] Recall that the LDE statistical metric for five sensors is used to provide the reference value for the ratio so as to eliminate Longfellow Events.

faithfully using power-law relationships; these expressions are referred to in this paper as the **Ballpark Estimates**.

The power-law equation for a Ballpark Estimate linear regression model is defined in terms of linear regression weights in (28), where the output variable y represents the Minimum, Mean, or Maximum of the Improvement Ratios for the Mean, 50%ile, 95%ile, or 99%ile LDE. [47] Two alternate expressions are given in (28), where the second is the form displayed as the trend line equations in the plots shown in Figure 92.

Expression (28) is used only for $N = 6$ to 24 sensors because Improvement Ratios are defined to be 1.0 for five sensors.

Figure 92 shows the Microsoft Excel trend lines, their equations, and R^2 values for these statistics. For example, the trend line equation for the *Maximum* of the Improvement Ratios for the Mean LDE (for all of the simulated configurations and error conditions in the Main Data Set for N immersed sensors) is displayed as $y = 2.7711x^{-0.703}$; in the notation of this paper and with an extra digit of precision in the exponent obtained from the more detailed linear regression, this would be written as $y = 2.7711\, N^{-0.7027}$ with y denoting the Maximum of the Improvement Ratios for the Mean LDE at the given value of N. The R^2 value for this linear regression model is 0.9879 showing an extremely close fit to the measured values. Similarly, the linear regression model for the *Minimum* of the Improvement Ratios for the Mean LDE would be written as $y = 4.1546\, N^{-1.0452}$ and the linear regression model for the *Mean* of the Improvement Ratios for the Mean LDE would be written as $y = 3.6026\, N^{-0.9263}$. The R^2 values for these two power-law linear regression models are also both close to unity indicating excellent goodness-of-fit.

It was noted in Section 8.2 that all of the linear regression models except those in this section were based on simulation data for $N = 3$ to 24 but are useful only for five and more sensors. It was also noted that experimentation showed that the best results for the Ballpark Estimate approach described here were obtained using the simulation data for $N = 5$ to 24. In a sense however, the same phenomenon occurred again in that it was found that the Ballpark Estimate linear regression models developed in this section must be applied only for $N = 6$ to 24; although the Ballpark Estimate linear

[47] Capitalization is used to help identify these long phrases as single terms.

regression models give poor results for five sensors, the Improvement Ratio for the Mean LDE is, by definition, exactly 1.0 for five sensors.

Figure 93 shows the trend lines for the same statistics and the same configurations and error conditions as above for standoff sensors. The linear regression model for the *Maximum* of the Improvement Ratios for the Mean LDE (for all of the simulated configurations in the Main Data Set for N standoff sensors) is $y = 2.9173\ N^{-0.7124}$, the linear regression model for the *Minimum* of the Improvement Ratios for the Mean LDE is $y = 4.135\, N^{-1.0812}$, and the linear regression model for the *Mean* of the Improvement Ratios for the Mean LDE is $y = 3.7142\, N^{-0.9192}$. Again, the R^2 values for all three power-law linear regression models are nearly unity.

Figure 94 and Figure 95 (for immersed and standoff sensors, respectively) show the power-law linear regression models for the Minimum, Mean, and Maximum of the Improvement Ratios for the 50%ile LDE. The envelopes for the Improvement Ratios for the 50%ile LDE are even tighter than those for the Improvement Ratios for the Mean LDE.

Figure 96 and Figure 97 show the power-law linear regression models for the three Improvement Ratios for the 95%ile LDE and Figure 98 and Figure 99 show the power-law linear regression models for the three Improvement Ratios for the 99%ile LDE.

The smallest R^2 value for any of these dozen linear regression models is 0.9530, indicating excellent goodness-of-fit.

Table 18 through Table 25 give the weights and R^2 values for all of the descriptive statistics for the Ballpark Estimate linear regression models.

These tables are used as follows. For example, suppose it is desired to estimate the Mean of the Improvement Ratios for the Mean LDE as a function of the number of immersed sensors.

First, from Table 18, the second line gives the weights for the Mean of the Improvement Ratios for the Mean LDE. The values for w_1 and either w_0 or e^{w_0} are plugged into the appropriate expression in (28) to obtain the linear regression model for the Mean of the Improvement Ratios for the Mean LDE for immersed sensors. Here, the second alternate expression for the Mean of the Improvement Ratios for the Mean LDE is used:

$$y = 3.6026\, N^{-0.9263} \quad . \tag{30}$$

(The corresponding expression for standoff sensors is obtained using Table 19, where the second line gives the weights for the Mean of the Improvement Ratios for the Mean LDE that are plugged into (28) to obtain the linear regression model for the Mean of the Improvement Ratios for the Mean LDE for standoff sensors:

$$y = 3.7142\, N^{-0.9192} \quad . \tag{31}$$

Expressions (30) and (31) are used in Section 12.4.)

Second, having obtained (30) for immersed sensors, the reduction in the Mean of the Improvement Ratios for the Mean LDE achieved by increasing the number of sensors can be estimated. Setting $N = 6$ in (30) yields the result that randomly selected configurations from the Main Data Set with six immersed sensors have $y = 0.6852$ or 68.52% of the Mean of the Improvement Ratios for the Mean LDE as the same configurations with only five sensors. Setting $N = 8$ in (30) estimates that eight immersed sensors have 52.49% of the Mean of the Improvement Ratios for the Mean LDE as the configurations with five sensors.

Expression (30) can also be solved for N to determine how many immersed sensors are needed to reduce the Mean of the Improvement Ratios for the Mean LDE to a target level. If a target value of $y = 0.25$ for the Mean of the Improvement Ratios for the Mean LDE were required, then the requisite value of N would be $\lceil 17.82 \rceil = 18$ immersed sensors; the estimated Mean of the Improvement Ratios for the Mean LDE with 18 immersed sensors would be 24.77%, which would achieve the required target value.

Bounds on the statistics for the Improvement Ratio for an LDE statistical metric are used as follows. From Table 18 and (30), the Minimum of the Improvement Ratios for the Mean LDE for immersed sensors is given by

$$y = 4.1546\, N^{-0.9669} \tag{32}$$

and the Maximum of the Improvement Ratios for the Mean LDE for immersed sensors is given by

$$y = 2.7711\, N^{-0.9879} \quad . \tag{33}$$

Setting $N = 6$ in (32) and (33) yields the lower and upper bounds of 63.86% and 78.68% for the Mean of the Improvement Ratios for the Mean LDE for eight immersed sensors compared to the same configurations with only five sensors. Setting $N = 8$ in (32) and (33) yield the lower and upper bounds of 47.28% and 64.28% for the Mean of the Improvement Ratios for the Mean LDE for eight immersed sensors compared to the same configurations with only five sensors.

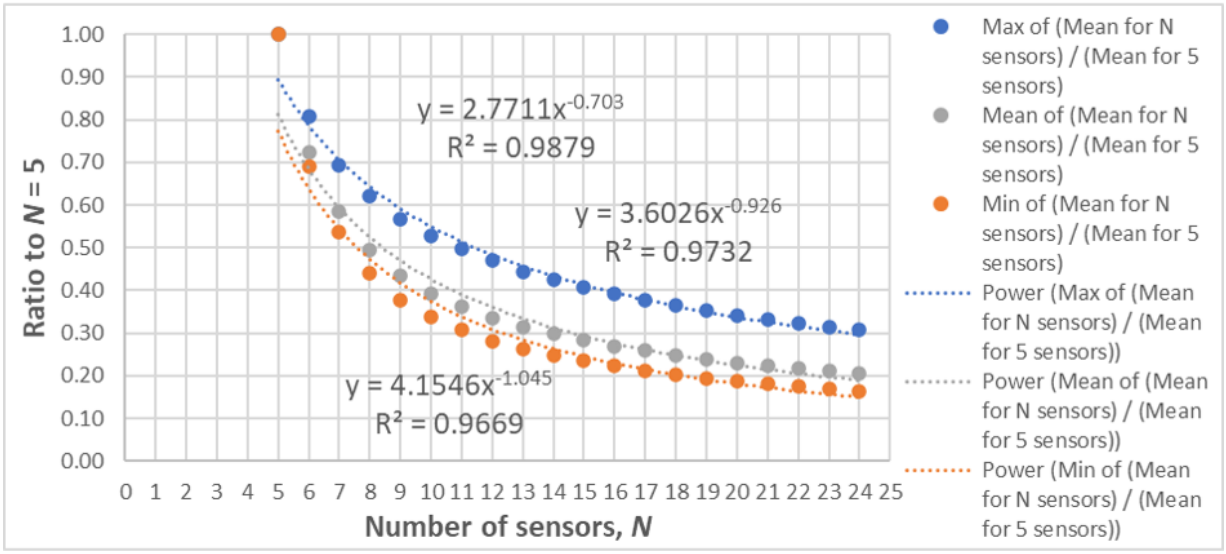

Figure 92: For the envelope shown in Figure 90, power-law trend lines and linear regression models are shown for the Minimum, Mean, and Maximum of the Improvement Ratios for the Mean LDE for immersed sensors.

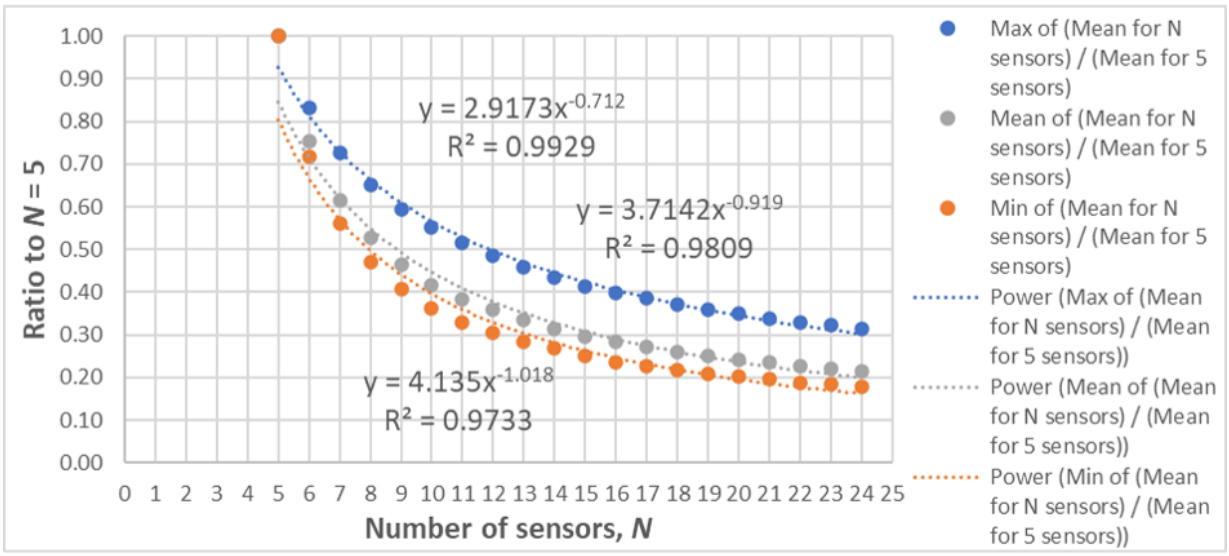

Figure 93: For the envelope shown in Figure 91, power-law trend lines and linear regression models are shown for the Minimum, Mean, and Maximum of the Improvement Ratios for the Mean LDE for standoff sensors.

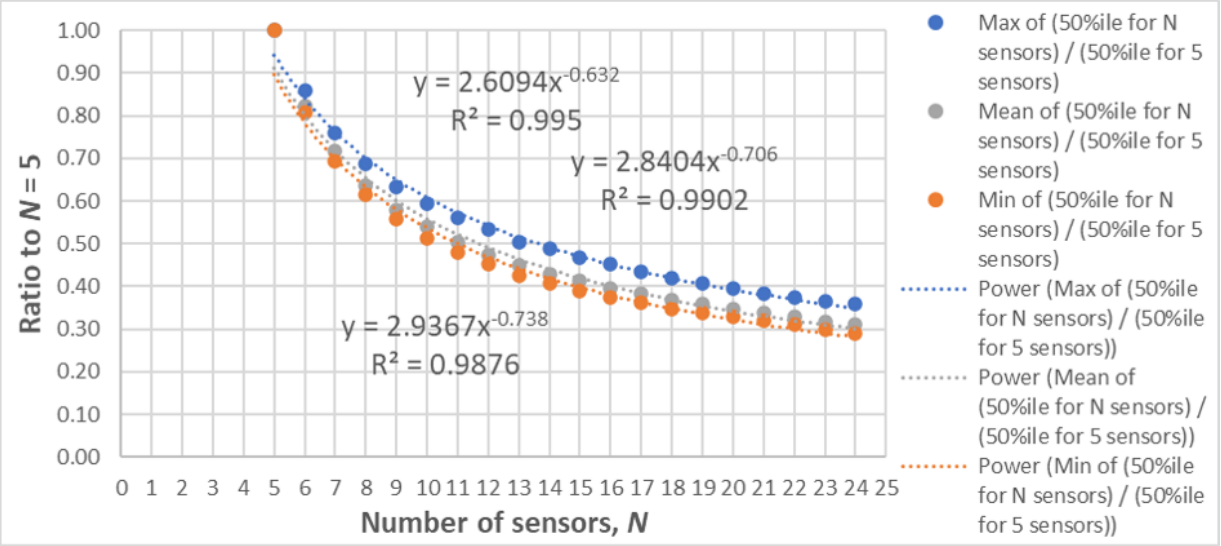

Figure 94: For envelope of the Improvement Ratios for the 50%ile LDE, power-law trend lines and linear regression models are shown for the Minimum, Mean, and Maximum of the Improvement Ratios for the 50%ile LDE for immersed sensors.

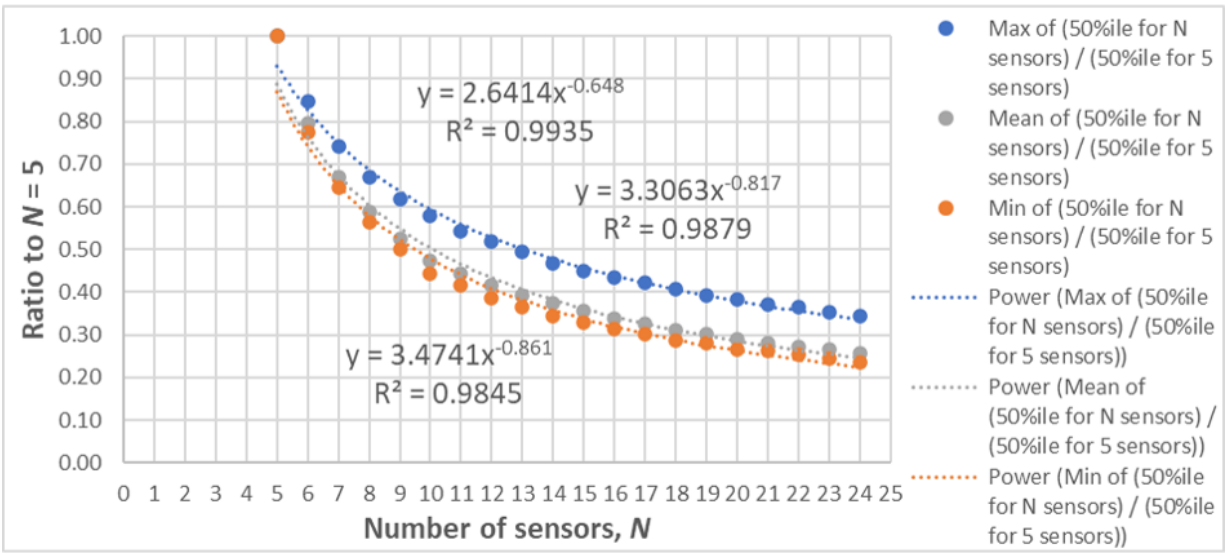

Figure 95: For envelope of the Improvement Ratios for the 50%ile LDE, power-law trend lines and linear regression models are shown for the Minimum, Mean, and Maximum of the Improvement Ratios for the 50%ile LDE for standoff sensors.

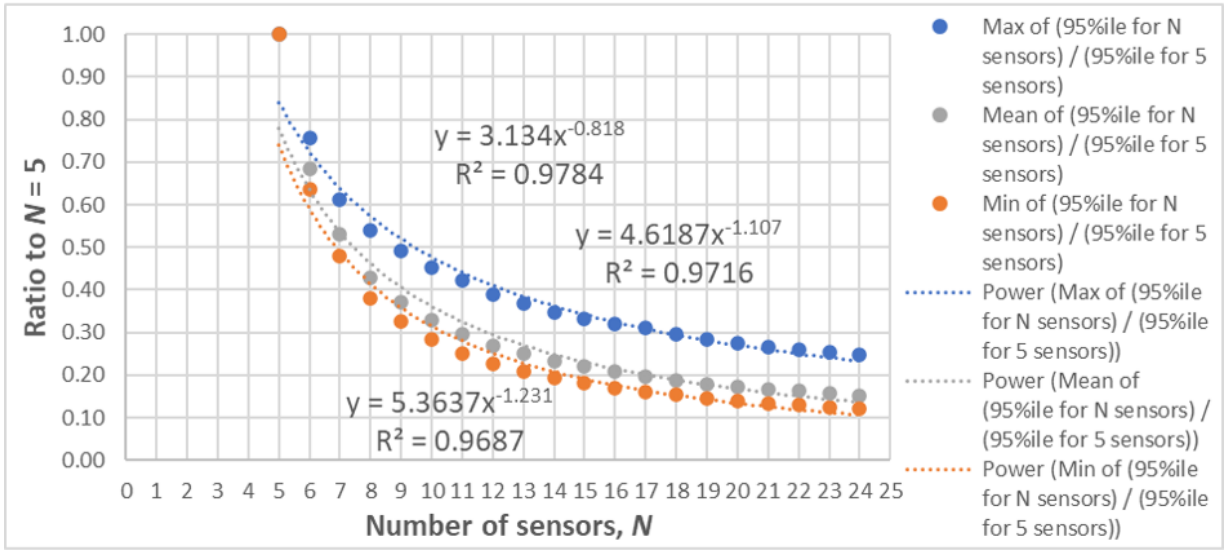

Figure 96: For envelope of the Improvement Ratios for the 95%ile LDE, power-law trend lines and linear regression models are shown for the Minimum, Mean, and Maximum of the Improvement Ratios for the 95%ile LDE for immersed sensors.

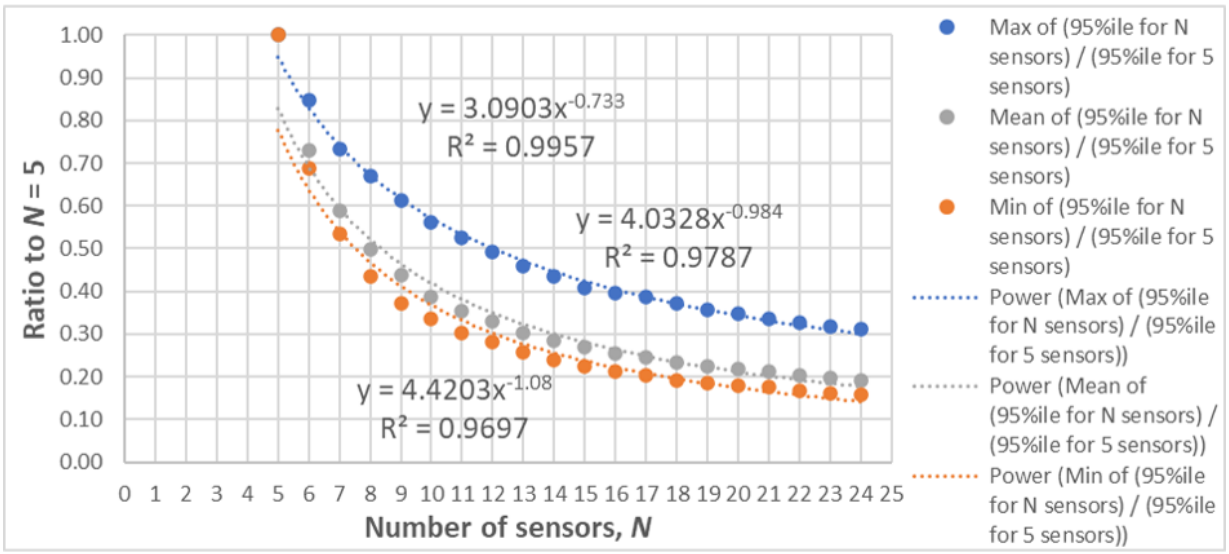

Figure 97: For envelope of the Improvement Ratios for the 95%ile LDE, power-law trend lines and linear regression models are shown for the Minimum, Mean, and Maximum of the Improvement Ratios for the 95%ile LDE for standoff sensors.

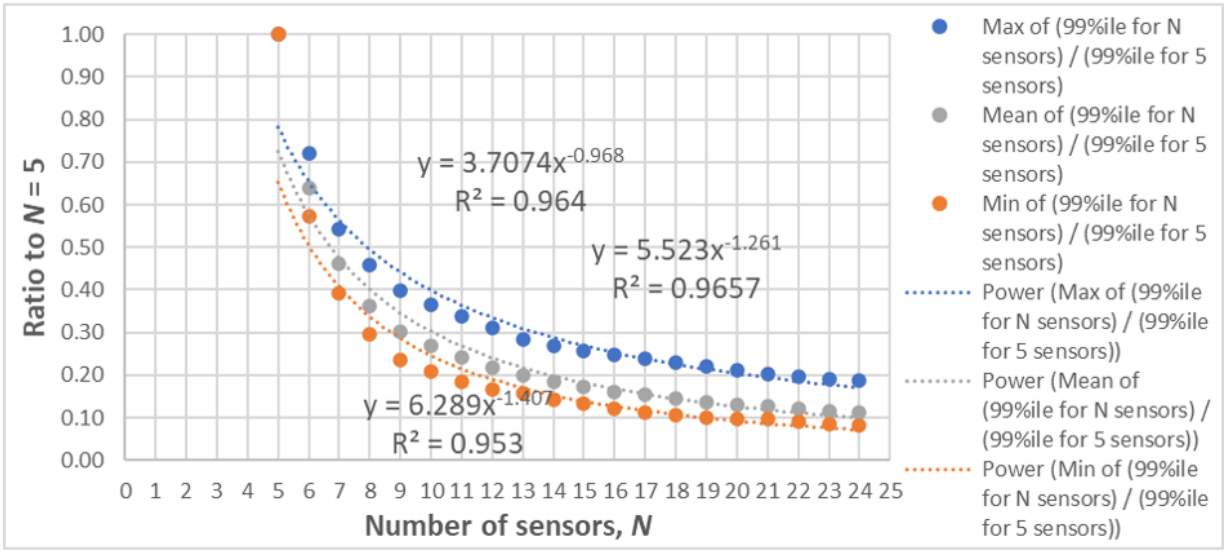

Figure 98: For envelope of the Improvement Ratios for the 99%ile LDE, power-law trend lines and linear regression models are shown for the Minimum, Mean, and Maximum of the Improvement Ratios for the 99%ile LDE for immersed sensors.

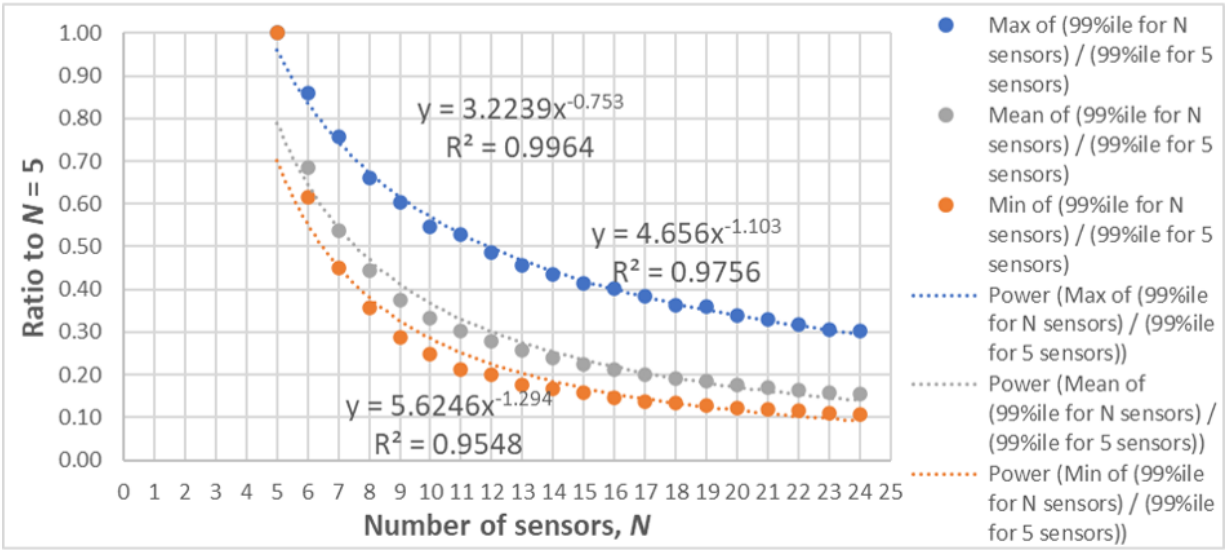

Figure 99: For envelope of the Improvement Ratios for the 99%ile LDE, power-law trend lines and linear regression models are shown for the Minimum, Mean, and Maximum of the Improvement Ratios for the 99%ile LDE for standoff sensors.

Table 18: Weights for power-law linear regression model for Minimum, Mean, and Maximum of the Improvement Ratios for the Mean LDE for immersed sensors, as shown in Figure 92.

Statistics for ratio: (Mean LDE for N sensors) / (Mean LDE for 5 sensors)	w_0	w_1	e^{w_0}	R^2
Max of ratio	1.0192	-0.7027	2.7711	0.9879
Mean of ratio	1.2817	-0.9263	3.6026	0.9732
Min of ratio	1.4242	-1.0452	4.1546	0.9669

Table 19: Weights for power-law linear regression model for Minimum, Mean, and Maximum of the Improvement Ratios for the Mean LDE for standoff sensors, as shown in Figure 93.

Statistics for ratio: (Mean LDE for N sensors) / (Mean LDE for 5 sensors)	w_0	w_1	e^{w_0}	R^2
Max of ratio	1.0707	-0.7124	2.9173	0.9929
Mean of ratio	1.3122	-0.9192	3.7142	0.9809
Min of ratio	1.4195	-1.0182	4.1350	0.9733

Table 20: Weights for power-law linear regression model for Minimum, Mean, and Maximum of the Improvement Ratios for the 50%ile LDE for immersed sensors, as shown in Figure 94.

Statistics for ratio: (50%ile LDE for N sensors) / (50%ile LDE for 5 sensors)	w_0	w_1	e^{w_0}	R^2
Max of ratio	0.9591	-0.6322	2.6094	0.9950
Mean of ratio	1.0439	-0.7063	2.8404	0.9902
Min of ratio	1.0773	-0.7377	2.9367	0.9876

Table 21: Weights for power-law linear regression model for Minimum, Mean, and Maximum of the Improvement Ratios for the 50%ile LDE for standoff sensors, as shown in Figure 95.

Statistics for ratio: (50%ile LDE for N sensors) / (50%ile LDE for 5 sensors)	w_0	w_1	e^{w_0}	R^2
Max of ratio	0.9713	-0.6479	2.6414	0.9935
Mean of ratio	1.1958	-0.8173	3.3063	0.9879
Min of ratio	1.2453	-0.8613	3.4741	0.9845

Table 22: Weights for power-law linear regression model for Minimum, Mean, and Maximum of the Improvement Ratios for the 95%ile LDE for immersed sensors, as shown in Figure 96.

Statistics for ratio: (95%ile LDE for N sensors) / (95%ile LDE for 5 sensors)	w_0	w_1	e^{w_0}	R^2
Max of ratio	1.1423	-0.8176	3.1340	0.9784
Mean of ratio	1.5301	-1.1067	4.6187	0.9716
Min of ratio	1.6797	-1.2310	5.3637	0.9687

Table 23: Weights for power-law linear regression model for Minimum, Mean, and Maximum of the Improvement Ratios for the 95%ile LDE for standoff sensors, as shown in Figure 97.

Statistics for ratio: (95%ile LDE for N sensors) / (95%ile LDE for 5 sensors)	w_0	w_1	e^{w_0}	R^2
Max of ratio	1.1283	-0.7332	3.0903	0.9957
Mean of ratio	1.3945	-0.9835	4.0328	0.9787
Min of ratio	1.4862	-1.0798	4.4203	0.9697

Table 24: Weights for power-law linear regression model for Minimum, Mean, and Maximum of the Improvement Ratios for the 99%ile LDE for immersed sensors, as shown in Figure 98.

Statistics for ratio: (99%ile LDE for N sensors) / (99%ile LDE for 5 sensors)	w_0	w_1	e^{w_0}	R^2
Max of ratio	1.3103	-0.9678	3.7074	0.9640
Mean of ratio	1.7089	-1.2606	5.5230	0.9657
Min of ratio	1.8388	-1.4070	6.2890	0.9530

Table 25: Weights for power-law linear regression model for Minimum, Mean, and Maximum of the Improvement Ratios for the 99%ile LDE for standoff sensors, as shown in Figure 99.

Statistics for ratio: (99%ile LDE for N sensors) / (99%ile LDE for 5 sensors)	w_0	w_1	e^{w_0}	R^2
Max of ratio	1.1706	-0.7525	3.2239	0.9964
Mean of ratio	1.5382	-1.1026	4.6560	0.9756
Min of ratio	1.7272	-1.2943	5.6246	0.9548

12.3 Reciprocal Approximations for the Mean of the Envelope of the Improvement Ratio for the Mean LDE

In Table 18 and Table 19, note that the w_1 weights for the Mean of the Improvement Ratios for the Mean LDE for both immersed and standoff sensors are close to negative one: they are -0.9263 and -0.9192, respectively. This fortunate situation indicates that (28) again can be approximated by a simple reciprocal function w_{RA}/N for these statistics. As the MAPE curve as a function of w_{RA} is convex, the value of w_{RA} that minimizes MAPE is easily found. This optimization process yielded the simplified expression for the Mean of the Improvement Ratios for the Mean LDE for immersed sensors

$$y = \frac{4.25}{N} \tag{34}$$

and the Mean of the Improvement Ratios for the Mean LDE for standoff sensors

$$y = \frac{4.50}{N} \quad . \tag{35}$$

These simplified expressions for the Ballpark Estimates are referred to as **Reciprocal Approximations**. As was the case for (28), these expressions are valid for $N = 6$ to 24 and the Improvement Ratio for the Mean LDE is defined to be exactly 1.0 for five sensors.

The close fits of (34) and (35) to the true mean values of the mean LDE are shown in Figure 100 and Figure 101 for immersed and standoff sensors, respectively. MAPE for (34) is 6.26% and MAPE for (35) is 5.69% over the range $N = 6$ to 24.

It must be emphasized that these MAPE values are with respect to the mean value of the mean LDE for *all* of the configurations and error conditions in the Main Data Set, with respect to a given number of sensors, rather than with respect to *specific configurations* as was done in previous sections.

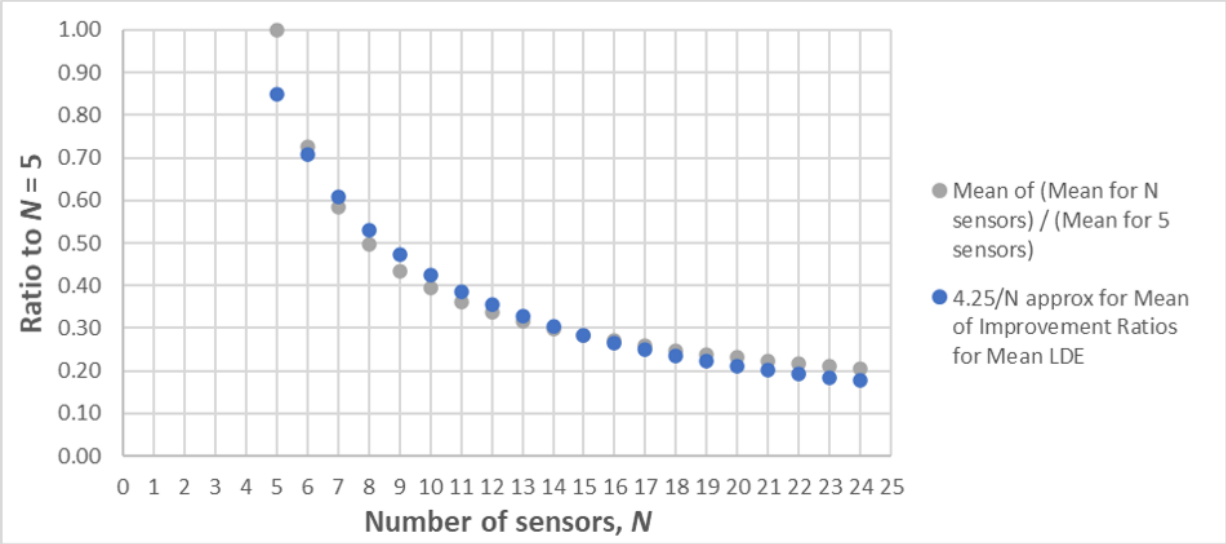

Figure 100: Reciprocal Approximation for the Mean of the Improvement Ratio for the Mean LDE for immersed sensors.

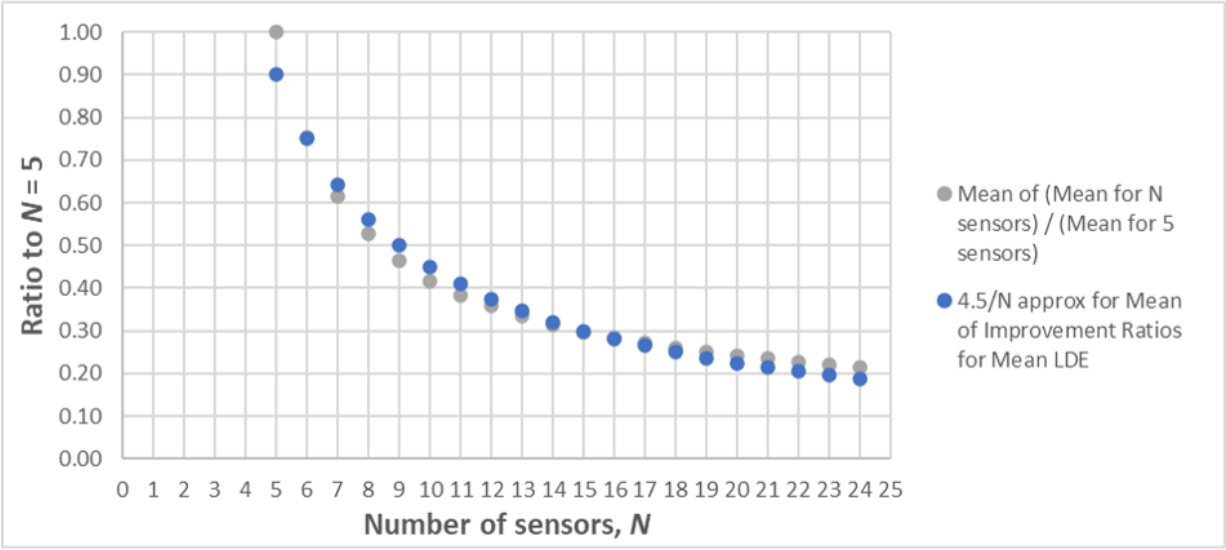

Figure 101: Reciprocal Approximation for the Mean of the Improvement Ratio for the Mean LDE for standoff sensors.

12.4 Testing the Ballpark Estimates and Reciprocal Approximations

The estimates of the descriptive statistics for the Ballpark Estimates and Reciprocal Approximations were developed only for the *envelope* of all of the configurations and error conditions contained in the Main Data Set, but it is instructive and irresistible to see how closely they model the *specific configurations*. Only the estimates for Mean of the Improvement Ratios for the Mean LDE were considered.

For all of the configurations with $N = 6$ to 24 immersed sensors in the Main Data Set, Ballpark Estimates of the Mean of the Improvement Ratios for the Mean LDE were obtained using (30). MAPE for those estimates was 12.06%, and the largest percentage error was −38.49%. Using the Reciprocal Approximation for the Mean of the Improvement Ratios for the Mean LDE given by (34), MAPE for those estimates was 11.45%, and the largest percentage error was −42.59%. For comparison, the MAPE achieved by the linear regression model presented in Section 10.1 was only 2.33% and the largest percentage error was 14.33% over the range of $N = 5$ to 24 immersed sensors.

Similarly, for all of the configurations with $N = 6$ to 24 standoff sensors, MAPE for the Ballpark Estimates given by (31) was 12.17%, and the largest percentage error was −36.50%. Using the Reciprocal Approximation for the Mean of the Improvement Ratios for the Mean LDE given by (34), MAPE for those estimates was 11.61%, and the largest percentage error was −40.49%. The MAPE achieved by the linear regression model presented in Section 10.1 was 2.43% and the largest percentage error was 15.31% over the range of $N = 5$ to 24 standoff sensors.

Clearly, the more detailed linear regression model that takes into account the specific altitude and search area side length provides much tighter estimates than the Ballpark Estimates and Reciprocal Approximations, but the trade-off of simplicity and fewer assumptions may make the Ballpark Estimates more attractive to a user.

13 Sensitivity to Variations in Sensor Altitude and Error Conditions

In the previous sections, all of the simulations set the coefficient of variation of the nominal altitude σ_{alt}/alt to be 5%. In addition, the Standard Error Conditions of $\sigma_{pos} = 10$ m position error and $\sigma_{time} = 30$ ns timing error were used. These notional amounts of variation in the configurations and error conditions were selected to be reasonable but not based on any actual military or civilian systems or scenarios.

This section explores the sensitivity of the results of this paper's analyses to ranges of values of σ_{alt}, σ_{pos}, and σ_{time}. The ranges are intended to be reasonable but not tied to any actual implementation.

13.1 Sensitivity to Variations in Nominal Altitude

A set of simulations was performed to determine how the standard deviation σ_{alt} about the mean altitude affects LDE. Only the mean LDE was considered. The simulated configurations had $N = 5$, 10, 15, and 20 immersed sensors in a search area with side length $side = 1{,}000$ m at nominal altitudes of $alt = 500$ m and 1,000 m. The Standard Error Conditions were used.

The coefficient of variation σ_{alt}/alt was varied over the values 0, 0.05, 0.1, 0.2, and 0.25. Thus, for $alt = 500$ m, the configurations used the values $\sigma_{alt} = 0$ m, 25 m, 50 m, 100 m, and 125 m. For $alt = 1{,}000$ m, the configurations used the values $\sigma_{alt} = 0$ m, 50 m, 100 m, 200 m, and 250 m.

Due to the long run times required, only 1,000 simulations of each configuration were performed.

The variation in mean LDE obtained for the configurations using the five simulated values of σ_{alt} for a given nominal altitude was used to assess the effect of σ_{alt} on LDE. Specifically, the *variation in mean LDE* is expressed here in the form similar to a "percent error" calculation: it is defined as the percentage difference between the maximum and minimum mean LDE (for the five values of σ_{alt}) for a configuration, with respect to the minimum mean LDE. Thus, the **percentage variation in mean LDE** is given by

$$\frac{(\text{max mean LDE}) \;-\; (\text{min mean LDE})}{(\text{min mean LDE})} \times 100\% \;\; . \tag{36}$$

It was found that the percentage variation in mean LDE was small for every combination of N and alt tested. For the numbers of sensors and the nominal altitudes identified above, the percentage variations in mean LDE were:

- 3.89% for $N = 5$ and $alt = 500$ m
- 3.00% for $N = 5$ and $alt = 1{,}000$ m
- 2.49% for $N = 10$ and $alt = 500$ m
- 5.10% for $N = 10$ and $alt = 1{,}000$ m
- 2.22% for $N = 15$ and $alt = 500$ m

- 6.02% for $N = 15$ and $alt = 1{,}000$ m
- 2.67% for $N = 20$ and $alt = 500$ m
- 6.65% for $N = 20$ and $alt = 1{,}000$ m

Within each set of mean LDE values for the five σ_{alt} per nominal altitude, there was no obvious pattern that indicated that mean LDE was worse for small or large σ_{alt}. Based on these small values of the percentage variations in mean LDE, it can be concluded that the model used in this paper is practically insensitive to the standard deviation of the nominal altitude of the sensors. [48]

[48] A formal test of hypothesis concerning the difference of two means would have to be conducted to confirm whether there is, in fact, *any* statistically significant difference in mean LDE for the ranges of σ_{alt} that were simulated.

13.2 Sensitivity to Variations in Error Conditions

The Standard Error Conditions used prior to this section fixed the value of σ_{pos} at 10 m and σ_{time} at 30 ns. This section explores the effect on mean LDE of varying either σ_{pos} or σ_{time} over a range of values with the other error condition set at zero.

A dozen combinations of simulated configurations were used with $N = 5$, 10, 15, and 20 immersed sensors in a search area with side length $side = 1{,}000$ m at nominal altitudes of $alt = 0$ m, 500 m, and 1,000 m with $\sigma_{alt} = alt/20$.

Due to the long run times required, only 1,000 simulations of each configuration were performed.

The figures-of-merit for these analyses were the mean LDE as well as the Improvement Ratio for the Mean LDE as defined in Section 12.1.

13.2.1 Varying Only Position Error Conditions

The effect of introducing position error alone was explored by varying σ_{pos} while σ_{time} was set to zero. The values of σ_{pos} varied from 5 m to 20 m, which were half to twice the standard error condition of $\sigma_{pos} = 10$ m used in the Main Data Set.

Figure 102 shows the mean LDE for the 12 simulated configurations over the given range of σ_{pos}. The major takeaway from this figure is that the mean LDE increased essentially linearly with the position error. Table 26 provides the linear regression models for (21) for each of the 12 simulated configurations, where w_1 is the slope of the best straight line estimate and w_0 is the intercept. The R^2 goodness-of-fit values are essentially unity.

Figure 103 shows how the Improvement Ratios for the Mean LDE increase as position error increases for sensors on the ground. The trend lines are very nearly parallel. The figure shows that position error is a factor for immersed sensors on the ground as the benefit of using more sensors is slightly reduced when σ_{pos} increases.

On the other hand, Figure 104 where $alt = 500$ m and Figure 105 where $alt = 1{,}000$ m show Improvement Ratio for the Mean LDE trend lines that are practically flat. This indicates, at least for the configurations and range of position errors considered here, that position error for immersed airborne sensors has little effect on the Improvement Ratio for the Mean LDE.

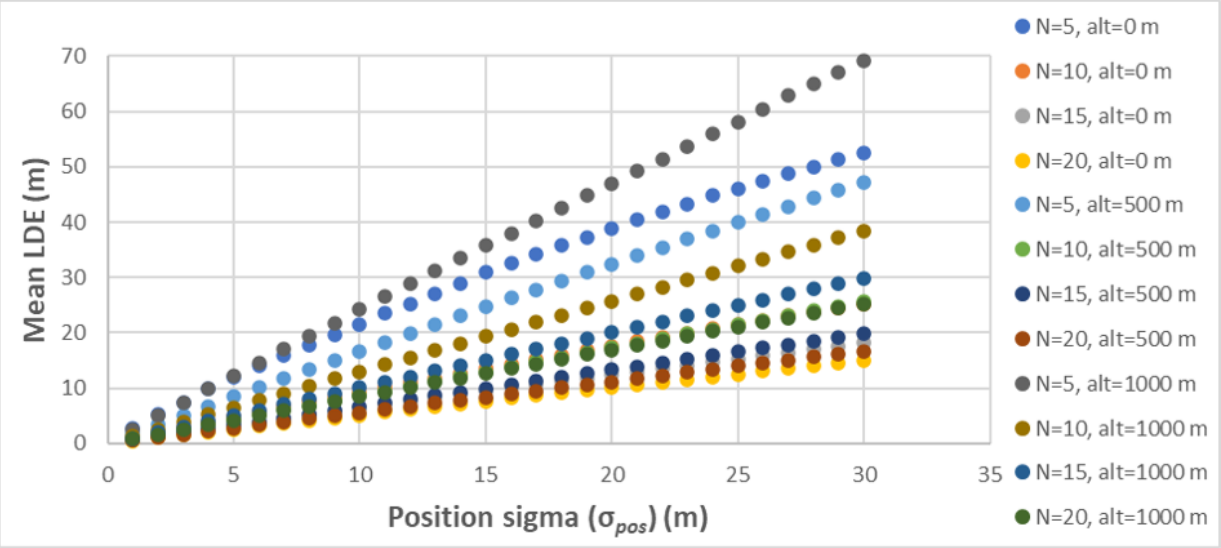

Figure 102: Mean LDE as a function of standard deviation of position error (σ_{pos}). See text for description of configurations and error conditions.

Table 26: Linear regression models for the mean LDE relationships as a function of σ_{pos} (in m) shown in Figure 102.

N	alt **(m)**	w_0	w_1	R^2
5	0	3.8997	1.6994	0.9930
10	0	0.7578	0.8334	0.9985
15	0	0.3366	0.6021	0.9994
20	0	0.1569	0.4981	0.9998
5	500	0.7706	1.5696	0.9995
10	500	0.1443	0.8530	1.0000
15	500	0.0745	0.6607	1.0000
20	500	0.0432	0.5575	1.0000
5	1000	0.9416	2.2947	0.9997
10	1000	0.1567	1.2783	1.0000
15	1000	0.0947	0.9965	1.0000
20	1000	0.0642	0.8412	1.0000

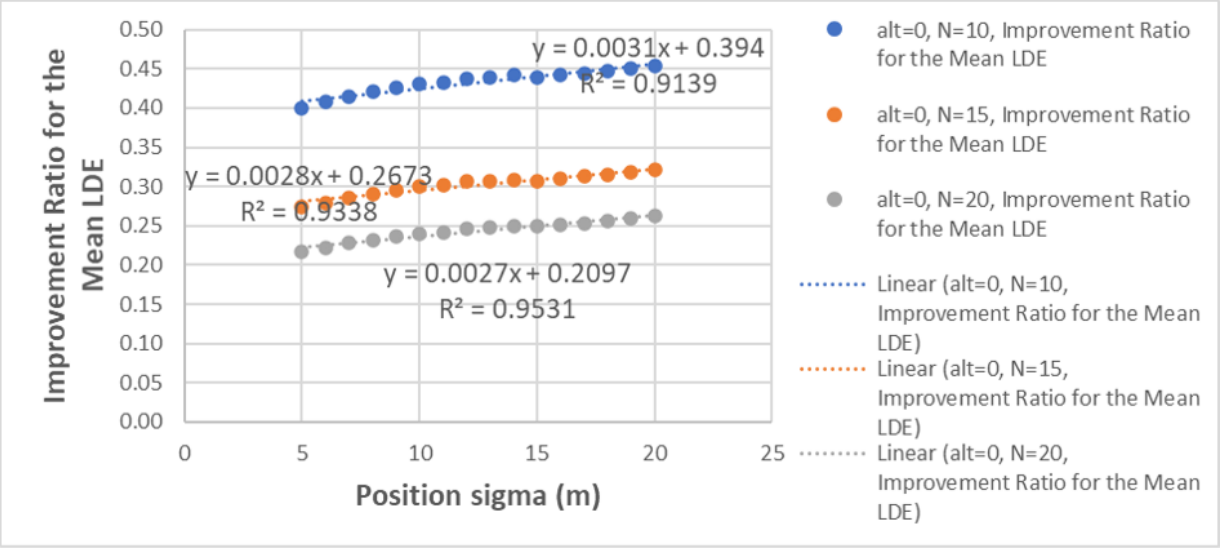

Figure 103: Improvement Ratios for the Mean LDE for immersed sensors on the ground, with trend lines and linear regression models, as a function of σ_{pos}. See text for description of configurations and error conditions.

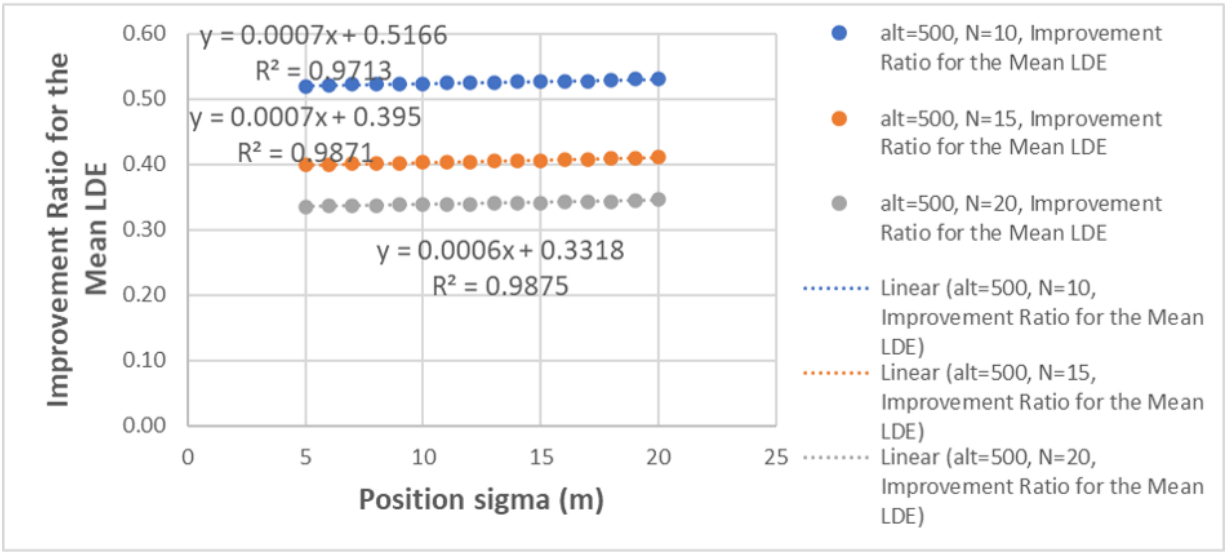

Figure 104: Improvement Ratios for the Mean LDE for immersed sensors at nominal altitudes of 500 m, with trend lines and linear regression models, as a function of σ_{pos}. See text for description of configurations and error conditions.

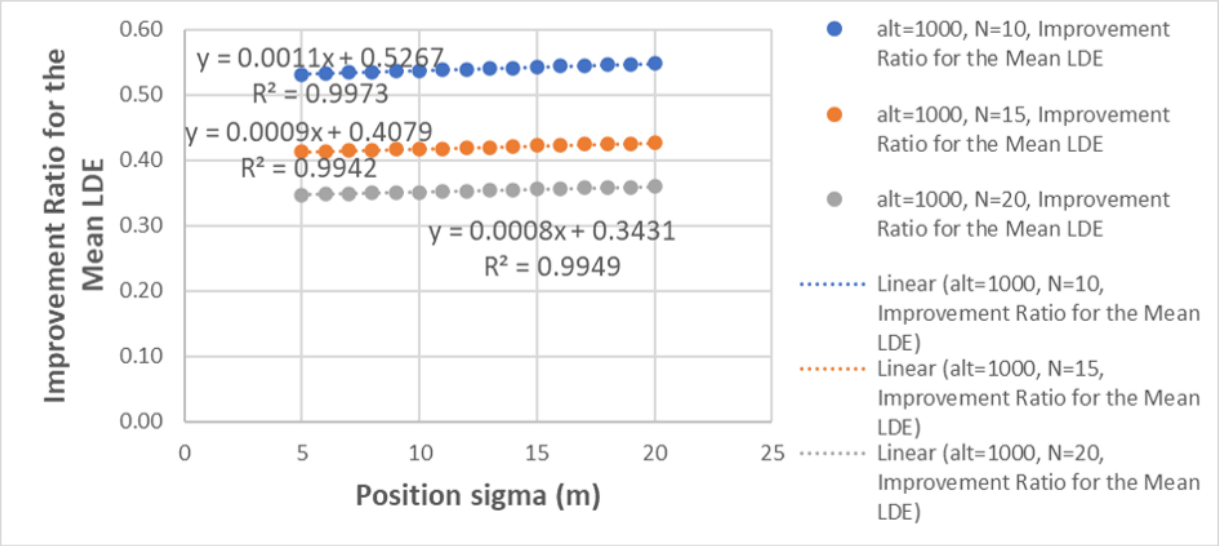

Figure 105: Improvement Ratios for the Mean LDE for immersed sensors at nominal altitudes of 1,000 m, with trend lines and linear regression models, as a function of σ_{pos}. See text for description of configurations and error conditions.

13.2.2 Varying Only Timing Error Conditions

The effect of introducing timing error alone was explored by varying σ_{time} while σ_{pos} was set to zero. The values of σ_{time} varied from 15 ns to 60 ns, which were half to twice the standard error condition of $\sigma_{time} = 30$ ns used in the Main Data Set.

Note that the plots and linear regression models are functions of σ_{time} in nanoseconds rather than in seconds.

Figure 106 shows the mean LDE for the 12 simulated configurations over the given range of σ_{time}. As was the case for position error, the clear observation from this figure is that the mean LDE increased essentially linearly with the timing error.

Table 27 provides the linear regression models for (21) for each of the 12 simulated configurations, where w_1 is the slope of the best straight line estimate and w_0 is the intercept. The R^2 goodness-of-fit values are again nearly indistinguishable from unity.

Figure 107 shows how the Improvement Ratios for the Mean LDE increase as timing errors increase for sensors on the ground. As for non-zero σ_{pos} alone, the trend lines are nearly parallel for the Improvement Ratios for the Mean LDE as a function of σ_{time}.

The slopes of the trend lines in Figure 107 (with timing error scaled in nanoseconds) are roughly half those in Figure 103 (with position error scaled in meters). Even so, it is clear that timing error is still a factor for immersed sensors on the ground and the benefit of using more sensors is slightly reduced even when only σ_{time} increased.

Figure 108 where $alt = 500$ m and Figure 109 where $alt = 1{,}000$ m show that the Improvement Ratios for the Mean LDE are nearly flat with respect to increases in σ_{time}. Thus, for the configurations and range of timing errors considered here, it appears that timing errors for immersed airborne sensors have little effect on the Improvement Ratios for the Mean LDE.

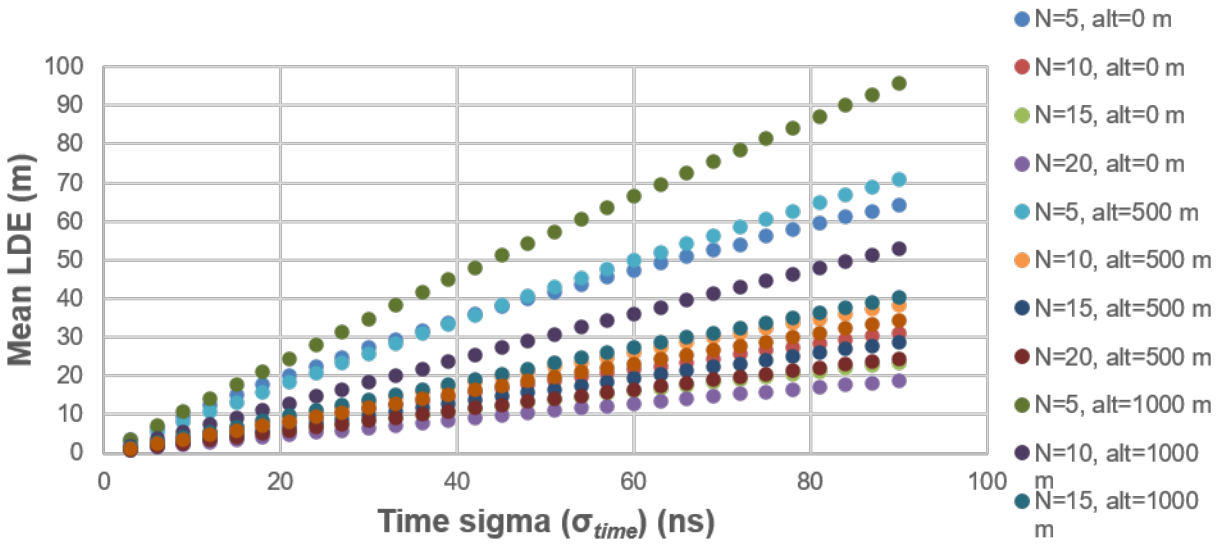

Figure 106: Mean LDE as a function of standard deviation of timing error (σ_{time}). See text for description of configurations and error conditions.

Table 27: Linear regression models for the mean LDE relationships as a function of σ_{time} (in ns) shown in Figure 106.

N	alt **(m)**	w_0	w_1	R^2
5	0	5.3424	0.6844	0.9919
10	0	0.8977	0.3425	0.9989
15	0	0.4421	0.2582	0.9994
20	0	0.2780	0.2087	0.9996
5	500	1.9009	0.7852	0.9984
10	500	0.3425	0.4273	0.9998
15	500	0.2050	0.3194	0.9999
20	500	0.1350	0.2723	0.9999
5	1000	2.3808	1.0570	0.9987
10	1000	0.4788	0.5898	0.9998
15	1000	0.2765	0.4479	0.9999
20	1000	0.1922	0.3825	0.9999

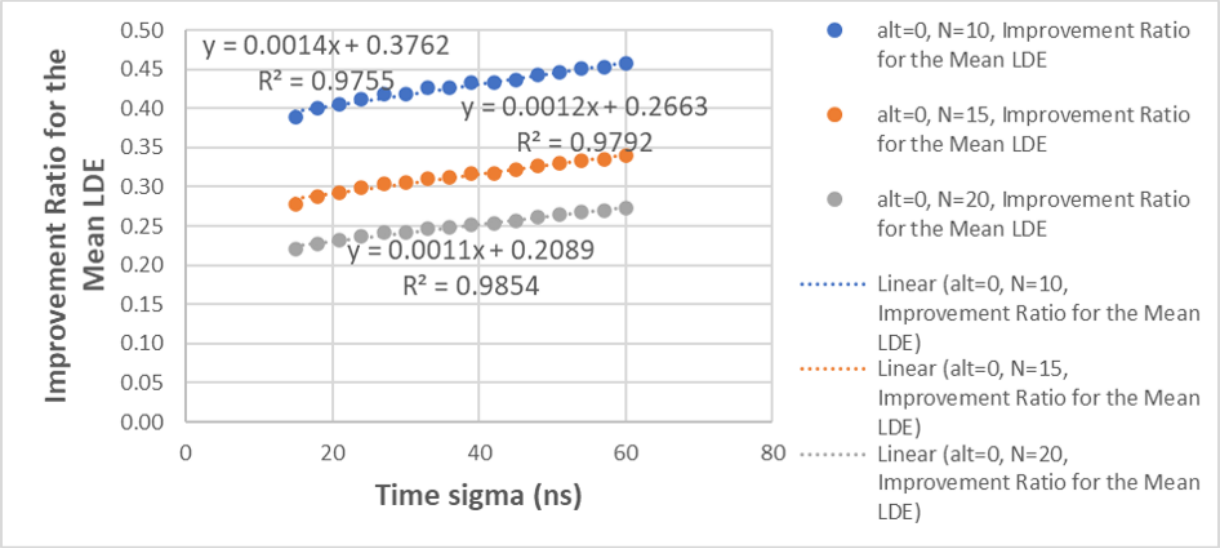

Figure 107: Improvement Ratios for the Mean LDE for immersed sensors on the ground, with trend lines and linear regression models, as a function of σ_{time}. See text for description of configurations and error conditions.

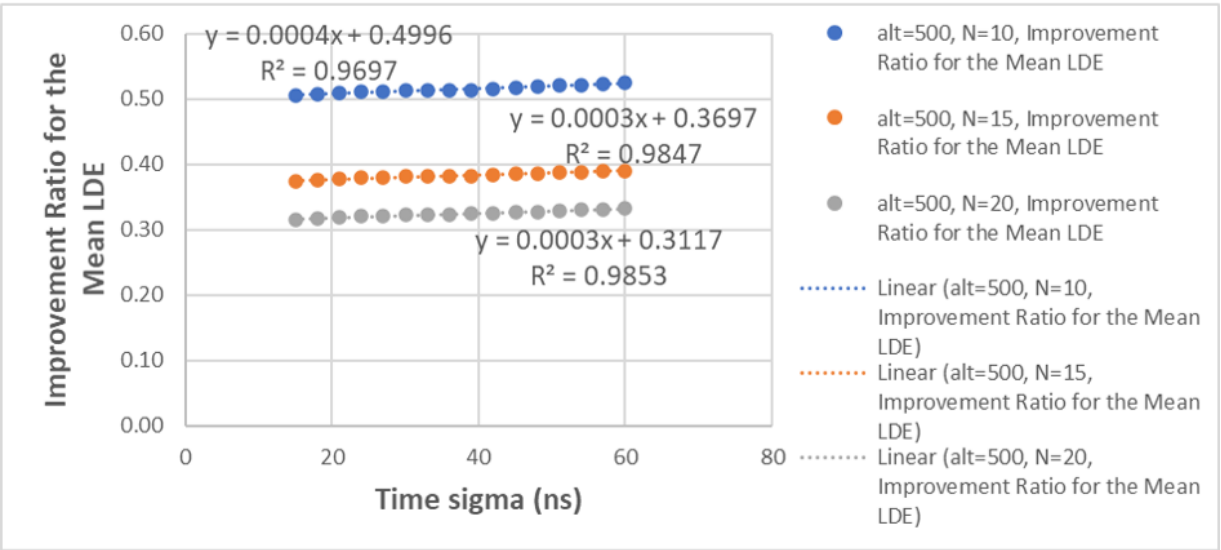

Figure 108: Improvement Ratios for the Mean LDE for immersed sensors at nominal altitudes of 500 m, with trend lines and linear regression models, as a function of σ_{time}. See text for description of configurations and error conditions.

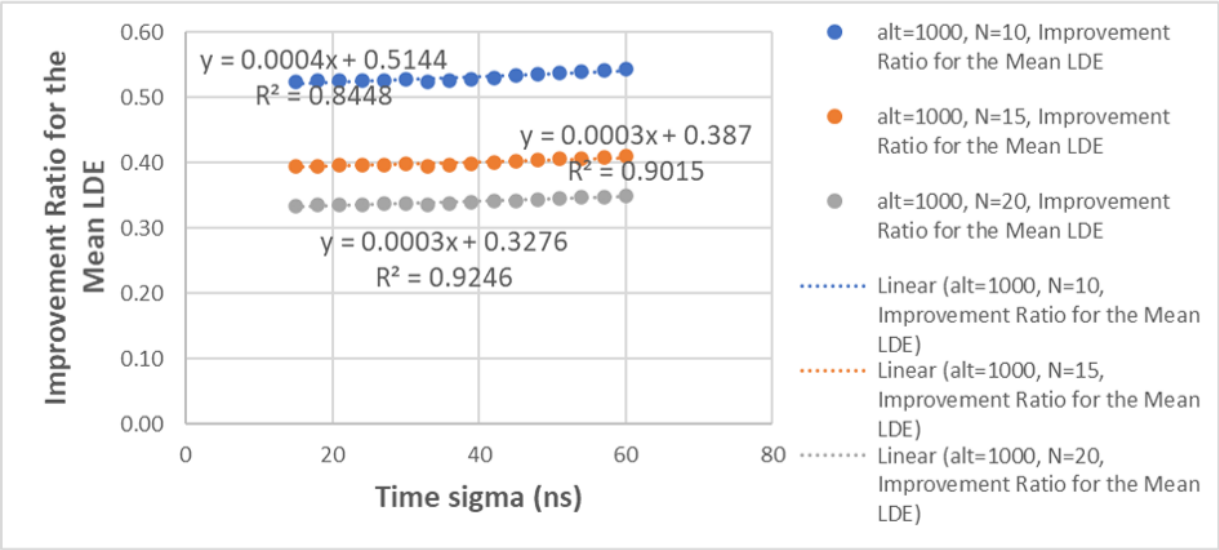

Figure 109: Improvement Ratios for the Mean LDE for immersed sensors at nominal altitudes of 1,000 m, with trend lines and linear regression models, as a function of σ_{time}. See text for description of configurations and error conditions.

13.2.3 Equivalent Values of σ_{pos} and σ_{time} for Mean LDE

The problem considered now is to how to determine the value of σ_{pos} that provides the same mean LDE as a given value of σ_{time}, or the value of σ_{time} that provides the same mean LDE as a given value of σ_{pos}, when only one of those error conditions is present.

As described in Section 13.2.1 and Section 13.2.2, Table 26 gives the linear regression model weights for mean LDE in terms of σ_{pos} (in m) and Table 27 gives the linear regression model weights for mean LDE in terms of σ_{time} (in ns). For given values of N and alt, the equations given by (21) by those two linear regression models can be set equal to each other and solved either for σ_{pos} in terms of σ_{time} or for σ_{time} in terms of σ_{pos}.

Table 28 gives the weights for the functions for these equivalences. The w_0 intercepts can effectively be disregarded. The w_1 weights for the conversion of a σ_{time} value to the value of σ_{pos} that yields the same mean LDE hover in the range of about 0.4 to 0.5. The w_1 weights for the conversion of a σ_{pos} value to the value of σ_{time} that yields the same mean LDE hover in the range of about 2 to 2.5.

Thus, it appears that an additional nanosecond of timing error standard deviation is equivalent to approximately an additional half (or a little less) of a meter of position error standard deviation or, conversely, an additional meter of position error standard deviation is equivalent to approximately two (or a little more) additional nanoseconds of timing error standard deviation.

Using $c = 3 \times 10^8$ m/sec as the speed of light, one meter is equivalent to 3.33 nanoseconds. This ratio is considerably higher than the approximation obtained here for the equivalence between position and timing error standard deviation for mean LDE.

It is not correct in general to take the inverse of a linear regression model. However, the linear fits based on the R^2 values are so good that the error percentages for all but the smallest values of σ_{pos} and σ_{time} were in the range of $\pm 5\%$ to less than $\pm 1\%$. This is certainly adequate for an overall understanding of the equivalence between these two types of error conditions.

Table 28: Weights for equivalences between the linear regression models for mean LDE in terms of standard deviations of position error (in m) and timing error (in ns) based on Table 26 and Table 27.

N	alt **(m)**	σ_{time} **to** σ_{pos}**:** w_0	σ_{time} **to** σ_{pos}**:** w_1	σ_{pos} **to** σ_{time}**:** w_0	σ_{pos} **to** σ_{time}**:** w_1
5	0	0.8490	0.4027	-2.1080	2.4830
10	0	0.1679	0.4109	-0.4086	2.4335
15	0	0.1752	0.4288	-0.4086	2.3321
20	0	0.2430	0.4190	-0.5800	2.3864
5	500	0.7201	0.5002	-1.4395	1.9991
10	500	0.2324	0.5009	-0.4640	1.9964
15	500	0.1975	0.4835	-0.4085	2.0682
20	500	0.1646	0.4885	-0.3370	2.0470
5	1000	0.6272	0.4606	-1.3616	2.1711
10	1000	0.2520	0.4614	-0.5461	2.1674
15	1000	0.1824	0.4495	-0.4059	2.2248
20	1000	0.1522	0.4547	-0.3346	2.1990

13.2.4 Sensor Position Errors and Timing Errors Are Not Linearly Additive

In spite of the findings in Section 13.2.3 that indicate that there are proportional equivalences between the effects of sensor position errors and timing errors on LDE, those errors do not add linearly. That is to say, the sum of the LDE resulting from pure position error and the LDE resulting from pure timing error does not equal the LDE resulting from position errors and timing errors. Thus, the principle of superposition does not apply.

Sufficient proof of this conclusion is provided by a few demonstrations involving combinations of the Standard Error Conditions. Mean LDE values were obtained from simulations of N = 5, 10, 15, and 20 immersed sensors in a search area with side length $side$ = 1,000 m at nominal altitudes of alt = 0 m, 500 m, and 1,000 m with $\sigma_{alt} = alt/20$. For the configurations with both position and timing errors (that is, with the Standard Error Conditions of $\sigma_{pos} = 10$ m and $\sigma_{time} = 30$ ns), the Main Data Set was used. For the configurations with only position error (σ_{pos} at 10 m) and the configurations with only timing error (σ_{time} at 30 ns), 1,000 simulations were performed to obtain the mean LDE.

The mean LDE for the position errors-only and timing errors-only were added for each configuration and compared to the mean LDE of the same configuration with both position and timing errors. The mean LDE resulting from introducing both position and timing errors was less than the sum of the mean LDE of the configurations with only one error condition.

The surprising result was observed that the ratio of the mean LDE with both position and timing errors to the sum of the mean LDE of the configurations with only one error condition was nearly a constant. The average value of the ratio for the set of configurations enumerated above was 0.704 and ranged only from 0.696 to 0.712.

Thus, it was shown that the principle of superposition did not hold for position errors and timing errors. Furthermore, in the case of these very limited experiments and specifically for mean LDE and the Standard Error Conditions used in this paper, the effect of the combination of both position and timing errors was only 70% of the sum of the individual effects of those errors conditions.

14 Estimating Location Distance Error for Sensor Error Conditions Wider than the Standard Error Conditions

The linear relationships of the Improvement Ratios for the Mean LDE with respect to varying position errors, timing errors, or both error conditions indicate that the same linear regression model approaches used in prior sections for the Main Data Set with the Standard Error Conditions would work under different error conditions. Therefore, two data sets with half- and twice-Standard Error Conditions were generated and Ballpark Estimates were obtained as was done in Section 12.2 for the Main Data Set and the Standard Error Conditions.

The half-standard error condition data set used the same configurations as in the Main Data Set but with the position and timing errors set to half the Standard Error Conditions: $\sigma_{pos} = 5$ m and $\sigma_{time} = 15$ ns. The twice-standard error condition data set used the same configurations but with the position and timing errors set to twice the Standard Error Conditions: $\sigma_{pos} = 20$ m and $\sigma_{time} = 60$ ns.

Due to the long run times required, only 200 simulations per configuration were performed for the half- and twice-standard error condition data sets.

14.1 Ballpark Estimates of the Improvement Ratio for the Mean LDE for Half- and Twice-Standard Error Conditions

Figure 110 shows the Minimum, Mean, and Maximum of the Improvement Ratios for the Mean LDE for immersed sensors in the case of half the standard position and timing error conditions used in the Main Data Set. As was the case with the Ballpark Estimates for the Main Data Set, the Ballpark Estimates for the half-Standard Error Conditions have power-law linear regression models with R^2 goodness-of-fit values that are nearly unity. The envelope (bounded by the minimum and maximum values) in Figure 110 for the half-Standard Error Conditions is slightly tighter than that in Figure 92 for immersed sensors in the Main Data Set.

Figure 111 shows the Minimum, Mean, and Maximum of the Improvement Ratios for the Mean LDE for standoff sensors in the case of half the standard position and timing error conditions used in the Main Data Set. The statements made in the paragraph immediately above apply to this figure as well, including the comparison to Figure 93 for standoff sensors in the Main Data Set.

Figure 112 for immersed sensors and Figure 113 for standoff sensors show the Minimum, Mean, and Maximum of the Improvement Ratios for the Mean LDE in the case of twice the standard position and timing error conditions used in the Main Data Set. The statements made in the two paragraphs immediately above hold for these configurations as well, except that the envelope for the standoff sensors with twice-Standard Error Conditions is slightly wider than those for the Standard Error Conditions or the half-Standard Error Conditions.

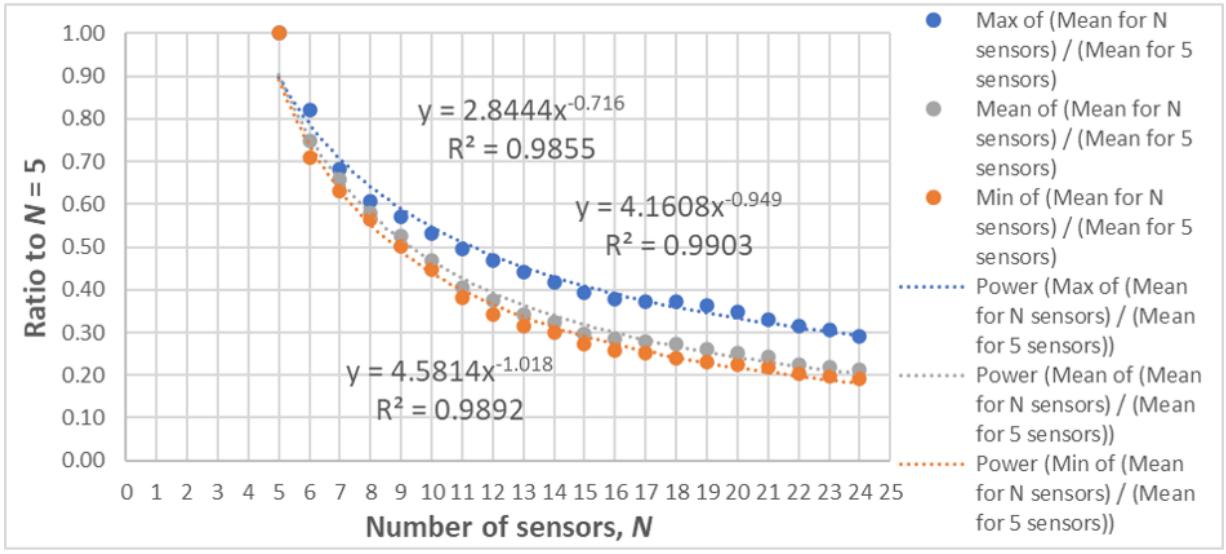

Figure 110: Minimum, Mean, and Maximum of the Improvement Ratios for the Mean LDE for immersed sensors in the case of half-standard position and timing error conditions, with trend lines and power-law linear regression models.

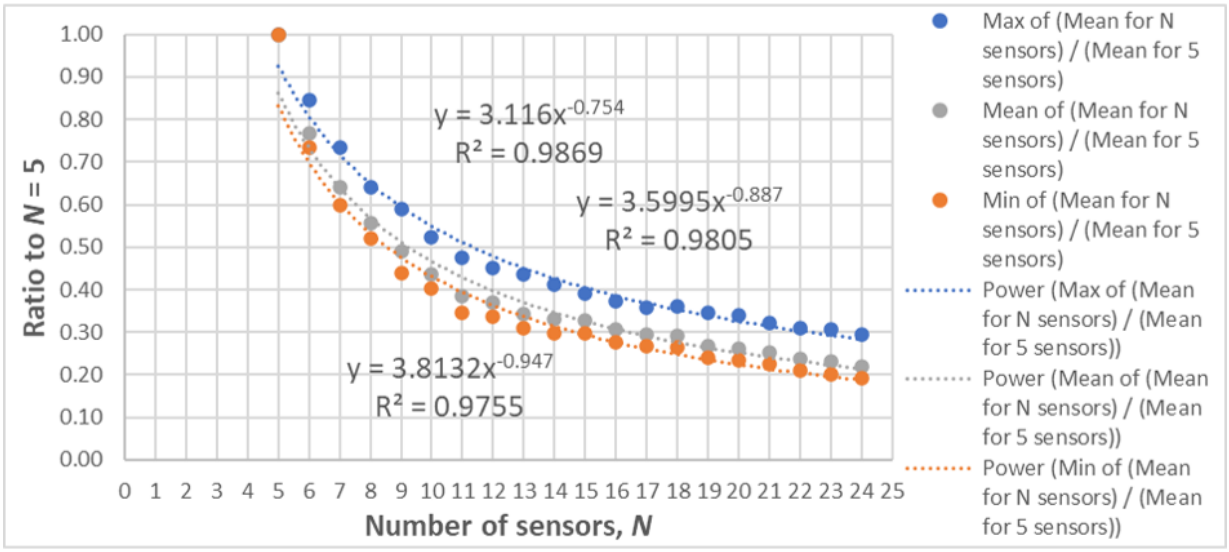

Figure 111: Minimum, Mean, and Maximum of the Improvement Ratios for the Mean LDE for standoff sensors in the case of half-standard position and timing error conditions, with trend lines and power-law linear regression models.

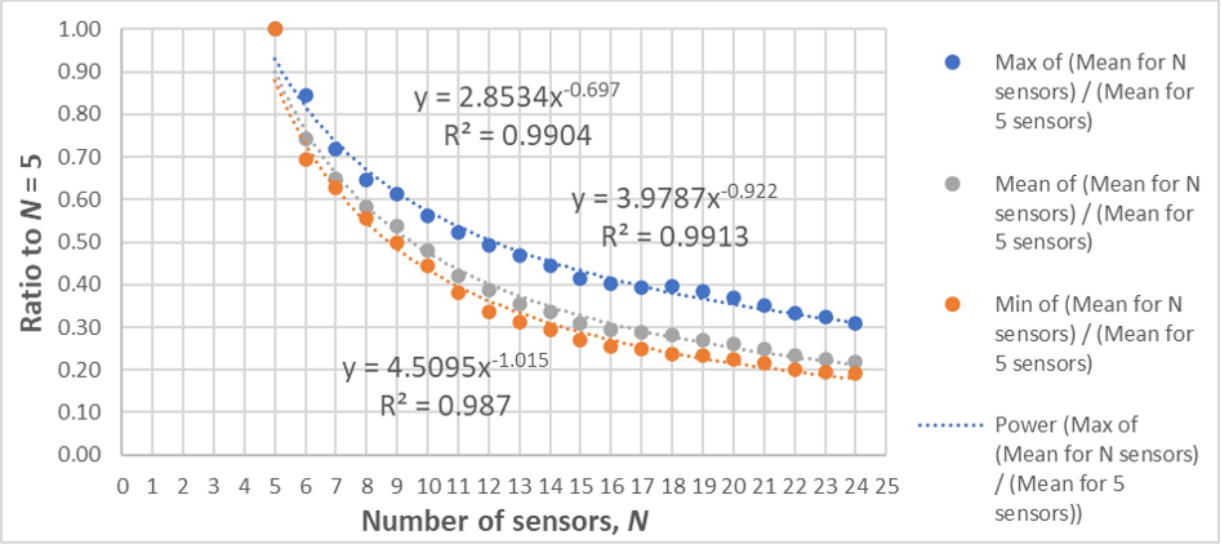

Figure 112: Minimum, Mean, and Maximum of the Improvement Ratios for the Mean LDE for immersed sensors in the case of twice-standard position and timing error conditions, with trend lines and power-law linear regression models.

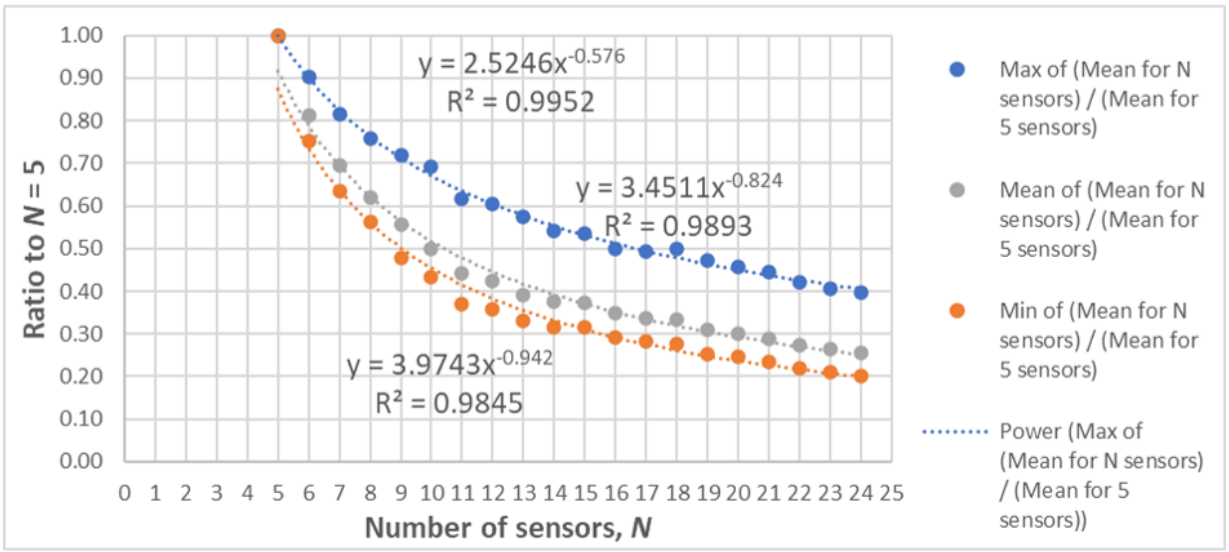

Figure 113: Minimum, Mean, and Maximum of the Improvement Ratios for the Mean LDE for standoff sensors in the case of twice-standard position and timing error conditions, with trend lines and power-law linear regression models.

14.2 Expanded Ballpark Estimates and Expanded Reciprocal Approximations for an Ensemble Data Set Incorporating All of the Error Conditions Simulated

Having the individual data sets with (σ_{pos}, σ_{time}) = (5 m, 15 ns), (10 m, 30 ns), and (20 m, 60 ns), [49] the next logical step was to pool them into a single **Ensemble Data Set** and obtain an **Expanded Ballpark Estimate** as well as an **Expanded Reciprocal Approximation**. [50]

Only the Improvement Ratios for the Mean LDE are considered in this section.

Initially, these estimates were applied to the envelope of the combined immersed and standoff configurations in the Ensemble Data Set, but the results were poor compared to the estimates based on the envelopes of the Ensemble Data Sets for immersed and standoff sensors separately.

Figure 114 shows the Expanded Ballpark Estimate for immersed sensors based on the envelope of the Ensemble Data Set. The power-law weights and R^2 values for the Expanded Ballpark Estimate linear regression models for the Minimum, Mean, and Maximum of the Improvement Ratios for the Mean LDE are given in Table 29. These weights are used in the appropriate expression in (28) as was described in Section 12.2 for the Ballpark Estimate of the Mean of the Improvement Ratios for the Mean LDE for the Main Data Set immersed sensors that used the values in Table 18.

Figure 115 shows the Expanded Ballpark Estimate for standoff sensors based on the envelope of the Ensemble Data Set. The power-law weights and R^2 values for the Expanded Ballpark Estimate linear regression models for the Minimum, Mean, and Maximum of the Improvement Ratios for the Mean LDE are given in Table 30. These weights are used in the appropriate expression in (28) as was described in Section 12.2 for the Ballpark Estimate of the Mean of the Improvement Ratios for the Mean LDE for the Main Data Set standoff sensors using the values in Table 19.

As done in Section 12.2, these data were used to estimate the Mean of the Improvement Ratios for the Mean LDE as a function of the number of

[49] That is, the data sets are those with the half-Standard Error Conditions, the Standard Error Conditions, and the twice-Standard Error Conditions.

[50] Capitalization is used to help identify these phrases as single terms.

immersed or standoff sensors for the Ensemble Data Set. From Table 29, the second line gives the weights for the Mean of the Improvement Ratios for the Mean LDE. The values for w_1 and either w_0 or e^{w_0} are plugged into the appropriate expression in (28) to obtain the linear regression model for the Mean of the Improvement Ratios for the Mean LDE for immersed sensors. As was done previously, the second alternate expression for the Mean of the Improvement Ratios for the Mean LDE is used:

$$y = 3.9184\, N^{-0.9333} \quad . \tag{37}$$

Similarly, for standoff sensors, from Table 30, the second line gives the weights for the Mean of the Improvement Ratios for the Mean LDE that are plugged into (28) to obtain the linear regression model for the Mean of the Improvement Ratios for the Mean LDE for standoff sensors:

$$y = 3.5768\, N^{-0.8747} \quad . \tag{38}$$

It can be seen in Table 29 and Table 30 that the w_1 weights for the Mean of the Improvement Ratios for the Mean LDE for both immersed and standoff sensors are close to negative one so, again, (28) can be approximated by a simple reciprocal function of N for these statistics. As was done in Section 12.4, weights were found for simplified expressions for the Mean of the Improvement Ratios for the Mean LDE for immersed sensors.

Thus, the Expanded Reciprocal Approximation for the Mean of Improvement Ratios for the Mean LDE for immersed sensors based on the Ensemble Data Set is

$$y = \frac{4.5}{N} \tag{39}$$

and the Expanded Reciprocal Approximation for the Mean of the Improvement Ratios for the Mean LDE for standoff sensors based on the Ensemble Data Set is

$$y = \frac{4.8}{N} \quad . \tag{40}$$

These expressions are valid for $N = 6$ to 24 and the Improvement Ratio for the Mean LDE is defined to be exactly 1.0 for five sensors.

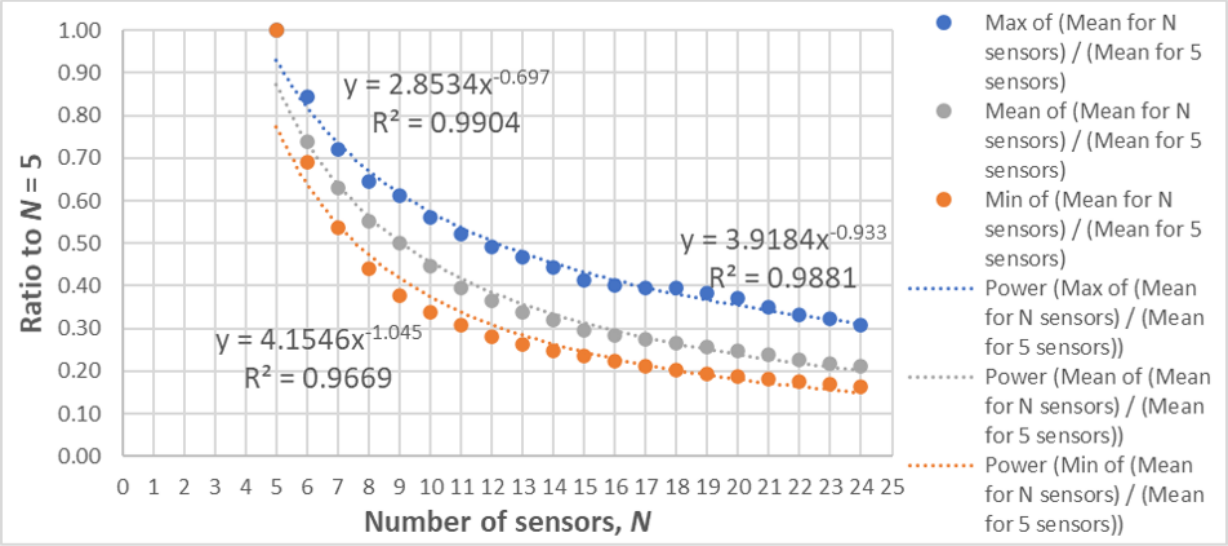

Figure 114: Expanded Ballpark Estimates of the Minimum, Mean, and Maximum of the Improvement Ratios for the Mean LDE based on Ensemble Data Set for immersed sensors, with trend lines and power-law linear regression models.

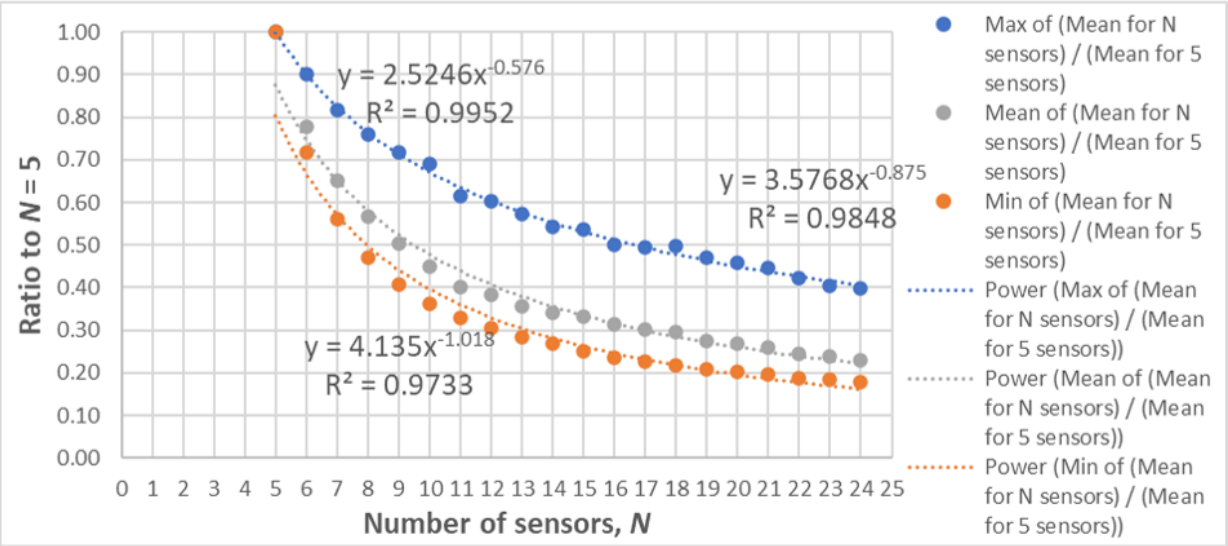

Figure 115: Expanded Ballpark Estimates Minimum, Mean, and Maximum of the Improvement Ratios for the Mean LDE based on Ensemble Data Set for standoff sensors, with trend lines and power-law linear regression models.

Table 29: Weights and R^2 for Expanded Ballpark Estimate linear regression models for immersed sensors shown in Figure 114.

Statistics for ratio: (Mean LDE for N sensors) / (Mean LDE for 5 sensors)	w_0	w_1	e^{w_0}	R^2
Max of ratio	1.0485	-0.6968	2.8534	0.9904
Mean of ratio	1.3657	-0.9333	3.9184	0.9881
Min of ratio	1.4242	-1.0452	4.1546	0.9669

Table 30: Weights and R^2 for Expanded Ballpark Estimate linear regression models for standoff sensors shown in Figure 115.

Statistics for ratio: (Mean LDE for N sensors) / (Mean LDE for 5 sensors)	w_0	w_1	e^{w_0}	R^2
Max of ratio	0.9261	-0.5756	2.5246	0.9952
Mean of ratio	1.2745	-0.8747	3.5768	0.9848
Min of ratio	1.4195	-1.0182	4.1350	0.9733

14.3 Testing the Expanded Ballpark Estimates and Reciprocal Approximations

The close fits of the Expanded Reciprocal Approximations for the Mean of the Improvement Ratios for the Mean LDE given by (39) and (40) to the actual values are shown in Figure 116 and Figure 117 for immersed and standoff sensors, respectively. MAPE for immersed sensors in the Ensemble Data Set obtained from (39) is 4.54% and MAPE for standoff sensors in the Ensemble Data Set obtained from (40) is 7.11% over the range $N = 6$ to 24. Again, these MAPE values are for the Reciprocal Approximations for the Mean of the Improvement Ratios for the Mean LDE for all of the configurations and error conditions in the Ensemble Data Set, with respect to a given number of sensors, rather than with respect to specific configurations.

The linear regression models for the Expanded Ballpark Estimates and Expanded Reciprocal Approximations were developed only for the *envelope* of all of the configurations and error conditions contained in the Ensemble Data Set, but once again it is irresistible to see how closely they model the specific configurations. As was done in Section 12, only the Mean of the Improvement Ratios for the Mean LDE was considered.

For all of the configurations with $N = 6$ to 24 immersed sensors in the Ensemble Data Set, Expanded Ballpark Estimates of the Mean of the Improvement Ratios for the Mean LDE were obtained using (37). MAPE for those estimates was 9.50%, and the largest percentage error was 36.45%. Using the Expanded Reciprocal Approximation for the Mean of the Improvement Ratios for the Mean LDE given by (39), MAPE for those estimates was 9.42%, and the largest percentage error was −39.49%.

Similarly, for all of the configurations with $N = 6$ to 24 standoff sensors in the Ensemble Data Set, MAPE for the Expanded Ballpark Estimates of the Mean of the Improvement Ratios for the Mean LDE given by (38) was 12.06%, and the largest percentage error was −44.12%. Using the Expanded Reciprocal Approximation for the Mean of the Improvement Ratios for the Mean LDE given by (39), MAPE for those estimates was 12.04%, and the largest percentage error was −49.64%.

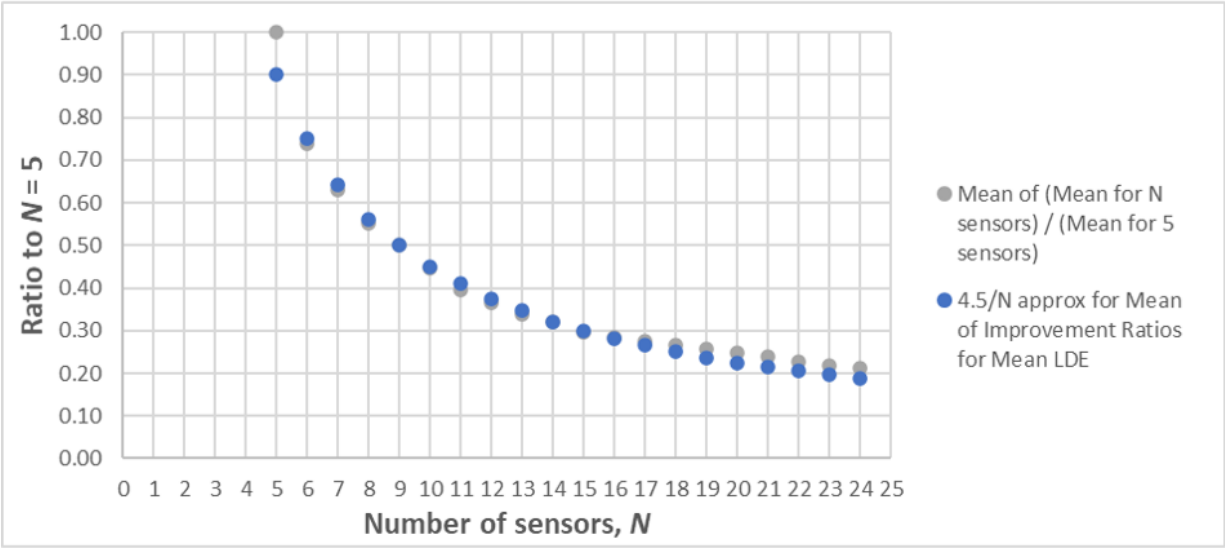

Figure 116: Mean of Improvement Ratio for the Mean LDE for immersed sensors and its Reciprocal Approximation given by (39).

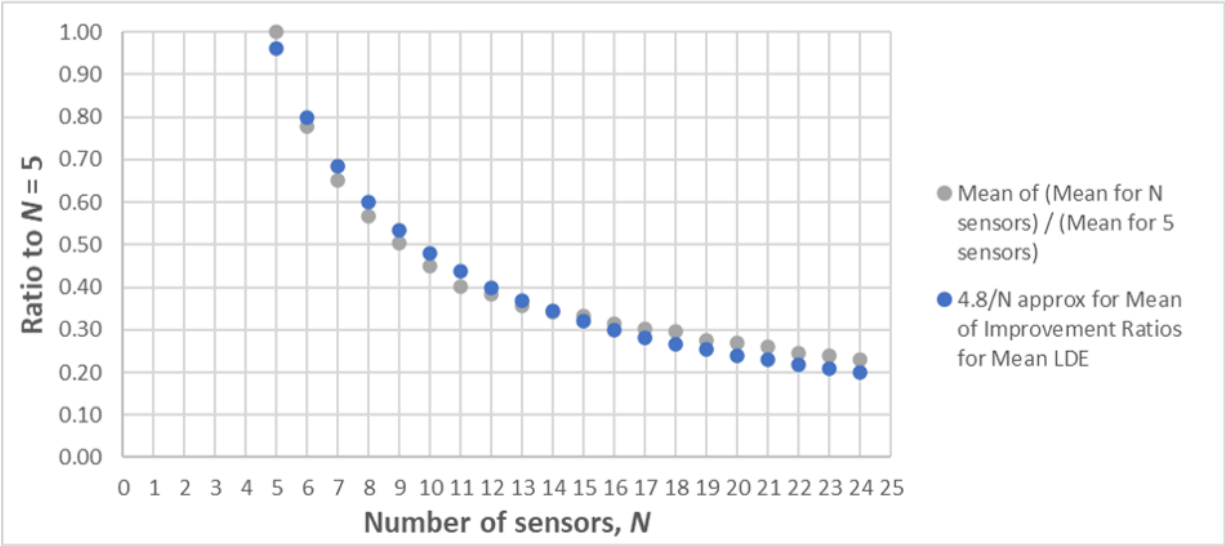

Figure 117: Mean of Improvement Ratio for the Mean LDE for standoff sensors and its Reciprocal Approximation given by (40).

15 Conclusions

The context of this work is the problem of geolocating an emitter on the ground by combining Time-difference-of-arrival (TDoA) measurements at pairs of sensors, where those sensors may be on the ground or in the air. Sensors may be immersed in or above the search area where the emitter is known to be located or they may be standoff in or above an adjacent area. The analyses used configurations with up to 24 sensors in most cases although behavior with up to 100 sensors was also considered.

The mainstream of this study was based on the assumption that the locations of the emitter and the sensors are random. An appendix considers a minor optimization where a minimum separation of the sensors is enforced.

The central question addressed in this paper has been to determine the trend of the relative improvement in geolocation accuracy as the number of sensors increases. The primary figure-of-merit for geolocation accuracy was the Location Distance Error (LDE) and the statistical metrics of its mean, 50%ile or median, 95%ile, and 99%ile. Additional LDE statistical metrics based on these statistical metrics were developed to quantify aspects of geolocation accuracy and its relative improvement.

The results in this paper were derived from large numbers of Monte Carlo simulations involving randomly generated geometries based on parameterized configurations of emitter and sensors. The locus of points that satisfy TDoA measurements between sensors form hyperboloids and, ideally, the emitter should be found at the intersection of those hyperboloids on the ground. The simulations implemented a grid-based TDoA solution method that found an estimated location for the emitter which minimized the sum of the squared TDoA errors compared to the true but unknown location of the emitter.

Most of the results in this paper were obtained using the "Main Data Set" consisting of a large number of configurations of immersed and standoff sensors with a wide range of nominal altitudes and search area side lengths. Numbers of sensors from three to 24 were included. For airborne sensors, their nominal altitude was assumed to vary with a Gaussian distribution about the mean altitude with a coefficient of variation of 5%. The "Standard Error Conditions" assumed zero-mean Gaussian distributions where position

error had a standard deviation of 10 m and timing error had a standard deviation of 30 ns.

This paper explored various methods for pairing sensors to obtain TDoA measurements and found that using all possible pairs gave the smallest mean LDE. Based on this finding, all of the results presented in this paper are based on simulations involving all pairs sensor pairing. However, it was pointed out that real-time geolocation applications may find that the quadratic growth in TDoA solution run time for all pairs sensor pairing is prohibitive and the benefit of the linear growth of Linearly Independent Pairs (LIP) sensor pairing or disjoint pairs sensor pairing outweighs the penalty of the larger mean LDE.

Even in the absence of position or timing errors, configurations with small numbers of sensors have many geometries where the LDE is very large. For example, in 10,000 simulations of three immersed sensors at nominal altitudes of 100 m, the largest LDE observed was more than 1.1 km in a 1 km $\times$ 1 km search area. More than 21% of error-free geometries with three sensors may have non-zero LDE. One common cause of this is where sensors are collinear, but this situation occurs unpredictably with many other geometries.

The phenomena where LDE values are unpredictably very small or very large are called "Longfellow Events" in this paper in honor of H.W. Longfellow. Paraphrasing the poet, one could say of LDE resulting from small numbers of sensors: "When they are good, they are very very good, but when they are bad they are horrid." At least in the case of all pairs sensor pairing, it was found that Longfellow Events can be largely avoided using configurations that consist of at least five sensors.

It was found that the LDE statistical metrics were roughly scale-invariant with the ratio of the nominal altitude of the sensors to the search area side length. The LDE statistical metric curves, as functions of that ratio, were convex so there were optimal altitudes for any given sizes of search area.

Multivariate linear regression was used to develop models of how the LDE statistical metrics varied as a function of the number of sensors (immersed or standoff), nominal altitude, and search area side lengths. A "shotgun approach" was used to find linear regression models with the smallest numbers of variables that maximized the coefficient of determination (R^2)

and minimized the Mean Absolute Percentage Error (MAPE). Even though the linear regression models were developed for five and more sensors, it was found that the models that included the data for three and more sensors were superior to those based only on five and more sensors.

For configurations with specific values for nominal altitude and search area lengths, it was found that the best linear regression models expressed the double logarithm of the LDE statistical metrics as linear functions of the double logarithm of the number of sensors. The R^2 values for these linear regression models were close to unity and MAPE values were small percentages.

While most of the configurations used in this paper were limited to a maximum of 24 sensors, experiments were conducted with up to 100 sensors to determine whether the results regarding the LDE statistical metrics were statistically significant. It was shown that the ± 3 standard error bounds for the mean LDE were extremely tight even when based only on 1,000 simulations per configuration; note that most of the results in this paper were based on 10,000 simulations per configuration. The apparent linearity of the double logarithm of the mean and 95%ile LDE with respect to the double logarithm of the number of sensors continued, with only slight downward bending, up to the limit of 100 sensors.

The extensive tabulation of linear regression model weights for specific configurations of nominal altitude and search area lengths was used as the basis for more general models for the LDE statistical metrics as functions of those parameters. This generalization again expressed the double logarithm of the LDE statistical metrics as a linear function of the double logarithm of the number of sensors, but the weights for these linear functions were obtained from the linear regression models for individual nominal altitudes and search area side lengths. The weights for the generalized linear regression models were, in turn, functions of nominal altitude and search area side lengths as transformed and combined variables.

As the central question addressed in this paper was to determine the trend in the relative improvement of LDE with respect to the number of sensors, the LDE-based figure-of-merit termed the "Improvement Ratio for an LDE statistical metric" was introduced. To avoid Longfellow Events, it was assumed that the value of a chosen LDE statistical metric with five sensors was the baseline against which geolocation improvement is measured.

For instance, the "Improvement Ratio for the Mean LDE for N sensors" was defined to be the ratio of the mean LDE for N sensors to the mean LDE for five sensors; the Improvement Ratios for the other LDE statistical metrics were defined similarly.

As an example, for immersed sensors on the ground in a 1 km $\times$ 1 km search area, the Improvement Ratio for the Mean LDE for eight sensors was found to be 0.5264, meaning that using eight sensors reduces the mean LDE to about 53% of that achieved using only five sensors.

It was determined that a power-law linear regression model was a good fit for the Improvement Ratios for the specific configurations in the Main Data Set. However, rather than once again extensively tabulate the weights for those linear regression models, the observation was made that the weights corresponding to the exponents of N in the power-law fits averaged fairly close to 1. This led to the formulation of a set of "Reciprocal Approximations" of the form w_{RA}/N, where w_{RA} is a tabulated value for one of the eight combinations of immersed or standoff sensor configurations and the mean, 50%ile, 95%ile, or 99%ile LDE. For example, the Reciprocal Approximation for the 95%ile LDE for standoff sensors is $3.80/N$ which has a MAPE of 11.56% with respect to the Improvement Ratios for the 95%ile LDE for all configurations in the Main Data Set for numbers of sensors ranging from six to 24.

For a given number of sensors and a specific LDE statistical metric, the Improvement Ratios for the configurations in the Main Data Set have a range of values. The next step was to work with the envelope of those ranges by finding linear regression models for their minimum, mean, and maximum; these models are called the "Ballpark Estimates."

There are 24 combinations of the Minimum, Mean, or Maximum of the Improvement Ratios for the Mean, 50%ile, 95%ile, or 99%ile LDE for immersed or standoff sensors. An example of one of those combinations would be the "Mean of the Improvement Ratio for the Mean LDE for immersed sensors."

It was found that power-law linear regression models were good fits for the two dozen Ballpark Estimates. The R^2 values for those linear regression models were close to 1, indicating excellent goodness-of-fit.

For example, for immersed sensors, the Reciprocal Approximations for the Mean LDE for eight sensors yield the bounds of 47% for the minimum, 52% for the mean, and 64% for the maximum for any configuration in the Main Data Set; those values give the range and expected value of the relative improvement achieved by increasing the number of sensors from the baseline of five sensors to eight.

While most of the weights corresponding to the exponents of N in the power-law fits for the Ballpark Estimates were not very close to 1, fortuitously that was the case for the Ballpark Estimates of the Mean of the Improvement Ratios for the Mean LDE. Thus, the Reciprocal Approximations for these Improvement Ratios were found to be $4.25/N$ and $4.50/N$ for immersed and standoff sensors, respectively. While these Reciprocal Approximations were developed for the mean values of the envelope of the Improvement Ratios, they had MAPE of only 11% and 12% with respect to the specific configurations with six and more immersed and standoff sensors, respectively.

Most of the results described in this paper were based on the assumption of sensor nominal altitude varying with a Gaussian distribution with a 5% standard deviation about the mean altitude and zero-mean Gaussian distributed position error with 10 m standard deviation and timing error with 30 ns standard deviation. These values were chosen to be reasonable but not based on any actual military or civilian system or scenarios. However, it was vital to establish the sensitivity of results to these parameters. Only mean LDE was considered as well as only a few configurations for immersed sensors.

It was found that the standard deviation of sensor nominal altitude had very little effect on mean LDE. In fact, the small percentages of difference in mean LDE did not even follow a consistent trend with respect to the coefficient of variation for the altitude.

Sensitivity to position error alone was gauged by varying the standard deviation of position error from half (5 m) to twice (20 m) the value used in the Standard Error Conditions of the Main Data Set. It was observed that the mean LDE varied linearly with position error for all of the configurations and numbers of sensors tested.

The mean LDE curves for given numbers of sensors were not parallel, however. Thus, when those results were expressed as Improvement Ratios for the Mean LDE, the Improvement Ratios for a given number of sensors varied linearly with small but positive slopes with respect to position error, although they were practically flat for non-zero altitudes. Thus, the Improvement Ratio degrades slightly for sensors on the ground as position error increases but practically not at all for airborne sensors.

Sensitivity to timing error alone was determined in a similar way by varying the standard deviation of timing error from half (15 ns) to twice (60 ns) the value used in the Standard Error Conditions of the Main Data Set. It was observed that the mean LDE varied linearly with timing error for all of the configurations and numbers of sensors tested.

As was the case for position error alone, the mean LDE curves for given numbers of sensors as a function of timing error were not parallel, so the Improvement Ratios for the Mean LDE varied linearly with small positive slopes with respect to timing error alone. The Improvement Ratios for sensors on the ground had the largest slopes, and those for airborne sensors were close to flat with respect to timing error.

When only position error or timing error is present, it was found that adding a meter of position error standard deviation was roughly equivalent to adding two nanoseconds of timing error standard deviation in terms of the resulting increase in mean LDE.

The effects of position errors and timing errors together do not possess the property of superposition; that is, their effects are not linearly additive. It was found that, for the configurations tested, the mean LDE for configurations with the Standard Error Conditions of 10 m position error standard deviation and 30 ns timing error standard deviation was only about 70% of the sum of the mean LDE for the configurations with position error or timing error alone.

Data sets were generated with half-Standard Error Conditions and twice-Standard Error Conditions, and those data sets were then combined with the Main Data Set to produce an "Ensemble Data Set." As was the case for the envelope of the Improvement Ratios for the Mean LDE for the Main Data Set, the power-law fits for the data sets with the half- and twice-Standard

Error Conditions and the Ensemble Data Set had R^2 values that were nearly unity, indicating excellent goodness-of-fit.

The power-law linear regression model fits for the Improvement Ratios for the Mean LDE for the Ensemble Data Set are referred to here as the "Expanded Ballpark Estimates." When the weights for those power-law fits were tabulated, it was observed that the exponents for the Expanded Ballpark Estimates for the Mean of the Improvement Ratio for the Mean LDE were close to 1. The "Expanded Reciprocal Approximations" for the Mean of the Improvement Ratio for the Mean LDE were found to be $4.5/N$ and $4.8/N$ for immersed and standoff sensors, respectively. Even though those Expanded Reciprocal Approximations were not developed for the individual configurations in the Ensemble Data Set, it was found that MAPE for the configurations with six and more immersed sensors was 9.42% and 12.04%, respectively.

An appendix that follows this section addresses the distribution of timing difference errors for sensor pair TDoA measurements under the assumption that timing errors and position errors for individual sensors have Gaussian distributions. Timing difference errors clearly are Gaussian because they are simply the difference of two Gaussian distributions. While timing difference error due to distance difference error is simply proportional to the distance difference error, the analysis is more complicated because the geometry of the RF signal path must be considered; the distribution of distance difference error was found to have a sharp peak at a distance difference slightly greater than zero and it had tails much smaller than those that would result from a Gaussian distribution.

A second appendix considers a means for improving LDE by simply enforcing a minimum xy distance between any two sensors to avoid small baselines between the foci of the hyperboloids. Based on a restricted set of configurations, it was shown that mean LDE appears to decrease linearly with the minimum xy separation. If it is assumed that the sensors move randomly and the geometries are just tested to see if they satisfy the minimum xy separation, then the application of this strategy is limited by the fact that the number of randomly generated geometries grows exponentially with the number of sensors. Ultimately, there is a packing limit on the number of sensors that can satisfy the minimum xy separation.

The benefit of enforcing minimum xy separation was looked at from the point of view of an equivalent number of sensors. For example, for immersed sensors on the ground in a 1 km $\times$ 1 km search area, ten sensors with an enforced 200 m minimum xy separation provide, on average, the mean LDE achieved by 14 sensors with no minimum separation.

This paper has provided a framework for determining the improvement in TDoA geolocation accuracy achieved by increasing the number of sensors. While the results obtained rely on the specific values of the parameters used in this paper, the analyses suggest how these results can be applied for other values of the parameters. Through a series of approximations with various degrees of goodness-of-fit and error percentages, the geolocation accuracy or its proportional improvement can be estimated.

The two most significant findings were the following. First, a minimum of five sensors, paired in all of their combinations, are needed to avoid having significant fractions of bad geometries that inherently results in poor emitter locations even without sensor position or timing error. Second, geolocation distance error, by several measures, appears to decrease roughly as the reciprocal of the number of sensors.

A Timing Difference Error Distributions as a Function of Distance and Timing Error Conditions

The LDE resulting from any of the sensor pairing methods described in this paper is affected by sensor position and timing errors, where those errors are assumed to have Gaussian distributions with zero mean and standard deviations σ_{pos} and σ_{time}, respectively. This appendix deals with the relationship between timing errors and timing difference errors as well as the relationship between sensor position errors, sensor distance errors, and sensor distance difference errors as they relate to the calculation of the TDoA of RF signals at pairs of sensors.

A.1 Distribution of Timing Error and Timing Difference Error

As described in Section 4.1.1 and Section 4.1.2, each simulation of a given configuration of emitter and sensors and error conditions creates a random geometry where sensor i is assigned a timing error t'_i that is Gaussian distributed with zero mean and standard deviation σ_{time}. The timing error t'_i is added to each pairwise TDoA calculation involving sensor i.

As described in Section 4.1.3, the timing difference error in a TDoA measurement between sensors with indices i and j is given by t'_i - t'_j. The difference of two Gaussian random variables is also Gaussian and, for the difference of any two distributions, the mean is the difference of the individual means and the variance is the sum of the individual variances [Rohatgi (1979)]. Thus, for the error model used in this paper, the distribution of the timing difference error for the TDoA measurement between any two sensors is Gaussian with zero mean and standard deviation $\sqrt{\sigma_{time}^2 + \sigma_{time}^2} = \sqrt{2}\,\sigma_{time}$.

A.2 Distribution of Distance Error and Distance Difference Error

Distance error, and thus distance difference error, is the result of sensor position errors. Figure 118 shows an instance of sensor i created in a simulation at the presumed position (x_i, y_i, z_i). As stated in Section 4.1.2, the true (but unknown) position (x_i', y_i', z_i') is also created with a position error magnitude given by the absolute value of a Gaussian distribution with zero mean with standard deviation σ_{pos}. For sensors on the ground, the angle of the position error is uniformly distributed in the xy-plane from 0° to 360°. For airborne sensors, the angle of the position error is uniformly distributed with respect to the three axes. The simulation places the emitter at the true (but unknown) location (x_e', y_e', z_e') on the ground (so $z_e' = 0$) in the search area.

In Figure 118, d_i is the Euclidean distance from the emitter to the presumed position of sensor i and d_i' is the Euclidean distance from the emitter to the true position of sensor i. For the purpose of this analysis, let d_i be specified in multiples of σ_{pos} and, without loss of generality, let $\sigma_{pos} = 1$ m.

The distance error with respect to the emitter is given by (3).

Figure 119 shows the distribution of the distance error where $d_i = 6$ m (thus, sensor i is $6\,\sigma_{pos}$ from the emitter). This histogram is based on 100,000 random generations of the true sensor position performed in Microsoft Excel. The histogram also shows a Gaussian distribution that has the same mean and standard deviation as that of the observed distribution of the distance error; it is clear that the distance error distribution is not Gaussian.

With $\sigma_{pos} = 1$ m, the observed mean magnitude of the sensor position error from the presumed position to the true position for the simulations represented in Figure 119 was 0.7953 m and the maximum for the 100,000 simulations was 4.1904 m. The mean sensor distance error was 0.0590 m with standard deviation of 0.4956 m. (These values varied slightly over multiple trials of 100,000 simulations.) For practical purposes, the standard deviation of the distribution of distance error converged to 0.5 m.

The mean of the distribution of distance error approached zero for larger values of d_i and was larger for smaller values of d_i, but was always greater than zero. This conclusion can be derived from Figure 118, where q is the

randomly generated magnitude of the sensor i position error and γ is the angle of the position error off the axis between the presumed sensor position and the emitter. If $d_i = d_i'$, then γ must be less than 90° and so the spherical cap facing the emitter must enclose less than half the volume of the sphere with radius q. Therefore, the probability that any randomly generated true position with position error magnitude equal to q for sensor i has $d_i' > d_i$ is greater than $1/2$ and thus the mean distance error is greater than zero.

Having an understanding of the distribution of the distance error associated with a single sensor i, now the distribution of the distance difference error between two sensors i and j, given by (6), can be addressed.

Because the directions of the position errors of two sensors are assumed to be independent, the relative positions of the two sensors are irrelevant for the purpose of determining the distribution of their distance difference errors.

For the sake of simplicity, let $d_i = d_j = 6$ m. Cases where the distances from the emitter to the presumed positions of two sensors are unequal will be discussed later.

Figure 120 shows the distribution of the distance difference error based on 100,000 simulations. Again, the histogram also shows a Gaussian distribution that has the same mean and standard deviation as that of the observed distribution of the distance difference error and it is clear that the distance difference error distribution is clearly not Gaussian as the peak is far sharper. For the case represented here, the mean of the distance difference error distribution was observed, over many trials of 100,000 simulations, to closely hover about zero as expected. The standard deviation of the distribution was observed to be 0.7073 m, which is close to the value of $\sqrt{0.5^2 + 0.5^2} = \sqrt{2}/2 = 0.7071$ m as expected.

Keeping $\sigma_{pos} = 1$ m, for $d_i = 4$ m and $d_j = 6$ m, the observed mean distance difference error was 0.0280 m and the standard deviation was 0.7064 m. For $d_i = 6$ m and $d_j = 10$ m, the observed mean distance difference error was 0.0262 m and the standard deviation was 0.7035 m. The standard deviation remained near $\sqrt{2}/2$ m as expected.

The mean and standard deviation of the distribution of the distance difference error for two sensors scale linearly with σ_{pos} in this model. Using

$\sigma_{pos} = 10$ m, let $d_i = 4\,\sigma_{pos} = 40$ m and $d_j = 6\,\sigma_{pos} = 60$ m. Then, based on the results above from the simulations, the mean of the distance difference error would be $0.0280\,\sigma_{pos} = 0.280$ m. The predicted standard deviation would be $0.7071\,\sigma_{pos} = 7.071$ m. The mean is very small and can probably be disregarded, while the standard deviation is significant when distance difference error is converted into timing difference error.

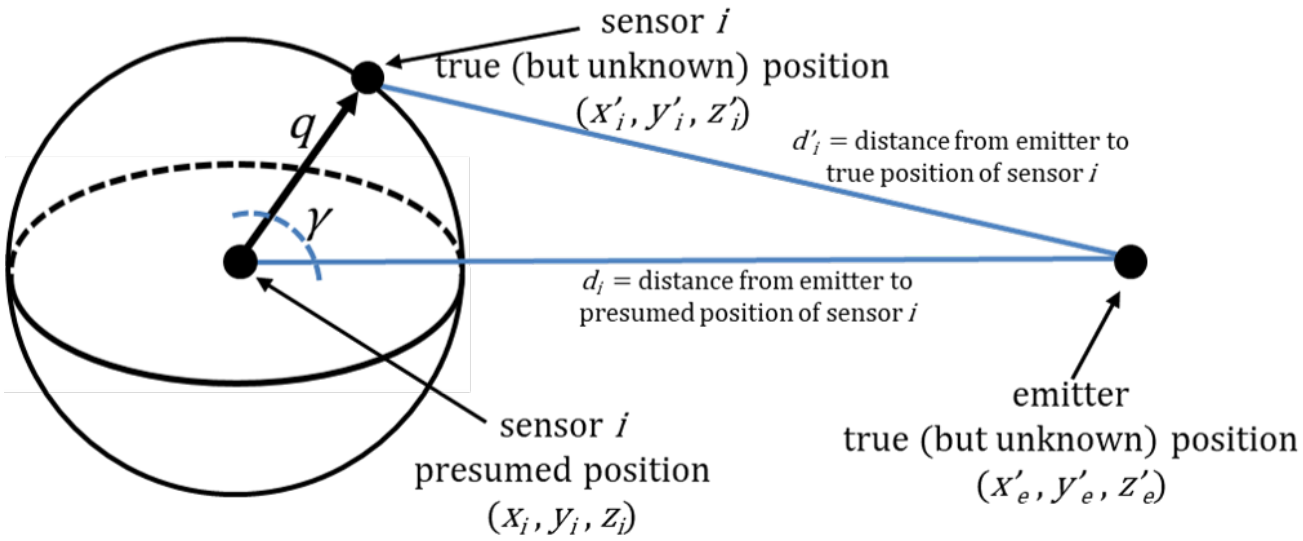

Figure 118: Sensor with position error showing distance from emitter at presumed sensor position and true sensor position.

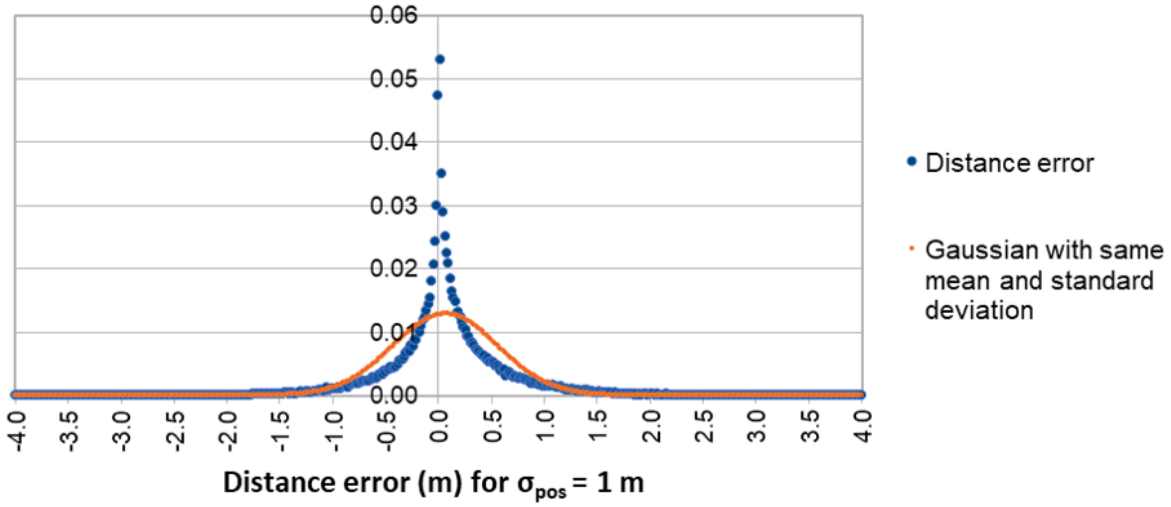

Figure 119: Distribution of *distance error* from an emitter in the case of sensor position error. See text for description of error conditions.

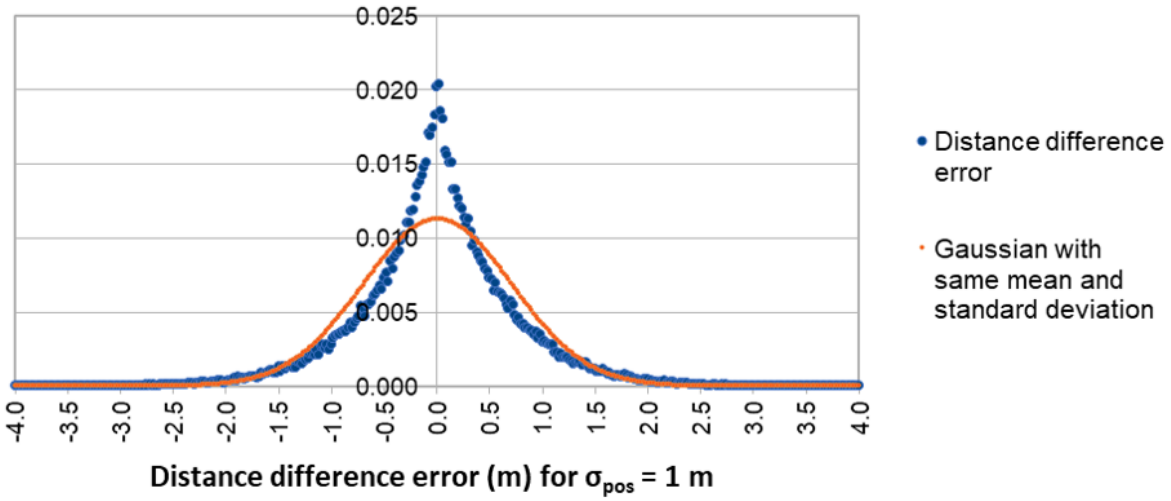

Figure 120: Distribution of *distance difference error* for two sensors from an emitter in the case of sensor position error. See text for description of error conditions.

A.3 Comparing the Effects of Timing Difference Error and Distance Difference Error

As stated in Section 4.1.2, most results obtained in this paper in the case of errors are based on simulations where the Standard Error Conditions $\sigma_{pos} = 10$ m and $\sigma_{time} = 30$ ns were used. They were chosen to be reasonable yet independent of any actual military or civilian systems or scenarios. They were also chosen to be somewhat commensurate in scale, as 10 m of distance is roughly equivalent to 30 ns at the speed of light c. Now, those values can be tested to determine how similar their effects are on TDoA timing difference error between pairs of sensors.

The mean of the timing difference error due to σ_{time} was shown in Appendix A.1 to be zero. The mean of the distance difference error due to σ_{pos} was shown to be non-zero but practically negligible. Thus, the analysis focuses on the effects on the standard deviations of the timing difference errors caused by the position and timing error conditions.

It was also shown in Appendix A.1 that the standard deviation of the timing difference error between two sensors is given by $\sqrt{2}\,\sigma_{time}$. For $\sigma_{time} = 30$ ns, the standard deviation of the TDoA time measurement between any two sensors would be 42.42 ns.

The standard deviation of the distance difference error between two sensors is given by $\sqrt{2}/2\,\sigma_{pos}$. Using $c = 3 \times 10^8$ m/sec as the speed of light, that distance (in m) is converted to time (in ns) as $\sqrt{2}/2\,\sigma_{pos} \times \frac{1 \text{ sec}}{3 \times 10^8 \text{ m}} \times \frac{10^9 \text{ ns}}{1 \text{ sec}}$ ns $= 10\sqrt{2}/2\,\sigma_{pos}$ ns $= 2.3570\,\sigma_{pos}$ ns, although, as noted earlier, the distribution of the distance difference error is not Gaussian. For $\sigma_{pos} = 10$ m, the standard deviation of the TDoA measurement between any two sensors would be 23.57 ns.

Thus, the standard deviation of the timing difference error between any two sensors due to the standard error condition of $\sigma_{time} = 30$ ns alone is 1.8X that of the timing difference error due to the standard error condition of $\sigma_{pos} = 10$ m alone.

Setting $\sigma_{pos} = 18$ m alone would equal the standard deviation of the timing difference error between any two sensors due to the error condition of $\sigma_{time} = 30$ ns alone. Setting $\sigma_{time} = 17$ ns alone would equal the standard

deviation of the timing difference error between any two sensors due to the error condition of $\sigma_{pos} = 10$ m alone.

In Section 13.2.3 it was found that, for the mean LDE based on simulations of a range of configurations with immersed sensors, a meter of position standard deviation is approximately equivalent to two (or a little more) nanoseconds of timing error standard deviation. This is a little larger than the calculated ratio of 1.8X for the equivalence between position (in m) and timing (in ns) error conditions for the standard deviation of the timing difference error between any two sensors. While these two problems are only indirectly related, it is still a good sanity check to see that the two ratios are relatively close in scale.

While it has been shown here that there is a proportional equivalence between position errors and timing errors in their impact on mean LDE, recall that it was shown in Section 13.2.4 that the principle of superposition does not apply to position errors and timing errors. That is, the LDE resulting from only position errors and the LDE resulting from only timing errors do not sum linearly to yield the LDE resulting from the combination of the same position and timing errors.

B Benefits of Enforcing Minimum xy Sensor Separation

The analyses in this paper have been based on the assumption that the sensors are placed randomly or their movements are random. Potential optimizations could involve eliminating poor geometries, such as collinear sensors, to avoid Longfellow Events. This is a very difficult task, as examples in Section 2 showed. This appendix considers the simplest possible geometric optimization, which would be to enforce a specified minimum xy separation between any two sensors

Sets of simulations were run with enforced minimum xy separation of 50 m, 100 m, 150 m, and 200 m, and the results were compared to the baseline of 0 m (that is, no minimum xy separation). The configurations consisted of $N = 3$ to 10 immersed sensors in a search area with side length $side = 1{,}000$ m at nominal altitudes of $alt = 0$ m and 500 m, with $\sigma_{alt} = alt/20$. The Standard Error Conditions $\sigma_{pos} = 10$ m and $\sigma_{time} = 30$ ns were used.

Due to the long run times required, only 1,000 simulations of each configuration were performed.

Two figures-of-merit are used. The first was the ratio of mean LDE with a specified enforced minimum xy separation to the mean LDE with zero minimum xy separation. The second was the equivalent number of sensors required for a configuration with zero minimum xy separation to achieve the mean LDE of a configuration with a specified enforced minimum xy separation.

B.1 Ratio of LDE With and Without Enforced Minimum xy Separation

For each simulation of a given configuration and minimum xy separation, random geometries were generated and used only if no two sensors violated the minimum xy separation requirement. Figure 121 shows two instances of ten sensors placed at random, where tight "clusters" of sensors appear. Figure 122 shows two instances of ten sensors placed at random with an enforced minimum of 200 m xy separation; the clusters of sensors have been eliminated.

Figure 123 shows the ratio (per configuration) of the number of random geometries generated and tested to the number of geometries that achieved the required minimum xy separation. For small minimum xy separation, the overhead was small. For minimum xy separation of 150 m, the ratio grew approximately as $e^{0.4261\,N}$. For minimum xy separation of 200 m, the ratio grew approximately as $e^{0.7883\,N}$ and, worse, the ratio for $N = 10$ sensors was nearly double the value predicted by that regression. For minimum xy separation of 200 m and $N = 10$ sensors, an average of 361 random geometries had to be generated and tested to obtain a single geometry that met the minimum xy separation requirement.

With a minimum xy separation of 200 m in a search area with side length 1,000 m, the greatest number of sensors for which that requirement could be satisfied was 14. Figure 124 shows two instances of 14 sensors placed at random with minimum xy separation of 200 m. The search was terminated after finding only those two geometries; based on only those two successes, the ratio of generated geometries to geometries that met the specified minimum xy separation requirement was 345,481.5. [51]

For stationary sensors, such overhead might be acceptable as a one-time cost while planning a sensor deployment. However, for sensors hosted on moving platforms, these ratios give an indication of the computational cost to find such geometries (literally on the fly) or the low probability that sensors in motion would, at random, satisfy the minimum xy separation requirement at any given instant of time.

[51] That is, in each case, more than a third of a million geometries were generated, tested, and rejected to find a geometry that satisfied the minimum xy separation of 200 m.

Figure 125 shows, for sensors on the ground, the ratio of the mean LDE for a given enforced minimum xy separation to the mean LDE with zero minimum xy separation. This figure-of-merit drops from 1.0 for zero minimum xy separation (by definition) to approximately 0.7 to 0.8 as the minimum xy separation increases to 200 m. There is no apparent trend for this ratio as a function of the number of sensors.

Figure 126 shows, for sensors at $alt = 500$ m, the ratio of the mean LDE for a given minimum xy separation to the mean LDE with zero minimum xy separation. The same observations given above for sensors on the ground apply here as well.

Figure 127 combines the data shown in Figure 125 and Figure 126 by plotting the average ratios for $N = 3$ to 10 for $alt = 0$ m and $alt = 500$ m. The average values for these two nominal altitudes were so close that it is fair to do a single linear regression for those combined data. The average ratio (over this range of N) appears to fall off linearly with the increase in minimum xy separation.

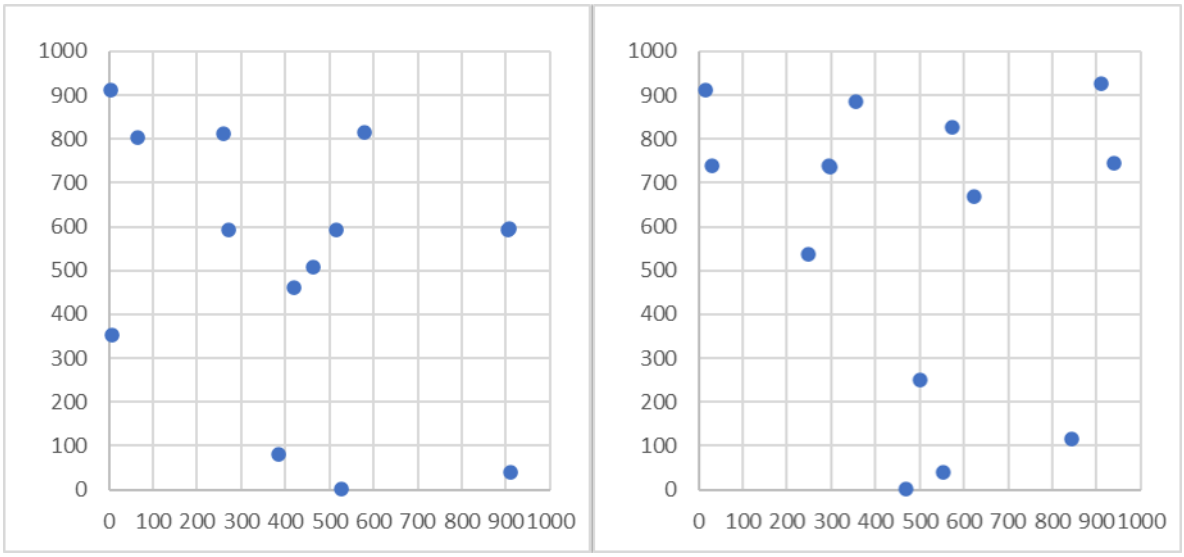

Figure 121: Two instances of ten immersed sensors with no enforced minimum xy separation.

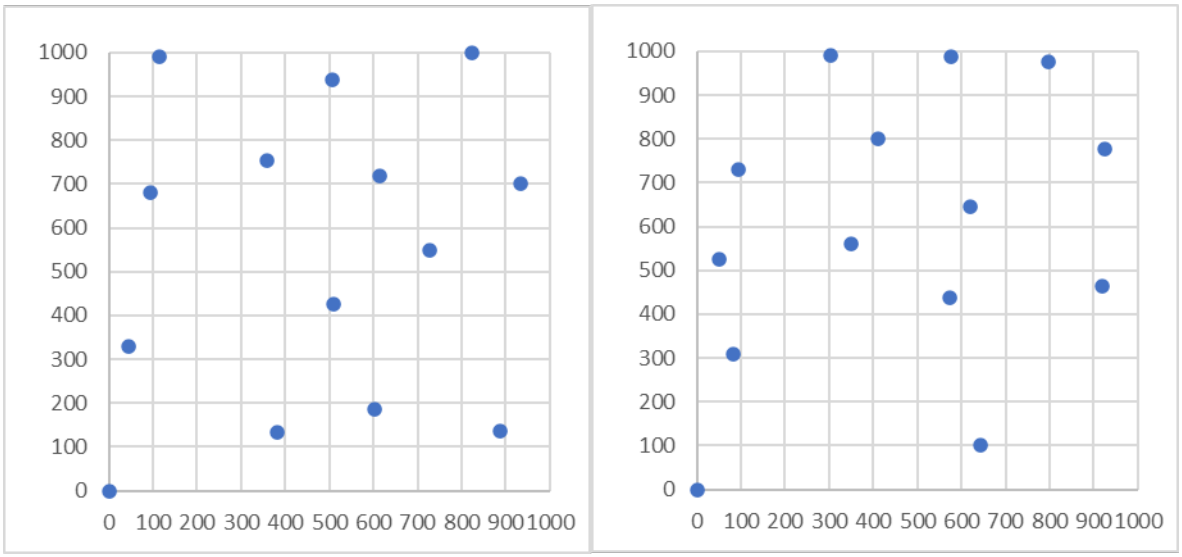

Figure 122: Two instances of ten immersed sensors with 200 m enforced minimum xy separation.

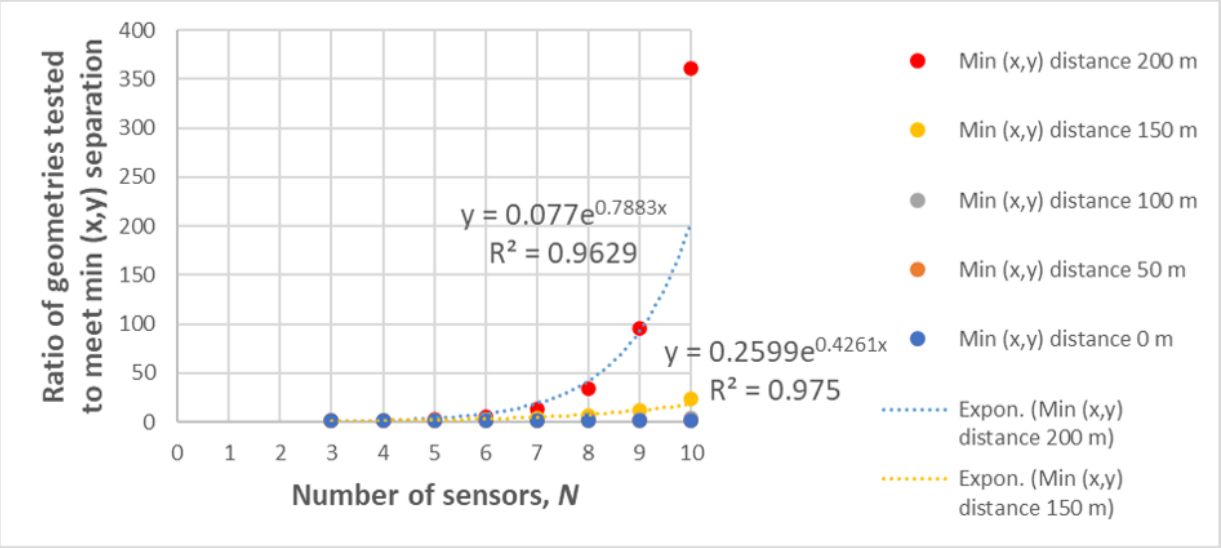

Figure 123: Ratio of the number of randomly generated geometries tested to the number of geometries that satisfied the required minimum xy separation, as a function of the number of sensors. Trend lines and exponential fits are given for growth of the ratios.

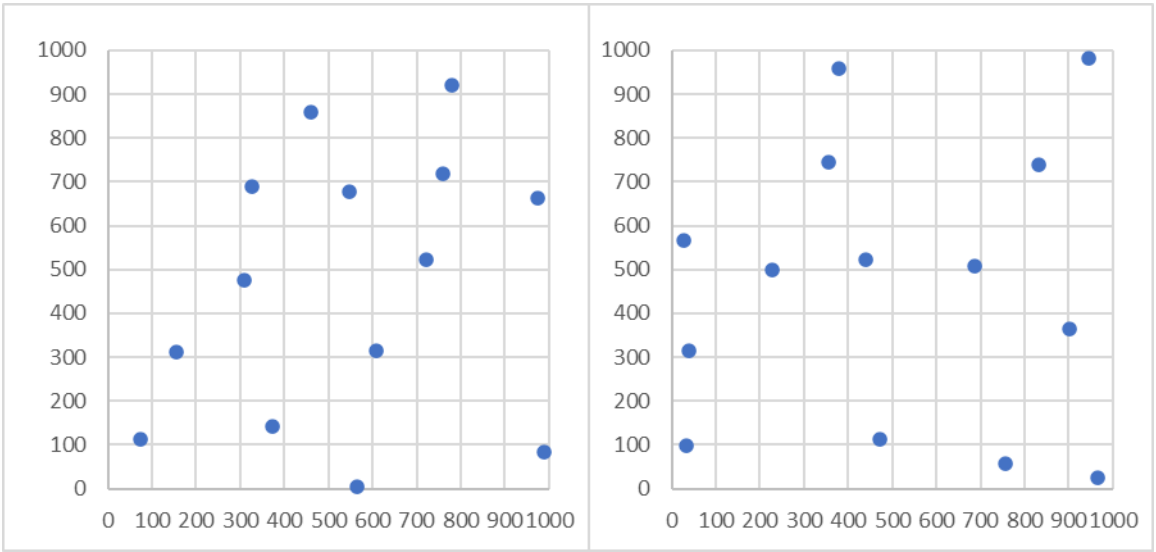

Figure 124: Two instances of 14 immersed sensors with 200 m enforced minimum xy separation. Only these two instances were found after a substantial run time.

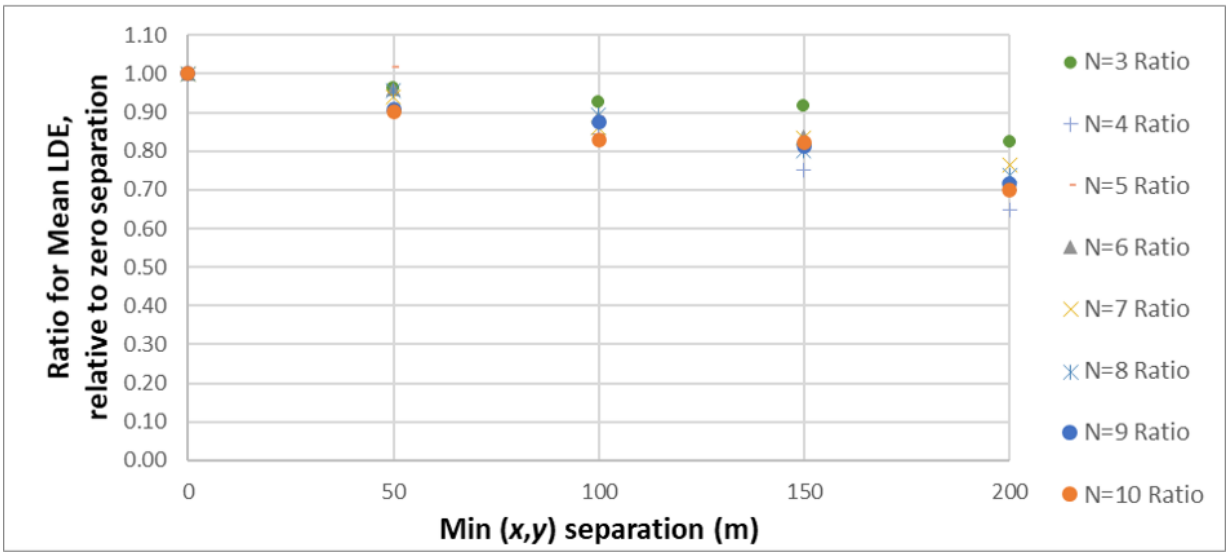

Figure 125: Ratio of the mean LDE for a given minimum xy to the mean LDE with no enforced minimum xy separation, for immersed sensors on the ground, with errors.

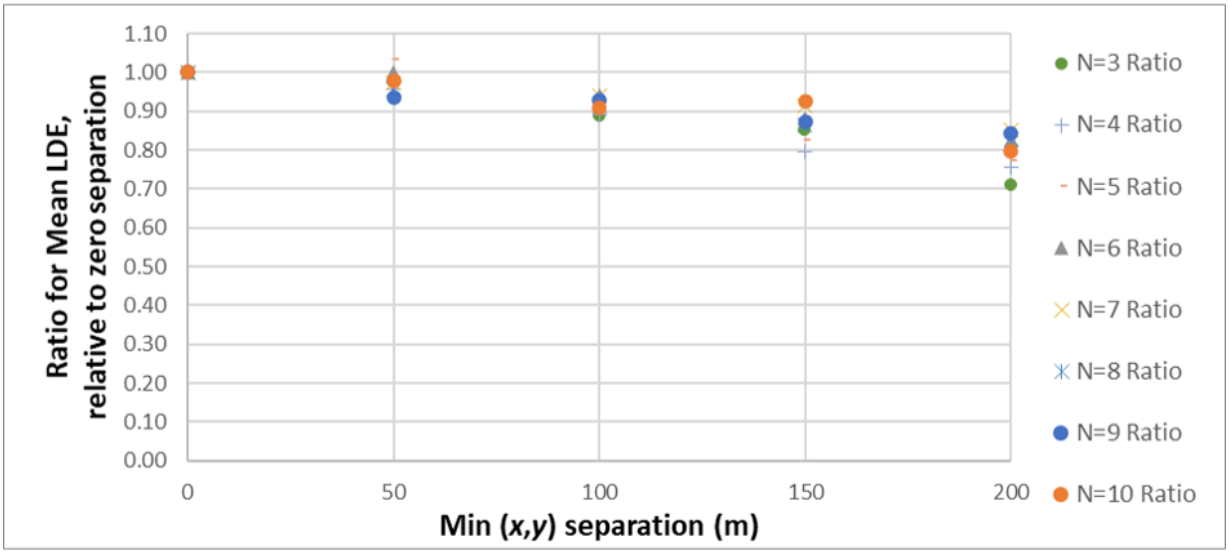

Figure 126: Ratio of the mean LDE for a given minimum xy to the mean LDE with no enforced minimum xy separation, for immersed sensors at nominal altitudes of 500 m, with errors.

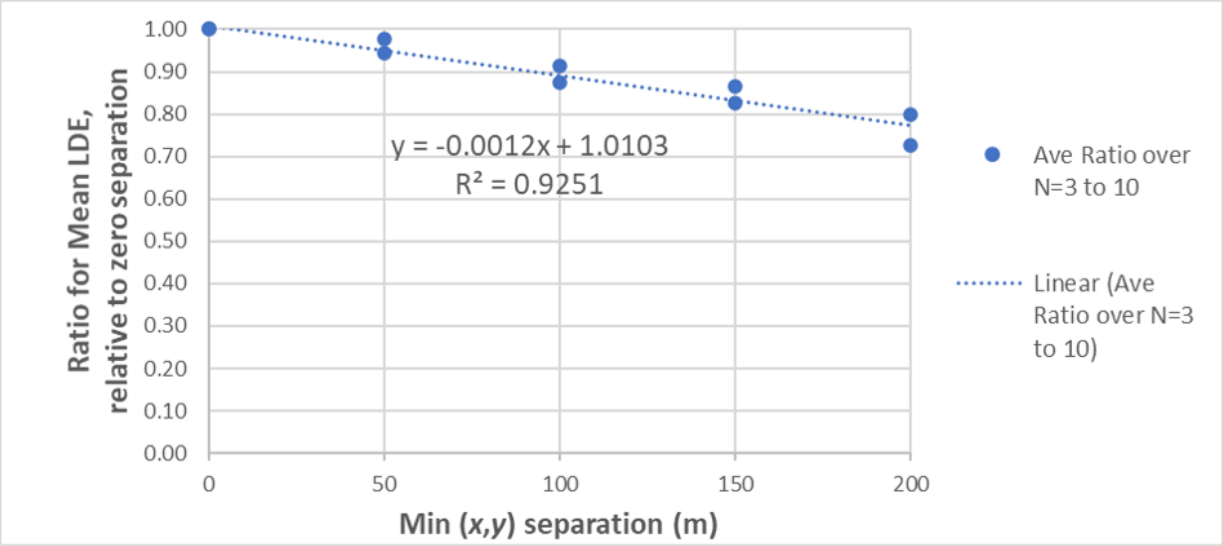

Figure 127: Trend line and linear regression model for combined data shown in Figure 125 and Figure 126.

B.2 Effectively Increasing the Number of Sensors by Enforcing Minimum xy Separation

The second figure-of-merit determines how a enforcing a minimum xy separation effectively increases the number of sensors. For a given N and specified minimum xy separation, let the **equivalent number of sensors** N_{equiv} denote the largest number of sensors with zero minimum xy separation that provide equal or greater mean LDE compared to that achieved by N sensors with the specified minimum xy separation enforced.

The measured mean LDE values from the Main Data Set were used to find N_{equiv} for $alt = 0$ m and $alt = 500$ m with minimum xy separation of 200 m. For $N = 3$ to 10, respectively, those values were:

$N_{equiv} = 3, 4, 6, 7, 8, 10, 12, 14$ immersed sensors for $alt = 0$ m, and

$N_{equiv} = 3, 4, 6, 7, 8, 9, 11, 13$ immersed sensors for $alt = 500$ m.

Thus, for example, five sensors with an enforced minimum xy separation of 200 m provide equal or better LDE compared to that achieved by six sensors without an enforced minimum xy separation, for both of these nominal altitudes.

As a test of the accuracy of the linear regression models presented in Section 9.3, (23) and the weights in Table 3 were used to obtain estimates for N_{equiv} from the mean LDE observed for the given minimum xy separation values. If y denotes such a mean LDE, then (23) and Table 3 yield $\ln\ln y = -0.8154 \ln\ln N + 1.6528$ for $alt = 0$ m and $\ln\ln y = -0.6663 \ln\ln N + 1.5584$ for $alt = 500$ m. Solving these expression for N_{equiv} yields

$$N_{equiv} = \exp(\exp\left\{\frac{1.6528 - \ln\ln y}{0.8154}\right\}) \quad \text{for } alt = 0 \text{ m} \tag{41}$$

s

and

$$N_{equiv} = \exp(\exp\left\{\frac{1.5584 - \ln\ln y}{0.6663}\right\}) \quad \text{for } alt = 500 \text{ m} \quad . \tag{42}$$

Using the mean LDE for minimum xy separation of 200 m for y, rounding the results of (41) and (42) gave

N_{equiv} = 3, 5, 6, 8, 8, 10, 12, 14 immersed sensors for alt = 0 m, and

N_{equiv} = 3, 5, 6, 8, 9, 10, 11, 13 immersed sensors for alt = 500 m,

which differed in the six instances noted in red font from the N_{equiv} values obtained using the measured values from the Main Data Set.

Better results were obtained by taking the floor instead of rounding the results of (41) and (42), which gave

N_{equiv} = 3, 4, 6, 7, 8, 10, 11, 14 immersed sensors for alt = 0 m, and

N_{equiv} = 3, 4, 6, 7, 8, 9, 10, 13 immersed sensors for alt = 500 m

which differed in only the two instances noted in red font from the N_{equiv} values obtained using the measured values from the Main Data Set.

This appendix has shown that enforcing a minimum xy separation between sensors improves mean LDE linearly with the amount of separation, with about a 20% to 30% reduction in mean LDE with a minimum xy separation of 200 m. For ten sensors, enforcing a minimum xy separation can provide the equivalent of adding up to four sensors compared to not enforcing a minimum xy separation.

Acknowledgment

Dr. Paul Ratazzi provided invaluable technical advice as well as making available the computational resources used to perform this work.

References

[Altman (2015)] D.G Altman, "Standard Deviations and Standard Errors," *BMJ*, https://doi.org/10.1136/bmj.331.7521.903, Oct 2005.

[Chan (1994)] Y.T. Chan and K.C. Ho, "A Simple and Efficient Estimator for Hyperbolic Location," in IEEE Transactions on Signal Processing, vol. 42, no. 8, pp. 1905-1915, Aug 1994.

[Chen (2013)] S. Chen and K.C. Ho, "Achieving Asymptotic Efficient Performance for Squared Range and Squared Range Difference Localizations," in *IEEE Transactions on Signal Processing*, vol. 61, no. 11, pp. 2836-2849, June 2013.

[El Gemayel (2014)] N. El Gemayel, H. Jäkel and F.K. Jondral, "Error Analysis of a Low Cost TDoA Sensor Network," IEEE/ION Position, Location and Navigation Symposium (PLANS), 2014.

[Gholami (2013)] M.R. Gholami, S. Gezici and E.G. Strom, "TDoA Based Positioning in the Presence of Unknown Clock Skew," *IEEE Transactions on Communications*, vol. 61, no. 6, pp. 2522-2534, Jun 2013.

[Hamdollahzadeh (2016)] M. Hamdollahzadeh, S. Adelipour, and F. Behnia, "Optimal Sensor Configuration for Two Dimensional Source Localization Based on TDoA/FDoA Measurements," *17th International Radar Symposium (IRS)*, 2016

[Ho (2007)] K.C. Ho, X. Lu, and L. Kovavisaruch, "Source Localization Using TDoA and FDoA Measurements in the Presence of Receiver Location Errors: Analysis and Solution," *IEEE Transactions on Signal Processing*, vol. 55, no. 2, pp. 684-696, Feb. 2007.

[Holleman (2012)] I. Holleman and A. Huuskonen, "Analytical Formulas for Refraction of Radiowaves from Exoatmospheric Sources," *Radio Science*, vol. 48, no. 3, pp. 226-231, May 2013.

[Hu (2006)] X. Hu, M. Chen, and M.L. Fowler, "Exploiting Data Compression Methods for Network-Level Management of Multi-Sensor Systems," *Proceedings, Mathematics of Data/Image Pattern Recognition, Compression, and Encryption with Applications IX, SPIE Optics + Photonics*, Aug 2006.

[Huie (2014)] L.M. Huie-Seversky, "Localization Under Adversary Misdirection," AFRL-RI-RS-TR-2014-274, DTIC #ADA611846, https://apps.dtic.mil/dtic/tr/fulltext/u2/a611846.pdf, Oct 2014.

[Kaune (2012)] R. Kaune, "Accuracy Studies for TDoA and TOA Localization," *IEEE 15th International Conference on Information Fusion*, 2012.

[Kim (2016)] S. Kim and H. Kim, "A New Metric of Absolute Percentage Error for Intermittent Demand Forecasts," *International Journal of Forecasting*, Elsevier, https://doi.org/10.1016/j.ijforecast.2015.12.003, 2016.

[Longfellow (1904)] H.W. Longfellow, "There Was a Little Girl," https://allnurseryrhymes.com/there-was-a-little-girl/. There are many versions of this poem, all of which may have first appeared in the early 1900s and 1910s long after Henry Wadsworth Longfellow's death in 1882. There appears to be an 1890 "Edison's Talking Doll" sound recording of a portion of the poem at https://commons.wikimedia.org/wiki/File:There_was_a_little_girl_(1890).ogg but this probably did not popularize the poem; the dolls were a commercial failure due to the fact they terrified children.

[MathWorks (2020)] MathWorks Documentation, "Coefficient of Determination (R-Squared)," https://www.mathworks.com/help/stats/coefficient-of-determination-r-squared.html.

[Montminy (2007)] M.B. Montminy, "Passive Geolocation of Low-Power Emitters in Urban Environments Using TDoA," Thesis AFIT/GE/ENG/07-16, DTIC #ADA471571, Mar 2007.

[Press (2002)] W.H. Press, S.A. Teukolsky, W.T. Vetterling, and B.P. Flannery, *Numerical Recipes in C++: The Art of Scientific Computing*, Cambridge University Press, New York NY, 2002.

[Qu (2012)] X. Qu and L. Xie, "Source Localization by TDoA with Random Sensor Position Errors - Part I: Static Sensors," *IEEE 15th International Conference on Information Fusion*, 2012.

[Rohatgi (1979)] V.K. Rohatgi, *An Introduction to Probability Theory and Mathematical Statistics*, John Wiley and Sons, New York, 1979.

[Sadaphal (2005)] V.P. Sadaphal and B.N. Jain, "Sensor Selection Heuristic in Sensor Networks," in D.A. Bader, M. Parashar, V. Sridhar, V.K. Prasanna (eds), *High Performance Computing – HiPC 2005*, *Lecture Notes in Computer Science*, vol. 3769, Springer, 2005.

[Smith (1987)] J. Smith and J. Abel, "Closed-Form Least-Squares Source Location Estimation from Range-Difference Measurements," in *IEEE Transactions on Acoustics, Speech, and Signal Processing*, vol. 35, no. 12, pp. 1661-1669, Dec 1987.

[Torrieri (1984)] D.J. Torrieri, "Statistical Theory of Passive Location Systems," in *IEEE Transactions on Aerospace and Electronic Systems*, vol. AES-20, no. 2, pp. 183-198, Mar 1984.

[Wang (2013)] Y. Wang and K.C. Ho, TDoA Source Localization in the Presence of Synchronization Clock Bias and Sensor Position Errors, *IEEE Transactions on Signal Processing*, vol. 61, no. 18, pp. 4532-4544, Sep 2013.

[Weisstein (2019a)] E.W. Weisstein, "Box-Muller Transformation," *MathWorld—A Wolfram Web Resource*: https://mathworld.wolfram.com/Box-MullerTransformation.html, original date of article unknown.

[Weisstein (2019b)] E.W. Weisstein, "Standard Error," *MathWorld—A Wolfram Web Resource*: https://mathworld.wolfram.com/StandardError.html, original date of article unknown.

[Zhang (2019)] T. Zhang, X. Mao, C. Zhao and J. Liu, "A Novel Grid Selection Method for Sky-Wave Time Difference of Arrival Localisation," *IET Radar, Sonar & Navigation,* vol. 13, no. 4, pp. 538-549, 2019.